Carbon Dioxide Utilisation: Unlocking Enhanced Properties for Oxygenated Polymers

Kam Charles Poon

Trinity College

Department of Inorganic Chemistry

University of Oxford

July 2024

A thesis submitted in partial fulfilment of the requirements for the degree of Doctor of Philosophy in Chemistry

For my family and my friends

"Chemists are dreamers.

We think up new molecules and bring them to life."

- Carolyn Bertozzi

Declaration

The work described in this thesis was conducted between September 2020 and July 2024 at the University of Oxford. This is the work of the author unless otherwise stated.

Kam C. Poon

Abstract

This thesis describes the synthesis of new oxygenated plastics and elastomers from CO_2 and bio-derived feedstocks, where non-covalent cross-linking interactions between chains are employed to improve and tune thermomechanical properties. Networks are established through reversible metal-ligand bonding, macromolecular entanglements, and thiol-ene crosslinking during vat photopolymerization 3D printing. This thesis aims to develop strategies to improve the thermomechanical properties of CO_2-derived polymers, to match those of the current petrochemical incumbents.

Chapter 1 provides an introduction to the latest progress in the development of sustainable and oxygenated plastics and elastomers. Specifically, polyesters and polycarbonates produced through lactone ring-opening polymerisation and epoxide/CO_2 ring-opening copolymerisation to form high molar mass homopolymers and ABA triblock polymers. The potential of macromolecular networking strategies and the chemistries to facilitate non-covalent interactions are discussed.

Chapter 2 reports new CO_2-derived thermoplastic elastomers (TPEs) together with a generally applicable method to augment tensile mechanical strength and Young's modulus without requiring material re-design. These TPEs combine high glass transition temperature (T_g) amorphous blocks comprising CO_2-derived poly(carbonates) (A-block), with low T_g poly(*ε*-decalactone), from castor oil, (B-block) in ABA structures. The poly(carbonate) blocks are selectively functionalized with metal-carboxylates, where the metals are Na(I), Mg(II), Ca(II), Zn(II) and Al(III). The colorless polymers, featuring <1 wt% metal, show tunable thermal (T_g), and mechanical (elongation at break, elasticity, creep-resistance) properties. The best elastomers show >50-fold higher Young's modulus and 21-times greater tensile strength, without compromise to elastic recovery, compared with the starting block

polymers. They have wide operating temperatures (−20 to 200 °C), high creep-resistance and yet remain recyclable.

Chapter 3 describes well-defined, high molar mass CO_2 terpolymers prepared from cyclohexene oxide (CHO), cyclopentene oxide (CPO), and CO_2 by using a [Zn(II)Mg(II)] catalyst. In the catalysis, CHO and CPO show reactivity ratios of 1.53 and 0.08 with CO_2, respectively; as such, the terpolymers have gradient structures. The poly(cyclohexene carbonate)-*grad*-poly(cyclopentene carbonate) (PCHC-*grad*-PCPC) have high molar masses (M_n >86 kg mol^{-1}) and good thermal stability (T_d > 250 °C). All the polymers are amorphous with a single, high glass transition temperature (96 < T_g < 108 °C). The polymer entanglement molar masses, determined using dynamic mechanical analyses, range from 4 < M_e < 23 kg mol^{-1} depending on the polymer composition (PCHC:PCPC). These polymers show superior mechanical performance to PCHC; specifically, the lead material ($PCHC_{0.28}$-grad-$PCPC_{0.72}$) shows 25% greater tensile strength and 160% higher tensile toughness. These new plastics are recycled, using cycles of reprocessing by compression moulding, four times without any loss in mechanical properties. They are also efficiently chemically recycled to selectively yield the two epoxide monomers, CHO and CPO, as well as carbon dioxide, with high activity (TOF = 270−1653 h^{-1}). The isolated recycled monomers are repolymerized to form a thermoplastic showing the same material properties.

Chapter 4 reports the successful additive manufacturing of a series of poly(carbonate-*b*-ester-*b*-carbonate) elastomers, derived from carbon dioxide and bio-derived ε-decalactone. By employing a highly active and selective [Co(II)Mg(II)] polymerisation catalyst, an ABA triblock copolymer (M_n = 6.3 kg mol^{-1}, $Đ_M$ = 1.26) was synthesised on a 200 g scale, formulated into resins which were 3D printed using digital light processing (DLP), and a thiol-ene-based crosslinking system. A series of elastomeric and degradable thermosets were produced, with varying thiol cross-linker length and poly(ethylene glycol) content, to produce complex triply

periodic geometries at high resolution. Thermomechanical characterisation of the materials reveals printing-induced microphase separation and tunable hydrophilicity. These findings highlight how utilising DLP can produce sustainable materials from low molar mass polyols quickly and at high resolution. The 3D printing of these functional materials may help to expedite the production of sustainable plastics and elastomers with potential to replace conventional petrochemical-based options.

Chapter 5 concludes the thesis and discusses future work to build on and extend the research.

Chapter 6 provides the experimental details for Chapters 2-4.

Chapter 7 is an appendix containing all supplementary information, figures, schemes, and tables that supports the results reported and discussed in Chapters 2-6.

Acknowledgments

First of all, I would like to thank Prof. Charlotte Williams for giving me the opportunity of a lifetime to complete my PhD in your incredible group. It has been nothing but an enormous privilege. Thank you for your unwavering support, guidance, and endless enthusiasm for research. I will be eternally grateful.

I have been lucky enough to work with and learn from the most amazing people during my time in the Williams Group, thank you: Greg, George, Fer, Shannon, Nora, Ryan, Thom, Gemma, Mati, Fran, Holly, Kat, Bonny, Maddie, Gloria, Wouter, Arron, Wilf, Lisa, Hui, Sandy, Edward, Brad, Diego, Víctor, Freya, Ploy, Jamie, Mantas, Lukas, Kira, Balu, Kristian, James, Sevven, Matylda, Tats, Rachel, Erica, Kate, Rosie, and David.

Greg – thank you for taking me under your wing on day one, for training me, and for all the cricket. George – I will never meet someone with more polymer knowledge than you, it has been a privilege to learn from such a master. Kat – thank you for being a phenomenal friend. I have loved our trips to the water cooler and having had the chance to see your genius in action up close. Holly – from my first day you went out of your way to make me feel welcome in the group. Your generosity and outrageous humour were an endless source of joy. Maddie – you never failed to make me smile even on the toughest days; it has been an honour working with you. Bonny – it has been a pleasure working with you and I can't wait to follow all your successes over the coming months and years. Thank you for the laughs and the savage takes. And of course, Fran – completing this journey alongside you has made it more fun and memorable than I ever expected. I couldn't have asked for a better friend. I'm going to miss you so much.

I am so grateful to Prof. Matthew Becker for welcoming me into his group with open arms during my research secondment at Duke. A special mention to Maddiy, Alex, Nicola,

Yin, Sam, Gigi, Cody, Emily, Anshu, and Matt for teaching me the art of 3D printing, showing me the beauty of North Carolina, and ensuring I tried the best BBQ the state has to offer.

I have been lucky to have some sensational housemates during my time in Oxford: Helen, Maya, James, and Matthew. It was always a pleasure to come home to you. Thank you for the memories, the food, and the shared covid isolation trauma.

Megan – we may have completed our PhDs in different cities but it always felt as if we were on this venture side by side. Who would have thought in fresher's week all those years ago we would be where we are today? Thank you for constantly supporting and inspiring me.

I am so grateful to the OxICFM CDT for funding me. In particular to Simon and Maitane for all the opportunities you have given me.

Thank you to Trinity College for your support, funding, and delicious meals over the past four years. Ashley – you are the lifeblood of our graduate community. I and the college are so lucky to have you in our corner.

It is hard for me to imagine completing this journey without my wonderful girlfriend. Mary, your love and support means more to me than you will ever realise. I can't wait to start the next chapter of our lives together by your side. You are my best friend, my home, and my greatest adventure.

And finally, Mum, Dad, and Mei Lan, it is impossible for me to put into words what you mean to me. You taught me what it means to be curious, what it means to explore, and what it means to follow my passions. You might not understand too much of what follows in this thesis but it exists because of you. I love you.

List of Publications

Toughening CO_2 -Derived Copolymer Elastomers Through Ionomer Networking

Kam C. Poon, Georgina L. Gregory, Gregory S. Sulley, Fernando Vidal, Charlotte K. Williams, *Adv. Mater.* **2023**, 35, e2302825. DOI: 10.1002/adma.202302825.

Controlled Carbon Dioxide Terpolymerizations to Deliver Toughened yet Recyclable Thermoplastics

Kam C. Poon, Madeleine L. Smith, Charlotte K. Williams, *Macromolecules* **2024**, *57*, 4199-4207. DOI: 10.1021./acs.macromol.4c00455

Digital Light Processing to Afford High Resolution and Degradable CO_2-Derived Copolymer Elastomers

Kam C. Poon, Maddison Segal, Alexander J. Bahnick, Yin Mei Chan, Chang Gao, Matthew L. Becker, Charlotte K. Williams, *Angew. Chem. Int. Ed.* **2024**, e202407794. DOI: 10.1002/anie.202407794.

List of Abbreviations

3D	Three-Dimensional
AGE	Allyl Glycidyl Ether
b	Block
BCC	Body-Centred Cubic
BDM	1,4-Benzenedimethanol
BPA	Bisphenol A
CAN	Covalent Adaptable Network
Cat.	Catalyst
CCU	Carbon Capture and Utilisation
CHD	Cyclohexane-1,2-diol
CHO	Cyclohexene Oxide
ε-CL	ε-Caprolactone
co	Copolymer
CO_2	Carbon Dioxide
COSY	Correlated Spectroscopy
Conv.	Conversion
CPMA	Carbic Anhydride
CPO	Cyclopentene Oxide
CTA	Chain Transfer Agent
$Đ_M$	Dispersity
DCM	Dichloromethane
ε-DL	ε-Decalactone
DLP	Digital Light Processing
DMA	Dynamic Mechanical Analysis

DMAP	4-Dimethylaminopyridine
DMTA	Dynamic Mechanical Thermal Analysis
DOSY	Diffusion Ordered Spectroscopy
DP	Degree of Polymerisation
DSC	Differential Scanning Calorimetry
DTC	5,5-Dimethyl-1,3-Dioxan-2-one
E'	Elastic Storage Modulus
E"	Elastic Loss Modulus
Equiv.	Equivalents
E_Y	Young's Modulus
f_{hard}	Hard Block Volume Fraction
G'	Sheer Storage Modulus
G"	Sheer Loss Modulus
GA	Glutaric Anhydride
grad	Gradient
HEX	Hexagonally Packed Cylinders
HMBC	Hetronuclear Multiple-Bond Coherence
HSQC	Hetronuclear Single Quantum Coherence
IR	Infrared
L	Ligand
LA	Lactide
LAM	Lamellae
LO	Limonene Oxide
M	Metal
MA	Maleic Anhydride
M_e	Entanglement Molar Mass

M_c	Critical Molar Mass
MeOH	Methanol
M_n	Number Average Molar Mass
mol%	Mole Percent
3-MPA	3-Mercaptopropionic
M_w	Weight Average Molar Mass
N	Degree of Polymerisation
NMR	Nuclear Magnetic Resonance
OCA	L-lactide-*O*-carboxyanhydride
OTW	Operating Temperature Window
PA	Phthalic Anhydride
PC	Poly(Carbonate)
PCHC	Poly(Cyclohexene Carbonate)
PCHPE	Poly(Cyclohexene Phthalate)
PCPC	Poly(Cyclopentene Carbonate)
PDL	Poly(ε-Decalactone)
PE	Poly(Ester)
PeCHC	Poly(Ethyl-Cyclohexene Carbonate)
PEG	Poly(Ethylene Glycol)
PET	Polyethylene Terephthalate
PJL	Poly(Jasmine Lactone)
PLA	Poly(Lactic Acid)
PLimC	Poly(Limonene Carbonate)
PLLA	Poly(L-Lactic Acid)
PO	Propylene Oxide

PPF	Poly(Propylene Fumerate)
PvCHC	Poly(Vinyl Cyclohexene Carbonate)
ran	Random
ROCOP	Ring-Opening Copolymerisation
ROP	Ring-Opening Polymerisation
SA	Succinic Anhydride
SAXS	Small Angle X-Ray Scattering
SEC	Size Exclusion Chromatography
t	Time
T	Temperature
Tan(δ)	Damping Coefficient
TCA	Tricyclic Anhydride
$T_{d,\,5\%}$	Degradation Temperature (5% mass loss)
T_g	Glass Transition Temperature
TGA	Thermogravimetric Analysis
THF	Tetrahydrofuran
TMC	Trimethylene Carbonate
TOF	Turnover Frequency
TON	Turnover Number
TPE	Thermoplastic Elastomer
U_T	Tensile Toughness
UV	Ultraviolet
vCHO	4-Vinyl-Cyclohexene Oxide
wt%	Weight Percent
δ-VL	δ- Valerolactone
W_d	Weight of Dried Polymer

W_o	Original Weight of Polymer
W_d	Weight of Dried Polymer
ε_b	Strain at Break
η	Viscosity
λ	Wavelength
μ	Micro
ν	Poisson Ratio
σ	Ultimate Tensile Strain
χ	Flory-Huggins Interaction Parameter

List of Figures, Schemes and Tables

Chapter 1: Introduction

Chapter 2: Toughening CO2-Derived Copolymer Elastomers Through Ionomer Networking

Chapter 3: Controlled Carbon Dioxide Terpolymerisations to Deliver Toughened Yet Recyclable Thermoplastics

Chapter 4: Digital Light Processing to Afford High Resolution and Degradable CO2-Derived Copolymer Elastomers

Table of Contents

CHAPTER 1

Introduction

1.1 Sustainable Polymers

A century on from their discovery, synthetic polymers have become ubiquitous in modern society.[1] From inexpensive packaging to specialised electronics, we are increasingly reliant on polymers in almost every aspect of our lives. However, the vast majority of plastics we produce are derived from fossil fuels and are unable to degrade within a reasonable timescale once disposed of.[2] This demand for plastics presents numerous environmental and societal challenges that urgently need addressing.[3] We may need new, bio-derived, biodegradable, and affordable materials with thermal and mechanical properties to challenge those of their environmentally persistent counterparts.[4] This chapter aims to outline some of the technical challenges we face, recent progress in the synthesis of sustainable polymers, and polymer networking strategies capable of improving their properties.

The versatile property profile of synthetic polymers, their durability, their low cost, and their light weight, have revolutionised almost every industrial sector. The complex architecture and topology of macromolecules offers numerous handles to tune their properties to highly specialised requirements, for a given application. These extraordinary properties have led to the mass production and adoption of polymers around the world. However, the durable and chemically inert nature of such materials have led to their accumulation throughout the environment. As a society we are now only starting to realise the extent of the damage this macro- and microplastic pollution is causing to the natural world.[5]

It is clear that a 'business as usual' response to this growing crisis is untenable. This would only lead to rapidly increasing plastic pollution over the coming decades. Instead, we urgently need both the reduction and replacement of plastic products (pre-consumption) as well as improved plastic waste disposal, collection, and recycling (post-consumption). This could result in an 80% reduction in oceanic plastic waste.[6] This multifaceted response is

inherently complex and will require decisive action from global policy decision makers around the world.

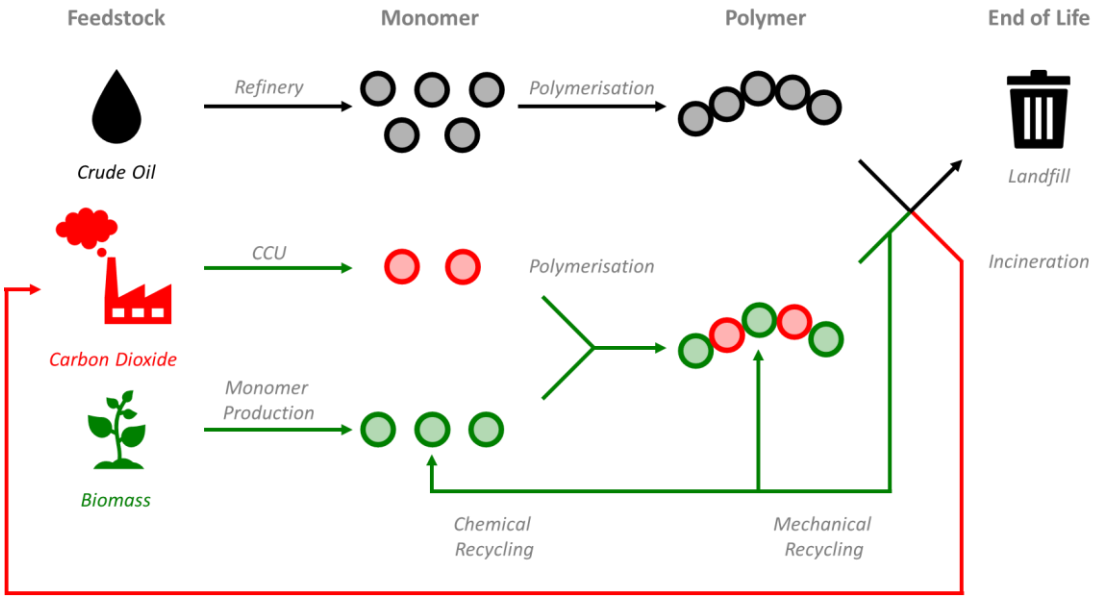

Figure 1.1. Schematic representation and comparison between linear and circular plastic economies.

Of the 6300 million metric tonnes of plastic waste generated, only 9% has been recycled.[7] Effective and efficient recycling is an essential cornerstone to addressing the plastic waste crisis. Unfortunately, it is predicted that the growth of plastic waste is outpacing current efforts to mitigate plastic pollution.[8] Current recycling technologies cannot meet the current, let alone future, needs for plastic waste recycling. These processes are severely limited by material degradation and incompatibilities from complicated wate streams. New and emerging recycling technologies need further development to be used at scale.[9, 10] There are three key instruments of change required to incentivise the accelerated development of recycling technologies: 1) Extended producer responsibility to ensure producers are physically and/or financially responsible for the plastic they produce; 2) Financially incentivising research into new recycling technologies through tax credits; and 3) Promoting the use of recycled plastic as a feedstock through coordinated regulatory policy.[4] This is essential to develop a truly circular

plastic economy and to move away from the well-established linear economy which is resulting in enormous levels of pollution (**Figure 1.1**).[11]

Physical plastic waste is not the only form of pollution that must be addressed. In 2015, 1.7 gigatonnes of carbon dioxide-equivalent (Gt-CO_2 equiv.) of greenhouse gas emissions were emitted from polymer production worldwide.[12] Without efforts to apply renewable energy, recycling and demand-management strategies, this is forecasted to rise to 6.5 Gt-CO_2 equiv. by 2050. Managing demand for polymers will be critical to help with decarbonisation but demand will continue to increase. Therefore, the adoption of bio-based and sustainable plastic alternatives is critical.[13] Furthermore, we specifically need new materials that can, not only rival but, outperform the petroleum derived incumbents.[14]

The design and development of new sustainable polymers is central to reducing plastic pollution, reducing emission from their production, and reducing our dependence on fossil-fuel derived monomers. Aliphatic oxygenated polymers have emerged as lead candidate materials. They are most commonly produced from the ring-opening polymerisation (ROP) of lactones or cyclic carbonates and the ring-opening copolymerisation (ROCOP) of epoxides with cyclic anhydrides or CO_2.[15] This offers a large pool of monomers to choose from, many of which can be produced from renewable sources like terpenes, vegetable oils or carbohydrates.[16] Moreover, CO_2 is a cheap, overly-abundant, waste product, which can be directly enchained with an epoxide to produce a polycarbonate.[17]

It is critical that new materials are designed with end-of-life options in mind. These materials must be able to be mechanically recycled, chemically recycled to monomer, and/or degraded on demand.[18, 19] The high concentration of ester and carbonate linkages within oxygenated polymers facilitate their acid or base catalysed hydrolysis into hydroxy acids, alcohols or CO_2. Furthermore, the catalysed depolymerisation of oxygenated polymer to

monomers is proving an increasingly viable route to recycle these renewable materials without sacrificing their mechanical performance.[20]

Despite the attractive monomer scope and multiple end-of-life options, oxygenated polymers exhibit sub-par mechanical properties. Often too brittle, the poor toughness restricts the potential applications for these materials, hindering their mass adoption.[21] It is imperative we design, develop, and produce new sustainable, oxygenated polymers with a holistic approach.[22] Monomer source, thermomechanical properties, end-of-life options must all be considered. We need new sustainable polymers with not only improved material properties but with approaches and strategies to augment, tune, and tailor those properties to given applications.

1.2 Heterocycle Ring-Opening Polymerisation and Heterocycle/Heteroallene Ring-Opening Copolymerisation

Since Wallace Carothers reported the thermally induced ring-opening polymerisation (ROP) of trimethylene carbonate (TMC) in 1932, heterocycle ROP has become of the most powerful tools to produce aliphatic polyesters, polycarbonates, and polyethers from lactones, cyclic carbonates and epoxides, respectively (**Figure 1.2**).[23] As concerns surrounding the finite availability of fossil resources and the environmental longevity of polyolefins have grown, the production of oxygenated polymers from ROP has become increasingly attractive.[24] The majority of commercial polyesters are synthesised by condensation polymerisation. Two key examples are polycarbonate (PC, from bisphenol A) and poly(ethylene terephthalate) (PET). While these are commonly used in packaging and as rigid engineering plastics, their synthesis

lacks control ($Đ_M$ > 2.0), and the removal of small molecule by-products is highly energy intensive.

On the other hand, lactone/cyclic carbonate ROP can produce polymers with high atom efficiency and precise control of the molar mass, end-group fidelity, tacticity and even stereochemistry.[25] Through catalyst and initiator selection, ROP can be employed to deliver liner, star-shaped, branched/graft, and cyclic polymers.[26] Furthermore, a mixed monomer feedstock can be used to produce random, statistical or gradient copolymers and sequential monomer addition can afford (multi-)block copolymers. The ROP of lactide (LA) is used to produce hundreds of thousands of tonnes of corn-derived poly(lactic acid) (PLA) plastic every year.[27] Despite the relatively low glass transition temperature (T_g) of PLA (60 °C), it is already finding growing use as a packaging material and in biomedical products, like stents and sutures.

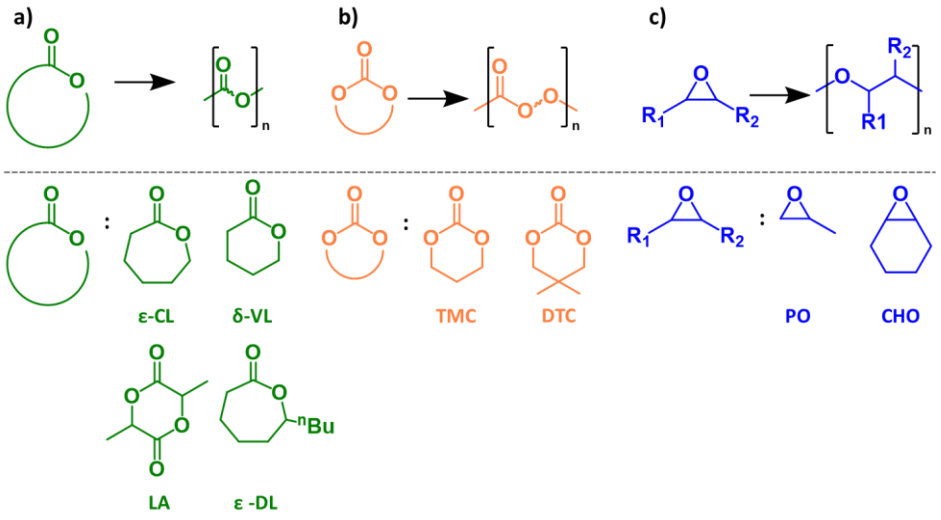

Figure 1.2. General ring-opening polymerisation (ROP) of a) lactones (cyclic esters), b) cyclic carbonates, and c) epoxides with key relevant monomers shown.

Discrete coordination complexes are most often utilised as homogeneous catalysts for ROP for their ease of synthesis, high turn-over frequencies (TOFs), and the ease of which they can be removed from the resulting polymeric materials.[28, 29] Recently, organocatalytic species

have received great attention as metal-free alternatives.[30] These organocatalysts are extremely promising but most are limited by their toxicity and the difficulty in removing them post-polymerisation. Many different lactone/cyclic carbonate ROP processes have been reported exploiting coordination-insertion, cationic, anionic, zwitterionic, and bio-chemical mechanisms. However, common to all, is the thermodynamic/enthalpic driving force of ring-strain release in the cyclic monomer.[31] As a result, the majority of monomers used in ROP are rings of three to eight atoms. The lack of ring strain exhibited in much larger cyclic monomers decreases this enthalpic driving force and the decreasing entropy, which arises from the loss in translational degrees of freedom of the polymer chain, can dominate. Subsequently, larger cyclic monomers are much harder to polymerise, although entropically driven heterocycle ROP is feasible. This need for ring strain limits the monomers available and, therefore, the diversity of polymer and material properties that are readily accessible from ROP.

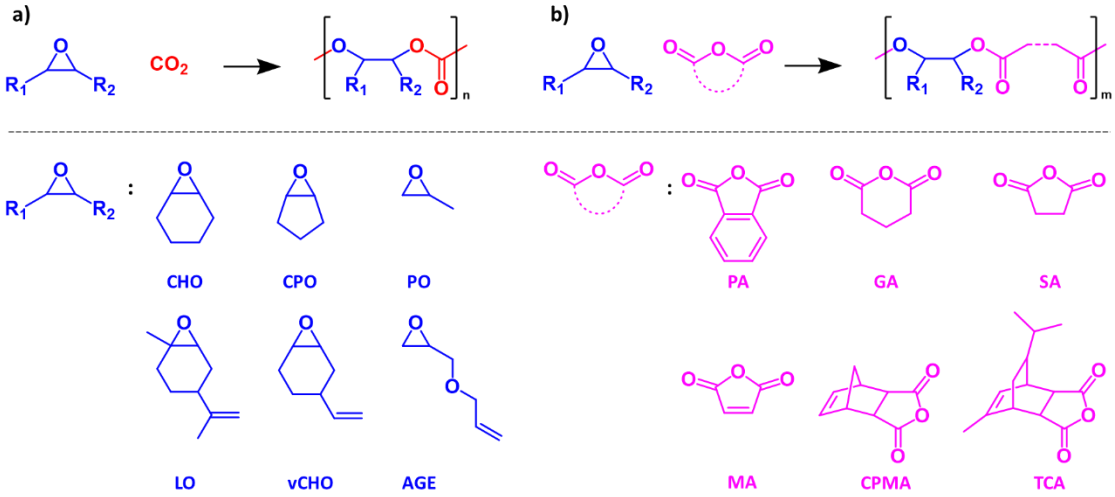

Figure 1.3. General ring-opening copolymerisation (ROCOP) of a) epoxide/CO_2 and b) epoxide/cyclic anhydride with key relevant monomers shown.

The (ROCOP) of epoxides with CO_2 or cyclic anhydrides is an alternative controlled means to produce aliphatic polycarbonates and polyesters respectively.[32] Unlike in lactone/cyclic carbonate ROP, two different co-monomers are enchained in a perfectly

alternating fashion and therefore allows for far greater structural diversity of the resulting polymers (**Figure 1.3**).[33] For example, in the ROCOP of epoxides with anhydrides there are two separate handles to tune thermomechanical properties. By introducing more flexible or rigid monomers the T_g can be decreased or increased respectively. For example, switching from rigid bi-cyclic cyclohexene oxide (CHO) to flexible mono-cyclic propylene oxide (PO) in the ROCOP with CO_2 results in a 90 °C reduction in the T_g.[34]

The best performing catalysts for ROCOP are metal complexes.[33] Specifically, it is now quite well established that heterodinuclear catalysts (those containing two metal centres) provide impressive TOFs, high selectivities, and obviate the need for toxic and heavy cocatalysts.[35] These two metal centres work in a synergistic fashion to afford efficient and effective ROP and ROCOP catalysis.[36] Initiation for both mechanisms begin with a reaction between the pre-catalyst and protic species, deliberately incorporated to control the molar mass of the final polymer or from residual impurities present in the monomers. The resulting metal-alkoxide intermediate then allows for propagation reactions to take place. Monomers are incorporated sequentially during ROCOP either through a) insertion of CO_2 into the alkoxide to form a carbonate intermediate, which goes on to attack and ring-open an epoxide to regenerate the alkoxide or b) the alkoxide attacks the anhydride to form a metal-carboxylate intermediate which ring-opens an epoxide and reform the starting alkoxide. During propagation, chain transfer reactions can occur more rapidly than the propagation reactions themselves. These are reactions in which the catalyst from a growing polymer chain switches between other chains with hydroxy end-groups, resulting in narrow molar masses. Finally, the polymerisation is terminated through the removal of monomer, reduction in temperature or addition of water and/or acids.

This vast monomer scope includes many potentially bio-derived monomers like CHO,[37, 38] limonene oxide (LO),[39] phthalic anhydride (PA),[40] and tricyclic anhydrides (TCA).[41] This wide

range of commercially available monomers allows for the introduction of functional groups which can impart desired material properties or offer downstream post-polymerisation functionalisation sites, allowing for further tuning of material properties.[42] Often bespoke and functionalised monomers must be synthesised to achieve equivalent functionality from lactone/cyclic carbonate ROP. These syntheses are often challenging, multi-step processes which have limited commercial potential.[43, 44] Furthermore, ROCOP allows for the incorporation of aromatic functionality into the polymer backbone which is particularly challenging in ROP.

Control of the molar mass achievable with ROP and ROCOP derives from tuning the ratio of protic species, which act as both initiators and chain transfer agents (CTA), and the loading of monomer in the reaction. As a result, low molar mass (M_n < 10 kg mol^{-1}) viscous liquids are easily accessible. These polyols are commonly used in the synthesis of polyurethanes (PUs) for applications as flexible and rigid foams, elastomers, coatings, and adhesives.[45-50] Conversely, in order to produce high molar mass materials (M_n > 100 kg mol^{-1}), pure monomers are required. Residual protic species like water can ring open lactones, epoxides and cyclic anhydrides to form hydroxy acids, diols and diacids, respectively, which can act as initiators and subsequently reduce the molar mass of the polymer produced. Extensive drying, distillation, and sublimation is often essential to remove these impurities and prepare monomers suitable for the synthesis of high molar mass materials. Due to this synthetic challenge, to date, there have been limited reports of high molar mass oxygenated polymers which can be processed into free-standing films.[51-57] Therefore, we are only in the infancy of understanding their thermomechanical properties and potential applications.

Both lactone/cyclic carbonate ROP and epoxide/CO_2 ROCOP can yield a wide range of different oxygenated and sustainable polymers. The structural diversity achievable results in a range of T_gs for the homopolymer spanning over 200 °C (**Figure 1.4**). We can relate the T_g

of these materials to the flexibility/rigidity of the polymer backbone. Incorporating aliphatic or aromatic rings results in a rigid plastic with elevated an T_g (in excess of 100 °C). On the other hand, polymers with long aliphatic segments within the backbone delivers soft viscoelastic liquids with T_gs below room temperature. While we can easily relate the repeat unit structure to the thermal properties, this is much more complicated with respect to mechanical properties. This is because there are numerous factors which influence the physical behaviour of the materials. These include the molar mass, dispersity, entanglement molar mass (M_e), interchain interactions, physical crosslinking, chain confirmation, and crystallinity. Deconvoluting the factors that determine the mechanical performance of an oxygenated homopolymer is complicated and to date, this has proven to be extremely challenging. This becomes increasingly complex for blends and co-, ter- or block polymer structures, where multiple structures interact on multiple length scales. It will be essential to understand the design principles that govern the production of new high performance oxygenated and sustainable polymeric materials to find alternatives capable of replacing the fossil-derived incumbents.

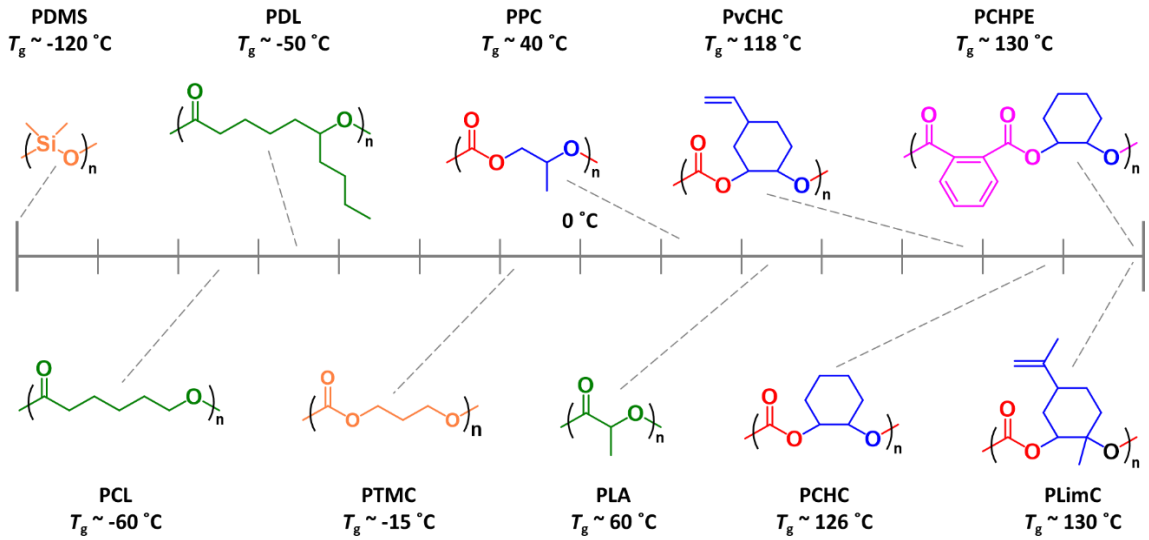

Figure 1.4. Glass transition (T_g) of key oxygenated homopolymers.

1.3 CO_2-Derived Polycarbonates

CO_2-derived polycarbonates, produced from CO_2/epoxide ROCOP, are an attractive class of materials and key in reducing the 1.7 Gt-CO_2 equiv. emitted every year.[10, 12] CO_2 is a cheap and abundant waste feedstock suitable for use in existing manufacturing infrastructure.[58] When directly used in the ROCOP with epoxides, CO_2 allows for a threefold reduction in greenhouse gas emissions relative to the corresponding polyether: for every molecule of CO_2 polymerised, two more are saved through the replacement of epoxide.[59-61]

Table 1.1: Uniaxial Tensile Properties of CO_2-Derived Polycarbonate Homopolymers

Polymer	[a]M_n [$Đ_M$]	[b]T_g (°C)	[c]σ (MPa)	[d]ε_b (%)	[e]E_y (GPa)	[f]U_T (MJ m^{-3})
PCHC[57]	121.6 [1.09]	126	40.0 ± 1.8	3.3 ± 0.3	2.16 ± 0.06	0.9 ± 0.1
PvCHC[57]	124.5 [1.06]	118	52.2 ± 1.0	4.9 ± 1.3	1.33 ± 0.11	1.6 ± 0.6
PCPC[57]	114.4 [1.06]	85	58.5 ± 1.7	7.1 ± 1.9	1.70 ± 0.09	2.9 ± 1.1
PeCHC[57]	72.6 [1.34]	105	46.7 ± 1.3	18.7 ± 4.2	1.31 ± 0.05	7.0 ± 1.5
PLimC[52]	53.4 [1.10]	130	55.0	15	0.95	-

[a]Determined by SEC. [b]Determined by DSC. [c]Ultimate tensile strength. [d]Strain at break. [e]Young's modulus. [f]Tensile toughness.

While low molar mass CO_2-derived polyols are increasingly employed in the synthesis of PUs, their potential as high molar mass materials remains unrealised (*vide supra*). Furthermore, while there are a handful of reports of high molar mass polycarbonates synthesised directly from CO_2, few authors have explored their thermomechanical properties. Rosetto *et al.* reported the synthesis of a series of polycarbonate homopolymers with molar masses, exceeding 100 kg mol^{-1}.[57] These materials were poly(cyclohexene carbonate) (PCHC),

poly(vinyl cyclohexene carbonate) (PvCHC), poly(cyclopentene carbonate) (PCPC), and an ethyl-substituted PeCHC, derived from the hydrogenation of PvCHC (**Table 1.1**).

Commonly reported PCHC displayed a high T_g but was extremely brittle with an elongation at break (ε) of 3%. Rheological analysis of PCHC elucidated the molar mass between macromolecular entanglements was 56 kg mol^{-1}. Therefore, it is unlikely that the material achieves the critical molar mass (M_c), where increasing molar mass does not improve mechanical performance. Typically M_c > 3-6 M_e.[62] This lack of entanglements results in a weak polymer network for the thermoplastic which severely limits the ability to process PCHC and subsequently, possible applications. Ultra-high molar masses (M_n >> 300 kg mol^{-1}) would be required to produce critically entangled PCHC. However, processing will likely be extremely challenging as a result of the high viscosity at elevated high molar mass.

Conversely, PCPC was found to have an M_e an order of magnitude lower than PCHC at 4 kg mol^{-1}. Consequently, at M_n ~ 100 kg mol^{-1} it is sufficiently entangled and the materials exhibits high tensile strengths (σ = 59 MPa) and a moderate elongation at break, double that of PCHC (7%). Its mechanical properties are similar to polystyrene and, with a higher T_g, its thermal properties are superior to poly(L-lactide) (PLLA).[63] Despite these impressive thermomechanical properties, PCPC exhibits a high but slightly reduced T_g of 85 °C, relative to 126 °C for PCHC.

PvCHC displayed a moderate improved tensile strength (52 MPa) and elongation at break compared to PCHC (5%). This improvement is attributed to the increased degrees of freedom provided by the pendent vinyl group. This effect is increased upon hydrogenation of the vinyl substituent. The ethyl substituent in PeCHC results in a slight reduction in tensile strength (47 MPa) but a much-improved strain at break (19%). As a result, the tensile toughness for PeCHC is over 200% greater than PvCHC, 100% greater than PCPC, and over 600% than PCHC.

Greiner and co-workers reported the synthesis of poly(limonene carbonate) (PLimC) as thermally resistant, hard and transparent plastic.[52] While they report the synthesis of high molar mass PLimC (M_n > 100 kg mol^{-1}) they only report mechanical testing on a lower mass sample (M_n > 53 kg mol^{-1}). Its M_e wasn't measured but might be quite high on the basis of the structural similarity to PCHC and PvCHC. PLimC is a particularly attractive bio-based polycarbonate as limonene oxide (LO) can be produced from naturally occurring limonene.[64] Limonene exists as a mixture of *cis* and *trans* isomers, in a 6:4 ratio, which can be extracted from citrus peel. PLimC has a high tensile strength (55 MPa) and relative to the other high molar mass CO_2-dervied polycarbonates discussed, has a high elongation at break (15%). While LO is an attractive monomer, it is challenging to polymerise. Zinc-β-diiminate are able to catalyse the ROCOP of LO with CO_2 however they can only polymerise the *trans* isomer.[65] This results in the 40% *cis* isomer going to waste. Kleij and co-workers reported an Al-(amine)tris(phenolate) catalysts which can polymerise both isomers but the molar mass achievable is very low due to the use of ionic cocatalysts.[66, 67]

Recent developments have revealed the potential for polycarbonates, prepared from the ROCOP of CO_2 and epoxides to be chemically recycled back to the constituent monomers.[57, 68-74] This depolymerisation can often be catalysed by the same species used for the polymerisation. Reforming monomer offers an attractive and alternative end-of-life option. After a material has been mechanically recycled to the point that the thermomechanical performance starts to deteriorate, the material can be transformed back to the constituent monomers and repolymerised to produce a virgin material. This further highlights the potential role CO_2-derived polycarbonates are able to play in a fully circular polymer economy.

1.4 Switch Polymerisation Catalysis

In attempt to mimic the complexity of natural biopolymers, various strategies have been developed to produce well-defined sequence controlled copolymers.[75] In 2014, Williams and co-workers reported a dinuclear, dizinc catalyst (**1a**, **Figure 1.5**), already known to be active for the ring-opening copolymerization (ROCOP) of epoxides and CO_2/cyclic anhydrides, was also active for the ROP of lactones.[76]

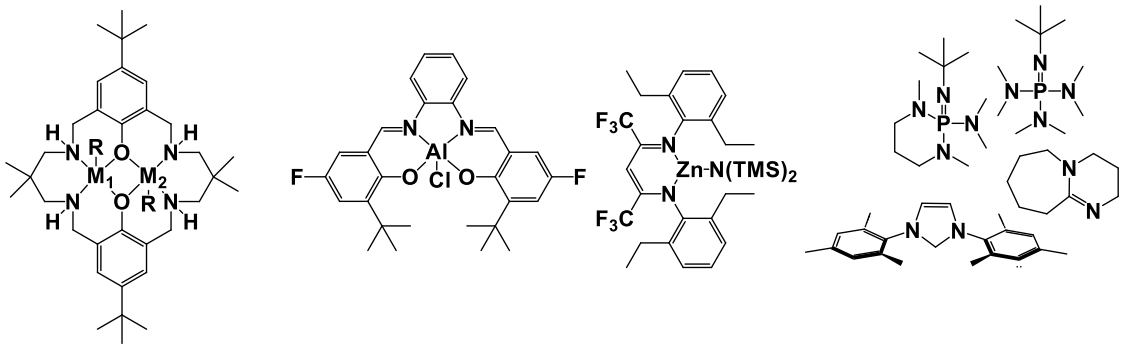

Figure 1.5. Examples of switch polymerisation catalysts.

The two mechanisms are bridged by a common metal-alkoxide intermediate and switching between the two mechanisms is possible through control over the chain end-group chemistry (**Figure 1.6**). The fast insertion of CO_2/cyclic anhydride (zeroth rate order) into the metal-alkoxide initiator forms a thermodynamically stable metal-carbonate/carboxylate, which must react with an epoxide to reform the bridging metal-alkoxide species. Therefore, lactone ROP only occurs when CO_2 or cyclic anhydride is fully consumed or when it is removed. This allows for a one-pot synthesis of (multi-)block sequence controlled copolymers through the triggering of switches. By combining lactone/cyclic carbonate ROP with epoxide/anhydride or CO_2 ROCOP, copolymers with both polyester and polycarbonate blocks were synthesised.[77] The large monomer scope containing lactones, epoxides, anhydrides, and heteroallenes creates

opportunities to tune structure and therefore properties, through the precise addition of specific functionalities.

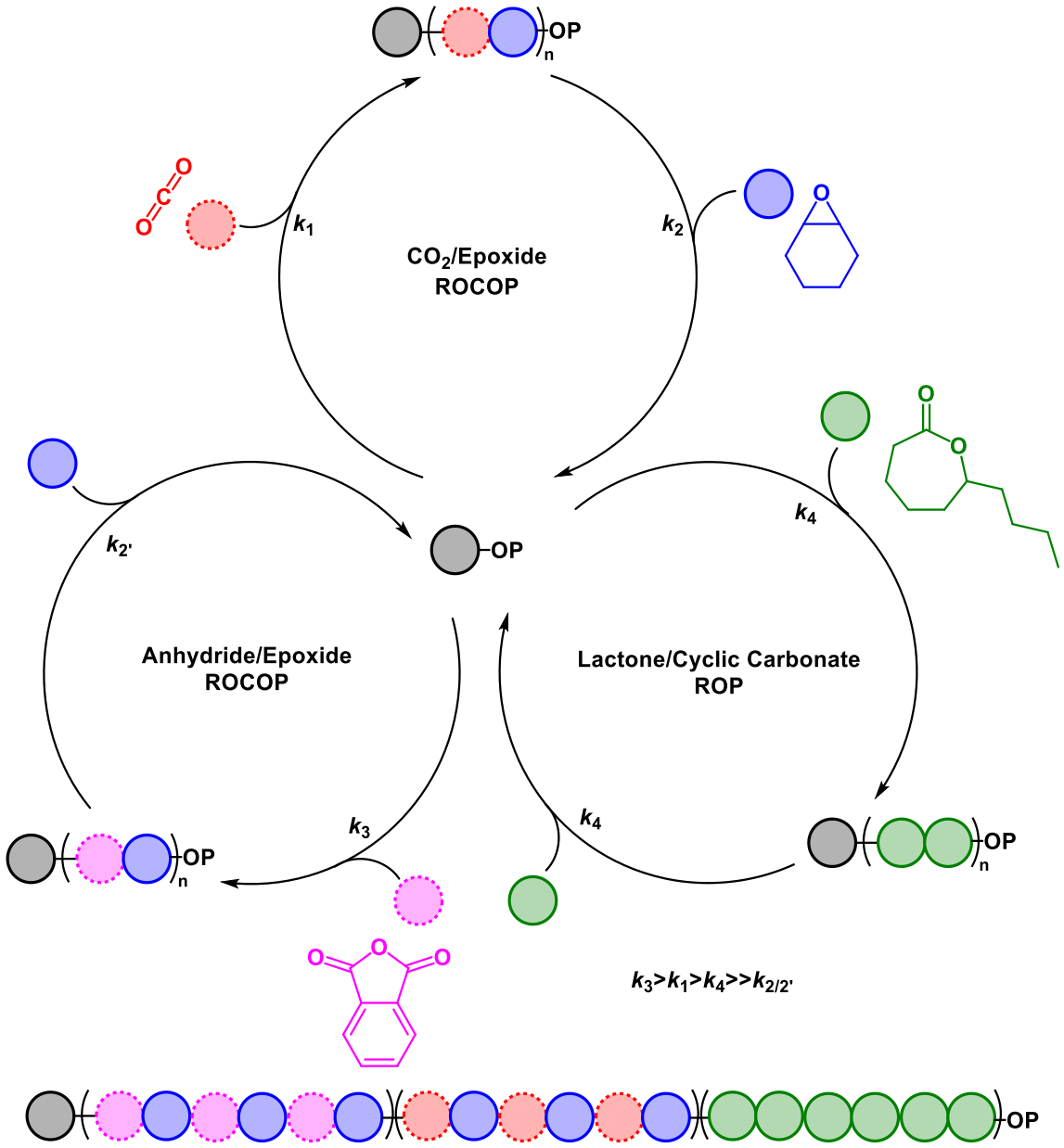

Figure 1.6. Possible switch catalysis polymerisations bridged by metal alkoxide intermediate.

Many other groups have since investigated switch catalysis and many other catalysts have been shown follow the same rules for switch polymerization.[78-80] These include, a dimagnesium (**1b**) species,[81] a heterodinuclear zinc/magnesium species (**1c**) which displays

superior activity to the homodinuclear dizinc species,[82, 83] an aluminium salphen catalyst shown to deliver copolymers with up to 27 blocks (**2**),[84] a β-diimine zinc complex also capable of producing statistical copolymers at low CO_2 pressures (**3**),[85] and a range of organic species (**4**).[86]

Since its discovery, there have been quite a few developments and advances in the use of switch polymerisation catalysis to expand the oxygenated block copolymer structures accessible. Low molar mass triblock copolymer polyols were produced from a mixed monomer feedstock of CHO, CO_2, and ε-caprolactone (ε-CL) with cyclohexane diol (CHD) acting as the CTA.[87] Due to the rapid insertion of CO_2 into the metal-alkoxide propagating species, a hydroxy telechelic block of PCHC was produced. By removing the CO_2 from the reaction mixture, the polymerisation mechanism switched to the ROP of ε-CL and the PCHC acted as a macroinitiator with polycaprolactone (PCL) forming the outer blocks. It was later shown that an analogous all polyester copolymer could be produced with the use of phthalic anhydride (PA), CHO, and ε-DL.[88] The central semi-aromatic block, poly(cyclohexene phthalate) (PCHPE), was formed first, due to the rapid anhydride insertion. Once the PA was completely consumed, the polydecalactone (PDL) blocks were installed to produce the low molar mass triblock copolymer.

Further studies revealed that a four-component monomer mixture of CHO, PA, ε-CL, and CO_2 could be employed to synthesise complex block copolymer structures from a single catalyst.[89] This study revealed the differences in monomer reactivity and shed light on how to produce oxygenated polymers with predictable composition and block sequences. This understanding was subsequently exploited to yield pentablock copolymers by combing lactone ROP, epoxide/CO_2 ROCOP, and epoxide/anhydride ROCOP in a one-pot synthesis.[90, 91] Switch polymerisation catalysis has also been used with a mixture of L-lactide-*O*-carboxyanhydride (OCA) and CHO in a closed one-pot reaction to produce poly(L-lactide-*b*-

cyclohexene carbonate).[92] The CO_2 liberated during the ROP of the OCA is recycled in the ROCOP with CHO, with up to 91% atom efficiency.

It is critical to consider how to characterise the block copolymers produced through switch polymerisation catalysis. This is essential to confirm the formation of a block copolymer structure and to understand the composition of the blocks within the chain.[93] There are several experimental methods to aid in this characterisation: 1) An increase in molar mass by size-exclusion chromatography (SEC) after switching polymerisation mechanism; 2) End-group analysis with the addition of 2-chloro-4,4,5,5-tetramethyl dioxaphospholane (**Figure 1.7**) followed by $^{31}P\{^{1}H\}$ NMR to determine the environment/block at the hydroxyl chain ends; [94] 3) A single diffusion coefficient would be observed by DOSY NMR for a block copolymer as opposed to two or more for a physical blend of homopolymers; 4) The presence of ^{1}H NMR signals corresponding to the repeat units immediately adjacent to neighbouring blocks, junction units, further confirm a block architecture; 5) $^{13}C\{^{1}H\}$ NMR can reveal the presence of signals corresponding to a random copolymer formed as a result of transesterification block scrambling; 6) A distinct change in thermomechanical properties (T_g, complex viscosity (η), tensile mechanical properties) should be observed for a block copolymer when compared to the constituent homopolymers and; 7) Repeated precipitations and washings shouldn't result in a change in relative ratios of the blocks however this ratio would result in a change for mixture of homopolymers as they are physically separated.

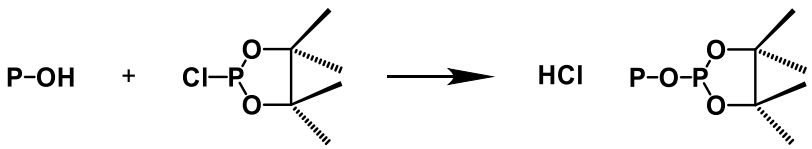

Figure 1.7. Hydroxyl end-capping with of 2-chloro-4,4,5,5-tetramethyl dioxaphospholane for end-group analysis.[94]

The majority of early studies into switch polymerisation catalysis produced only low molar mass block copolymers and subsequently, the materials are viscous liquids and no mechanical testing on the materials was conducted. Higher molar masses (M_n > 50 kg mol^{-1}) would usually be required to produce free standing films. One option is to use higher monomer loadings in the polymer synthesis however, this would require a low loading of CTA and minimal protic impurities in the monomers. Another option is to carry out an isocyanate coupling with the low M_n polyols. The chain extension of the triblock copolymers results in a high molar mass multi-block copolymer. The isocyanate coupling of a PDL-PCHPE-PDL triblock copolymer resulted in a range of tough elastomers and self-healing plastics depending on the content (wt%) of PCHPE within the material.[95]

1.5 Thermoplastic Elastomers (TPEs)

Thermoplastic elastomers (TPEs) are reprocessable alternatives to vulcanized rubber since they feature physical, rather than chemical, cross-linking, hence enabling efficient material recycling. They are industrially important in automotives (tubing, tyres), electronics (cables), apparel (shoe soles) and speciality products (sports equipment and medical devices).[96] Petrochemical TPEs are derived from a range of olefins including styrene, butadiene, ethene, octene, propene or acrylates.[97] Block polymer TPEs feature phase-separated ABA structures, where the A domains comprise of rigid or glassy polymer blocks (T_g or T_m > room temperature) and B domains, the majority phase, are elastomers (T_g and T_m < room temperature). Physical crosslinks between the hard domains in combination with the flexible and extendible nature of the soft domains yields a material exhibiting both high ultimate tensile strength (σ) and strain (ε_b) at break.[98, 99] Commercial TPEs typically exhibit ultimate tensile

strengths of 20-40 MPa, Young's moduli of >6 MPa, and with an elongations at break of >650%.[98]

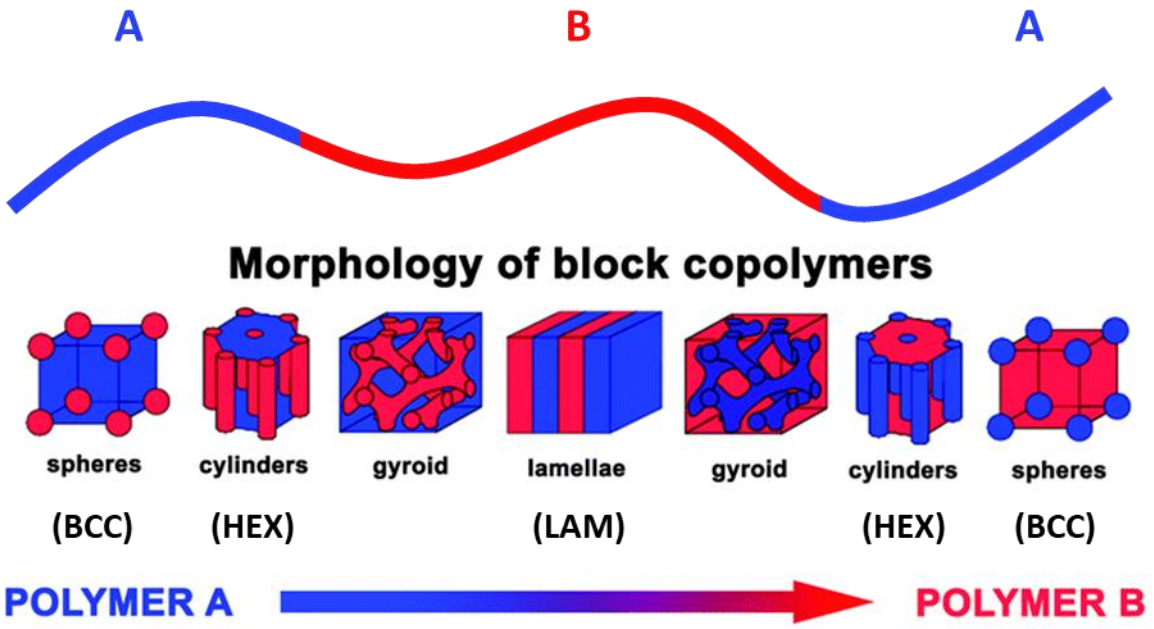

Figure 1.8. Comparison of morphological arrangements of immiscible A and B blocks in an ABA triblock copolymer. Reproduced and adapted from Ref. 100 with permission from the Royal Society of Chemistry.[100]

The desirable properties of TPEs arise from the incompatibility of the A and B blocks.[101] Unfavourable block interactions drive the phase separation of the copolymers in the solid state. This leads to the polymers self-organising into nanosized regions of the two pure domains and the observation of two T_gs, matching that of the T_g the pure constituent homopolymer. This typically results in fractions of the glassy block within an elastomeric matrix. The precise morphology can be body-centred cubic (BCC) spheres, hexagonally-packed cylinders (HEX), gyroid or lamellae (**Figure 1.8**) and are characterised by indexing the small-angle X-ray scattering pattern. The morphology adopted, and therefore the mechanical performance of the material, is determined by (i) the degree of polymerization N, (ii) the volume fraction (composition) of the hard block f_{hard}, (iii) the polymer architecture, and (iv) the Flory-Huggins

interaction parameter χ.[102, 103] Consequently, when designing a new TPE, the macroscopic properties of the material can be tuned by altering the molar mass of the polymer and the chemical composition of the A and B blocks, where the weight% (wt%) of the blocks can be used as a proxy for the volume fraction of the respective block. Block polymers with the best elastomeric performance typically feature ~20–30 wt% A-block compositions and have overall M_n > 60 kg mol^{-1}.[104] The resulting microphase-separated morphology for elastomers is typically BCC or HEX.[96]

The syntheses of the ABA block polyolefins requires careful control over monomer addition timing, macro-monomer purification and, in some case, very low temperatures with the associated energy inputs.[96] Therefore, sustainable materials need straight-forward polymer syntheses, ideally operating with a single catalyst, and in one reactor to compete with existing procedures.

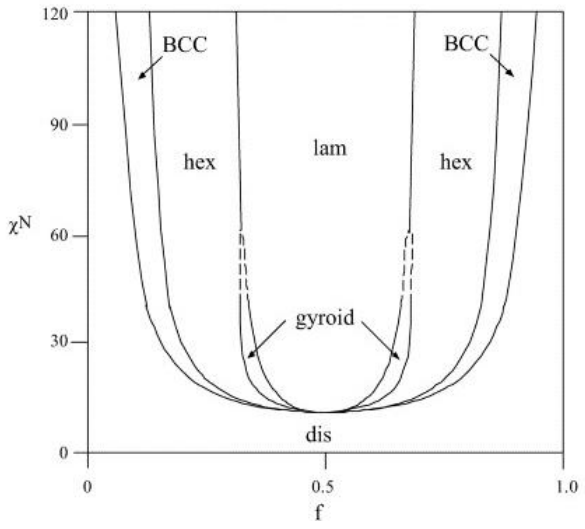

Figure 1.9. Phase diagram for conformationally symmetrical diblock or triblock copolymer. Reproduced and adapted from Ref. 105 with permission from Elsevier.[105]

Sustainable oxygenated homopolymers are often extremely brittle or exist as viscous liquids under ambient conditions. Not only does this limit their potential applications but

consequently, they fail to match the property profile of incumbent petroleum derived materials. Utilising a block polymer design can significantly enhance the mechanical properties of bio-derived polymers. Previously reported oxygenated ABA triblock copolymers (**Figure 1.10**) are subsequently discussed and their mechanical performance compared (**Figure 1.11**). Hillmyer and co-workers pioneered the development of sustainable oxygenated TPEs.[106] Hillmyer's work has explored the synthesis of ABA copolymers through the ring-opening polymerization (ROP) of two or more bio-derived lactone monomers to produce TPEs with varying central mid-blocks and PLA outer blocks.

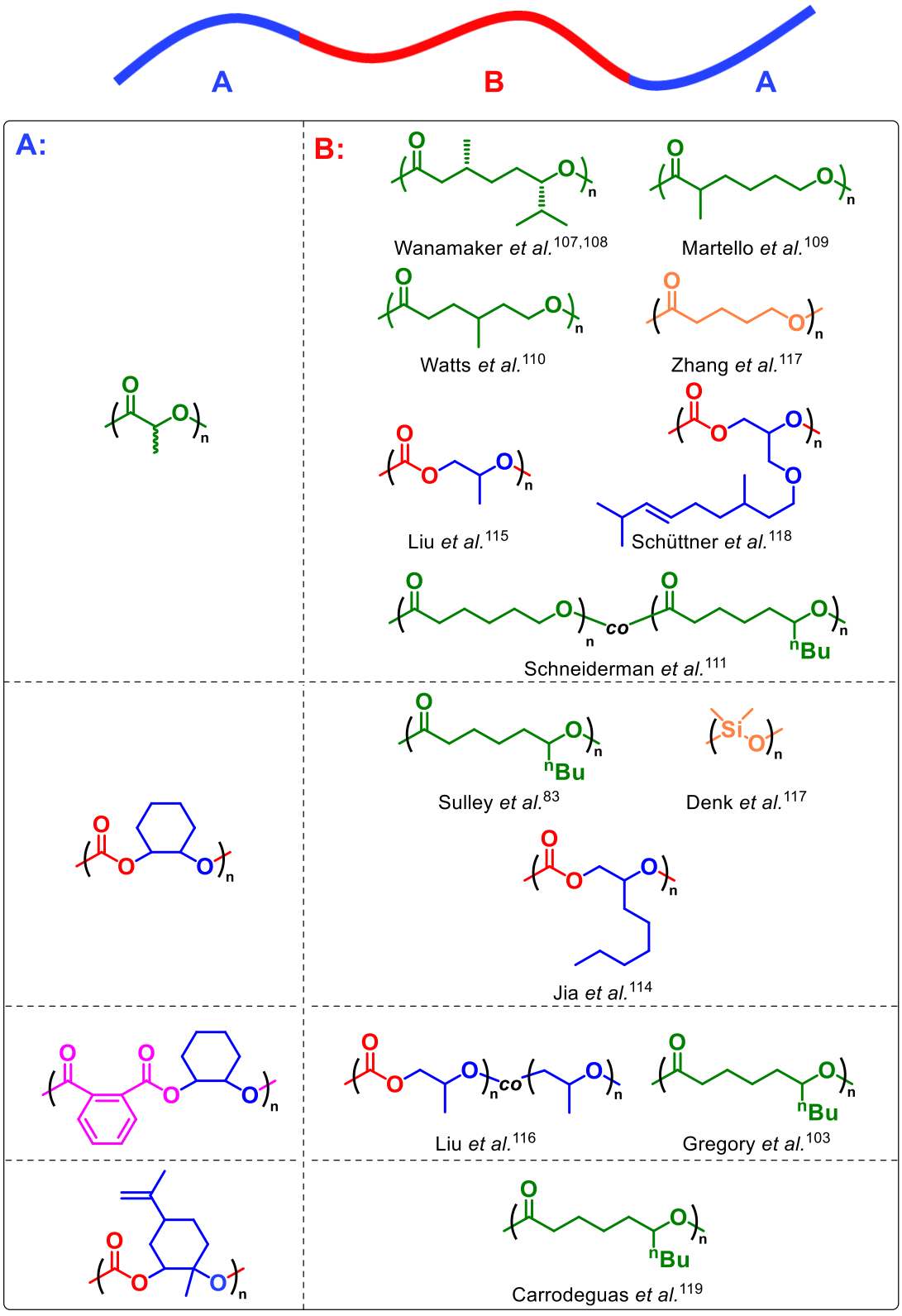

Figure 1.10. Previously reported block combinations for the synthesis of oxygenated ABA triblock copolymer TPEs and plastics.

Wanamaker *et al.* reported poly(lactide-*b*-menthide-*b*-lactide) (PLA-PM-PLA), where the lactide monomers used for the end blocks are derived from the natural carbohydrates found in corn and the menthide soft block is derived from menthol, extracted from mint.[107] The block copolymer was synthesised through the ROP of menthide, using a $ZnEt_2$ catalyst, to produce α,ω-hydroxy telechelic polymenthide (B). Upon addition of lactide, and a $AlEt_3$ catalyst, the polylactide end blocks (A) were synthesised to produce the final ABA copolymer. The resulting ABA triblock copolymers behaved as elastomers, with a moderate ultimate tensile strength and Young's modulus of 1.7 MPa and 1.4 MPa respectively, and with a high elongation at break of 960%. The relatively low T_g of the atactic PLA (60 °C) outer blocks limits the operating temperature window (OTW) of these TPEs (-20 °C to 60 °C).

Replacing the outer blocks with semi-crystalline PLLA facilitates enhanced physical cross-linking over the fully amorphous stereo-irregular counterparts.[108] The introduction of isotactic PLA improves the mechanical properties of the resulting elastomers, with an ultimate tensile strength of 20 MPa, Young's modulus of 25 MPa, and an elongation at break of 750%. Blends of the ABA block copolymers with PLLA and PDLA outer blocks were produced to form stereocomplexes. This further enhanced the physical crosslinking in the semi-crystalline domains and resulted in ultimate tensile strengths of 21 MPa, Young's modulus of 37 MPa and elongations at break of 1000%. Not only does the use of stereoregular PLA improve the mechanical properties of the TPE but it widens the OTW. The T_m of the outer blocks was observed at ~150 °C, resulting in a 90 °C increase in upper operating temperature. Moreover, the T_m increased further to over 200 °C upon formation of the stereocomplexes.

An analogous synthetic procedure was later employed to produce ABA triblock copolymer TPEs, using a $Sn(Oct)_2$ catalyst, with varying central block compositions. Martello *et al.* used 6-methyl-ε-caprolactone and Watts *et al.* used γ-methyl-ε-caprolactone, to form TPEs with PLA outer blocks flanking poly(6-methyl-ε-caprolactone) and poly(γ-methyl-ε-caprolactone),

respectively.[109, 110] The poly(6-methyl-ε-caprolactone) containing ABA triblock copolymer exhibited good mechanical properties: an ultimate tensile strength of 4.2 MPa, Young's modulus of 31 MPa and an elongation at break of 1360%. Poly(γ-methyl-ε-caprolactone) was found to have a low M_e of 2.9 kg mol^{-1} and subsequently produced tough TPEs when used in an ABA triblock copolymer, ultimate tensile strength of 24 MPa, Young's modulus of 4.8 MPa, and an elongation at break of 1029%.

Schneiderman *et al.* went on to study the use of poly(ε-caprolactone-*co*-ε-decalactone) as a central block with PLA outer blocks.[111] The incorporation of poly(ε-decalactone) supressed the crystallinity of poly(ε-caprolactone) and resulted in a low T_g miscible block. The copolymer mid-block was used to produce TPEs with an ultimate tensile strength of 18 MPa, Young's modulus of 3.5 MPa, and an elongation at break of 1200%. The improvement in mechanical properties, relative to the purely PDL midblock TPE, is attributed to the reduced entanglement molar mass of the central block.

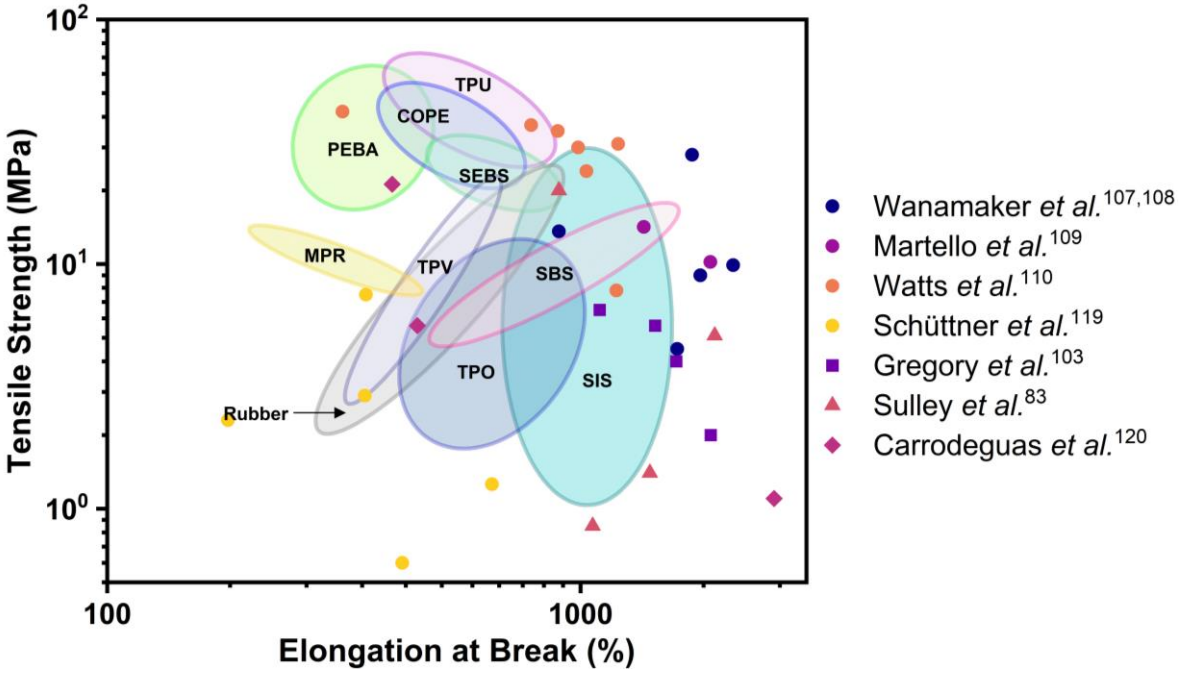

Figure 1.11. Ashby plot of oxygenated ABA triblock copolymers compared to incumbent petrochemical-derived TPEs.

PDL and PLA were employed in the synthesis of ABA triblock copolymer which were chain extended by Hillmyer in an isocyanate coupling to produce higher order multiblock copolymers.[112] These materials were injection moulded and displayed superior mechanical properties than when compression moulded. This improvement is attributed to sheer-induced domain alignment. The best performing specimens displayed an ultimate tensile strength of 6.7 MPa, a Young's modulus of 3.4 MPa, and a strain at break of 1020%.

Feng and co-workers have synthesised a range of CO_2-derived polycarbonate ABA triblock copolymer plastics, using a triethyl borate catalyst. Jia *et al.* reported an all polycarbonate ABA triblock copolymer featuring a poly(octene carbonate) central block with PCHC outer blocks, which resulted in elastomers with an ultimate tensile strength of up to 3.2 MPa, a Young's modulus of 2.5 MPa, and an elongation at break of 454%.[113] In related work, Feng reported the synthesis of ABA triblock copolymers featuring a poly(propylene carbonate-*co*-propylene oxide) central block with flanking poly(*N*-tosyl propylene urethane) blocks to produce toughened plastics which display superior mechanical properties to polyethylenes. The best performing triblock copolymer exhibited an ultimate tensile strength of 29.2 MPa, Young's modulus of 1.3 GPa, and an elongation at break of 476%.

Liu *et al.* proceeded to improve the mechanical properties through the synthesis of a series of triblock copolymers with stereoregular PLA A blocks with polycarbonate B blocks.[114] A plethora of polycarbonate central blocks were explored, with the use of ethylene oxide, propylene oxide, butylene oxide, and octene oxide all employed. The best performing plastic featured a poly(propylene carbonate) mid-block with an ultimate tensile strength of 32.6 MPa, Young's modulus of 1.2 GPa, and an elongation at break of 654%. Finally, Lui *et al.* also reported the synthesis of a series of heat-resistant thermoplastics through the formation of a poly(cyclohexene phthalate-*b*-propylene carbonate-*ran*-ether-*b*-cyclohexene phthalate) triblock

copolymer.[115] An ultimate tensile strength of 25.7 MPa, Young's modulus of 38.0 MPa and an elongation at break of 835% was determined for the linear triblock copolymer produced.

Zhang *et al.* synthesised fully degradable TPEs composed of a poly(1,3-trimethylene carbonate) (PTMC) central block with semi-crystalline PLA outer blocks.[116] A range of elastomers and plastics were produced with varying PLA contents however, the inconsistent processing conditions and mechanical testing procedures convolute evaluation of the performance of these triblock copolymers. Denk *et al.* reported ABA triblock copolymers where PCHC and poly(dimethyl siloxane) (PDMS) are used as the A and B blocks respectively.[117] The high polycarbonate content across the series of materials resulted in a range of plastics with mechanical properties superior to PCHC. The toughest plastic exhibited an ultimate tensile strength of 27.9 MPa, a Young's modulus of 1.7 GPa, and an elongation at break of 18%.

Schüttner *et al.* reported the synthesis of TPEs with a poly(citronellyl glycidyl ether carbonate) central block and PLA outer blocks.[118] This is a rare example of a low T_g central block formed through the ROCOP of CO_2 and a bio-derived epoxide. The resulting soft elastomers exhibited a maximum tensile strength of 2.9 MPa, Young's moduli ranging from 0.15 to 1 MPa and elongations at break up to 600%.

While the PLA containing TPEs discussed display good mechanical properties, they require challenging processing conditions as a result of the semi-crystalline outer blocks regularly used. Furthermore, the scope of potential monomers which can be utilised from ROP alone is narrow. Switchable catalysis allows for the coupling of epoxide/CO_2 ring-opening copolymerization (ROCOP) with cyclic ester ring-opening polymerization (ROP), using a single catalyst and reactor process.[77] Williams and co-workers used a [Zn(II)Mg(II)] heterodinuclear metal catalyst to produce high molar mass ABA triblock copolymers,

comprising CO_2-polycarbonate PCHC (A-blocks) and castor oil-derived PDL (B-block).[83] The catalysis was well-controlled and as the CO_2 content was increased, the polymer properties varied from adhesives, to low-strength elastomers, to toughened plastics. The best performing elastomer contained 26 wt% PCHC however, was very weak relative to commercial styrenic TPEs, exhibiting an ultimate tensile strength of 1.4 MPa, Young's modulus of 3.9 MPa, and elongation at break of 1400%.

Williams and co-workers explored the synthesis of TPEs with alternative outer blocks, while retaining the attractive, fully amorphous, low T_g, central PDL block. Switching from PCHC to PLimC outer blocks yielded a weakened material, with the best elastomer displaying an ultimate tensile strength of 1.1 MPa, Young's modulus of 2.0 MPa, and an elongation at break of 2563%.[119] The ROCOP of CHO with PA is an effective means to produce semi-aromatic, amorphous, outer blocks in a PDL containing TPE.[104] The best performing elastomer of these all polyester ABA triblock copolymers displayed an ultimate tensile strength of 6.5 MPa, Young's modulus of 5.0 MPa, and an elongation at break of 6.5%.

The oxygenated triblock copolymers discussed are all promising candidates to replace incumbent, petroleum derived, plastics and thermoplastic elastomers. While the best performing materials possess mechanical properties comparable to some of the commercial petrochemical products, they fail to offer property improvements (**Figure 1.11**). Sustainable alternative materials should not only match the property profile of current petrochemical-derived polymers but exceed them in order to enable their widespread adoption. Furthermore, it is imperative to design materials where the thermomechanical properties can be simply tuned without complete material re-design and re-optimisation. The formation of polymer networks is proving to be an attractive means to strengthen, toughen and tune the thermomechanical properties of polymeric materials and, in some cases, retaining the potential for mechanical recycling.[120]

1.6 Polymer Networks

The covalent cross-linking of polymer chains can transform individual macromolecules into a single molecule with an effectively infinite molar mass.[121] These cross-links restrict the segmental motion of chains and subsequently the flow of a, otherwise, viscous liquid to produce a solid material. Strong covalent cross-linking results in a thermoset, a material which is incapable of undergoing thermal reprocessing. A material behaves as an elastomer when the polymer chains cross-linked have a T_g below room temperature, for example, natural rubber. A T_g greater than room temperature typically gives rise to a rigid solid, for example, epoxy structural adhesives. While these materials are extremely useful in a wide array of applications, the inability to mechanically recycle them limits their end-of-life options.

Transient, reversible, and dynamic cross-linking is widely employed in nature to bestow soft materials with impressive mechanical properties. These interactions can reinforce interchain interactions in plastics and in the hard domains of TPEs to strengthen and toughen the bulk mechanical properties. Furthermore, these interactions can offer equivalent improvements in mechanical performance as covalent cross-linking, without sacrificing the ability to reprocess and recycle. These non-covalent interactions can be classified into three categories: strong physical cross-linking, weak physical cross-linking, and dynamic covalent cross-linking (**Figure 1.12**).

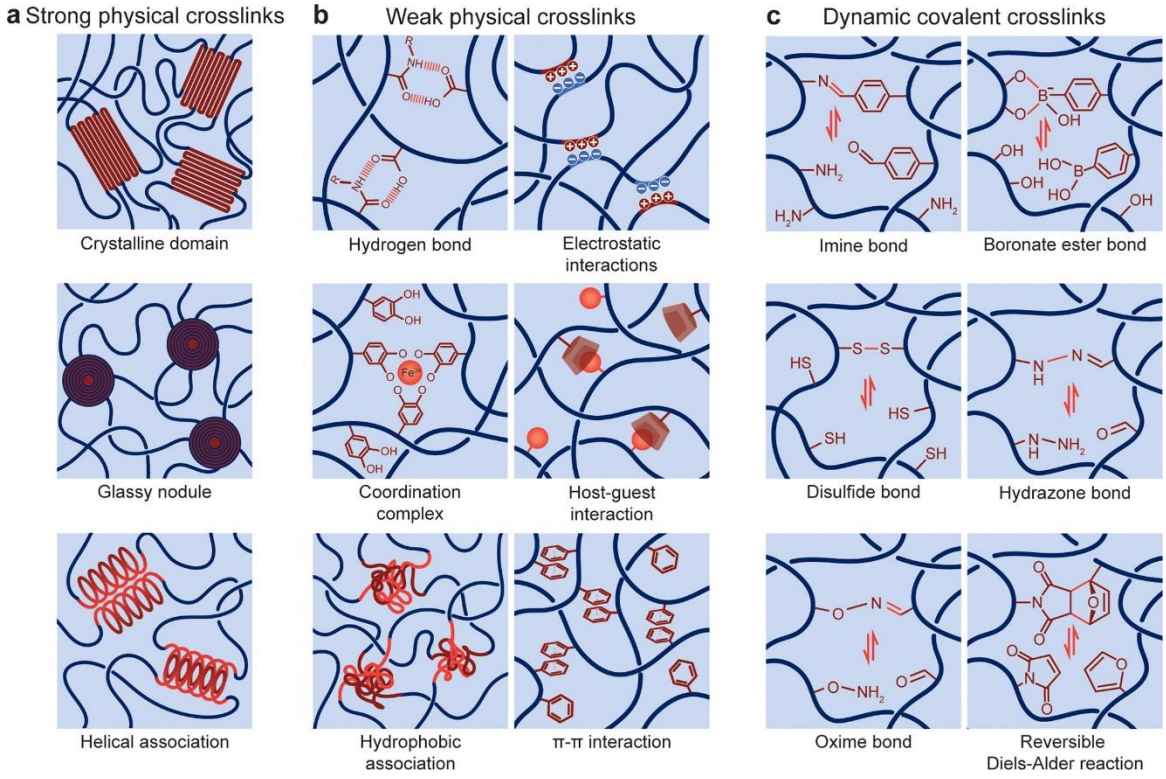

Figure 1.12. Schematic representation of non-covalent macromolecular networking interactions. Reproduced from Ref. 120 with permission from the American Chemical Society.[120]

As previously discussed, introducing crystalline domains into a material, such as a TPE, is an extremely effective means to incorporate strong physical cross-linking.[108] These intrinsically high-energy phases reduce the likelihood of chain pull-out from a domain, reinforcing and strengthening the material. The introduction of high T_g blocks and, therefore, physical cross-linking from glassy, domains can also act to reinforce inter-chain interactions.[83] The advantage of glassy, as opposed to crystalline, domains is the simplification of processing conditions. Semi-crystalline regions require controlled heating and cooling to produce a constant degree of crystallinity and reproducible mechanical properties. Furthermore, similar strong physical cross-linking can arise from the packing of helical polymers, such as collagen in nature, to form nanofibers.[122]

Weaker physical interactions are capable of forming cross-linked materials, however, the relatively low strength of these interactions can give rise to transient and reversible interactions. These interactions can arise from intra-molecular interactions such as hydrogen bonding, electrostatic interactions, and π-π stacking. Weak physical cross-linking can also arise from supramolecular interactions, such as the association of hydrophobic domains in microphase separated hydrogels or host-guest interactions. Metal-ligand interactions are commonly employed by living organisms to form coordination complexes capable of reinforcing a polymer matrix.[123] These are a powerful means to control and tune the resulting mechanical properties. The control over the metal and the ligand used facilitates the control over both the cross-link strength and the timescale of that interaction.[124]

Dynamic covalent cross-linking can be introduced through the inclusion of reactive moieties along the polymer chain which can reversibly associate and dissociate during high temperature processing. These functionalities include: imine bonds, boronate ester bonds, disulfide bonds, hydrazone bonds, oxime bonds, and reversible Diels-Alder reactions. Leibler and co-workers first reported the synthesis of these covalent adaptable networks (CANs) or vitrimers in 2011, exploiting the transesterification of hydroxy-ester networks.[125] Since then, the development of vitrimers has flourished to provide an array of new materials.[126] While this new class of materials show great promise, they are typically hindered by their intense and inherent colour, esoteric chemistries, tendency to creep, and by a need for an associative exchange mechanism to maintain properties.

To date, there have been only a few examples of the use of dynamic covalent or strong and weak cross-linking to toughen bio-renewable and oxygenated TPEs. Vidal *et al.* reported the synthesis of high T_g boron-containing polyesters through the ROCOP of a pinacol boronic ester-phthalic anhydride with various epoxides.[127] Deprotection to form pendent boronic acids followed by dehydration results dynamic covalent cross-linking through the formation of

boroxine rings. These boron-containing polyester are utilised as the A-block in AB and ABA triblock copolymers, with PDL as the B-block. While these materials behave as elastomers, the tensile mechanical properties are not reported. This is in part due to the instability of the boroxine cross-links which hydrolyse even in the presence of trace quantities of water. This environmental instability likely limits the applications accessible when employing this form of dynamic network.

Yang *et al.* reported the synthesis of fully CO_2-derived poly(cyclohexene carbonate-*b*-allyl glycidyl ether carbonate-*b*-cyclohexene carbonate) TPEs.[128] The pendent alkenes in the central block were functionalised to install diols to every repeat unit of the block and the addition of a boronic ester generated the formation of a healable thermoplastic elastomer. The TPEs reported behave as moderate elastomers with the strongest exhibiting an ultimate tensile strength of 6.7 MPa, Young's modulus of 10.1 MPa and an elongation at break of 250%. Unfortunately, the change in mechanical properties upon formation of the dynamic boronic ester network were not reported.

An alternative approach by Zhao *et al.* demonstrated that the mechanical properties of a CO_2-based polyurethane thermoset could be tuned by varying the ratio of rigid CO_2-polycarbonate to the soft polyester.[129] These materials were synthesized through the grafting of poly(γ-methyl-ε-caprolactone) onto pendent alcohol groups decorating a poly(vinyl cyclohexene oxide-*co*-cyclohexene oxide) backbone, followed by isocyanate coupling.

Clarke *et al.* report the synthesis of an all-acrylic ABA triblock copolymer where the outer A-blocks were functionalised with pendent carboxylic acids.[130] The outer blocks dehydrate upon heating to 200 °C and an acid-anhydride dynamic network was established. This improved creep-resistance and the mechanical properties of the triblock copolymer. The best performing material exhibited a Young's modulus of 2.9 GPa ultimate tensile strength of

42 MPa and an elongation at break of 123%. This reflected a 5700 times, 20 times, and 5.4 times improvement in Young's modulus, ultimate tensile strength and elongation at break respectively. While the magnitude of enhancement of mechanical properties is notable, the materials require 24 hours of thermal compression to be mechanically recycled due to the slow timescale of the acid-anhydride exchange.

Another example of a networked TPE with a fully saturated carbon backbone is reported by Robertson and co-workers. Ding *et al.* reported the synthesis of ABA triblock TPEs with poly(styrene) as the outer block and a copolymer of poly(lauryl acrylate), derived from vegetable oils, and poly(acrylamide) as the central block.[131] The poly(acrylamide) formed a transient hydrogen bonding network which reduced the effective entanglement molar mass and improved the mechanical properties. This resulted in an over 10 times increase in ultimate tensile strength and a 2 times increase in elongation at break, however, precise results from mechanical testing are not reported.

Gregory *et al.* reported the synthesis of ionomer networks of all polyester triblock copolymer elastomers.[132] These feature a PDL central block and semi-aromatic outer blocks, which were functionalised to install pendent carboxylic acids and were neutralised to form sodium and lithium ionomers. This strategy improved the mechanical performance of the TPEs without compromising the ability to thermally reprocess the materials. The Young's modulus, ultimate tensile strength, and elongation at break of the best performing elastomer were 8.8 MPa, 19.5 MPa and 2420% respectively. This reflected a 19 times increase in modulus and a 59 time increase in tensile strength, with no significant loss in the elongation at break.

Gregory *et al.* later utilised an analogous approach to produce TPEs with a PTMC central block flanked by the same semi-aromatic outer blocks.[133] Functionalisation to produce zinc ionomers improved the mechanical properties of the already high-performance

elastomers. The PTMC central block was able to undergo strain-induced crystallisation upon extension. The formation of crystallites stiffens the material and results in a rapid increase in stress at approximately 400% strain. The best unfunctionalised TPE exhibited a Young's modulus of 7.1 MPa, ultimate tensile strength of 25.9 MPa, and an elongation at break of 822%. The addition of the Zn(II) ionomeric cross-links resulted in a Young's modulus of 41.6 MPa, an ultimate tensile strength of 62.3 MPa and an elongation at break of 851%. This reflected a 5.9 times and 2.4 times increase in modulus and tensile strength respectively. These results highlight the great potential of metal-ligand cross-linking to enhance and tune the mechanical properties of sustainable oxygenated polymers.

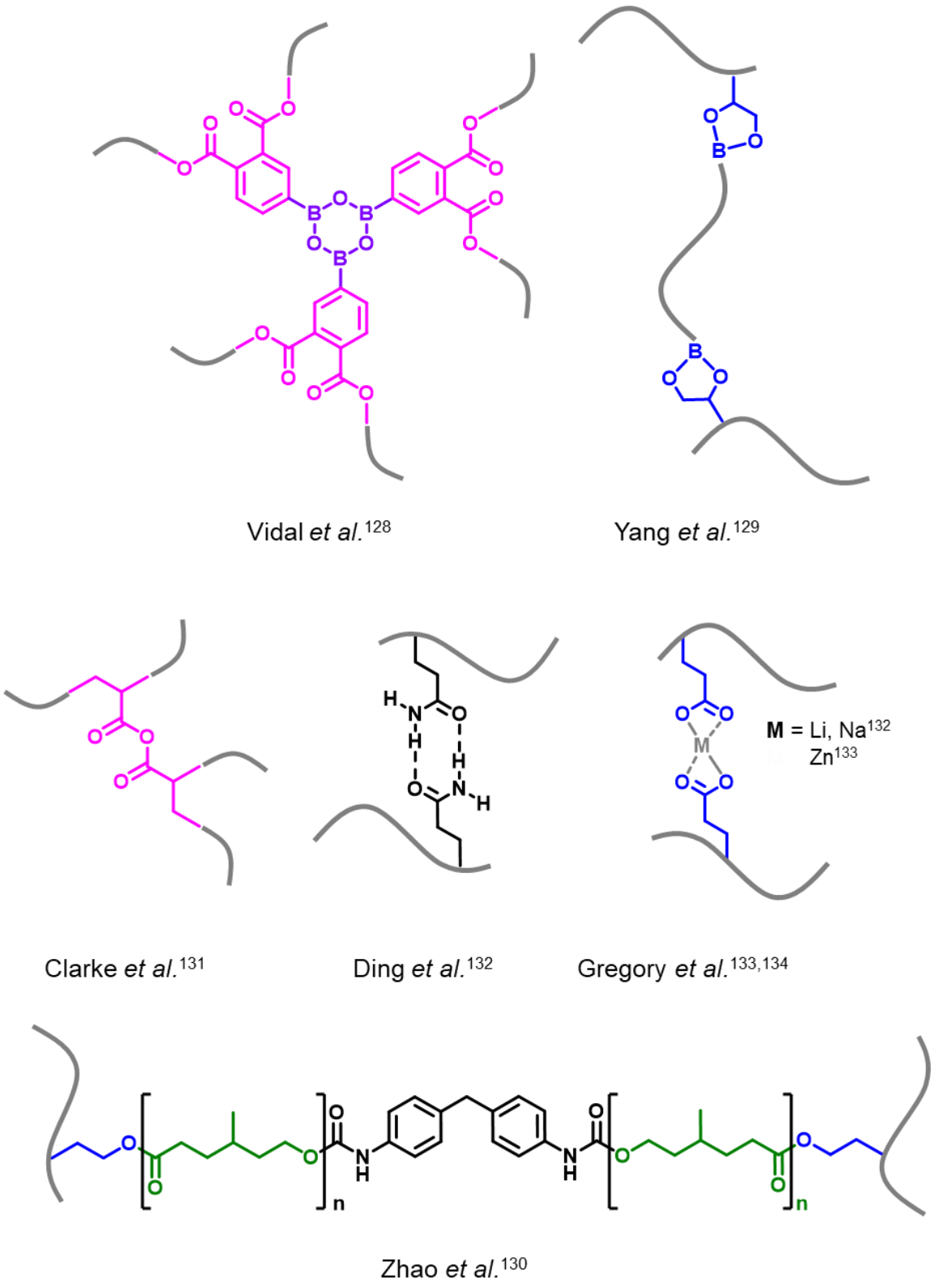

Figure 1.13. Previously reported ABA triblock copolymer networks.

1.7 Aims and Objectives

The main objective of this thesis is to explore how the formation of polymeric networks can enhance the mechanical properties of CO_2- and bio-derived plastics and elastomers. The principle questions this thesis aims to answer are: 1) Can metal-ligand interactions be used to toughen and tune the thermomechanical properties of oxygenated elastomers without compromising the ability to mechanically recycle?; 2) How does regulation of the entanglement molar mass influence the thermomechanical properties of terpolymer plastics?; 3) Is it possible to 3D print sustainable polyols as degradable and elastic thermosets in high resolution? These studies aim to expand the property profile of CO_2-derived polycarbonates through the development of new functional materials. In each instance, exploration of the end-of-life options of the materials should be undertaken, leading to a final question: 4) Is it possible to bridge the divide between the performance of these CO_2-derived polycarbonates and the petro-polymers used today?

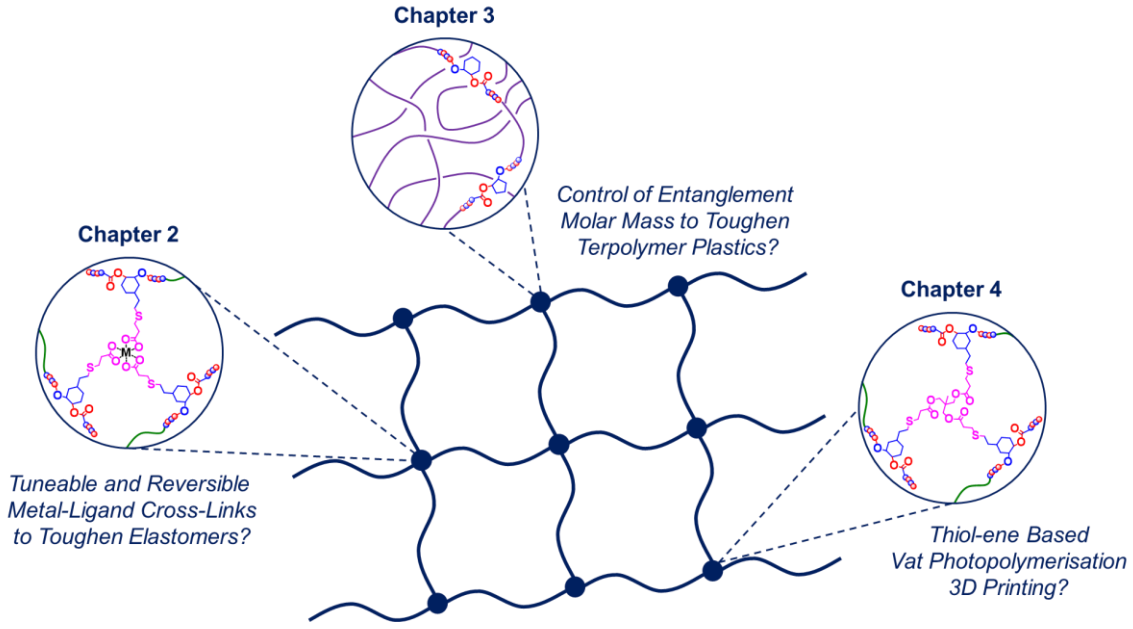

Figure 1.14. Aims and objectives of this thesis – the formation of polymer networks to toughen and tune the thermomechanical properties of CO_2- and bio-derived materials.

1.8 References

(1) Mülhaupt, R. Hermann Staudinger and the origin of macromolecular chemistry. *Angew. Chem. Int. Edit.* **2004**, *43* (9), 1054-1063. DOI: 10.1002/anie.200330070.
(2) Ostle, C.; Thompson, R. C.; Broughton, D.; Gregory, L.; Wootton, M.; Johns, D. G. The rise in ocean plastics evidenced from a 60-year time series. *Nat. Commun.* **2019**, *10* (1), 1622. DOI: 10.1038/s41467-019-09506-1.
(3) MacLeod, M.; Arp, H. P. H.; Tekman, M. B.; Jahnke, A. The global threat from plastic pollution. *Science* **2021**, *373* (6550), 61-65. DOI: 10.1126/science.abg5433.
(4) Vidal, F.; van der Marel, E. R.; Kerr, R. W. F.; McElroy, C.; Schroeder, N.; Mitchell, C.; Rosetto, G.; Chen, T. T. D.; Bailey, R. M.; Hepburn, C.; et al. Designing a circular carbon and plastics economy for a sustainable future. *Nature* **2024**, *626* (7997), 45-57. DOI: 10.1038/s41586-023-06939-z.
(5) Lau, W. W. Y.; Shiran, Y.; Bailey, R. M.; Cook, E.; Stuchtey, M. R.; Koskella, J.; Velis, C. A.; Godfrey, L.; Boucher, J.; Murphy, M. B.; et al. Evaluating scenarios toward zero plastic pollution. *Science* **2020**, *369* (6510), 1455- 1461. DOI: 10.1126/science.aba9475.
(6) Horejs, C. Solutions to plastic pollution. *Nat. Rev. Mater.* **2020**, *5* (9), 641-641. DOI: 10.1038/s41578-020-00237-0.
(7) Geyer, R.; Jambeck, J. R.; Law, K. L. Production, use, and fate of all plastics ever made. *Sci. Adv.* **2017**, *3* (7), e1700782. DOI: 10.1126/sciadv.1700782.
(8) Borrelle, S. B.; Ringma, J.; Law, K. L.; Monnahan, C. C.; Lebreton, L.; McGivern, A.; Murphy, E.; Jambeck, J.; Leonard, G. H.; Hilleary, M. A.; et al. Predicted growth in plastic waste exceeds efforts to mitigate plastic pollution. *Science* **2020**, *369* (6510), 1515-1518. DOI: 10.1126/science.aba3656.
(9) Jehanno, C.; Alty, J. W.; Roosen, M.; De Meester, S.; Dove, A. P.; Chen, E. Y. X.; Leibfarth, F. A.; Sardon, H. Critical advances and future opportunities in upcycling commodity polymers. *Nature* **2022**, *603* (7903), 803-814. DOI: 10.1038/s41586-021-04350-0.
(10) Singh, A.; Rorrer, N. A.; Nicholson, S. R.; Erickson, E.; DesVeaux, J. S.; Avelino, A. F. T.; Lamers, P.; Bhatt, A.; Zhang, Y. M.; Avery, G.; et al. Techno-economic, life-cycle, and socioeconomic impact analysis of enzymatic recycling of poly(ethylene terephthalate). *Joule* **2021**, *5* (9), 2479-2503. DOI: 10.1016/j.joule.2021.06.015.
(11) Bachmann, M.; Zibunas, C.; Hartmann, J.; Tulus, V.; Suh, S.; Guillén-Gosálbez, G.; Bardow, A. Towards circular plastics within planetary boundaries. *Nat. Sustain.* **2023**, *6* (5), 599-610. DOI: 10.1038/s41893-022-01054-9.
(12) Zheng, J. J.; Suh, S. Strategies to reduce the global carbon footprint of plastics. *Nat. Clim. Change* **2019**, *9* (5), 374-378. DOI: 10.1038/s41558-019-0459-z.
(13) Rosenboom, J. G.; Langer, R.; Traverso, G. Bioplastics for a circular economy. *Nat. Rev. Mater.* **2022**, *7* (2), 117-137. DOI: 10.1038/s41578-021-00407-8.
(14) Cywar, R. M.; Rorrer, N. A.; Hoyt, C. B.; Beckham, G. T.; Chen, E. Y. X. Bio-based polymers with performance-advantaged properties. *Nat. Rev. Mater.* **2022**, *7* (2), 83-103. DOI: 10.1038/s41578-021-00363-3.
(15) Zhang, X. Y.; Fevre, M.; Jones, G. O.; Waymouth, R. M. Catalysis as an Enabling Science for Sustainable Polymers. *Chem. Rev.* **2018**, *118* (2), 839-885. DOI: 10.1021/acs.chemrev.7b00329.
(16) Zhu, Y. Q.; Romain, C.; Williams, C. K. Sustainable polymers from renewable resources. *Nature* **2016**, *540* (7633), 354-362. DOI: 10.1038/nature21001.
(17) Carus, M.; Dammer, L.; Raschka, A.; Skoczinski, P. Renewable carbon: Key to a sustainable and future-oriented chemical and plastic industry: Definition, strategy, measures and potential. *Greenh. Gases Sci. Technol.* **2020**, *10* (3), 488-505. DOI: 10.1002/ghg.1992.

(18) Hong, M.; Chen, E. Y. X. Chemically recyclable polymers: a circular economy approach to sustainability. *Green Chem.* **2017**, *19* (16), 3692-3706. DOI: 10.1039/c7gc01496a.
(19) Law, K. L.; Narayan, R. Reducing environmental plastic pollution by designing polymer materials for managed end-of-life. *Nat. Rev. Mater.* **2022**, *7* (2), 104-116. DOI: 10.1038/s41578-021-00382-0.
(20) Coates, G. W.; Getzler, Y. D. Y. L. Chemical recycling to monomer for an ideal, circular polymer economy. *Nat. Rev. Mater.* **2020**, *5* (7), 501-516. DOI: 10.1038/s41578-020-0190-4.
(21) Schneiderman, D. K.; Hillmyer, M. A. There Is a Great Future in Sustainable Polymers. *Macromolecules* **2017**, *50* (10), 3733-3750. DOI: 10.1021/acs.macromol.7b00293.
(22) Haque, F. M.; Ishibashi, J. S. A.; Lidston, C. A. L.; Shao, H. L.; Bates, F. S.; Chang, A. B.; Coates, G. W.; Cramer, C. J.; Dauenhauer, P. J.; Dichtel, W. R.; et al. Defining the Macromolecules of Tomorrow through Synergistic Sustainable Polymer Research. *Chem. Rev.* **2022**, *122* (6), 6322-6373. DOI: 10.1021/acs.chemrev.1c00173.
(23) Carothers, W. H.; Dorough, G. L.; Natta, F. J. v. STUDIES OF POLYMERIZATION AND RING FORMATION. X. THE REVERSIBLE POLYMERIZATION OF SIX-MEMBERED CYCLIC ESTERS. *J. Am. Chem. Soc.* **1932**, *54* (2), 761-772. DOI: 10.1021/ja01341a046.
(24) Li, Z.; Shen, Y.; Li, Z. B. Ring-Opening Polymerization of Lactones to Prepare Closed-Loop Recyclable Polyesters. *Macromolecules* **2024**, *57* (5), 1919-1940. DOI: 10.1021/acs.macromol.3c01912.
(25) Xie, X. Y.; Huo, Z. Y.; Jang, E.; Tong, R. Recent advances in enantioselective ring-opening polymerization and copolymerization. *Commun. Chem.* **2023**, *6* (1), 202. DOI: 10.1038/s42004-023-01007-z.
(26) Shaver, M.; Buchard, A. Ring opening polymerisation. *Eur. Polym. J.* **2020**, *129*, 109600. DOI: 10.1016/j.eurpolymj.2020.109600.
(27) Inkinen, S.; Hakkarainen, M.; Albertsson, A. C.; Södergård, A. From Lactic Acid to Poly(lactic acid) (PLA): Characterization and Analysis of PLA and Its Precursors. *Biomacromolecules* **2011**, *12* (3), 523-532. DOI: 10.1021/bm101302t.
(28) Sarazin, Y.; Carpentier, J. F. Discrete Cationic Complexes for Ring-Opening Polymerization Catalysis of Cyclic Esters and Epoxides. *Chem. Rev.* **2015**, *115* (9), 3564-3614. DOI: 10.1021/acs.chemrev.5b00033.
(29) Gruszka, W.; Garden, J. A. Advances in heterometallic ring-opening (co)polymerisation catalysis. *Nat. Commun.* **2021**, *12* (1), 3252. DOI: 10.1038/s41467-021-23192-y.
(30) Kamber, N. E.; Jeong, W.; Waymouth, R. M.; Pratt, R. C.; Lohmeijer, B. G. G.; Hedrick, J. L. Organocatalytic ring-opening polymerization. *Chem. Rev.* **2007**, *107* (12), 5813-5840. DOI: 10.1021/cr068415b.
(31) Nuyken, O.; Pask, S. D. Ring-Opening Polymerization-An Introductory Review. *Polymers* **2013**, *5* (2), 361-403. DOI: 10.3390/polym5020361.
(32) Plajer, A. J.; Williams, C. K. Heterocycle/Heteroallene Ring-Opening Copolymerization: Selective Catalysis Delivering Alternating Copolymers. *Angew. Chem. Int. Edit.* **2022**, *61* (1). DOI: 10.1002/anie.202104495.
(33) Paul, S.; Zhu, Y. Q.; Romain, C.; Brooks, R.; Saini, P. K.; Williams, C. K. Ring-opening copolymerization (ROCOP): synthesis and properties of polyesters and polycarbonates. *Chem. Commun.* **2015**, *51* (30), 6459-6479. DOI: 10.1039/c4cc10113h.
(34) Kember, M. R.; Buchard, A.; Williams, C. K. Catalysts for CO2/epoxide copolymerisation. *Chem. Commun.* **2011**, *47* (1), 141-163. DOI: 10.1039/c0cc02207a.
(35) Diment, W. T.; Lindeboom, W.; Fiorentini, F.; Deacy, A. C.; Williams, C. K. Synergic Heterodinuclear Catalysts for the Ring-Opening Copolymerization (ROCOP) of Epoxides, Carbon Dioxide, and Anhydrides. *Acc. Chem. Res.* **2022**, *55* (15), 1997-2010. DOI: 10.1021/acs.accounts.2c00197.

(36) Longo, J. M.; Sanford, M. J.; Coates, G. W. Ring-Opening Copolymerization of Epoxides and Cyclic Anhydrides with Discrete Metal Complexes: Structure-Property Relationships. *Chem. Rev.* **2016**, *116* (24), 15167-15197. DOI: 10.1021/acs.chemrev.6b00553.
(37) Winkler, M.; Romain, C.; Meier, M. A. R.; Williams, C. K. Renewable polycarbonates and polyesters from 1,4-cyclohexadiene. *Green Chem.* **2015**, *17* (1), 300-306. DOI: 10.1039/c4gc01353k.
(38) Mathers, R. T.; Shreve, M. J.; Meyler, E.; Damodaran, K.; Iwig, D. F.; Kelley, D. J. Synthesis and Polymerization of Renewable 1,3-Cyclohexadiene Using Metathesis, Isomerization, and Cascade Reactions with Late-metal Catalysts. *Macromol. Rapid. Comm.* **2011**, *32* (17), 1338-1342. DOI: 10.1002/marc.201100104.
(39) Parrino, F.; Fidalgo, A.; Palmisano, L.; Ilharco, L. M.; Pagliaro, M.; Ciriminna, R. Polymers of Limonene Oxide and Carbon Dioxide: Polycarbonates of the Solar Economy. *ACS Omega* **2018**, *3* (5), 4884-4890. DOI: 10.1021/acsomega.8b00644.
(40) Shao, X. J.; Su, L. J.; Zhang, J. J.; Tian, Z. S.; Zhang, N.; Wang, Y. X.; Wang, H. L.; Cui, X. J.; Hou, X. L.; Deng, T. S. Green Production of Phthalic Anhydride from Biobased Furan and Maleic Anhydride by an Acid Resin Catalyst. *ACS Sustain. Chem. Eng.* **2021**, *9* (43), 14385-14394. DOI: 10.1021/acssuschemeng.1c03974.
(41) Dakshinamoorthy, D.; Weinstock, A. K.; Damodaran, K.; Iwig, D. F.; Mathers, R. T. Diglycerol-Based Polyesters: Melt Polymerization with Hydrophobic Anhydrides. *ChemSusChem* **2014**, *7* (10), 2923-2929. DOI: 10.1002/cssc.201402249.
(42) Gauthier, M. A.; Gibson, M. I.; Klok, H. A. Synthesis of Functional Polymers by Post-Polymerization Modification. *Angew. Chem. Int. Edit.* **2009**, *48* (1), 48-58. DOI: 10.1002/anie.200801951.
(43) Shi, C. X.; Reilly, L. T.; Chen, E. Y. X. Hybrid Monomer Design Synergizing Property Trade-offs in Developing Polymers for Circularity and Performance. *Angew. Chem. Int. Edit.* **2023**, *62* (31), e202301850 DOI: 10.1002/anie.202301850.
(44) Schneiderman, D. K.; Hillmyer, M. A. Aliphatic Polyester Block Polymer Design. *Macromolecules* **2016**, *49* (7), 2419-2428. DOI: 10.1021/acs.macromol.6b00211.
(45) Lee, S. H.; Cyriac, A.; Jeon, J. Y.; Lee, B. Y. Preparation of thermoplastic polyurethanes using in situ generated poly(propylene carbonate)-diols. *Polym. Chem.* **2012**, *3* (5), 1215-1220. DOI: 10.1039/c2py00010e.
(46) Langanke, J.; Wolf, A.; Hofmann, J.; Böhm, K.; Subhani, M. A.; Müller, T. E.; Leitner, W.; Gürtler, C. Carbon dioxide (CO2) as sustainable feedstock for polyurethane production. *Green Chem.* **2014**, *16* (4), 1865-1870. DOI: 10.1039/c3gc41788c.
(47) DeBolt, M.; Kiziltas, A.; Mielewski, D.; Waddington, S.; Nagridge, M. J. Flexible polyurethane foams formulated with polyols derived from waste carbon dioxide. *J. Appl. Polym. Sci.* **2016**, *133* (45). DOI: 10.1002/app.44086.
(48) Alagi, P.; Ghorpade, R.; Choi, Y. J.; Patil, U.; Kim, I.; Baik, J. H.; Hong, S. C. Carbon Dioxide-Based Polyols as Sustainable Feedstock of Thermoplastic Polyurethane for Corrosion-Resistant Metal Coating. *ACS Sustain. Chem. Eng.* **2017**, *5* (5), 3871-3881. DOI: 10.1021/acssuschemeng.6b03046.
(49) Stösser, T.; Li, C. L.; Unruangsri, J.; Saini, P. K.; Sablong, R. J.; Meier, M. A. R.; Williams, C. K.; Koning, C. Bio-derived polymers for coating applications: comparing poly(limonene carbonate) and poly (cyclohexadiene carbonate). *Polym. Chem.* **2017**, *8* (39), 6099-6105. DOI: 10.1039/c7py01223c.
(50) Scharfenberg, M.; Hilf, J.; Frey, H. Functional Polycarbonates from Carbon Dioxide and Tailored Epoxide Monomers: Degradable Materials and Their Application Potential. *Adv. Funct. Mater.* **2018**, *28* (10), 1704302. DOI: 10.1002/adfm.201704302.
(51) Hauenstein, O.; Agarwal, S.; Greiner, A. Bio-based polycarbonate as synthetic toolbox. *Nat. Commun.* **2016**, *7*, 11862. DOI: 10.1038/ncomms11862.

(52) Hauenstein, O.; Reiter, M.; Agarwal, S.; Rieger, B.; Greiner, A. Bio-based polycarbonate from limonene oxide and CO2 with high molecular weight, excellent thermal resistance, hardness and transparency. *Green Chem.* **2016**, *18* (3), 760-770. DOI: 10.1039/c5gc01694k.
(53) Jia, M. C.; Hadjichristidis, N.; Gnanou, Y.; Feng, X. S. Monomodal Ultrahigh-Molar-Mass Polycarbonate Homopolymers and Diblock Copolymers by Anionic Copolymerization of Epoxides with CO. *ACS Macro. Lett.* **2019**, *8* (12), 1594-1598. DOI: 10.1021/acsmacrolett.9b00854.
(54) Kernbichl, S.; Rieger, B. Aliphatic polycarbonates derived from epoxides and CO2: A comparative study of poly(cyclohexene carbonate) and poly(limonene carbonate). *Polymer* **2020**, *205*, 122667. DOI: 10.1016/j.polymer.2020.122667.
(55) Diment, W. T.; Williams, C. K. Chain end-group selectivity using an organometallic Al(iii)/K(i) ring-opening copolymerization catalyst delivers high molar mass, monodisperse polyesters. *Chem. Sci.* **2022**, *13* (29), 8543-8549. DOI: 10.1039/d2sc02752f.
(56) Zhang, J. B.; Wang, L. B.; Liu, S. F.; Li, Z. B. Synthesis of Diverse Polycarbonates by Organocatalytic Copolymerization of CO2 and Epoxides: From High Pressure and Temperature to Ambient Conditions. *Angew. Chem. Int. Edit.* **2022**, *61* (4), e202111197 DOI: 10.1002/anie.202111197.
(57) Rosetto, G.; Vidal, F.; Mcguire, T. M.; Kerr, R. W. F.; Williams, C. K. High Molar Mass Polycarbonates as Closed-Loop Recyclable Thermoplastics. *J. Am. Chem. Soc.* **2024**, *146* (12), 8381-8393. DOI: 10.1021/jacs.3c14170.
(58) Hepburn, C.; Adlen, E.; Beddington, J.; Carter, E. A.; Fuss, S.; Mac Dowell, N.; Minx, J. C.; Smith, P.; Williams, C. K. The technological and economic prospects for CO2 utilization and removal. *Nature* **2019**, *575* (7781), 87-97. DOI: 10.1038/s41586-019-1681-6.
(59) Artz, J.; Müller, T. E.; Thenert, K.; Kleinekorte, J.; Meys, R.; Sternberg, A.; Bardow, A.; Leitner, W. Sustainable Conversion of Carbon Dioxide: An Integrated Review of Catalysis and Life Cycle Assessment. *Chem. Rev.* **2018**, *118* (2), 434-504. DOI: 10.1021/acs.chemrev.7b00435.
(60) von der Assen, N.; Bardow, A. Life cycle assessment of polyols for polyurethane production using CO2 as feedstock: insights from an industrial case study. *Green Chem.* **2014**, *16* (6), 3272-3280. DOI: 10.1039/c4gc00513a.
(61) von der Assen, N.; Jung, J.; Bardow, A. Life-cycle assessment of carbon dioxide capture and utilization: avoiding the pitfalls. *Energ. Environ. Sci.* **2013**, *6* (9), 2721-2734. DOI: 10.1039/c3ee41151f.
(62) Ferry, J. D. *Viscoelastic Properties of Polymers*; Wiley, 1980.
(63) Tripathi, N.; Misra, M.; Mohanty, A. K. Durable Polylactic Acid (PLA)-Based Sustainable Engineered Blends and Biocomposites: Recent Developments, Challenges, and Opportunities. *ACS Eng. Au.* **2021**, *1* (1), 7-38. DOI: 10.1021/acsengineeringau.1c00011.
(64) Ciriminna, R.; Lomeli-Rodriguez, M.; Carà, P. D.; Lopez-Sanchez, J. A.; Pagliaro, M. Limonene: a versatile chemical of the bioeconomy. *Chem. Commun.* **2014**, *50* (97), 15288-15296. DOI: 10.1039/c4cc06147k.
(65) Byrne, C. M.; Allen, S. D.; Lobkovsky, E. B.; Coates, G. W. Alternating copolymerization of limonene oxide and carbon dioxide. *J. Am. Chem. Soc.* **2004**, *126* (37), 11404-11405. DOI: 10.1021/ja0472580.
(66) Carrodeguas, L. P.; González-Fabra, J.; Castro-Gómez, F.; Bo, C.; Kleij, A. W. Al(III)-Catalysed Formation of Poly(limonene)carbonate: DFT Analysis of the Origin of Stereoregularity. *Chem. Eur. J.* **2015**, *21* (16), 6115-6122. DOI: 10.1002/chem.201406334.
(67) Kindermann, N.; Cristòfol, A.; Kleij, A. W. Access to Biorenewable Polycarbonates with Unusual Glass Transition Temperature (Tg) Modulation. *ACS Catal.* **2017**, *7* (6), 3860-3863. DOI: 10.1021/acscatal.7b00770.

(68) Darensbourg, D. J.; Wei, S. H.; Yeung, A. D.; Ellis, W. C. An Efficient Method of Depolymerization of Poly(cyclopentene carbonate) to Its Comonomers: Cyclopentene Oxide and Carbon Dioxide. *Macromolecules* **2013**, *46* (15), 5850-5855. DOI: 10.1021/ma401286x.
(69) Darensbourg, D. J.; Yeung, A. D.; Wei, S. H. Base initiated depolymerization of polycarbonates to epoxide and carbon dioxide co-monomers: a computational study. *Green Chem.* **2013**, *15* (6), 1578-1583. DOI: 10.1039/c3gc40475g.
(70) Li, C. L.; Sablong, R. J.; van Benthem, R. A. T. M.; Koning, C. E. Unique Base-Initiated Depolymerization of Limonene-Derived Polycarbonates. *ACS Macro. Lett.* **2017**, *6* (7), 684-688. DOI: 10.1021/acsmacrolett.7b00310.
(71) Liu, Y.; Zhou, H.; Guo, J. Z.; Ren, W. M.; Lu, X. B. Completely Recyclable Monomers and Polycarbonate: Approach to Sustainable Polymers. *Angew. Chem. Int. Edit.* **2017**, *56* (17), 4862-4866. DOI: 10.1002/anie.201701438.
(72) McGuire, T. M.; Deacy, A. C.; Buchard, A.; Williams, C. K. Solid-State Chemical Recycling of Polycarbonates to Epoxides and Carbon Dioxide Using a Heterodinuclear Mg(II)Co(II) Catalyst. *J. Am. Chem. Soc.* **2022**, *144* (40), 18444-18449. DOI: 10.1021/jacs.2c06937.
(73) Singer, F. N.; Deacy, A. C.; McGuire, T. M.; Williams, C. K.; Buchard, A. Chemical Recycling of Poly(Cyclohexene Carbonate) Using a Di-Mg(II) Catalyst. *Angew. Chem. Int. Edit.* **2022**, *61* (26), e202201785. DOI: 10.1002/anie.202201785.
(74) Yu, Y.; Gao, B.; Liu, Y.; Lu, X. B. Efficient and Selective Chemical Recycling of CO2-Based Alicyclic Polycarbonates via Catalytic Pyrolysis. *Angew. Chem. Int. Edit.* **2022**, *61* (34), e202204492. DOI: 10.1002/anie.202204492.
(75) Bates, F. S.; Hillmyer, M. A.; Lodge, T. P.; Bates, C. M.; Delaney, K. T.; Fredrickson, G. H. Multiblock Polymers: Panacea or Pandora's Box? *Science* **2012**, *336* (6080), 434-440. DOI: 10.1126/science.1215368.
(76) Romain, C.; Williams, C. K. Chemoselective Polymerization Control: From Mixed-Monomer Feedstock to Copolymers. *Angew. Chem. Int. Edit.* **2014**, *53* (6), 1607-1610. DOI: 10.1002/anie.201309575.
(77) Deacy, A. C.; Gregory, G. L.; Sulley, G. S.; Chen, T. T. D.; Williams, C. K. Sequence Control from Mixtures: Switchable Polymerization Catalysis and Future Materials Applications. *J. Am. Chem. Soc.* **2021**, *143* (27), 10021-10040. DOI: 10.1021/jacs.1c03250.
(78) Isnard, F.; Carratù, M.; Lamberti, M.; Venditto, V.; Mazzeo, M. Copolymerization of cyclic esters, epoxides and anhydrides: evidence of the dual role of the monomers in the reaction mixture. *Catal. Sci. Technol.* **2018**, *8* (19), 5034-5043. DOI: 10.1039/c8cy01174e.
(79) Reiter, M.; Vagin, S.; Kronast, A.; Jandl, C.; Rieger, B. A Lewis acid β-diiminato-zinc-complex as all-rounder for co- and terpolymerisation of various epoxides with carbon dioxide. *Chem. Sci.* **2017**, *8* (3), 1876-1882. DOI: 10.1039/c6sc04477h.
(80) Stösser, T.; Sulley, G. S.; Gregory, G. L.; Williams, C. K. Easy access to oxygenated block polymers via switchable catalysis. *Nat. Commun.* **2019**, *10*, 2668. DOI: 10.1038/s41467-019-10481-w.
(81) Saini, P. K.; Fiorani, G.; Mathers, R. T.; Williams, C. K. Zinc versus Magnesium: Orthogonal Catalyst Reactivity in Selective Polymerizations of Epoxides, Bio-derived Anhydrides and Carbon Dioxide. *Chem. Eur. J.* **2017**, *23* (18), 4260-4265. DOI: 10.1002/chem.201605690.
(82) Deacy, A. C.; Durr, C. B.; Garden, J. A.; White, A. J. P.; Williams, C. K. Groups 1, 2 and Zn(II) Heterodinuclear Catalysts for Epoxide/CO2 Ring-Opening Copolymerization. *Inorg. Chem.* **2018**, *57* (24), 15575-15583. DOI: 10.1021/acs.inorgchem.8b02923.
(83) Sulley, G. S.; Gregory, G. L.; Chen, T. T. D.; Carrodeguas, L. P.; Trott, G.; Santmarti, A.; Lee, K. Y.; Terrill, N. J.; Williams, C. K. Switchable Catalysis Improves the Properties of CO2-Derived Polymers: Poly(cyclohexene carbonate-b-ε-decalactone-b-cyclohexene carbonate)

Adhesives, Elastomers, and Toughened Plastics. *J. Am. Chem. Soc.* **2020**, *142* (9), 4367-4378. DOI: 10.1021/jacs.9b13106.
(84) Stöesser, T.; Mulryan, D.; Williams, C. K. Switch Catalysis To Deliver Multi-Block Polyesters from Mixtures of Propene Oxide, Lactide, and Phthalic Anhydride. *Angew. Chem. Int. Edit.* **2018**, *57* (51), 16893-16897. DOI: 10.1002/anie.201810245.
(85) Kernbichl, S.; Reiter, M.; Adams, F.; Vagin, S.; Rieger, B. CO2-Controlled One-Pot Synthesis of AB, ABA Block, and Statistical Terpolymers from β-Butyrolactone, Epoxides, and CO2. *J. Am. Chem. Soc.* **2017**, *139* (20), 6787-6790. DOI: 10.1021/jacs.7b01295.
(86) Ji, H. Y.; Wang, B.; Pan, L.; Li, Y. S. One-Step Access to Sequence-Controlled Block Copolymers by Self-Switchable Organocatalytic Multicomponent Polymerization. *Angew. Chem. Int. Edit.* **2018**, *57* (51), 16888-16892. DOI: 10.1002/anie.201810083.
(87) Paul, S.; Romain, C.; Shaw, J.; Williams, C. K. Sequence Selective Polymerization Catalysis: A New Route to ABA Block Copoly(ester-b-carbonate-b-ester). *Macromolecules* **2015**, *48* (17), 6047-6056. DOI: 10.1021/acs.macromol.5b01293.
(88) Zhu, Y. Q.; Romain, C.; Williams, C. K. Selective Polymerization Catalysis: Controlling the Metal Chain End Group to Prepare Block Copolyesters. *J. Am. Chem. Soc.* **2015**, *137* (38), 12179-12182. DOI: 10.1021/jacs.5b04541.
(89) Romain, C.; Zhu, Y. Q.; Dingwall, P.; Paul, S.; Rzepa, H. S.; Buchard, A.; Williams, C. K. Chemoselective Polymerizations from Mixtures of Epoxide, Lactone, Anhydride, and Carbon Dioxide. *J. Am. Chem. Soc.* **2016**, *138* (12), 4120-4131. DOI: 10.1021/jacs.5b13070.
(90) Chen, T. T. D.; Zhu, Y. Q.; Williams, C. K. Pentablock Copolymer from Tetracomponent Monomer Mixture Using a Switchable Dizinc Catalyst. *Macromolecules* **2018**, *51* (14), 5346-5351. DOI: 10.1021/acs.macromol.8b01224.
(91) Rosetto, G.; Deacy, A. C.; Williams, C. K. Mg(ii) heterodinuclear catalysts delivering carbon dioxide derived multi-block polymers. *Chem. Sci.* **2021**, *12* (37), 12315-12325. DOI: 10.1039/d1sc03856g.
(92) Raman, S. K.; Raja, R.; Arnold, P. L.; Davidson, M. G.; Williams, C. K. Waste not, want not: CO2 (re)cycling into block polymers. *Chem. Commun.* **2019**, *55* (51), 7315-7318. DOI: 10.1039/c9cc02459j.
(93) Stosser, T.; Chen, T. T. D.; Zhu, Y.; Williams, C. K. 'Switch' catalysis: from monomer mixtures to sequence-controlled block copolymers. *Philos. T. R. Soc. A* **2018**, *376*, 2017066. DOI: 10.1098/rsta.2017.0066.
(94) Spyros, A.; Argyropoulos, D. S.; Marchessault, R. H. A study of poly(hydroxyalkanoate)s by quantitative P31 NMR spectroscopy: Molecular weight and chain cleavage. *Macromolecules* **1997**, *30* (2), 327-329. DOI: DOI 10.1021/ma9601979.
(95) Zhu, Y. Q.; Radlauer, M. R.; Schneiderman, D. K.; Shaffer, M. S. P.; Hillmyer, M. A.; Williams, C. K. Multiblock Polyesters Demonstrating High Elasticity and Shape Memory Effects. *Macromolecules* **2018**, *51* (7), 2466-2475. DOI: 10.1021/acs.macromol.7b02690.
(96) Wang, W. Y.; Lu, W.; Goodwin, A.; Wang, H. Q.; Yin, P. C.; Kang, N. G.; Hong, K. L.; Mays, J. W. Recent advances in thermoplastic elastomers from living polymerizations: Macromolecular architectures and supramolecular chemistry. *Prog Polym Sci* **2019**, *95*, 1-31. DOI: 10.1016/j.progpolymsci.2019.04.002.
(97) Sun, M. H.; Xiao, Y. K.; Liu, K.; Yang, X.; Liu, P. W.; Jie, S. Y.; Hu, J. J.; Shi, S. B.; Wang, Q. Y.; Lim, K. H.; et al. Synthesis and characterization of polyolefin thermoplastic elastomers: A review. *Can. J. Chem. Eng.* **2023**, *101* (9), 4886-4906. DOI: 10.1002/cjce.24825.
(98) Holden, G.; Bishop, E. T.; Legge, N. R. Thermoplastic Elastomers. *J. Polym. Sci. Pol. Sym.* **1969**, (26), 37-57.
(99) Tong, J. D.; Jerôme, R. Dependence of the ultimate tensile strength of thermoplastic elastomers of the triblock type on the molecular weight between chain entanglements of the central block. *Macromolecules* **2000**, *33* (5), 1479-1481. DOI: DOI 10.1021/ma990404f.

(100) Fodor, C.; Kali, G.; Thomann, R.; Thomann, Y.; Iván, B.; Mülhaupt, R. Nanophasic morphologies as a function of the composition and molecular weight of the macromolecular cross-linker in poly(*N*-vinylimidazole)-*I*-poly(tetrahydrofuran) amphiphilic conetworks: bicontinuous domain structure in broad composition ranges. *RSC Adv.* **2017**, *7* (12), 6827-6834. DOI: 10.1039/c6ra25356c.
(101) Hermel, T. J.; Hahn, S. F.; Chaffin, K. A.; Gerberich, W. W.; Bates, F. S. Role of molecular architecture in mechanical failure of glassy/semicrystalline block copolymers: CEC vs CECEC lamellae. *Macromolecules* **2003**, *36* (7), 2190-2193. DOI: 10.1021/ma021754w.
(102) Feng, H. B.; Lu, X. Y.; Wang, W. Y.; Kang, N. G.; Mays, J. W. Block Copolymers: Synthesis, Self-Assembly, and Applications. *Polymers* **2017**, *9* (10), 494. DOI: 10.3390/polym9100494.
(103) Sinturel, C.; Bates, F. S.; Hillmyer, M. A. High χ-Low N Block Polymers: How Far Can We Go? *ACS Macro. Lett.* **2015**, *4* (9), 1044-1050. DOI: 10.1021/acsmacrolett.5b00472.
(104) Gregory, G. L.; Sulley, G. S.; Carrodeguas, L. P.; Chen, T. T. D.; Santmarti, A.; Terrill, N. J.; Lee, K. Y.; Williams, C. K. Triblock polyester thermoplastic elastomers with semi-aromatic polymer end blocks by ring-opening copolymerization. *Chem. Sci.* **2020**, *11* (25), 6567-6581. DOI: 10.1039/d0sc00463d.
(105) Castelletto, V.; Hamley, I. W. Morphologies of block copolymer melts. *Curr. Opin. Solid. St. M.* **2004**, *8* (6), 426-438. DOI: 10.1016/j.cossms.2005.06.001.
(106) Hillmyer, M. A.; Tolman, W. B. Aliphatic Polyester Block Polymers: Renewable, Degradable, and Sustainable. *Acc. Chem. Res.* **2014**, *47* (8), 2390-2396. DOI: 10.1021/ar500121d.
(107) Wanamaker, C. L.; O'Leary, L. E.; Lynd, N. A.; Hillmyer, M. A.; Tolman, W. B. Renewable-resource thermoplastic elastomers based on polylactide and polymenthide. *Biomacromolecules* **2007**, *8* (11), 3634-3640. DOI: 10.1021/bm700699g.
(108) Wanamaker, C. L.; Bluemle, M. J.; Pitet, L. M.; O'Leary, L. E.; Tolman, W. B.; Hillmyer, M. A. Consequences of Polylactide Stereochemistry on the Properties of Polylactide-Polymenthide-Polylactide Thermoplastic Elastomers. *Biomacromolecules* **2009**, *10* (10), 2904-2911. DOI: 10.1021/bm900721p.
(109) Martello, M. T.; Hillmyer, M. A. Polylactide-Poly(6-methyl-ε-caprolactone)-Polylactide Thermoplastic Elastomers. *Macromolecules* **2011**, *44* (21), 8537-8545. DOI: 10.1021/ma201063t.
(110) Watts, A.; Kurokawa, N.; Hillmyer, M. A. Strong, Resilient, and Sustainable Aliphatic Polyester Thermoplastic Elastomers. *Biomacromolecules* **2017**, *18* (6), 1845-1854. DOI: 10.1021/acs.biomac.7b00283.
(111) Schneiderman, D. K.; Hill, E. M.; Martello, M. T.; Hillmyer, M. A. Poly(lactide)-*block*-poly(ε-caprolactone-*block*-ε-decalactone)-*block*-poly(lactide) copolymer elastomers. *Polym. Chem.* **2015**, *6* (19), 3641-3651. DOI: 10.1039/c5py00202h.
(112) Martello, M. T.; Schneiderman, D. K.; Hillmyer, M. A. Synthesis and Melt Processing of Sustainable Poly(ε-decalactone)-b-Poly(lactide) Multiblock Thermoplastic Elastomers. *ACS Sustain. Chem. Eng.* **2014**, *2* (11), 2519-2526. DOI: 10.1021/sc500412a.
(113) Jia, M. C.; Zhang, D. Y.; de Kort, G. W.; Wilsens, C. H. R. M.; Rastogi, S.; Hadjichristidis, N.; Gnanou, Y.; Feng, X. S. All-Polycarbonate Thermoplastic Elastomers Based on Triblock Copolymers Derived from Triethylborane-Mediated Sequential Copolymerization of CO2 with Various Epoxides. *Macromolecules* **2020**, *53* (13), 5297-5307. DOI: 10.1021/acs.macromol.0c01068.
(114) Liu, J. J.; Jia, M. C.; Gnanou, Y.; Feng, X. S. One-Pot Synthesis of CO2-Based Polylactide-b-Poly(ether carbonate)-b-Polylactide Triblock Copolymers and Their Mechanical Properties. *Macromolecules* **2023**, *56* (4), 1615-1624. DOI: 10.1021/acs.macromol.2c02522.

(115) Liu, J. J.; Jia, M. C.; Gnanou, Y.; Feng, X. S. Heat-Resistant CO2-Based Polycarbonate Thermoplastics. *Macromolecules* **2024**, *57* (11), 5380-5388. DOI: 10.1021/acs.macromol.4c00885.
(116) Zhang, Z.; Grijpma, D. W.; Feijen, J. Triblock Copolymers Based on 1,3-Trimethylene Carbonate and Lactide as Biodegradable Thermoplastic Elastomers. *Macromol. Chem. Phys.* **2004**, *205* (7), 867-875. DOI: 10.1002/macp.200300184.
(117) Denk, A.; Grossmann, P.; Rieger, B. Soft Side of Aliphatic Polycarbonates: with PCHC-b-PDMS Copolymers toward Ductile Materials. *Macromolecules* **2023**, *56* (11), 4318-4324. DOI: 10.1021/acs.macromol.2c02433.
(118) Schüttner, S.; Gardiner, C.; Petrov, F.; Fotaras, N.; Preis, J.; Floudas, G.; Frey, H. Biobased Thermoplastic Elastomers Derived from Citronellyl Glycidyl Ether, CO2, and Polylactide. *Macromolecules* **2023**, *56* (20), 8247-8259. DOI: 10.1021/acs.macromol.3c01329.
(119) Carrodeguas, L. P.; Chen, T. T. D.; Gregory, G. L.; Sulley, G. S.; Williams, C. K. High elasticity, chemically recyclable, thermoplastics from bio-based monomers: carbon dioxide, limonene oxide and ε-decalactone. *Green Chem.* **2020**, *22* (23), 8298-8307. DOI: 10.1039/d0gc02295k.
(120) Zhao, X. H.; Chen, X. Y.; Yuk, H.; Lin, S. T.; Liu, X. Y.; Parada, G. Soft Materials by Design: Unconventional Polymer Networks Give Extreme Properties. *Chem. Rev.* **2021**, *121* (8), 4309-4372. DOI: 10.1021/acs.chemrev.0c01088.
(121) Rubinstein, M.; Colby, R. H. *Polymer Physics*; Oxford University Press, 2003.
(122) O'Leary, L. E.; Fallas, J. A.; Bakota, E. L.; Kang, M. K.; Hartgerink, J. D. Multi-hierarchical self-assembly of a collagen mimetic peptide from triple helix to nanofibre and hydrogel. *Nat. Chem.* **2011**, *3* (10), 821-828. DOI: 10.1038/nchem.1123.
(123) Grindy, S. C.; Learsch, R.; Mozhdehi, D.; Cheng, J.; Barrett, D. G.; Guan, Z. B.; Messersmith, P. B.; Holten-Andersen, N. Control of hierarchical polymer mechanics with bioinspired metal-coordination dynamics. *Nat. Mater.* **2015**, *14* (12), 1210-1216. DOI: DOI 10.1038/nmat4401.
(124) Khare, E.; Holten-Andersen, N.; Buehler, M. J. Transition-metal coordinate bonds for bioinspired macromolecules with tunable mechanical properties. *Nat. Rev. Mater.* **2021**, *6* (5), 421-436. DOI: 10.1038/s41578-020-00270-z.
(125) Montarnal, D.; Capelot, M.; Tournilhac, F.; Leibler, L. Silica-Like Malleable Materials from Permanent Organic Networks. *Science* **2011**, *334* (6058), 965-968. DOI: 10.1126/science.1212648.
(126) Guerre, M.; Taplan, C.; Winne, J. M.; Du Prez, F. E. Vitrimers: directing chemical reactivity to control material properties. *Chem. Sci.* **2020**, *11* (19), 4855-4870. DOI: 10.1039/d0sc01069c.
(127) Vidal, F.; Smith, S.; Williams, C. K. Ring Opening Copolymerization of Boron-Containing Anhydride with Epoxides as a Controlled Platform to Functional Polyesters. *J. Am. Chem. Soc.* **2023**, *145* (25), 13888-13900. DOI: 10.1021/jacs.3c03261.
(128) Yang, G. W.; Wu, G. P. High-Efficiency Construction of CO2-Based Healable Thermoplastic Elastomers via a Tandem Synthetic Strategy. *ACS Sustain. Chem. Eng.* **2019**, *7* (1), 1372-1380. DOI: 10.1021/acssuschemeng.8b05084.
(129) Zhao, J. K.; Yang, G. W.; Zhu, X. F.; Wu, G. P. Highly elastic and degradable thermoset elastomers from CO2-based polycarbonates and bioderived polyesters. *Polym. Chem.* **2019**, *10* (38), 5265-5270. DOI: 10.1039/c9py01085h.
(130) Clarke, R. W.; McGraw, M. L.; Newell, B. S.; Chen, E. Y. X. Thermomechanical activation achieving orthogonal working/healing conditions of nanostructured tri-block copolymer thermosets. *Cell Rep. Phys. Sci.* **2021**, *2* (7). DOI: 10.1016/j.xcrp.2021.100483.
(131) Ding, W. Y.; Robertson, M. L. Sustainable thermoplastic elastomers with a transient network. *Eur. Polym. J.* **2019**, *113*, 411-423. DOI: 10.1016/j.eurpolymj.2019.01.010.

(132) Gregory, G. L.; Williams, C. K. Exploiting Sodium Coordination in Alternating Monomer Sequences to Toughen Degradable Block Polyester Thermoplastic Elastomers. *Macromolecules* **2022**, *55* (6), 2290-2299. DOI: 10.1021/acs.macromol.2c00068.
(133) Gregory, G. L.; Sulley, G. S.; Kimpel, J.; Lagodzinska, M.; Häfele, L.; Carrodeguas, L. P.; Williams, C. K. Block Poly(carbonate-ester) Ionomers as High-Performance and Recyclable Thermoplastic Elastomers. *Angew. Chem. Int. Edit.* **2022**, *61* (47), e202210748 DOI: 10.1002/anie.202210748.

CHAPTER 2

Toughening CO_2-Derived Copolymer Elastomers Through Ionomer Networking

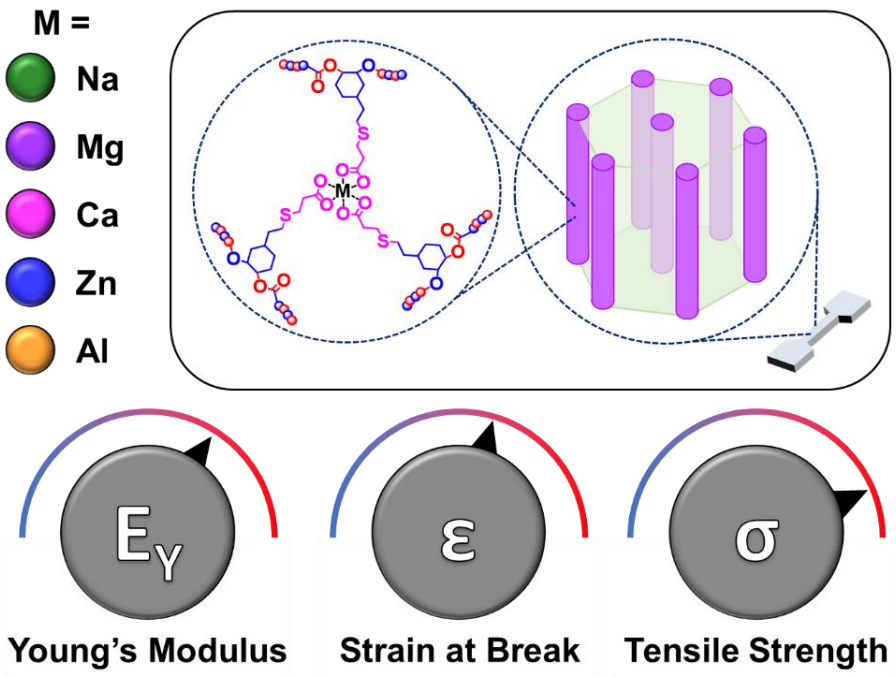

2.1 Introduction

In Nature, biopolymer-metal networks are often utilised to reinforce and toughen materials. Examples include peptide-iron-catechol complexes employed by marine mussels in byssal threads to adhere them to rocks in tidal regions;[1] zinc complexes that harden insect mandibles;[2] and calcium-polymer bonds which provide structural support in shells, bones, and skeletons.[3] Here, metal-polymer coordination chemistry is selected as a means to moderate elastomer properties since both the binding energy (thermodynamics) and ligand exchange lability (kinetics) are tuneable. This should allow for enhanced thermomechanical properties while maintaining the ability to mechanically reprocess the material. We hypothesised that from a common precursor, elastomeric properties might be modified by changing both the metal and loading used. This strategy could be advantageous since it would eliminate the need for new monomers or stereocomplex crystallisations to toughen thermoplastic elastomers (TPEs), both of which can be difficult to scale, control and may impact negatively upon recycling.

In fact, commercial elastomer-metal networks are known, sometimes referred to as ionomers when low metal loadings are applied. For example, the TPE ionomer Surlyn™ is a random copolymer of ethylene and methacrylic acid reinforced with sodium ions and is used in food packaging, medical devices, and sporting goods. So far, commercial ionomers feature rather ill-defined polymer structures and so deconvoluting influences of metal coordination chemistry would be very challenging. Recently, the incorporation of metals into better-defined polymer matrices has drawn interest for their responsive luminescence, self-healing, catalytic, and toughening potential.[4-7] Many of these materials have specific but limited applications, in part because of their intense colours.

Well-defined polymer-metal complex interactions are much better understood in soft materials, like hydrogels, and have shown real promise in improving material properties.[8-10]

There is much less investigation of their potential to moderate plastics or elastomers; material classes typically exhibiting 100-1000 times greater tensile strength and 10-100,000 times higher Young's modulus than gels. By applying strategies adopted in modern hydrogels, elastomers and plastics have the potential for dramatic improvements in mechanical properties.[11-16] One example, from Valentine *et al.*, demonstrated that incorporating iron-catechol interactions into a very low tensile strength polyether improved tensile strength and toughness.[17] In 2022, Williams and co-workers reported ABA block polymer TPEs (A=polyester, B= polyester/carbonate) featuring sodium-, or zinc-carboxylate complexation in the hard domains which showed high tensile strengths and Young's moduli.[18, 19] The correlations between material properties and either the nature of, or loading of, different metals is under-explored.

2.2 Aims

The work in this chapter aims to synthesise and characterise new types of carbon dioxide- (CO_2) and bio-derived TPEs. These are described together with a generally applicable method to augment thermomechanical properties without requiring material re-design. CO_2-derived polycarbonate, poly(vinyl-cyclohexene carbonate) (A-block), and bio-derived polyester, poly(ε-decalactone) (B-block), will be combined in an ABA block copolymer. These TPEs will combine high glass transition temperature (T_g) amorphous poly(carbonates) blocks (A-blocks), with low T_g poly(ε-decalactone) (B-block), derived from castor oil, in ABA structures.

The poly(carbonate) blocks will be selectively functionalised with metal-carboxylates through thiol-ene post polymerisation functionalisation. The polymer coordination chemistry will then be investigated with sodium(I), magnesium(II), calcium(II), zinc(II) or aluminium(III) as a strategy to reinforce A-block domains in TPEs. These metals are selected to be colourless, Earth-abundant, inexpensive, low-weight, non-toxic, and to feature strong bonding to carboxylic acids. The goals are to discover methods to moderate the TPE tensile strength, Young's modulus, and toughness without compromising elasticity, elastic recovery or recyclability.

The steps taken to achieve these aims will involve: 1) Synthesising poly(carbonate-*b*-ester-*b*-carbonate) triblock copolymers featuring alkene functionality in the outer blocks, this will then be exploited to install carboxylate ligands to every repeat unit of the poly(carbonate) blocks and coordinated to various metals and in various quantities; 2) The thermomechanical properties will then be explored to elucidate how valency and ionic radii of the metals employed can be used to tune material properties; 3) The ability for these novel materials to be mechanically recycled and degrade in aqueous environments will be studied. In future, it is hoped these materials could substitute high-volume petrochemical elastomers and be utilised in high-growth fields like medicine, robotics, and electronics.

2.3 Ionomer Synthesis

2.3.1 Synthesis of ABA Triblock Copolymer

The ABA triblock copolymer, poly(vinylcyclohexene carbonate-*b*-ε-decalactone-*b*-vinylcyclohexene carbonate) (PvCHC-PDL-PvCHC) was prepared using switchable catalysis in a one-pot process with a heterodinuclear [LZnMg(C_6F_5)$_2$] catalyst and 1,4-benzenedimethanol (BDM), as both initiator and chain transfer agent (CTA) (**Scheme 2.1**). Starting from a mixture of ε-decalactone (ε-DL) and 4-vinyl-cyclohexene oxide (vCHO), the [Zn(II)Mg(II)] metal catalyst first carries out the ring-opening polymerisation (ROP) of ε-DL, forming only a hydroxy telechelic poly(ε-decalactone) (PDL B-block). Next, the steel reactor was pressurised with CO_2 (20 bar), triggering a switch in polymerisation mechanism to the alternating ring-opening copolymerisation (ROCOP) of CO_2/epoxide and forming the desired ABA triblock copolymer (Figure S7.2.1). The benefits of this highly selective and well-controlled catalytic system are: (i) no need for any intermediate polymer isolation or purification, and (ii) production of monomodal, high molar mass polymers with high end-group fidelity (M_n > 50 kg mol^{-1}, $Đ_M$ = 1.2).[20]

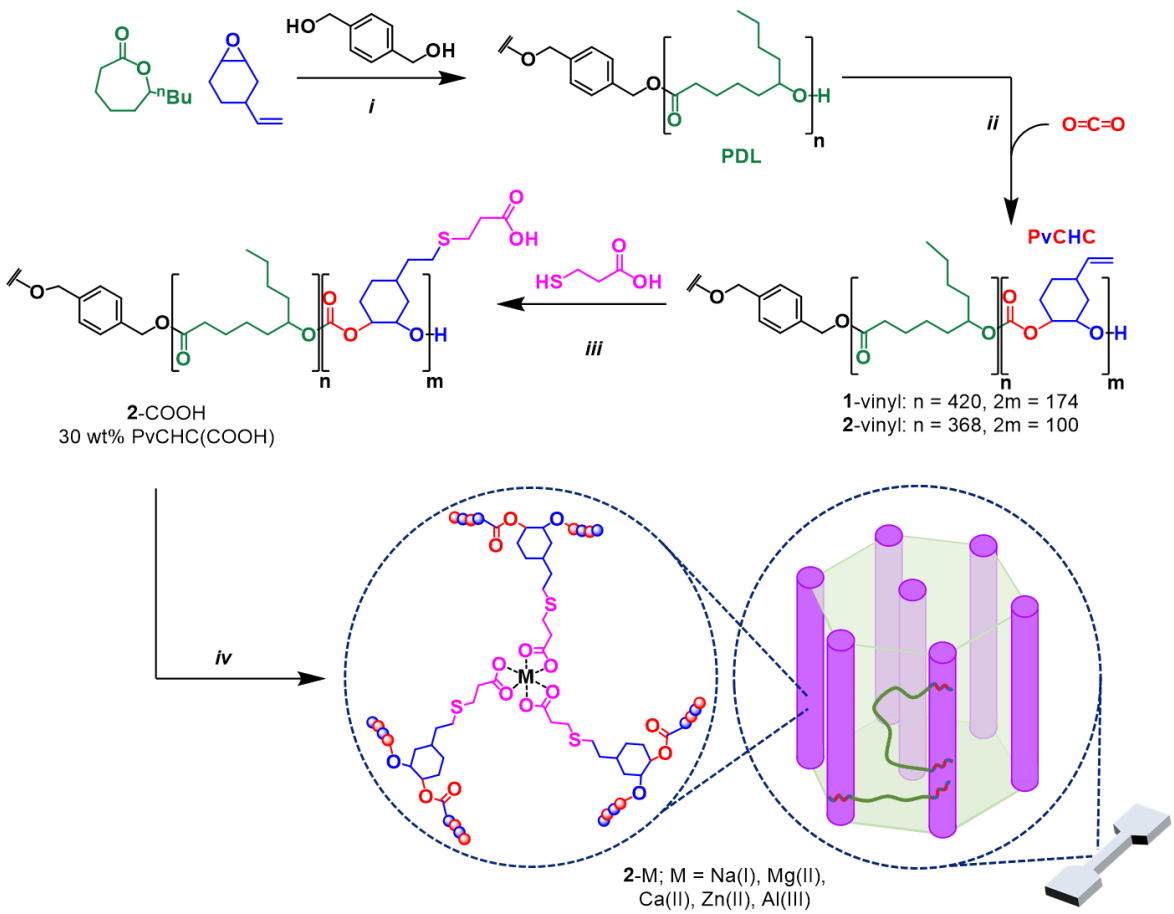

Scheme 2.1. Synthesis of poly(carbonate-*b*-ester-*b*-carbonate) ionomers. (i) *ε*-DL ROP at 80 °C catalysed by [LZnMg(C_6F_5)$_2$] with BDM as bifunctional initiator, where [Cat]$_0$/[BDM]$_0$/[ε-DL]$_0$ = 1/4/1644 (**1**-vinyl), [ε-DL]$_0$ = 1.7 M, toluene. (ii) CO_2/vCHO ROCOP, CO_2 (20 bar), 80 °C. PvCHC-PDL-PvCHC (**1**-vinyl): $M_{n,\,SEC}$ = 97 kg mol^{-1}($Đ_M$ = 1.09), 29 wt% PvCHC by ^{1}H NMR spectroscopy. **2**-vinyl: $M_{n,\,SEC}$ = 67 kg mol^{-1}($Đ_M$ = 1.12), 21 wt% PvCHC. (iii) Thiol-ene functionalisation (rt, 1 h) with 3- mercaptopropionic acid (3-MPA) and DMPA photoinitiator, 365 nm. [**2**-vinyl] = 5 wt %, THF. For P_{COOH}CHC-PDL-P_{COOH}CHC (**2**-COOH), 30 wt% P_{COOH}CHC. (iv) Coordination of Na(I), Mg(II), Ca(II), Zn(II) and Al(III) to P_{COOH}CHC carboxylate ligands. [**2**-COOH] = 5 wt%, THF. [COOH]$_0$/[M]$_0$ = 10/1 for screening of the different metal crosslinkers. 50 mM stock solutions of NaOTf, Al(OTf)$_3$ in THF and Mg(OTf)$_2$, Ca(OTf)$_2$, Zn(OTf)$_2$) in H_2O used to add desired quantity of metals.

As an example of how this reaction was conducted, ε-DL, vCHO, BDM and [LZnMg(C_6F_5)$_2$] catalyst were dissolved in toluene and reacted at 80 °C, for 120 min ([LZnMg(C_6F_5)$_2$]$_0$ = 1.0 mM, [LZnMg(C_6F_5)$_2$]:[BDM]:[vCHO]:[ε-DL] = 1:4:938:1645). The ROP of ε-DL occurred in high conversion to form the PDL block (90%, TOF = 740 h^{-1}), as confirmed by ^{1}H NMR spectroscopy from a reaction aliquot (**Table 2.1**). Then, the reaction mixture was transferred into a pressurised steel Parr reactor, the atmosphere was replaced with CO_2 (20 bar), and heated to 80 °C to switch to the efficient ROCOP of vCHO/CO_2. After stirring for 48 h, the reactor was cooled and depressurised, at which point analysis by ^{1}H NMR spectroscopy indicated 84% conversion to the desired PvCHC 'hard' blocks (>99% CO_2 selectivity, >99% polymer selectivity, TOF = 13 h^{-1}).

Table 2.1: Summary of Polymerisation Conditions and Results

	PDL ROP				**PvCHC**-PDL-**PvCHC** ROCOP				
	Temp (°C)	Time (min)	[a]Conv. (%)	[b]$M_{n,SEC}$ [c]$[Đ_M]$ (kg mol^{-1})	Temp. (°C)	Time (h)	[a]Conv. (%)	[b]$M_{n,SEC}$ [c]$[Đ_M]$ (kg mol^{-1})	[d]$M_{n,NMR}$ (kg mol^{-1})
1-vinyl	80	120	90	81.8 [1.12]	80	48	84	96.7 [1.09]	100.7
2-vinyl	80	90	89	41.4 [1.11]	80	48	80	67.3 [1.12]	79.4

[a]Determined from ^{1}H NMR spectrum of crude polymer sample. [b]Determined from SEC analysis (THF, 1 mL min^{-1}); calibrated with narrow poly(styrene) standards. [c]M_w/M_n. [d]Determined from ^{1}H NMR spectrum of purified polymer sample.

Further analysis by ^{1}H NMR spectroscopy, of the isolated material after precipitation (**1**-vinyl) in MeOH, established it comprised 29 wt% PvCHC (A-block). This value was deduced by comparing integrals of resonances at 2.27 ppm (PDL main-chain –C*H*$_2$–) and 5.76 ppm (PvCHC –C*H*=CH$_2$) (**Figure 2.1**). By comparing the integrals of the initiator (BDM) aromatic resonances at, 7.34 ppm, with those corresponding to PDL and PvCHC, at 2.27 and 5.76 ppm respectively, $M_{n,\,NMR}$ was calculated as 100.7 kg mol^{-1} and the average DPs for the blocks were 87:420:87 (PvCHC-PDL-PvCHC). ^{13}C{^{1}H} and ^{1}H - ^{13}C HSQC NMR spectroscopy provided additional support for the PvCHC-PDL-PvCHC triblock copolymer structure (Figure S7.2.2-S7.2.3).

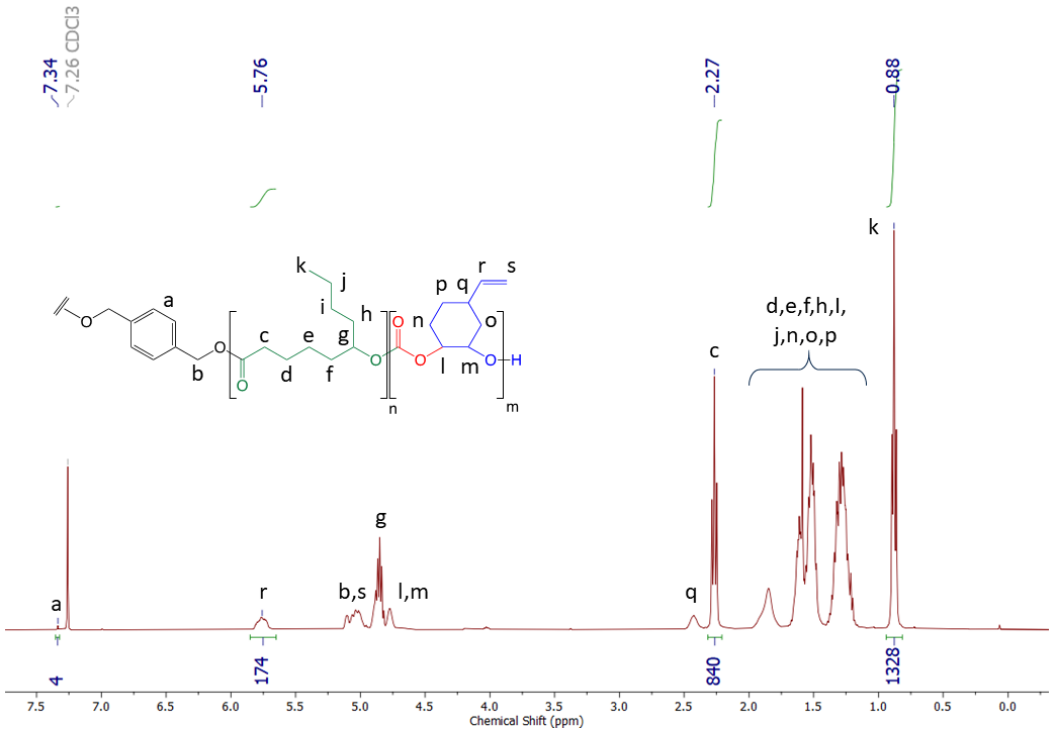

Figure 2.1: ^{1}H NMR (400 MHz, $CDCl_3$) spectrum of poly(vinylcyclohexene carbonate-*b*-ε-decalactone-*b*-vinylcyclohexene carbonate) (**1**-vinyl) triblock copolymer.

This material, **1**-vinyl, showed a high molar mass (number average molecular weight, M_n = 97 kg mol^{-1}) and narrow dispersity ($Đ_M$ = 1.09) which were determined by size-exclusion chromatography, SEC (**Figure 2.2**). There was an significant increase in molar mass by SEC for **1**-vinyl triblock copolymer relative to the intermediatory PDL block. This indicated that the CO_2/vCHO ROCOP was initiated from the hydroxy telechelic end groups of PDL, and that **1**-vinyl adopts a triblock copolymer architecture.

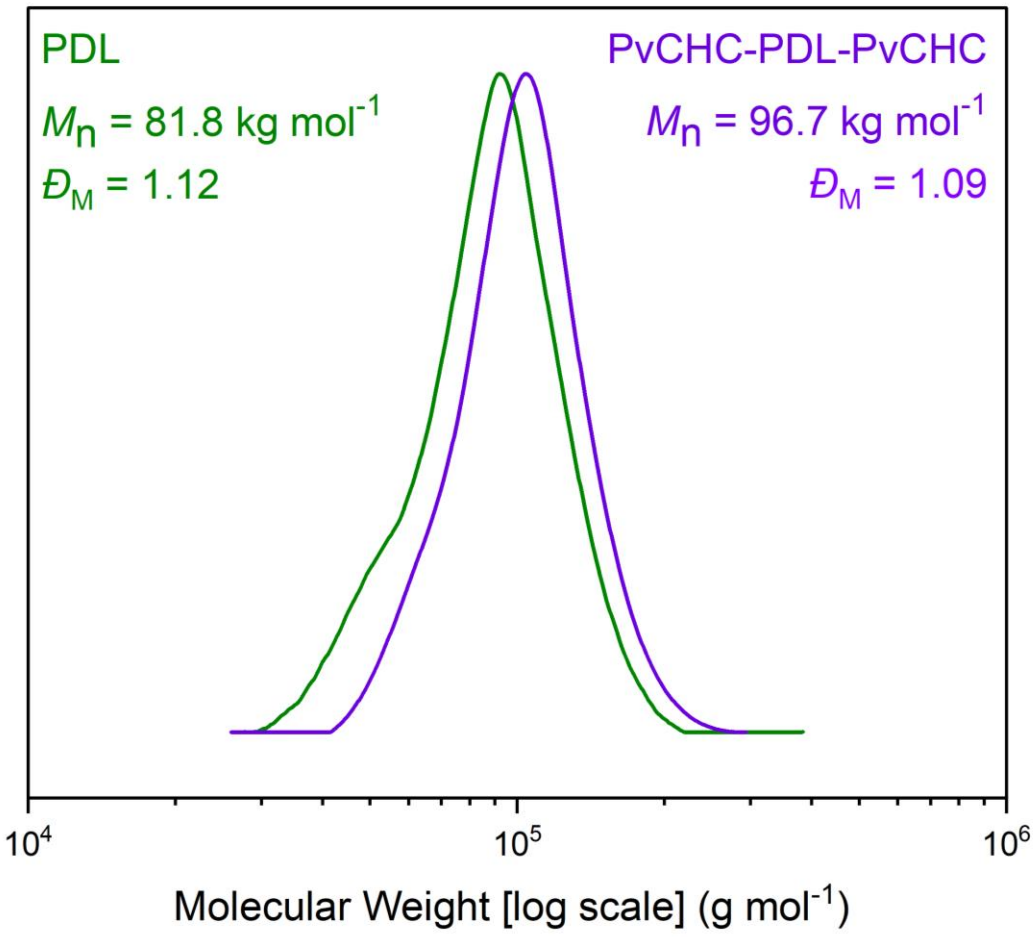

Figure 2.2: SEC (THF, 1 mL min^{-1}) traces for PDL block aliquot and purified PvCHC-PDL-PvCHC (**1**-vinyl). Calibrated with poly(styrene) standards.

The desired ABA triblock copolymer structure was further confirmed by analysis of chain end-groups, by $^{31}P\{^{1}H\}$ NMR spectroscopy after treatment with a phospholane reagent (2-chloro-4,4,5,5-tetramethyl dioxaphospholane), which showed the exclusive formation of hydroxyl telechelic polymers originating from the outer PvCHC (A-block) at 146.8 ppm and the absence of PDL hydroxy end-groups at 147.1 ppm (**Figure 2.3**).[21] Moreover, this disappearance of PDL end-groups confirms no transesterification taking place during the polymerisation, which would result in block scrambling and the presence of both PvCHC and PDL end-group.

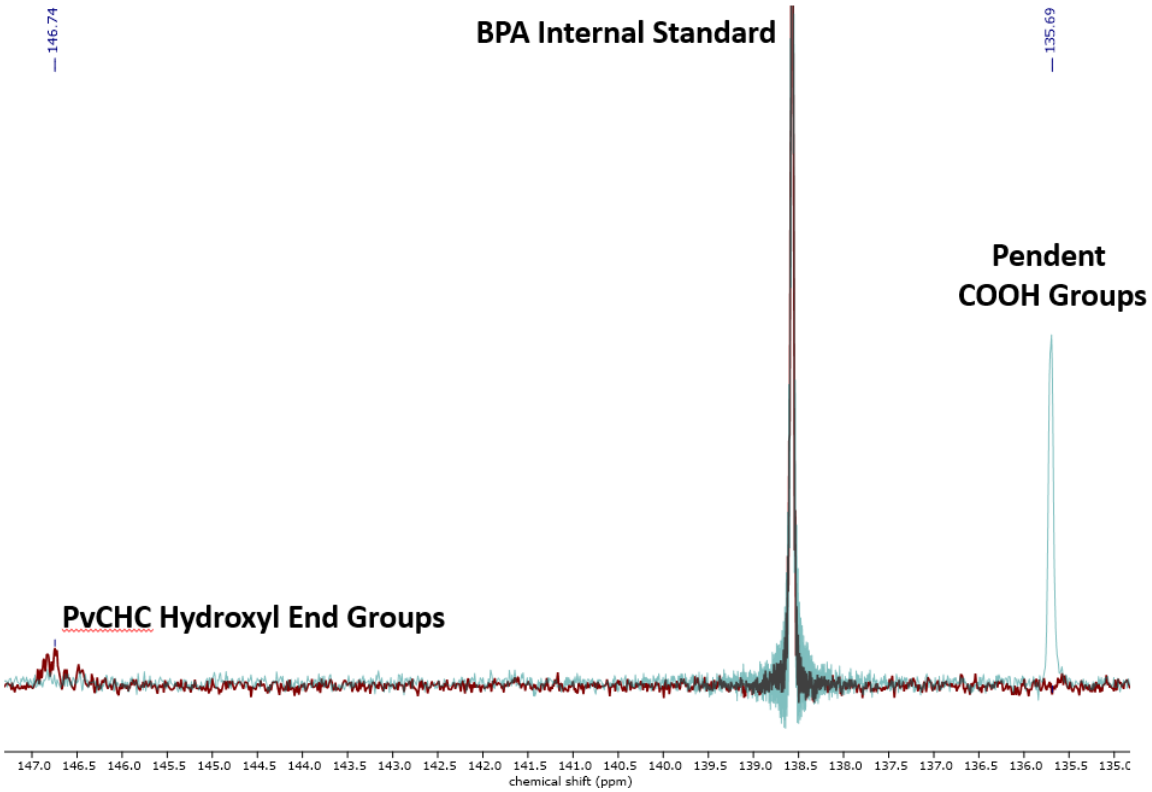

Figure 2.3: $^{31}P\{^{1}H\}$ NMR end-group analysis of **1**-vinyl poly(vinylcyclohexene carbonate-*b*-ε-decalactone-*b*-vinylcyclohexene carbonate) [red] triblock copolymer and thiol-ene functionalised **2**-COOH [blue]. No signal for PDL hydroxyl end-groups (147.1 ppm) observed for either material.

2D DOSY ^{1}H NMR spectroscopy displayed a single diffusion coefficient for all signals consistent with the blocks in a copolymer (**Figure 2.4**). This is further evidence of the formation of a block copolymer architecture opposed to a mixture of homopolymers.

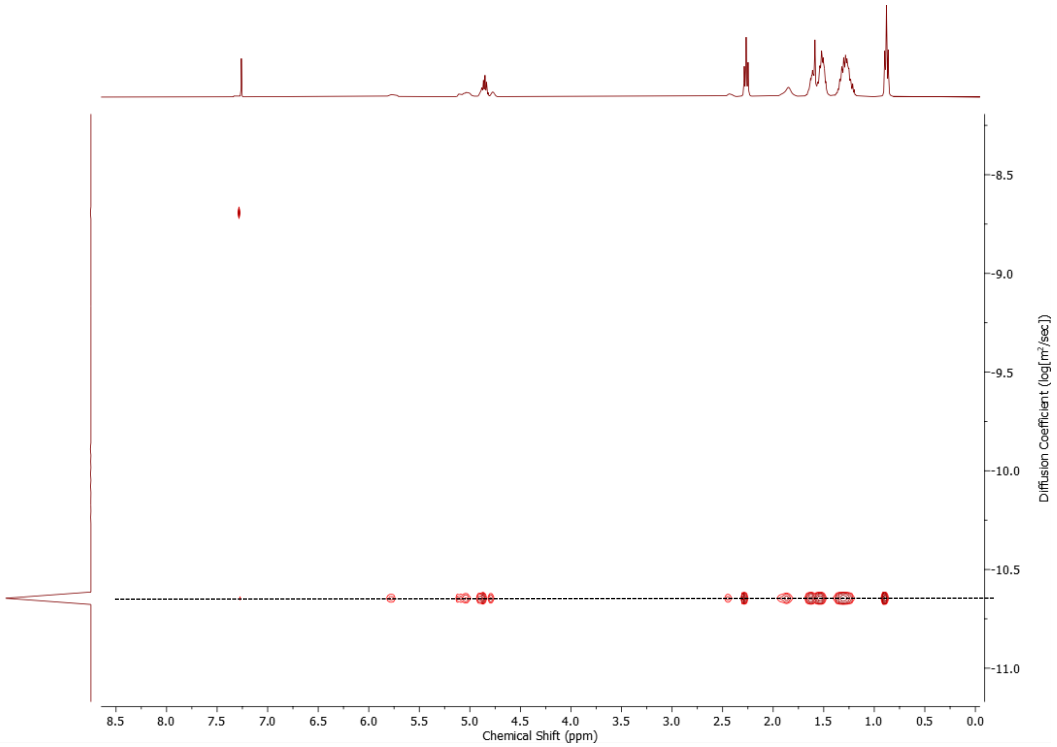

Figure 2.4: ^{1}H DOSY NMR (500 MHz, $CDCl_3$) spectrum of poly(vinylcyclohexene carbonate-*b*-ε-decalactone-*b*-vinylcyclohexene carbonate) (**1**-vinyl) triblock copolymer.

2.3.2 Thiol-ene Functionalisation

Next, carboxylic acids were installed onto every polycarbonate repeat by using a UV-initiated 'thiol-ene' reaction between the polymer vinyl substituents and 3-mercaptopropionic acid (3-MPA). To allow for proper comparison between equivalent 'unfunctionalised' and ionomeric elastomers, a constant polycarbonate (A-block) weight fraction (%) was used for all polymers. Here the weight fractions of the constituent blocks is used as a proxy for their volume fractions and handle to maintain consistent microphase separated morphologies across the series of materials. Accordingly, a second unfunctionalised block polymer featuring a lower (21 wt%) polycarbonate content was synthesised (**2**-vinyl), with this material delivering 30 wt%

polycarbonate block and an $M_{n,\,NMR}$ of 106.6 kg mol^{-1} after carboxylic acid installation (**2**-COOH, **Table 2.2**).

Table 2.2: ABA Triblock Characterisation Data

Polymer	[a]DP PvCHC : PDL : PvCHC	[a]wt% Hard Block	[a]$M_{n,NMR}$ [kg mol^{-1}]	[b]$M_{n,SEC}$ [kg mol^{-1}]	[c]$Đ_M$	Classification
1-vinyl	87 : 420 : 87	29	100.7	96.7	1.09	Elastomer
2-vinyl	50 : 368 : 50	21	79.4	67.3	1.12	Viscoelastic Liquid
2-COOH	50 : 368 : 50	30	106.6	43.0	1.45	Elastomer

[a]Determined from ^{1}H NMR spectrum of purified samples (**Figure 2.1**). [b]Determined from SEC analysis (THF, 1 mL min^{-1}); calibrated with narrow poly(styrene) standards (**Figure 2.2 & 2.7**). [c]M_w/M_n.

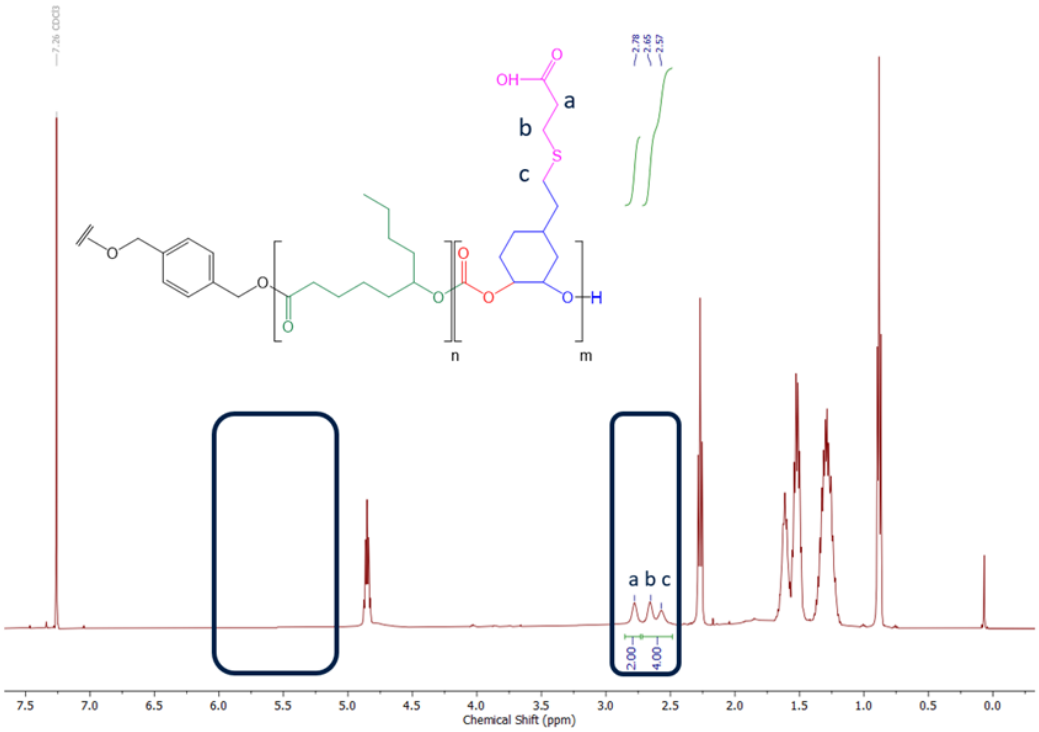

Figure 2.5: ^{1}H NMR (400 MHz, $CDCl_3$) spectrum of P_{COOH}CHC-PDL- P_{COOH}CHC (**2**-COOH).

Quantitative carboxylic acid functionalisation was confirmed using ^{1}H NMR spectroscopy, which showed the disappearance of the vinyl resonances at 4.98 and 5.76 ppm and the appearance of three new signals at 2.57, 2.65 and 2.78 ppm corresponding to the pendent carboxylic acid side chains (**Figure 2.5**). The ^{13}C{^{1}H} NMR spectra confirmed complete consumption of the vinyl signals (114, 142 ppm) and formation of a new carboxylic acid signal (177 ppm) without changes to polymer carbonate resonances (153 ppm, **Figure 2.6**).

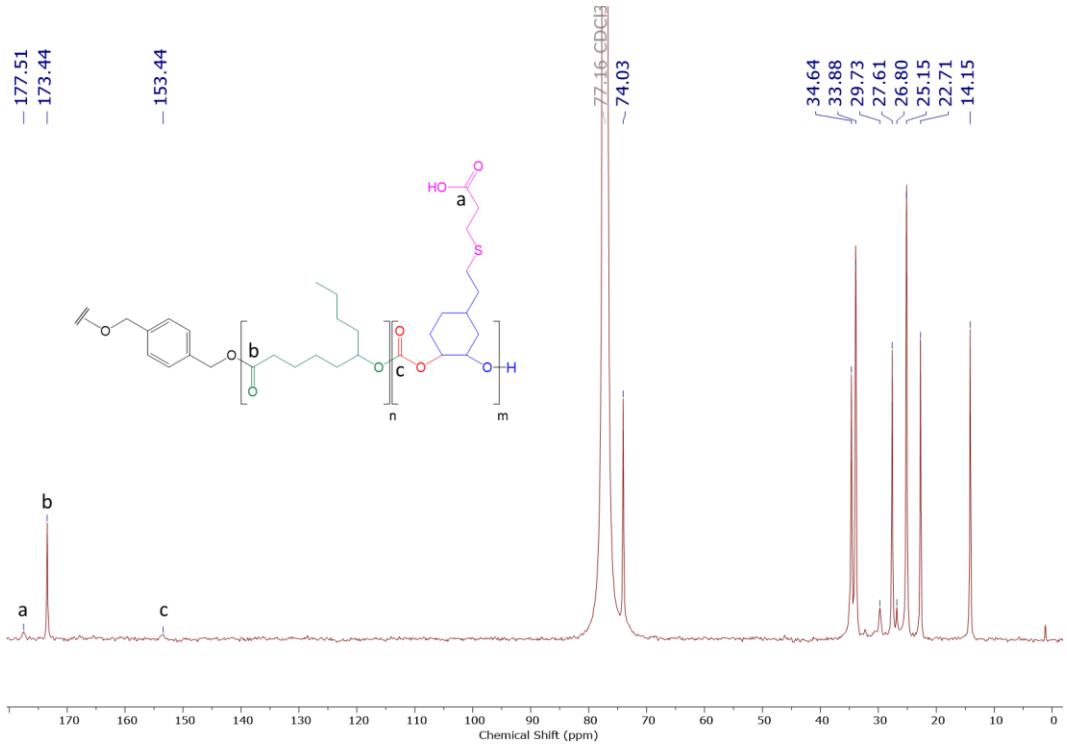

Figure 2.6: ^{13}C NMR (100.58 MHz, $CDCl_3$) spectrum of functionalised P_{COOH}CHC-PDL-P_{COOH}CHC (**2**-COOH).

SEC analyses revealed a slight decrease in the overall polymer molar mass after functionalisation, but with retention of a monomodal distribution (**2**-COOH, **Figure 2.7**). The decrease in molar mass is likely an SEC feature since the carboxylic acids are likely to significantly change the polymers' hydrodynamic radius. By capping the pendant carboxylic acid groups through the addition of an excess of 2-chloro-4,4,5,5-tetramethyl

dioxaphospholane, the inter-chain hydrogen bonding was disrupted and SEC revealed an increase in average molar mass and narrowing of dispersity (**Figure 2.3 & 2.7**). The $M_{n,NMR}$ showed the expected increase in molar mass after functionalisation. There was no evidence for any backbone degradation or high molar mass shouldering/tailing indicative of vinyl-vinyl crosslinking, by either SEC or NMR analyses.

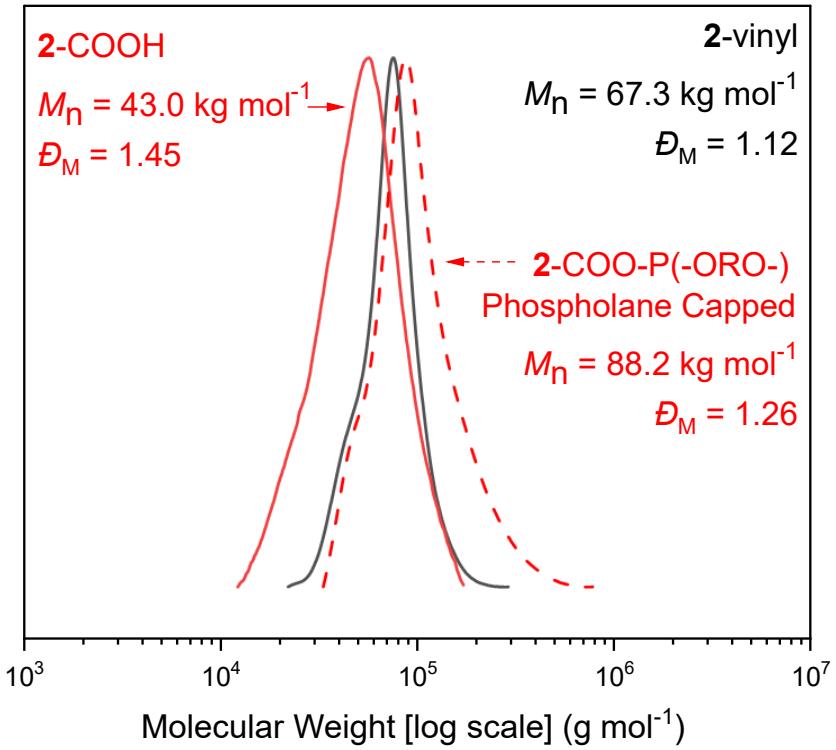

Figure S2.7: SEC (THF, 1 mL min^{-1}) traces for purified PvCHC-PDL-PvCHC (**2**-vinyl), functionalised P_{COOH}CHC-PDL- P_{COOH}CHC (**2**-COOH) and phospholane capped **2**-COOH. Calibrated with poly(styrene) standards.

The ^{1}H DOSY NMR spectrum showed a single diffusion coefficient consistent with the polymer structure (Figure S7.2.4). There was also a significant change in material properties, with **2**-vinyl behaving as a viscoelastic liquid, while **2**-COOH is an elastomeric solid (**Figure 2.8**).

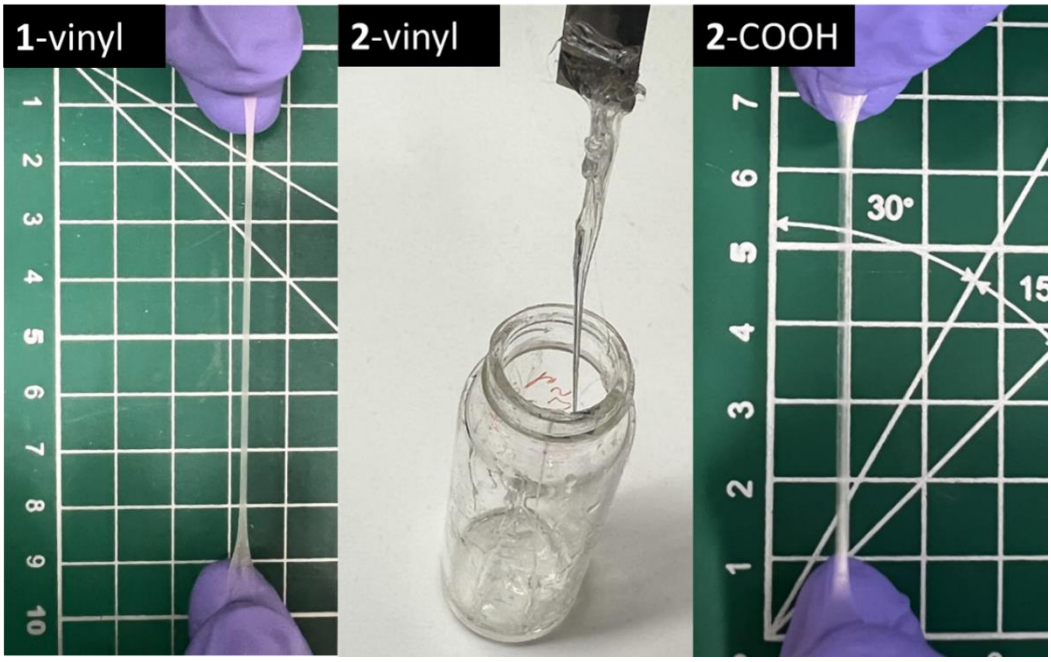

Figure 2.8: Photograph of viscoelastic liquid **2**-vinyl and elastic solids **1**-vinyl and **2**-COOH.

The IR spectra showed the disappearance of the vinyl resonance (1641 cm^{-1}) indicative of complete thiol-ene functionalisation (**Figure 2.9**). A broadening of the carbonyl resonance (1728 cm^{-1}) arises from the addition of acid carbonyl groups within the material as a result of the post-polymerisation functionalisation.

2.3.3 Metal Complexation

From **2**-COOH, a series of metal complex ionomers were synthesised using sodium(I), magnesium(II), calcium(II), zinc(II), and aluminium(III). These metals were selected on the basis of Earth-abundance, low cost, low weight, their strong precedent for reacting with carboxylic acids, and lack of colour upon coordination. By using mono-, di- and trivalent metals it is possible to compare the influences of metal ionic radii and coordination chemistries on the elastomer properties. All ionomer syntheses were scalable; thus, 10.4 g of **2**-vinyl was transformed into 9.0 g of **2**-COOH which was used for all subsequent metal complexation reactions. To investigate the influences of the different metals, a common molar ratio of (Polymer)-COOH : metal, 10:1 was targeted, i.e. 10, 20 or 30% metal-carboxylate formation

and neutralisation depending upon the valency of the metal. The ionomers were each synthesised by stirring a solution of **2**-COOH (5 wt% in THF) with the appropriate metal triflate salt (a 50 mM solution of NaOTf, $Al(OTf)_3$ in THF, or $Mg(OTf)_2$, $Ca(OTf)_2$, $Zn(OTf)_2$ in H_2O) for 10 minutes, at room temperature. Triflate salts were employed due to their favorable solubility in organic solvents, their weakly coordinating counter anion, and to maintain a consistent synthetic protocol, allowing for fair comparisons to be made between the ionomers produced. The products were precipitated (methanol), washed with water to remove any released triflic acid, dried under reduced pressure and compression moulded into thin films (120 °C, 1 tonne, 10 min). The resulting films had variable but low metal weight contents (0.3- 0.8 wt% overall) and consistent metal mol% (10%).

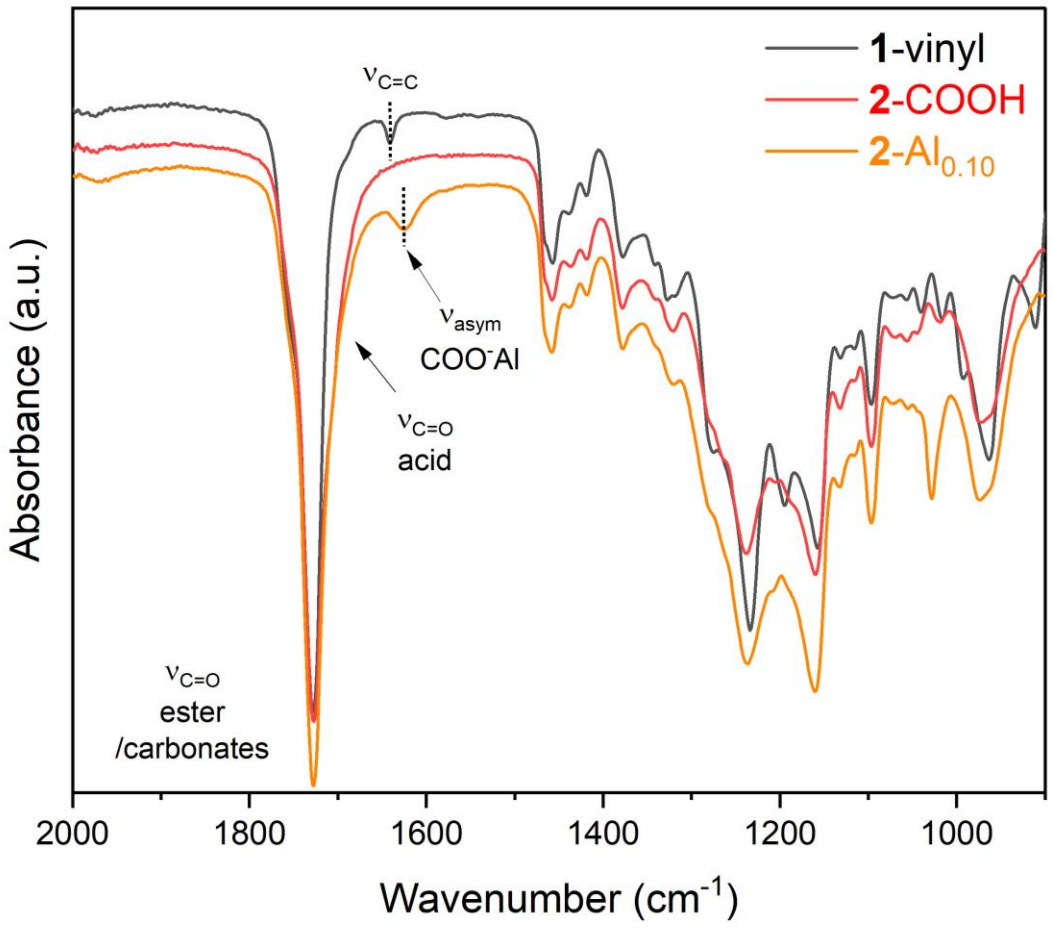

Figure 2.9. FTIR spectra of polymer films comparing the unfunctionalised (**1**-vinyl), carboxylic acid functionalised (**2** COOH) and aluminium ionomer (**2**-$Al_{0.10}$) materials.

The samples are henceforth referred to as **2**-$M_{x.xx}$, (M = metal employed, x.xx = metal loading relative to COOH groups). Formation of the $(-COO)_xM$ moieties (x = 1, 2, or 3) in the final film was supported by a range of spectroscopic techniques. FTIR spectroscopy confirms the metal-carboxylate coordination as exemplified by **2**-$Al_{0.10}$ showed a clear peak at 1627 cm^{-1} consistent with metal carboxylate formation (**Figures 2.9** & S7.2.5-S7.2.11).[16, 18, 22, 23] For **2**-$Na_{0.10}$, **2**-$Mg_{0.10}$, **2**-$Ca_{0.10}$, **2**-$Zn_{0.10}$ clear metal-carboxylate peaks could not be easily observed. This is attributed to the low concentration of metal-carboxylate bonds for the mono- and divalent metals. However, when this concentration was increased in the synthesis of **2**-$Na_{1.00}$, **2**-$Mg_{1.00}$, **2**-$Ca_{1.00}$ and **2**-$Zn_{1.00}$, new signals at 1570, 1567, 1578 and 1574 cm^{-1}, respectively, were observed. All the ionomer films appeared optically transparent and this was confirmed by UV-vis spectroscopy of all films produced (**Figures 2.10** & S7.2.12-S7.2.20). Optical transparency is critical to ensure these ionomers are suitable for a whide range of applications, avoiding the limitations of other intensely coloured networked materials.

Figure 3.10: Photo of colourless **2**-$Al_{0.10}$ disk on printed colour background.

Coordination of Al(III) to the carboxylate ligands was also confirmed by solid-state ^{27}Al NMR spectroscopy using a film of **2**-$Al_{0.10}$ (**Figure 2.11**). Signals at 182 and -202 ppm, which arise from ^{27}Al-^{19}F coupling in $Al(OTf)_3$ disappeared, consistent with the loss of triflate anions, and a new broad singlet at -6 ppm suggests there is a single aluminium-carboxylate coordination environment within the ionomer network.

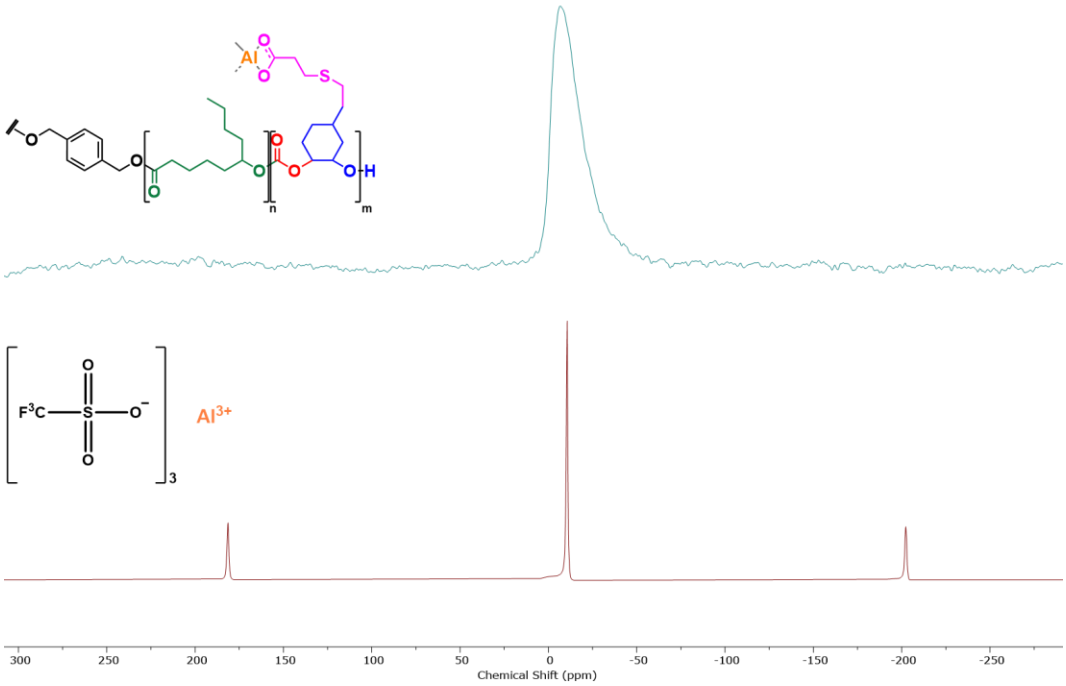

Figure 2.11: Solid-state ^{27}Al NMR spectra of **2**-$Al_{0.10}$ film (top) and aluminium triflate precursor (bottom).

2.4 Material Characterisation

2.4.1 Thermal Properties

The polymeric materials were all amorphous with phase-separated microstructures, as determined by differential scanning calorimetry (DSC). Indeed, the two glass transition temperatures (T_g) observed in the DSC thermograms are consistent with the values observed for the constituent polymer blocks (**Figure 2.12**). The lower glass transition temperature ($-46 \leq T_g \leq -54$ °C) corresponds to the PDL block. Interestingly, samples with **2**-COOH and **2**-$M_{x.xx}$ displayed slightly lower values, in both DSC and dynamic mechanical thermal analyses (DMTA) profiles, likely due to greater block incompatibility between the non-polar PDL and more hydrophilic hard-blocks. The upper glass transition temperature, corresponding to the hard-blocks, was only detected by DSC for the unfunctionalised **1**-vinyl (T_g = 105 °C) however could be observed by DMTA (*vide infra*).

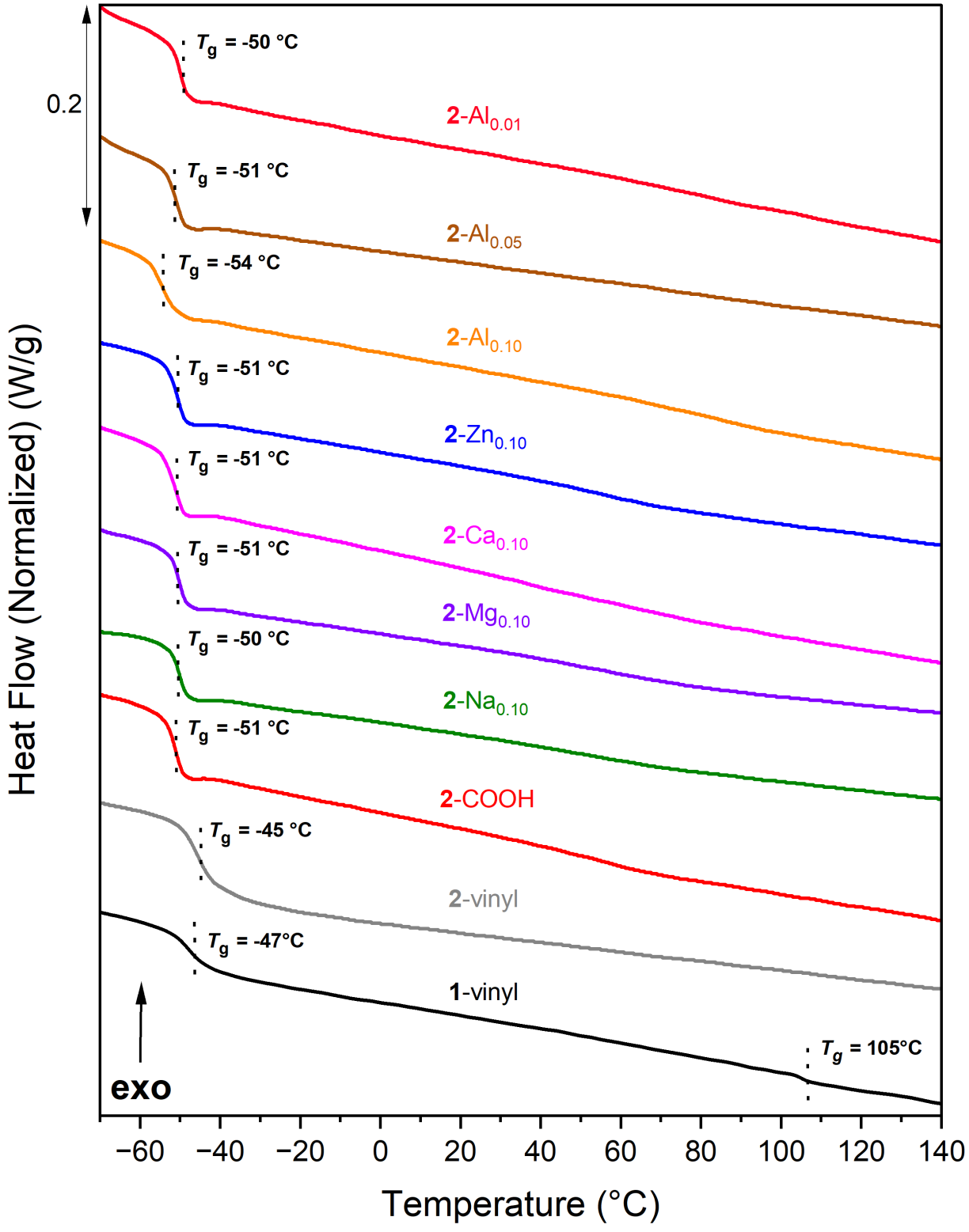

Figure 2.12: Differential Scanning Calorimetry (DSC) data for the polymers.

A better insight into the thermal transition and thermomechanical propeties of the PvCHC functionalised A-block domains was obtained by DMTA. Temperature ramps were conducted on thin films under tension for all the materials (3 °C min^{-1}, 0.1 % strain, 1Hz), from -80 to 250 °C or when the material deformed to the limits of the geometry. Thus, thin films of **2**-COOH, **2**-$Na_{0.10}$, **2**-$Mg_{0.10}$, **2**-$Ca_{0.10}$ and **2**-$Zn_{0.10}$ displayed distinct peaks in their tan(δ) profile (80–100 °C, **Figure 2.13, 2.14**, S7.2.21-S7.2.27, Table S7.2.1), a clear indicator of the T_g of the polycarbonate blocks.

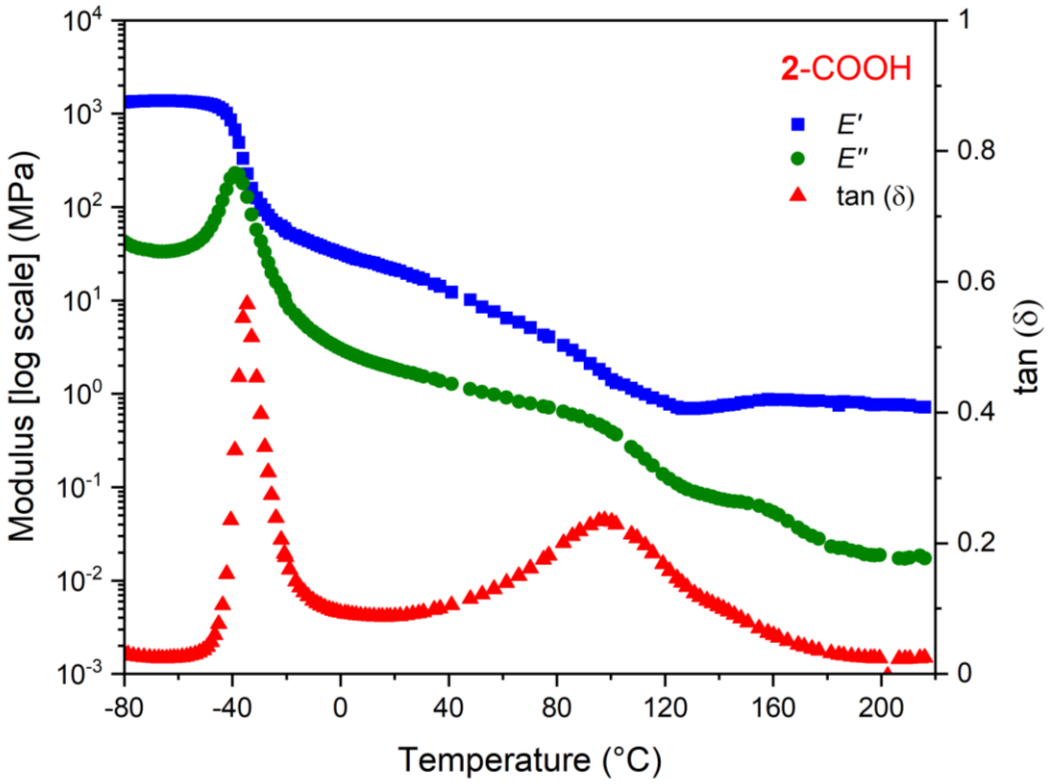

Figure 4.13: Dynamic mechanical thermal analysis (DMTA) temperature sweeps for the carboxylic acid functionalised materials **2**-COOH.

For **2**-$Al_{0.10}$, a low-intensity, diffuse peak at a significantly higher temperature (136 °C) was attributed to greater crosslink density afforded by the trivalent metal which restricts chain segmental motion. This property provides the material with an extended rubbery plateau

compared to the other ionomers spanning, from -20 to 200 ˚C, over-which range the material maintained its constant storage modulus.

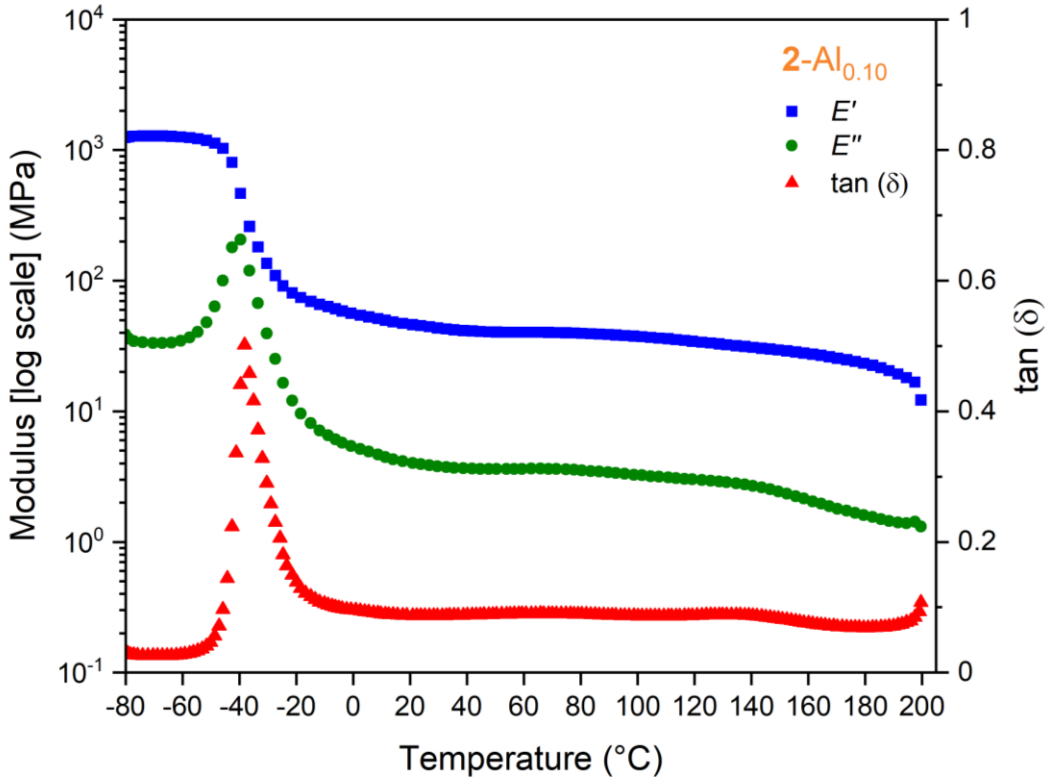

Figure 5.14: Dynamic mechanical thermal analysis (DMTA) temperature sweeps for the aluminium ionomer **2**-$Al_{0.10}$.

Finally, the high thermal stability, as determined by thermogravimetric analysis ($T_{d,5\%}$ > 250 ˚C), indicates a wide processing window for all polymers (Figures S7.2.28-S2.7.37). For all materials reported, there is a low-temperature shoulder on the principal peak in the derivative of the mass loss curve. This more clearly shows that the mass loss occurs in two stages. This is not as clear as one might expect in just the thermogram as the weight content of the polycarbonate blocks is low in the elastomeric regime. The derivative better shows that the polycarbonate A-blocks are degrading first, followed by the central PDL B-block. This suggests that thermal degradation occurs by a chain end-initiated decomposition.

2.4.2 Small-Angle X-Ray Scattering

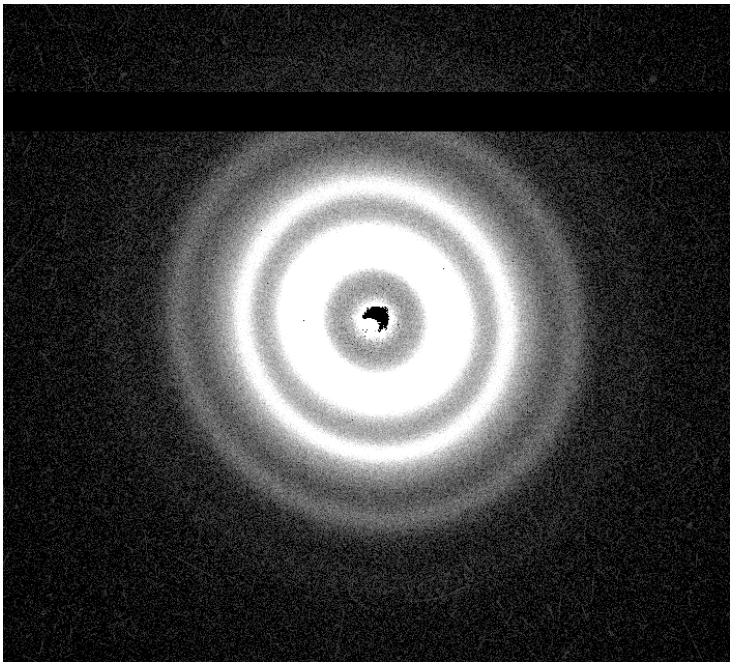

Figure 2.15: Representative SAXS scattering pattern (**2**-$Al_{0.05}$).

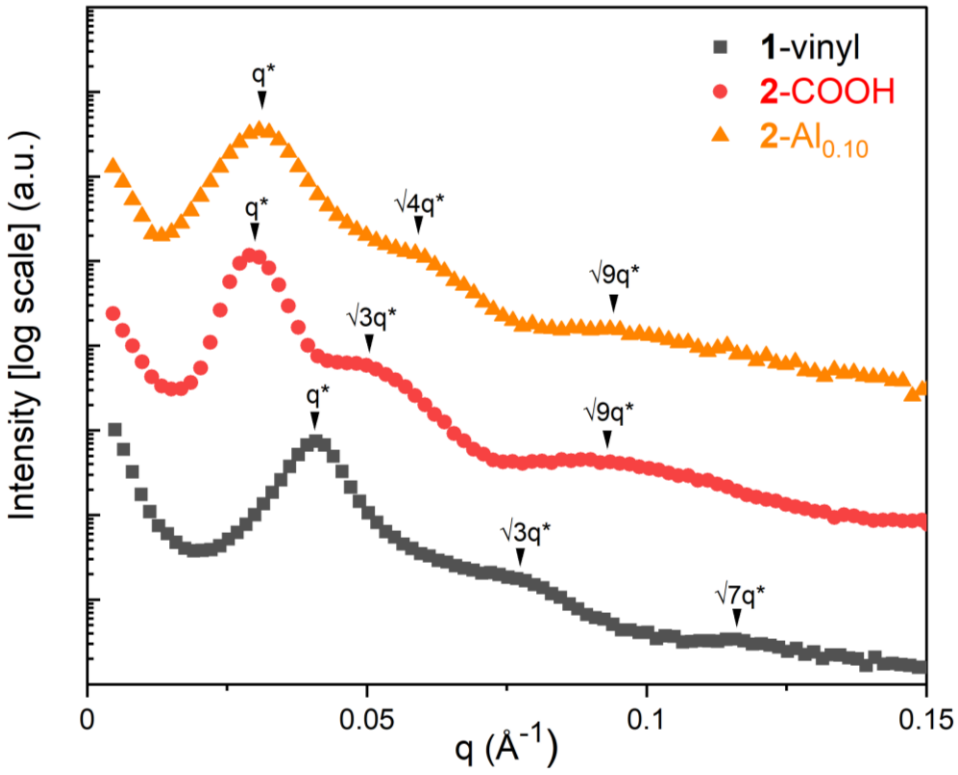

Figure 2.16: Room-temperature small-angle X-ray scattering (SAXS) profiles showing principle scattering peaks (q*) and higher-order peaks (q/q*).

To better understand the block polymer morphologies, small-angle X-ray scattering (SAXS) was conducted on all films, at room temperature (**Figure 2.15**). No pre-treatment was conducted to better reflect the 'true morphology' of samples used in subsequent mechanical testing (**Table 2.3** & Figures S7.2.38-S7.2.43). All polymers exhibit hexagonally packed cylindrical morphologies, as indicated by common higher-order scattering peaks ($q/q^* = \sqrt{3}$, $\sqrt{4}$, $\sqrt{7}$ and $\sqrt{9}$). This finding is important since it allows for comparisons of the metal influences without altering their phase-separated microstructures. The domain sizes ($d = 2\pi/q^*$), determined from the principle scattering peaks (q^*), increased slightly after functionalisation from 15 nm for **1**-vinyl to 21 and 20 nm for **2**-COOH and **2**-$Al_{0.10}$, respectively (**Figure 2.16, Table 2.3**). All the ionomers have domain sizes between 20 and 27 nm. This increase in domain spacing upon functionalisation is consistent with both carboxylic acid hydrogen bonding and metal-ligand coordination interactions within the hard domains.

Table 2.3: Summary of the SAXS data.

Material	q^*/ Å^{-1}	d/nm	High Order Peaks /q/q^*	Assigned Morphology
1-vinyl	0.041	15.4	$\sqrt{3}$, $\sqrt{7}$	HEX
2-COOH	0.029	21.4	$\sqrt{3}$, $\sqrt{9}$	HEX
2-$Na_{0.10}$	0.026	23.4	$\sqrt{4}$, $\sqrt{12}$	HEX
2-$Mg_{0.10}$	0.031	20.2	$\sqrt{3}$, $\sqrt{9}$	HEX
2-$Ca_{0.10}$	0.028	22.2	$\sqrt{3}$, $\sqrt{9}$	HEX
2-$Zn_{0.10}$	0.030	20.9	$\sqrt{4}$, $\sqrt{9}$	HEX
2-$Al_{0.10}$	0.031	20.2	$\sqrt{4}$, $\sqrt{9}$	HEX
2-$Al_{0.05}$	0.023	27.2	$\sqrt{4}$, $\sqrt{9}$, $\sqrt{13}$	HEX
2-$Al_{0.01}$	0.027	23.0	$\sqrt{4}$, $\sqrt{9}$	HEX

Where q^* = principle scattering peak ($d = 2\pi/q^*$), HEX = hexagonally packed cylinders.

2.4.3 Mechanical Properties

To study how the mechanical properties changed with metal-carboxylate coordination chemistry and to assess the stress-strain relationships of the thermoplastic elastomers, specimens were subjected to uniaxial extension experiments, according to ISO 527 (10 mm min^{-1}) (**Figure 2.17**). It was anticipated that a range of mechanical properties would be accessed by changing the valency and ionic radii of the metals. For each material, five repeat experiments were conducted, and the average values and errors, for the Young's modulus, tensile strength, strain at break and tensile toughness were compared (**Table 2.4**).

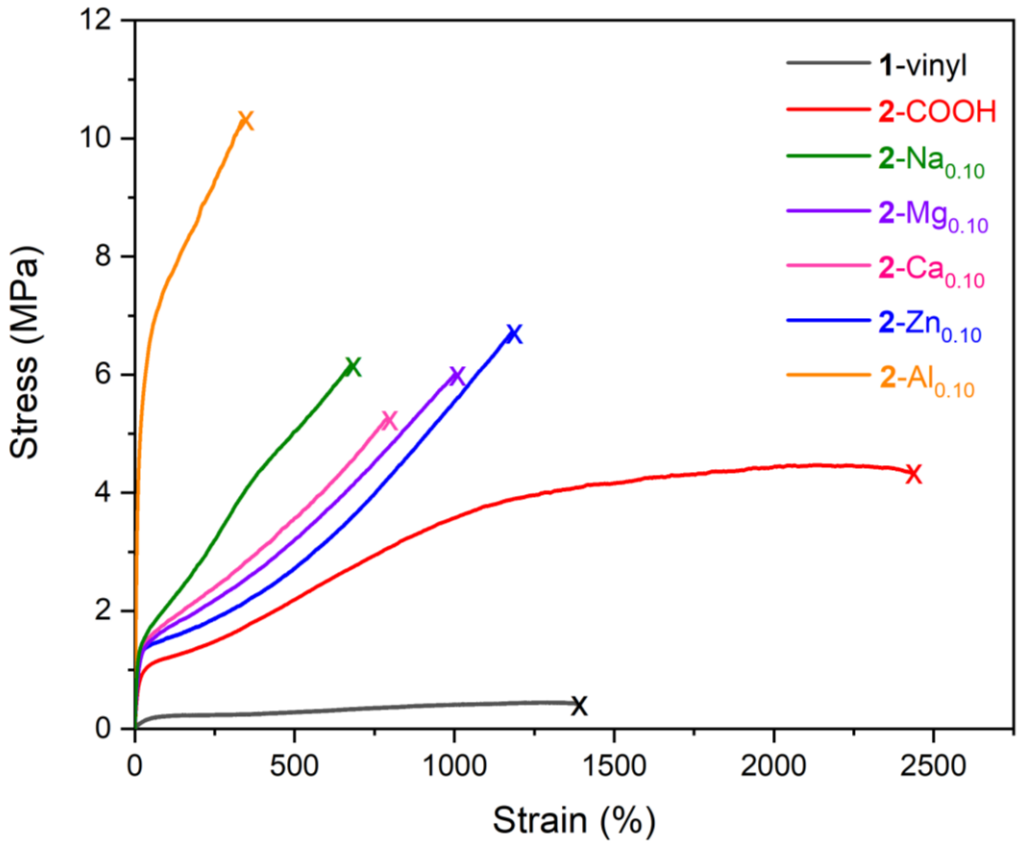

Figure 2.17: Representative stress-strain curves (10 mm min^{-1} extension rate).

Table 2.4: Summary of thermal and mechanical properties of CO_2-derived triblock copolymer elastomers.

Polymer	Metal [wt%]	[a]T_{g1}, [°C]	[b]T_{g2} [°C]	[c]$T_{d,5\%}$ [°C]	[d]E_y [MPa]	[e]σ [MPa]	[f]ε_b [%]	[g]U_T [MJ m^{-3}]	[h]Elastic Recovery [%]
1-vinyl	0.00	-46	105*	309	1.0 ± 0.1	0.5 ± 0.02	1373 ± 93	4.7 ± 0.3	81
2-COOH	0.00	-51	100	287	9.0 ± 0.4	4.4 ± 0.1	2615 ± 175	88.4 ± 7.6	92
2-$Na_{0.10}$	0.29	-50	91	285	18.8 ± 1.3	6.4 ± 0.4	610 ± 59	24.4 ± 3.4	78
2-$Mg_{0.10}$	0.30	-51	80	290	11.5 ± 0.4	6.0 ± 0.3	996 ± 62	33.9 ± 2.1	88
2-$Ca_{0.10}$	0.50	-51	82	290	13.2 ± 0.2	5.2 ± 0.7	790 ± 81	24.3 ± 4.8	88
2-$Zn_{0.10}$	0.82	-51	86	275	11.8 ± 0.6	6.2 ± 0.6	1156 ± 87	37.7 ± 6.0	89
2-$Al_{0.10}$	0.34	-54	136	273	51.5 ± 3.2	10.3 ± 0.3	361 ± 21	29.4 ± 2.2	99
2-$Al_{0.05}$	0.17	-50	121	258	21.5 ± 1.0	9.6 ± 0.3	462 ± 24	30.8 ± 2.3	78
2-$Al_{0.01}$	0.03	-50	100	270	12.4 ± 3.0	6.3 ± 0.4	630 ± 57	23.9 ± 3.0	82

[a]Lower glass transition temperature from DSC, [b]upper glass transition temperature from peak in tan(δ) in DMTA, *from DSC. [c]Thermal degradation behavior is reported as the temperature at 5% mass loss, determined by TGA. [d]Young's modulus. [e]Tensile strength. [f]Strain at break. [g]Tensile toughness (area under the stress-strain curve). Mean values ± std. dev. from measurements conducted independently on 5 specimens. [h]Elastic recovery determined from zero-force stress recovery experiment, materials were allowed to recover for 30 min from 0.3 ε_b.

Samples showed tensile strengths from 1–10 MPa and elongations at break from 300–2600%. All samples show stress-strain relationships, consistent with elastomeric behavior. The unfunctionalised polymer **1**-vinyl shows a very low tensile strength, 0.5 MPa, and high elongation at break (1373%). There are clear material property benefits to the carboxylic acid functionalisation in improving mechanical performance. Comparing materials with identical hard block content, **1**-vinyl (unfunctionalised) and **2**-COOH, reveals a 9-fold increase in Young's modulus (1.0 to 9.0 MPa), a 10-fold increase in tensile strength (0.5 to 4.4 MPa), a 2-fold increase in elongation at break (1373 to 2615%), and a 19-fold increase in tensile toughness (4.7 to 88.4 MJ m^{-3}). These superior properties are attributed to enhanced phase separation and the hydrogen bonding reinforcing the hard block. The mechanical properties

were also significantly influenced by the different metals (Figure 3b). All displayed superior characteristics relative to **1**-vinyl and **2**-COOH, albeit with very high elongations at break (< 1200%). Interestingly, monovalent **2**-$Na_{0.10}$ displayed the greatest Young's modulus and tensile strength relative to all the metal(I) and metal(II) ionomers studied, which was tentatively attributed to the sodium carboxylate clustering/aggregation in the hard domains.[16]

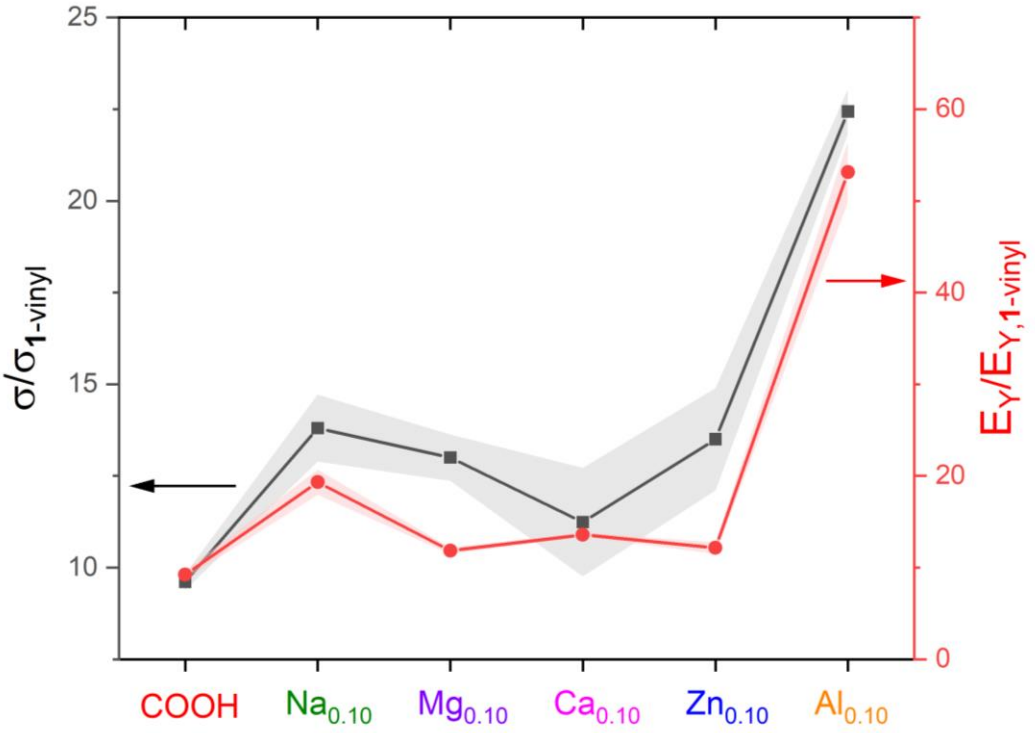

Figure 2.18: Improvement in tensile strength and Young's modulus relative to unfunctionalised **1**-vinyl.

2-$Al_{0.10}$ shows the most dramatic increase in tensile strength (52-fold) and Young's modulus (21-fold) relative to the unfunctionalised triblock copolymer. The trivalent Al(III) ions enable greater crosslinking which reinforces the hard domains and strengthens the material. The gains in stiffness and strength result in some slight reductions in elongation at break, but samples are able to achieve strains in excess of 350%, which is certainly sufficient for many TPE applications.[24, 25] The significant improvements in tensile strength and Young's modulus demonstrate the benefits of metal ion coordination and exemplify how a common

starting polymer can be rapidly adjusted to meet specific material property demands (**Figure 2.18**).

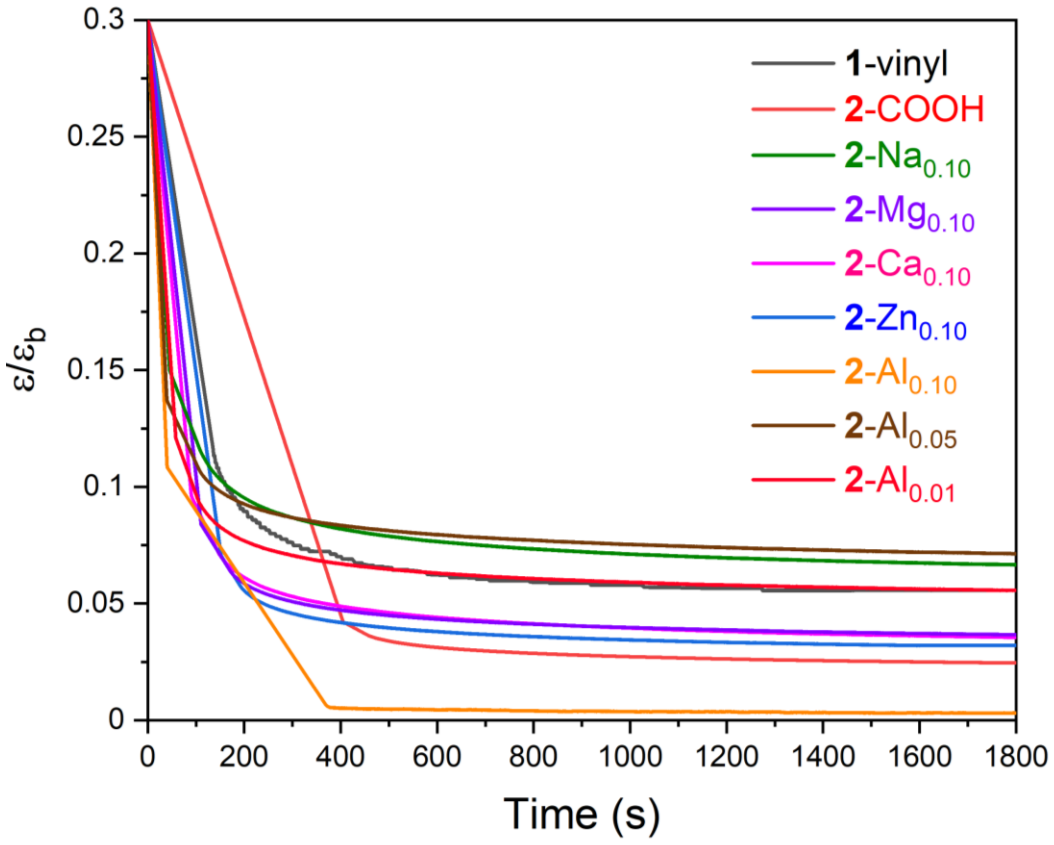

Figure 2.19: Zero force recovery experiments of all elastomers.

The elastic recovery was assessed by zero-force stress recovery experiments. Samples were strained to 30% of the elongation at break and allowed to freely recover for 30 min, i.e. under zero force/stress. Elastic recovery is the original length of the specimen relative to that after the 30 min recovery period (**Table 2.4, Figure 2.19**). **2**-COOH shows better elastic recovery, 92%, than the unfunctionalised polymer, likely as a result of dynamic inter-chain hydrogen bonding.[18] All the ionomers show high elastic recovery values, with **2**-$Mg_{0.10}$, **2**-$Ca_{0.10}$ and **2**-$Zn_{0.10}$ being 88–89%. The lead sample is, once again, **2**-$Al_{0.10}$ which displays an impressive 99% elastic recovery. It is proposed that the Al(III) ions anchor the hard blocks and reduce chain pull-out, thereby driving efficient elastic recovery.[26]

In most applications, elastomers must also resist mechanical creep, or permanent deformation under applied stress.[26] To assess these aspects, rheological creep-recovery experiments were conducted using **1**-vinyl, **2**-COOH and **2**-$Al_{0.10}$ (**Figure 2.20**). The experiments were conducted at 30 °C, at a constant stress (5 kPa) for four periods of 100 s, each followed by 100 s of 0 Pa stress to recover. During the first cycle, **1**-vinyl exhibited 11% strain which increased to 16% by the fourth cycle – i.e. it showed significant creep. On the other hand, **2**-COOH and **2**-$Al_{0.10}$ only showed 2.0 and 0.9% strain, respectively, in the first cycles which did not increase in subsequent cycles. This excellent creep resistance is likely the result of improved hard-domain interactions.

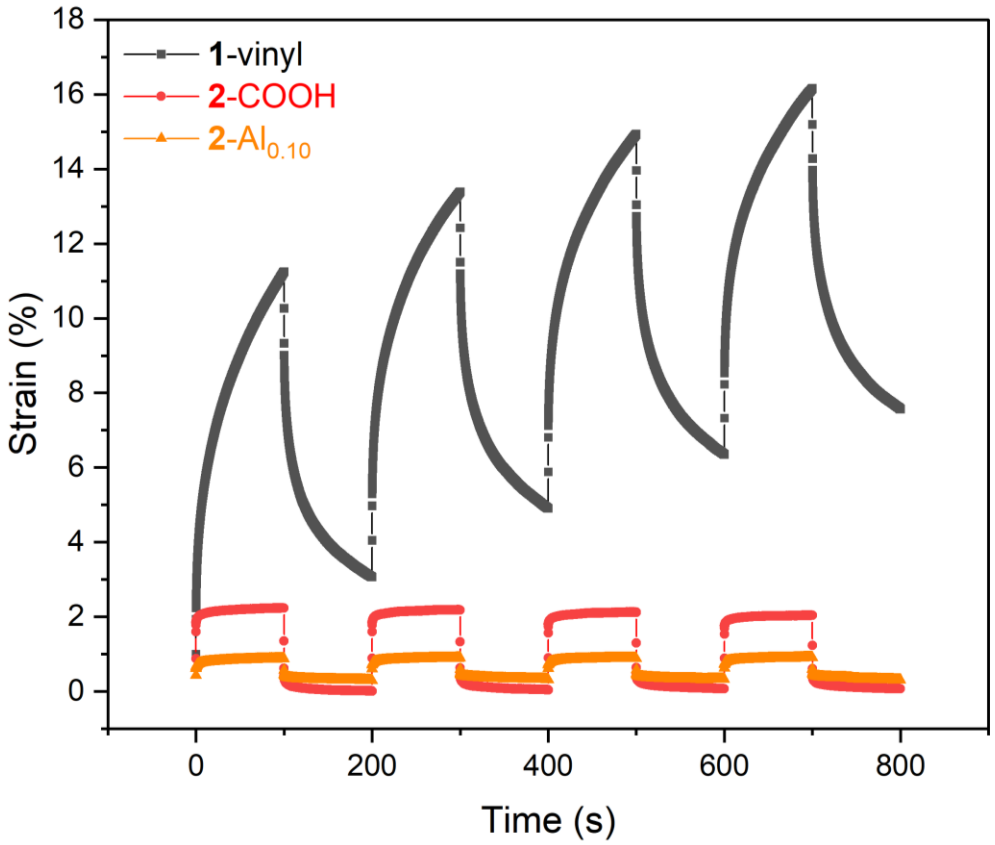

Figure 2.20: Creep-recovery experiments at 30 °C, 5 kPa.

Given the high tensile strength, elastic recovery and creep resistance of the Al(III) ionomer, four different metal loadings were examined (as mol% metal vs. carboxylic acid groups), targeting both lower (**2**-$Al_{0.01}$, **2**-$Al_{0.05}$) and higher (**2**-$Al_{0.12}$ and **2**-$Al_{0.15}$) metal contents.

The latter two samples (i.e. 12 and 15 mol%) were too densely crosslinked for subsequent processing either by solvent casting or compression moulding. On the other hand, **2**-$Al_{0.01}$ and **2**-$Al_{0.05}$ were both successfully processed into thin films and uniaxial tensile testing allowed comparisons of Young's moduli, tensile strengths and strains at break of the ionomers (**Figure 2.21**). The tensile strength correlates with the amount of Al(III) in the samples (0.03-0.34 wt%) and these experiments further demonstrate the potential tuning of tensile mechanical properties according to particular applications needs.

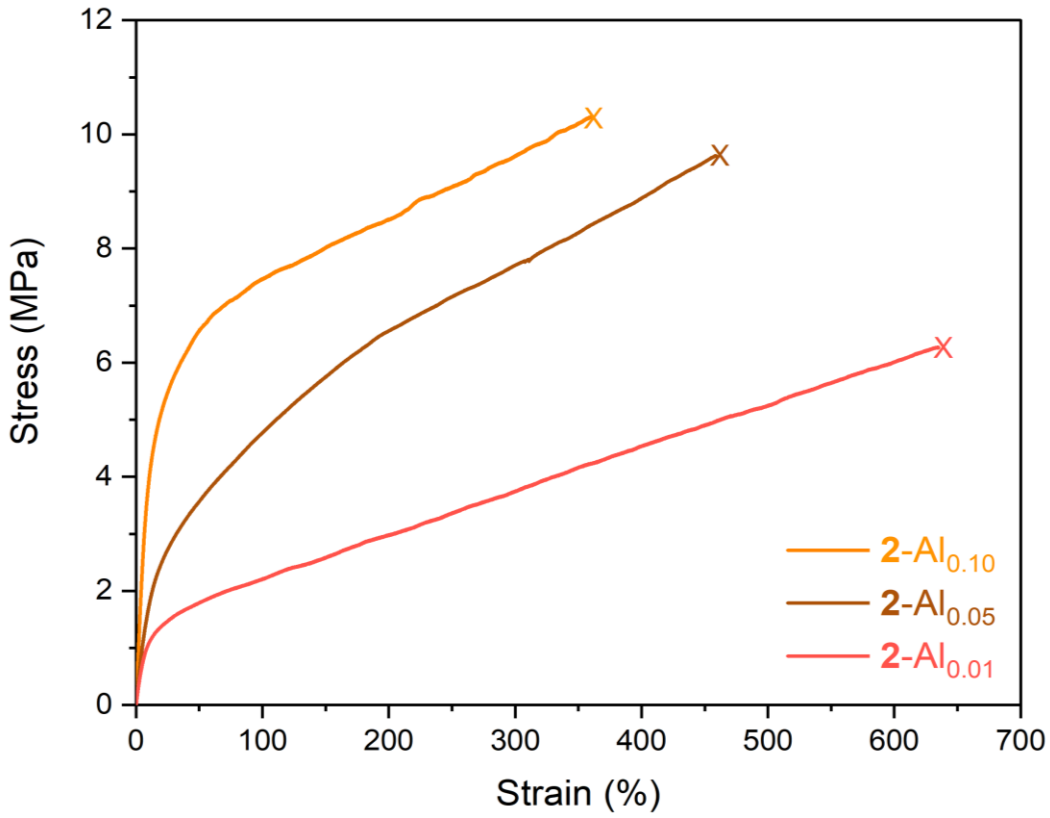

Figure 2.21: Representative stress-strain curves (10 mm min^{-1} extension rate) for ionomers containing 10, 5 and 1 mol% aluminium with respect to pendent COOH groups.

To qualitatively investigate the influences of ionomer crosslink density, samples were subjected to solvent swelling experiments; in which lower swelling indices correlate with more strongly cross-linked networks. Uniform ionomer disks (8 mm diameter, ~200 μm thick) were submerged in THF for 72 h, then dried (vacuum oven, 72 h) and weighed (both swollen and

dried) to determine the swelling index and gel content respectively (**Figure 2.22** and Table S7.2.2). All ionomers showed high gel contents, from 92-99%, highlighting their resistance to organic solvents. The swelling indices are highest for the metal(II) ionomers, indicating less effective crosslinking. In contrast, **2**-$Na_{0.10}$ has a lower swelling index, consistent with the proposed sodium carboxylate aggregation. The lead sample, **2**-$Al_{0.10}$ has the lowest swelling index and the highest crosslink density of all the materials. Further, as the Al(III) loading decreased, the swelling indices increased, consistent with reduced crosslinking (**Figure 2.22**). Overall, the swelling indices of all the Al(III) samples are the lowest suggesting that even at very low loadings of Al(III) there is a maximised crosslink density. This notion is consistent with the tensile mechanical data, where **2**-$Al_{0.01}$ has the greatest tensile strength even though it is applied at 1/10 the metal loading of the M(II) ions. This finding is significant since it allows for the highest mechanical strengths/Young's moduli using the lowest quantities of metal.

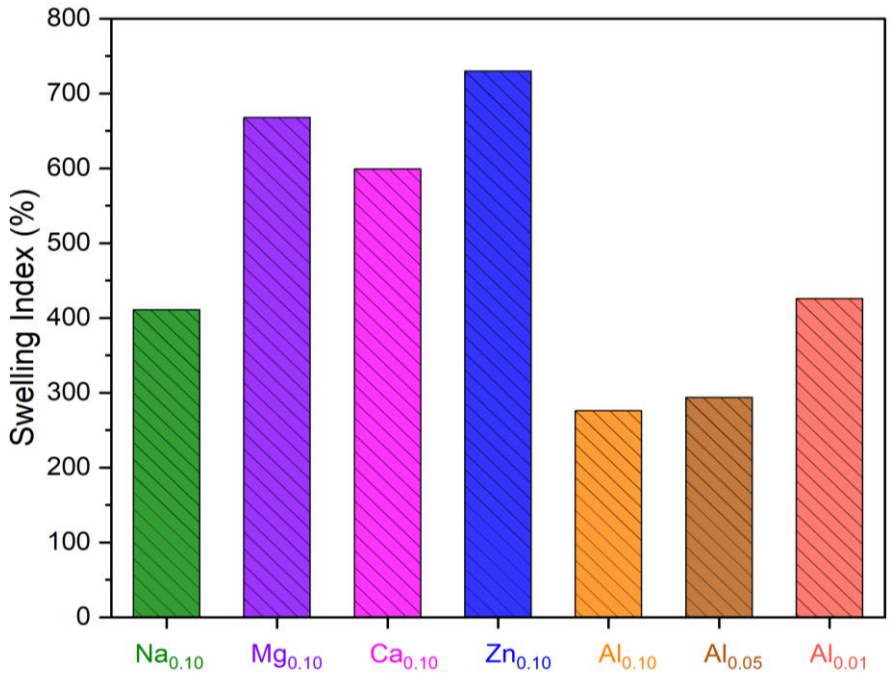

Figure 2.22: Swelling index after swelling polymer samples in THF for 72 hours of all ionomers.

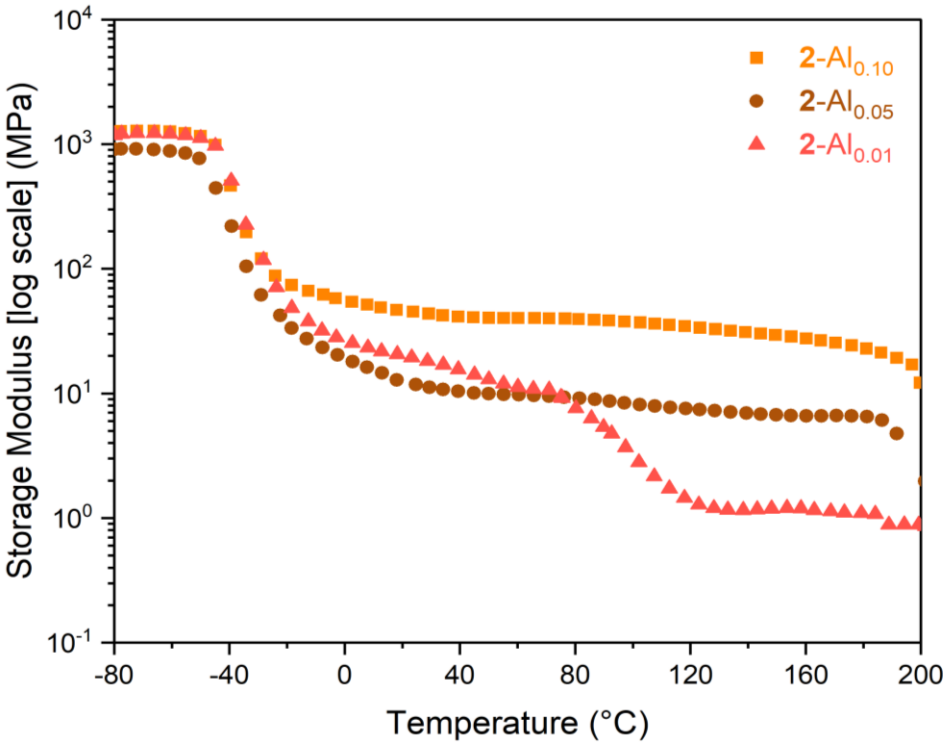

Figure 2.23: Storage moduli from dynamic mechanical temperature analysis (DMTA) temperature sweeps of **2**-$Al_{0.10}$, **2**-$Al_{0.05}$, **2**-$Al_{0.01}$.

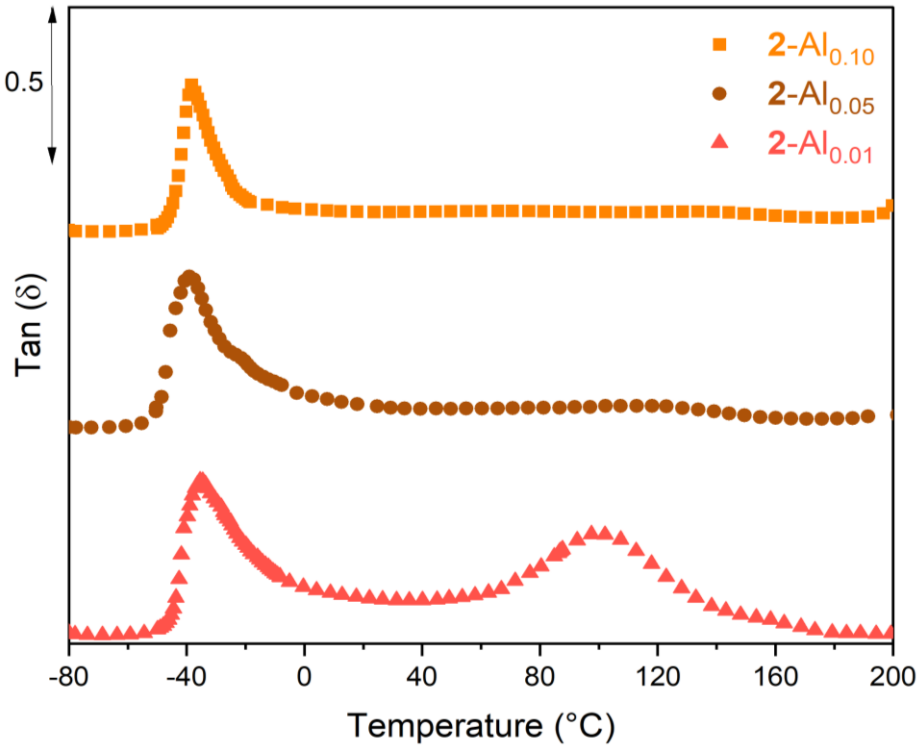

Figure 2.24: Tan(δ) profiles from dynamic mechanical temperature analysis (DMTA) temperature sweeps of **2**-$Al_{0.10}$, **2**-$Al_{0.05}$, **2**-$Al_{0.01}$.

Given the promising performances of the Al(III) ionomers, their dynamic mechanical properties were investigated. All samples show wide-ranging rubbery plateau regions (**Figure 2.23**). The plateau moduli of the Al(III) ionomers decrease with metal loading, particularly at elevated temperatures (34.3, 7.5 and 1.3 MPa at 120 °C for **2**-$Al_{0.10}$, **2**-$Al_{0.05}$ and **2**-$Al_{0.01}$ respectively). At Al(III) contents 5-10%, the storage modulus is maintained to temperatures of 200 °C (which is well above the notional $T_{g,upper}$, **Figure 2.24**) and the materials show a wide operating temperature range of -38–200 °C. It is proposed there is sufficient crosslinking in **2**-$Al_{0.10}$ and **2**-$Al_{0.05}$ to restrict chain mobility. As a result, the upper glass transition temperature is raised and suppressed.

2.5 Mechanical Recycling

Polymers designed to facilitate reprocessing could be advantageous in facilitating their end-of-life treatments since the energy required for mechanical recycling is usually significantly lower than for chemical recycling.[27, 28] One advantage of these reversible chemical bonds should be their facility to undergo thermal reprocessing. Accordingly, the lead sample **2**-$Al_{0.01}$ was successfully reprocessed three times, at 140 °C, without any compromise in thermal or mechanical properties (**Figure 2.25**). These data show the potential to efficiently recycle both manufacturing scraps and even waste thermoplastic elastomer samples by simple heating protocols (above $T_{g,upper}$) and without any material decomposition.

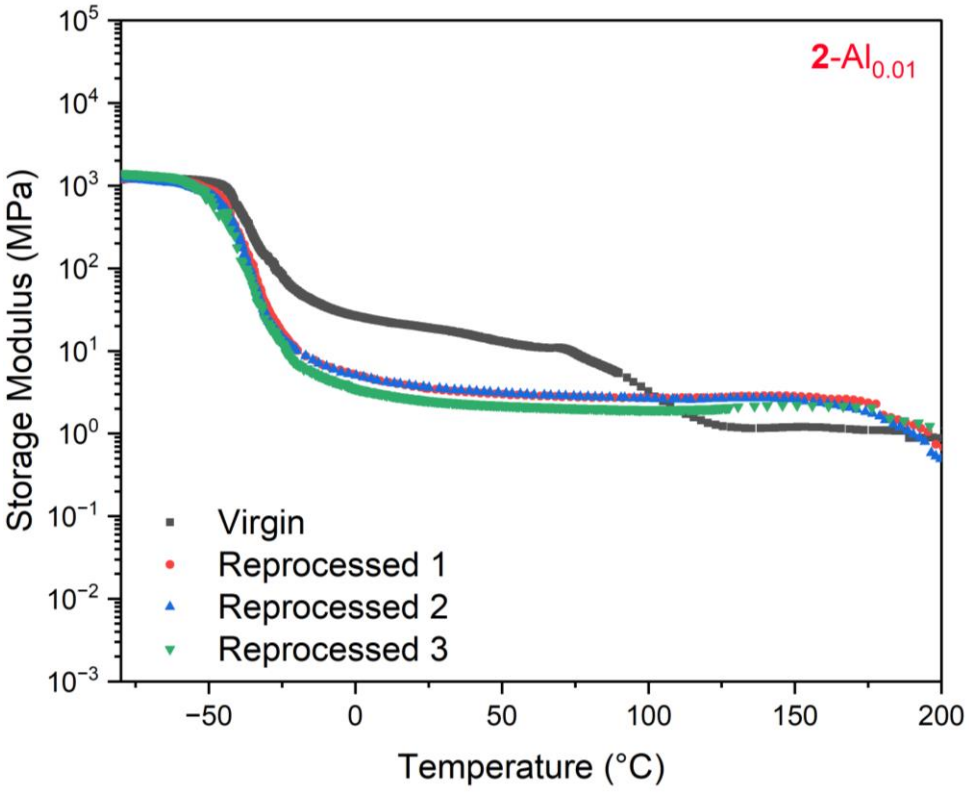

Figure 2.25: Dynamic Mechanical Thermal Analysis (DMTA) for "virgin" and "reprocessed" films of **2**-$Al_{0.01}$

Following the first reprocessing cycle, there is only a single rubbery plateau observed. This change in DMTA profile is attributed to the further thermal annealing of the polymer in which, kinetically trapped domains are released. After a second and third reprocessing cycle, there is no observable difference in the DMA profiles. This suggests that after complete annealing is achieved, there is no further change in the mechanical and thermal properties with repeated mechanical recycling.

2.6 Aqueous Stability

The aqueous stability of the polymers and ionomers was investigated by water swelling and base-catalysed accelerated hydrolyses. For the aqueous swelling experiments, disks of **1**-vinyl, **2**-COOH and **2**-$Al_{0.10}$ (16 mm diameter, ~200 μm thick) were submerged in deionised water (pH = 7) and their swollen mass measured over time (**Figure 2.26**). There were slight differences, with **2**-COOH and **2**-$Al_{0.10}$ showing increased water uptake. Over 5 months no significant degradation occurred, which is advantageous for any environmental exposure of products.

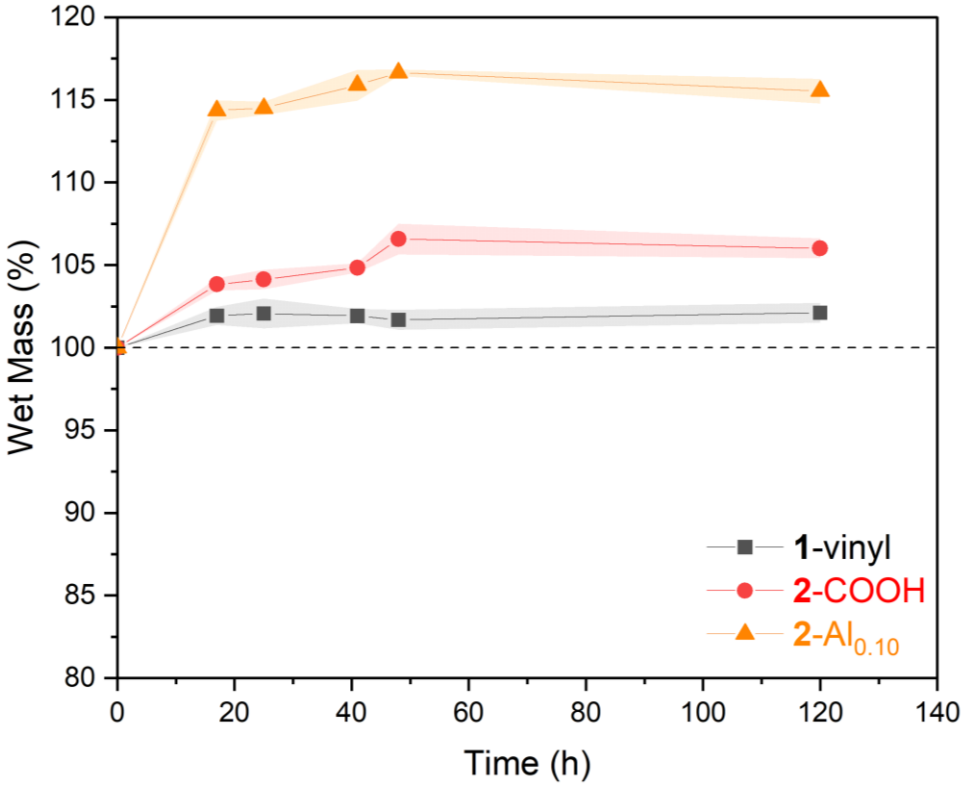

Figure 2.26: Swelling study in deionised water (pH = 7).

To confirm the stability of the samples, the storage moduli were monitored as a function of the relative humidity using representative samples of **1**-vinyl, **2**-COOH and **2**-$Al_{0.10}$ (**Figure 2.27**). All three materials maintained constant values for storage moduli from 0 - 80% relative humidity demonstrating good stabilities over the duration of the experiments, since the majority component of all samples is hydrophobic PDL. This prevents any compromise to sample mechanical integrity even in the most extreme of humid environments.

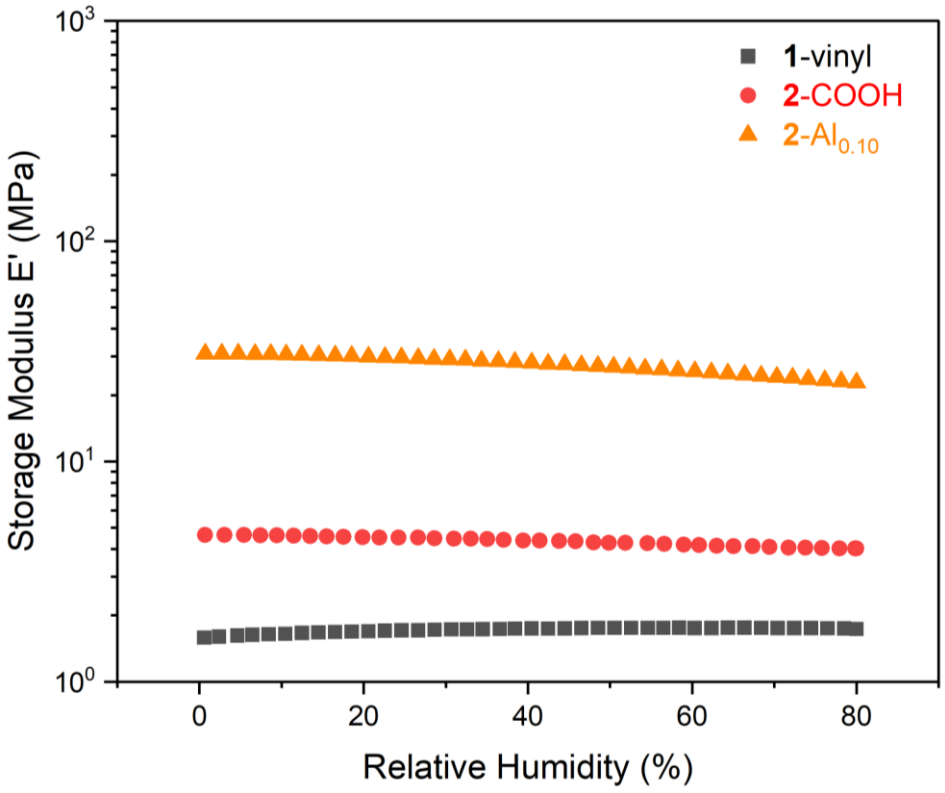

Figure 2.27: Storage moduli profiles from DMA relative humidity sweeps for **1**-vinyl, **2**-COOH and **2**-$Al_{0.10}$.

Finally, accelerated aging experiments were conducted using a strong base. Accordingly, disks of **1**-vinyl, **2**-COOH and **2**-$Al_{0.10}$ (16 mm diameter, ~200 μm thick) were submerged in 1 M NaOH solutions at room temperature and mass loss over time was measured (**Figure 2.28**). The Al(III) ionomer, **2**-$Al_{0.10}$, showed significantly faster hydrolysis compared to **1**-vinyl or **2**-COOH, achieving 50% mass loss over 5 months. In future, these accelerated hydrolyses could be exploited and accelerated, e.g. with higher temperatures, for chemical recycling.

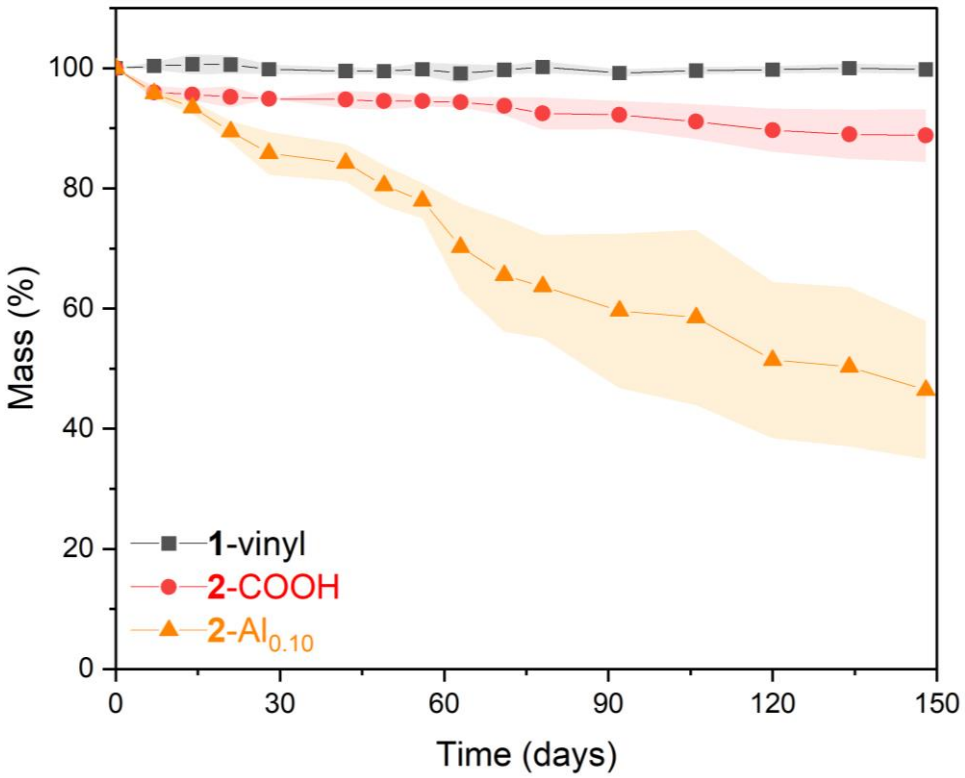

Figure 2.28: Polymer Films with accelerated degradation in basic aqueous media, (1 M NaOH, pH = 14, RT).

2.7 Discussion

The ABA block polymers are derived from CO_2, a common waste product abundant as a co-product of chemical/bio-chemical manufacturing, and ε-decalactone, sourced from castor oil via ricinoleic acid.[29, 30] As such, these polymers comprise ~75 wt% renewable resources and using efficient chemistry, simple carboxylic acid substituents were installed at regular sites through the polycarbonate 'hard' blocks. These carboxylic acid groups coordinate metals including Na(I), Mg(II), Ca(II), Zn(II) and Al(III) to make new ionomer elastomers. The overall metal loadings were very low in all samples, <1 wt%, allowing for optical transparency, but despite these low loadings, the nature of the metal, and specifically its oxidation state or valency controls the polymers' thermal and mechanical properties. In particular, the greatest tensile strengths were afforded by low quantities of Al(III) and the products combined broad operating temperatures with high upper service temperatures (-20–200 °C). The latter temperature exceeds those of TPEs featuring PLA (~60 °C),[31] polystyrene (~100 °C),[24] or poly(cyclohexene-*alt*-phthalate) (~120 °C) hard blocks.[32] There are significant benefits to using low quantities of metals to increase tensile mechanical strengths and toughness, no compromise in elastic recovery and reduced creep. Further, the elastomers can be reprocessed thermally which should help future recycling. There are two areas of novelty or property moderation that are worth more detailed contextualisation *vs.* the literature.

2.7.1 CO_2-Derived Elastomers

The first is the distinct improvements to the properties of carbon dioxide-derived polymers (PC) afforded by the metal carboxylates. These new polymers (~5 wt% CO_2) access previously inaccessible regions of property space compared with other CO_2-derived polymer elastomers (**Figure 2.29**). Compared with other elastomers featuring the same polyester 'soft' block (i.e. PDL), the ionomers showed significant increases in all tensile mechanical properties, i.e. they performed better than equivalent materials using poly(cyclohexene carbonate), poly(vinyl cyclohexene carbonate) or poly(limonene carbonate) 'hard blocks'.[33, 34] Further, the increases in tensile strength do not compromise elasticity, with materials showing high elastic recovery and high creep-resistance. The new polymers also improved upon prior reported carbon dioxide-derived polycarbonate elastomers.

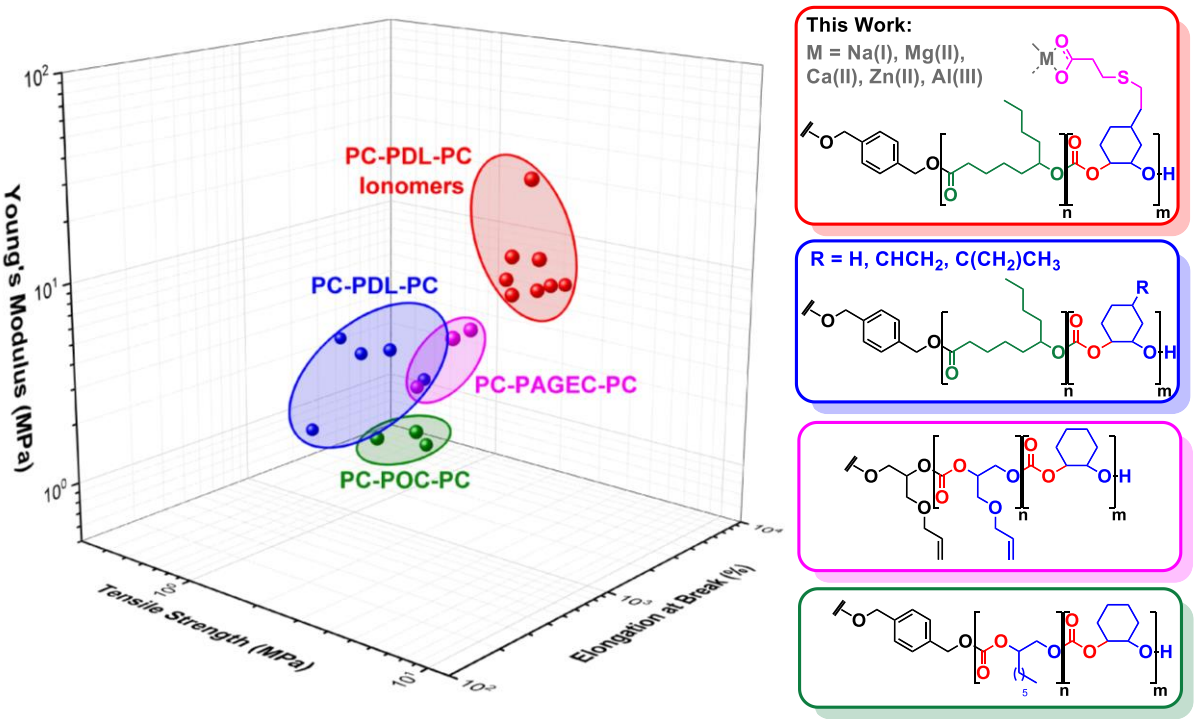

Figure 2.29. Ashby plot for literature CO_2-TPEs & CO_2 ionomers (this work). Where PC = Polycarbonate, PDL =Poly(ε-decalactone), PAGEC = Poly(allyl glycidyl ether carbonate),[35] and POC = Poly(octene carbonate).[36] PC-PDL-PC: ABA triblock polymers with PDL B-blocks and CO_2/epoxide (cyclohexene oxide, 4-vinyl cyclohexene oxide and limonene oxide).[33, 34]

Compared with materials featuring 'soft blocks' such as poly(allyl glycidyl ether carbonate) (PAGEC) or poly(octene carbonate) (POC), these ionomeric elastomers showed over 50 and 200% higher tensile strengths and over 400 and 1900% higher Young's moduli, respectively, and maintained the same poly(cyclohexene carbonate) hard blocks.[35, 36] Since the production of the current materials was highly controlled, there is a range of future options to combine different lactones, epoxides or heterocumulenes to fine-tune properties. If higher bio-based content were desired, a hard-block polymer comprising limonene oxide (LO) and carbon dioxide could be targeted, since both its catalysis and 'hard block' properties are benchmarked.[34] The step-changes in mechanical performances afforded by these ABA block polymers, compared with the current state-of-the-art polymers, offer significant scope for future property explorations and expand the range and application potential for carbon dioxide-derived plastics.

2.7.2 Toughening Strategies

The second feature is the facility to 'tune' properties without requiring any polymer backbone re-design or changes to processing conditions. This aspect is significant since prior solutions to these challenges generally involved new monomers and polymers. Whilst appropriate in academic discovery, there could be some disbenefits to moderating properties through changes to monomer chemistry, since in every new product the monomer syntheses, polymerisation catalysts and conditions must be (re)optimised. There are also a number of known approaches to increasing elastomer tensile strengths and comparably metal ion coordination appears promising.

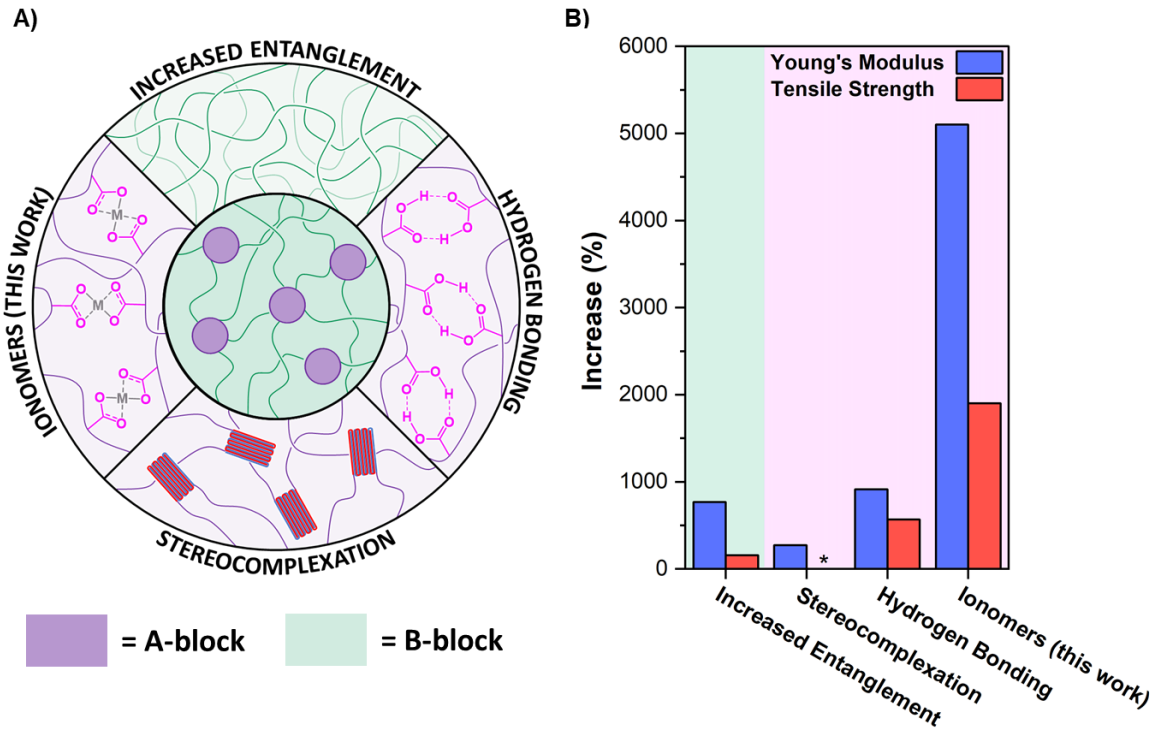

Figure 2.30. (A) Schematic representation of various approaches to increase mechanical properties of TPEs. (B) The resulting improvement of the strategy relative to unfunctionalised material. *No increase.

One excellent approach has been to increase the soft-block entanglement by using B-block polymers showing low entanglement molar mass (M_e). This strategy has allowed up to a 767% increase in Young's modulus and a 157% increase in tensile strength (compared with equivalent polymers applying soft blocks with higher M_e).[37] Alternatively, the hard-blocks can be reinforced by (co-)crystallisation, for example by PLLA/PDLA stereo-complexation, which achieved 273% higher Young's modulus but did little to change the overall tensile strength (compared with PLLA materials alone).[38] Despite the undoubted successes of the prior approaches, installing metal complexes allows for greater increases in properties of 1900% in tensile strengths and 5100% in Young's moduli (**Figure 2.30** & Table S7.2.3). Given the magnitude of the increment is controlled by the quantity of the added metal, it's easily feasible to moderate properties of a very wide range of values.

Finally, the metal ion coordination strategy should be practically achievable and this work has deliberately focused on precision structures using inexpensive monomers combined with low-cost, colourless, and Earth-abundant metals to improve future sustainability and applicability. Materials were prepared using controlled switchable polymerisations, combining commercial lactone ROP and epoxide/carbon dioxide ROCOP, with a single catalyst. The precision block polymer structures allow for high control and regulation over both the extent and site of metal ion coordination and subsequent properties. In future, a range of different coordination chemistries should be explored to provide an understanding of the relationships between inorganic macromolecular chemistry and macroscopic properties.

2.8 Summary and Future Work

2.8.1 Conclusion

Installing metal-carboxylate bonds within the hard domains of a CO_2- and bio-derived triblock copolymer thermoplastic elastomers allowed for control over and improvements to tensile mechanical properties. Materials were prepared with <1 wt% metal yet showed significantly higher tensile strengths, and toughness whilst maintaining high elasticity, elastic recovery and creep resistance. Well-controlled polymer syntheses ensured regular placement of coordination sites along the chain, allowing for accurate control over the crosslinking density and tuning the thermal and mechanical properties. Using <1 wt% aluminium in the polymers resulted in a 52-fold increase in the material's Young's modulus and a 21-fold increase in tensile strength relative to the starting polymer. The ionomeric polymers showed wide operating (-20–200 °C), were also recyclable by compression moulding, and showed good environmental stability.

2.8.2 Future Work

This new chemistry should be applicable to many other monomer combinations, polymer structures and metal-ligand coordination chemistries providing an exciting array of future materials and mechanisms for property tuning.

There are two key areas of further research with respect to the metal-ligand interactions within the ionomers: 1) the exploration of a wider array of metal crosslinkers and 2) the use of different ligands appended to the outer blocks of the TPE. While only sodium, magnesium, calcium, zinc, and aluminium were explored in this work, there are a plethora of other metals which could be employed to provided added functionality to the materials. For example, the incorporation of iron(III) into the polymer network should provide similar thermomechanical

properties to that of aluminium(III) but instil magneto-responsive properties to the material.[39] While this would result in a coloured polymer, it could potentially allow for magnetic actuation and subsequently applications in soft robotics and/or biomedical applications.[40] Furthermore, as the iron centres would be surrounded by pendent carboxylic acid ligands, the iron(III) could undergo photoreduction to iron(II) to change the crosslinking density within the network and ultimately the mechanical properties of the polymer.[41]

Changing the chosen ligand incorporated into the TPE backbone could have dramatic influences on the exchange dynamics of the ionomeric interactions. Catachol ligands have been extensively explored within biomimetic hydrogels and phosphonic acid ligands have been shown to be extremely effective in conductive composite cathode binders due to their favourable interfacial adhesion properties.[42, 43] These two classes of ligands would likely be extremely effective to toughen triblock copolymer elastomers. To probe these thermodynamics and kinetics formally, a series of low molar mass PvCHC (below entanglement molar mass M_e) could be used as a rheologically simple model for the outer 'hard' TPE blocks reported here. Thiol-ene functionalisation of the homopolymer to append varying ligands followed by the addition of metal salts to fully neutralise the ligands would yield a series of brittle and powdery ionomers. However, rheological stress-relaxation and creep-recovery experiments at varying temperatures would provide activation energies for metal-ligand bond exchange and for viscous flow respectively.[44, 45] As the metal-ligand exchange has been deconvoluted from entanglements within the blocks, hydrogen bonding, and order-to-disorder transitions. By developing a series of materials with varying ligands, the role of the ligand on both the thermodynamics and kinetics of the ionomeric exchange process could be established, allowing for a further handle to tune material properties and lead towards more targeted ionomer design.

The final avenue of further investigation is to produce analogous ionomers with 'soft' and 'hard' blocks with varying compositions. The ROP of trimethylene carbonate to produce poly(trimethylene carbonate) (PTMC) as the central 'soft' block of the TPE would likely result in CO_2-derived TPEs with greater strength and toughness. Under strain, PTMC chains can align and reversibly crystalise. PTMC blocks within TPEs have been shown to undergo strain-induced crystallisation, leading to a dramatic uptick in stress.[19] This would not only open up a new area of property space to for CO_2-derived copolymer elastomers but increase the CO_2 content of the material as PTMC can be produced directly from 1,3-propanediol and CO_2.[46] Alternatively, the ROCOP of CO_2 and monocyclic epoxides such as ally glycidyl ether could produce a low T_g 'soft' block to incorporate additional CO_2 into the ionomers while also providing vinyl functionality in the soft block, which could be used for further functionalisation.[35, 36]

Finally, replacing vCHO with vinyl containing limonene oxide or 1,4-cyclohexadiene oxide would produce TPEs with similar material properties to the ones reported here but increase the bio-based content of the materials.[47, 48] Furthermore, by synthesising a triblock copolymer with a terpolymer block composed limonene oxide and 1,4-cyclohexadiene oxide and CO_2, would allow for orthogonal functionalisation, facilitating the addition of multiple ligands and/or hydrophilic/hydrophobic side chains. [49] This ability to diversify and fine tune multiple material properties will be critical. In future sustainable polymers need to show a wide variety of properties to replace current petrochemical plastics and elastics.

2.9 References

(1) Degtyar, E.; Harrington, M. J.; Politi, Y.; Fratzl, P. The Mechanical Role of Metal Ions in Biogenic Protein-Based Materials. *Angew. Chem., Int. Ed.* **2014**, *53* (45), 12026-12044. DOI: 10.1002/anie.201404272.
(2) Hillerton, J. E.; Vincent, J. F. V. The Specific Location of Zinc in Insect Mandibles. *J. Exp. Biol.* **1982**, *101*, 333.
(3) Fantner, G. E.; Hassenkam, T.; Kindt, J. H.; Weaver, J. C.; Birkedal, H.; Pechenik, L.; Cutroni, J. A.; Cidade, G. A. G.; Stucky, G. D.; Morse, D. E.; et al. Sacrificial bonds and hidden length dissipate energy as mineralized fibrils separate during bone fracture. *Nat. Mater.* **2005**, *4* (8), 612-616. DOI: 10.1038/nmat1428.
(4) Zhao, X. H.; Chen, X. Y.; Yuk, H.; Lin, S. T.; Liu, X. Y.; Parada, G. Soft Materials by Design: Unconventional Polymer Networks Give Extreme Properties. *Chem. Rev.* **2021**, *121* (8), 4309-4372. DOI: 10.1021/acs.chemrev.0c01088.
(5) Wei, Z. C.; Duan, H. Y.; Weng, G. S.; He, J. Metals in polymers: hybridization enables new functions. *J. Mater. Chem. C.* **2020**, *8* (45), 15956-15980. DOI: 10.1039/d0tc03810e.
(6) Mozhdehi, D.; Ayala, S.; Cromwell, O. R.; Guan, Z. B. Self-Healing Multiphase Polymers via Dynamic Metal-Ligand Interactions. *J. Am. Chem. Soc.* **2014**, *136* (46), 16128-16131. DOI: 10.1021/ja5097094.
(7) Brown, C. M.; Lundberg, D. J.; Lamb, J. R.; Kevlishvili, I.; Kleinschmidt, D.; Alfaraj, Y. S.; Kulik, H. J.; Ottaviani, M. F.; Oldenhuis, N. J.; Johnson, J. A. Endohedrally Functionalized Metal-Organic Cage-Cross-Linked Polymer Gels as Modular Heterogeneous Catalysts. *J. Am. Chem. Soc.* **2022**, *144* (29), 13276-13284. DOI: 10.1021/jacs.2c04289.
(8) Piepenbrock, M. O. M.; Lloyd, G. O.; Clarke, N.; Steed, J. W. Metal- and Anion-Binding Supramolecular Gels. *Chem. Rev.* **2010**, *110* (4), 1960-2004. DOI: 10.1021/cr9003067.
(9) Grindy, S. C.; Learsch, R.; Mozhdehi, D.; Cheng, J.; Barrett, D. G.; Guan, Z. B.; Messersmith, P. B.; Holten-Andersen, N. Control of hierarchical polymer mechanics with bioinspired metal-coordination dynamics. *Nat. Mater.* **2015**, *14* (12), 1210-1216. DOI: DOI 10.1038/nmat4401.
(10) Creton, C. 50th Anniversary Perspective: Networks and Gels: Soft but Dynamic and Tough. *Macromolecules* **2017**, *50* (21), 8297-8316. DOI: 10.1021/acs.macromol.7b01698.
(11) Potaufeux, J. E.; Odent, J.; Notta-Cuvier, D.; Lauro, F.; Raquez, J. M. A comprehensive review of the structures and properties of ionic polymeric materials. *Polym. Chem.* **2020**, *11* (37), 5914-5936. DOI: 10.1039/d0py00770f.
(12) Khare, E.; Holten-Andersen, N.; Buehler, M. J. Transition-metal coordinate bonds for bioinspired macromolecules with tunable mechanical properties. *Nat. Rev. Mater.* **2021**, *6* (5), 421-436. DOI: 10.1038/s41578-020-00270-z.
(13) Wang, W. T.; Zhang, J.; Jiang, F.; Wang, X. H.; Wang, Z. G. Reprocessable Supramolecular Thermoplastic BAB-Type Triblock Copolymer Elastomers with Enhanced Tensile Strength and Toughness via Metal-Ligand Coordination. *ACS Appl. Polym. Mater.* **2019**, *1* (3), 571-583. DOI: 10.1021/acsapm.8b00277.
(14) Li, C. H.; Wang, C.; Keplinger, C.; Zuo, J. L.; Jin, L.; Sun, Y.; Zheng, P.; Cao, Y.; Lissel, F.; Linder, C.; et al. A highly stretchable autonomous self-healing elastomer. *Nat. Chem.* **2016**, *8* (6), 619-625. DOI: 10.1038/Nchem.2492.
(15) Lai, J. C.; Li, L.; Wang, D. P.; Zhang, M. H.; Mo, S. R.; Wang, X.; Zeng, K. Y.; Li, C. H.; Jiang, Q.; You, X. Z.; et al. A rigid and healable polymer cross-linked by weak but abundant Zn(II)-carboxylate interactions. *Nat. Commun.* **2018**, *9*. DOI: 10.1038/s41467-018-05285-3.
(16) Miwa, Y.; Kurachi, J.; Kohbara, Y.; Kutsumizu, S. Dynamic ionic crosslinks enable high strength and ultrastretchability in a single elastomer. *Commun. Chem.,* **2018**, *1*. DOI: 10.1038/s42004-017-0004-9.

(17) Filippidi, E.; Cristiani, T. R.; Eisenbach, C. D.; Waite, J. H.; Israelachvili, J. N.; Ahn, B. K.; Valentine, M. T. Toughening elastomers using mussel-inspired iron-catechol complexes. *Science* **2017**, *358* (6362), 502-505. DOI: 10.1126/science.aao0350.
(18) Gregory, G. L.; Williams, C. K. Exploiting Sodium Coordination in Alternating Monomer Sequences to Toughen Degradable Block Polyester Thermoplastic Elastomers. *Macromolecules* **2022**, *55* (6), 2290-2299. DOI: 10.1021/acs.macromol.2c00068.
(19) Gregory, G. L.; Sulley, G. S.; Kimpel, J.; Lagodzinska, M.; Hafele, L.; Carrodeguas, L. P.; Williams, C. K. Block Poly(carbonate-ester) Ionomers as High-Performance and Recyclable Thermoplastic Elastomers. *Angew. Chem., Int. Ed.* **2022**, *61* (47). DOI: 10.1002/anie.202210748.
(20) Deacy, A. C.; Gregory, G. L.; Sulley, G. S.; Chen, T. T. D.; Williams, C. K. Sequence Control from Mixtures: Switchable Polymerization Catalysis and Future Materials Applications. *J. Am. Chem. Soc.* **2021**, *143* (27), 10021-10040. DOI: 10.1021/jacs.1c03250.
(21) Spyros, A.; Argyropoulos, D. S.; Marchessault, R. H. A study of poly(hydroxyalkanoate)s by quantitative P-31 NMR spectroscopy: Molecular weight and chain cleavage. *Macromolecules* **1997**, *30* (2), 327-329. DOI: DOI 10.1021/ma9601979.
(22) Kajita, T.; Tanaka, H.; Noro, A.; Matsushita, Y.; Nozawa, A.; Isobe, K.; Oda, R.; Hashimoto, S. Extremely tough block polymer-based thermoplastic elastomers with strongly associated but dynamically responsive noncovalent cross-links. *Polymer* **2021**, *217*. DOI: 10.1016/j.polymer.2021.123419.
(23) Otero, V.; Sanches, D.; Montagner, C.; Vilarigues, M.; Carlyle, L.; Lopes, J. A.; Melo, M. J. Characterisation of metal carboxylates by Raman and infrared spectroscopy in works of art. *J. Raman. Spectrosc.* **2014**, *45* (11-12), 1197-1206. DOI: 10.1002/jrs.4520.
(24) Drobny, J. G. *Handbook of Thermoplastic Elastomers, 2nd Edition*; 2014.
(25) Fasolka, M. J.; Mayes, A. M. Block copolymer thin films: Physics and applications. *Annu. Rev. Mater. Res.* **2001**, *31*, 323-355. DOI: DOI 10.1146/annurev.matsci.31.1.323.
(26) Clarke, R. W.; McGraw, M. L.; Newell, B. S.; Chen, E. Y. X. Thermomechanical activation achieving orthogonal working/healing conditions of nanostructured tri-block copolymer thermosets. *Cell. Rep. Phys. Sci.* **2021**, *2* (7). DOI: 10.1016/j.xcrp.2021.100483.
(27) Piemonte, V.; Sabatini, S.; Gironi, F. Chemical Recycling of PLA: A Great Opportunity Towards the Sustainable Development? *J. Polym. Environ.* **2013**, *21* (3), 640-647. DOI: 10.1007/s10924-013-0608-9.
(28) de Andrade, M. F. C.; Souza, P. M. S.; Cavalett, O.; Morales, A. R. Life Cycle Assessment of Poly(Lactic Acid) (PLA): Comparison Between Chemical Recycling, Mechanical Recycling and Composting. *J. Polym. Environ.* **2016**, *24* (4), 372-384. DOI: 10.1007/s10924-016-0787-2.
(29) Chapman, A. M.; Keyworth, C.; Kember, M. R.; Lennox, A. J. J.; Williams, C. K. Adding Value to Power Station Captured CO2: Tolerant Zn and Mg Homogeneous Catalysts for Polycarbonate Polyol Production. *ACS Catal.* **2015**, *5* (3), 1581-1588. DOI: 10.1021/cs501798s.
(30) Zhu, Y. Q.; Radlauer, M. R.; Schneiderman, D. K.; Shaffer, M. S. P.; Hillmyer, M. A.; Williams, C. K. Multiblock Polyesters Demonstrating High Elasticity and Shape Memory Effects. *Macromolecules* **2018**, *51* (7), 2466-2475. DOI: 10.1021/acs.macromol.7b02690.
(31) Arias, V.; Hoglund, A.; Odelius, K.; Albertsson, A. C. Tuning the Degradation Profiles of Poly(L-lactide)-Based Materials through Miscibility. *Biomacromolecules* **2014**, *15* (1), 391-402. DOI: 10.1021/bm401667b.
(32) Gregory, G. L.; Sulley, G. S.; Carrodeguas, L. P.; Chen, T. T. D.; Santmarti, A.; Terrill, N. J.; Lee, K. Y.; Williams, C. K. Triblock polyester thermoplastic elastomers with semi-aromatic polymer end blocks by ring-opening copolymerization. *Chem. Sci.* **2020**, *11* (25), 6567-6581. DOI: 10.1039/d0sc00463d.
(33) Sulley, G. S.; Gregory, G. L.; Chen, T. T. D.; Carrodeguas, L. P.; Trott, G.; Santmarti, A.; Lee, K. Y.; Terrill, N. J.; Williams, C. K. Switchable Catalysis Improves the Properties of CO2-

Derived Polymers: Poly(cyclohexene carbonate-b-epsilon-decalactone-b-cyclohexene carbonate) Adhesives, Elastomers, and Toughened Plastics. *J. Am. Chem. Soc.* **2020**, *142* (9), 4367-4378. DOI: 10.1021/jacs.9b13106.
(34) Carrodeguas, L. P.; Chen, T. T. D.; Gregory, G. L.; Sulley, G. S.; Williams, C. K. High elasticity, chemically recyclable, thermoplastics from bio-based monomers: carbon dioxide, limonene oxide and epsilon-decalactone. *Green Chem.* **2020**, *22* (23), 8298-8307. DOI: 10.1039/d0gc02295k.
(35) Yang, G. W.; Wu, G. P. High-Efficiency Construction of CO2-Based Healable Thermoplastic Elastomers via a Tandem Synthetic Strategy. *ACS Sustain. Chem. Eng.* **2019**, *7* (1), 1372-1380. DOI: 10.1021/acssuschemeng.8b05084.
(36) Jia, M. C.; Zhang, D. Y.; de Kort, G. W.; Wilsens, C. H. R. M.; Rastogi, S.; Hadjichristidis, N.; Gnanou, Y.; Feng, X. S. All-Polycarbonate Thermoplastic Elastomers Based on Triblock Copolymers Derived from Triethylborane-Mediated Sequential Copolymerization of CO2 with Various Epoxides. *Macromolecules* **2020**, *53* (13), 5297-5307. DOI: 10.1021/acs.macromol.0c01068.
(37) Watts, A.; Kurokawa, N.; Hillmyer, M. A. Strong, Resilient, and Sustainable Aliphatic Polyester Thermoplastic Elastomers. *Biomacromolecules* **2017**, *18* (6), 1845-1854. DOI: 10.1021/acs.biomac.7b00283.
(38) Wanamaker, C. L.; Bluemle, M. J.; Pitet, L. M.; O'Leary, L. E.; Tolman, W. B.; Hillmyer, M. A. Consequences of Polylactide Stereochemistry on the Properties of Polylactide-Polymenthide-Polylactide Thermoplastic Elastomers. *Biomacromolecules* **2009**, *10* (10), 2904-2911. DOI: 10.1021/bm900721p.
(39) Song, J.; Kim, S.; Saouaf, O.; Owens, C.; McKinley, G. H.; Holten-Andersen, N. Soft Viscoelastic Magnetic Hydrogels from the In Situ Mineralization of Iron Oxide in Metal-Coordinate Polymer Networks. *ACS Appl. Mater. Interfaces* **2023**, *15* (45), 52874-52882. DOI: 10.1021/acsami.3c08145 From NLM Publisher.
(40) Kim, Y.; Zhao, X. Magnetic Soft Materials and Robots. *Chem. Rev.* **2022**, *122* (5), 5317-5364. DOI: 10.1021/acs.chemrev.1c00481 From NLM Medline.
(41) Lueder, U.; Jorgensen, B. B.; Kappler, A.; Schmidt, C. Photochemistry of iron in aquatic environments. *Environ. Sci. Process Impacts* **2020**, *22* (1), 12-24. DOI: 10.1039/c9em00415g From NLM Medline.
(42) Holten-Andersen, N.; Harrington, M. J.; Birkedal, H.; Lee, B. P.; Messersmith, P. B.; Lee, K. Y.; Waite, J. H. pH-induced metal-ligand cross-links inspired by mussel yield self-healing polymer networks with near-covalent elastic moduli. *Proc. Natl. Acad. Sci. U. S. A.* **2011**, *108* (7), 2651-2655. DOI: 10.1073/pnas.1015862108 From NLM Medline.
(43) Gregory, G. L.; Gao, H.; Liu, B.; Gao, X.; Rees, G. J.; Pasta, M.; Bruce, P. G.; Williams, C. K. Buffering Volume Change in Solid-State Battery Composite Cathodes with CO(2)-Derived Block Polycarbonate Ethers. *J. Am. Chem. Soc.* **2022**, *144* (38), 17477-17486. DOI: 10.1021/jacs.2c06138 From NLM PubMed-not-MEDLINE.
(44) Montarnal, D.; Capelot, M.; Tournilhac, F.; Leibler, L. Silica-like malleable materials from permanent organic networks. *Science* **2011**, *334* (6058), 965-968. DOI: 10.1126/science.1212648 From NLM PubMed-not-MEDLINE.
(45) Mondal, S.; Lessard, J. J.; Meena, C. L.; Sanjayan, G. J.; Sumerlin, B. S. Janus Cross-links in Supramolecular Networks. *J. Am. Chem. Soc.* **2022**, *144* (2), 845-853. DOI: 10.1021/jacs.1c10606 From NLM PubMed-not-MEDLINE.
(46) McGuire, T. M.; López-Vidal, E. M.; Gregory, G. L.; Buchard, A. Synthesis of 5-to 8-membered cyclic carbonates from diols and CO2: A one-step, atmospheric pressure and ambient temperature procedure. *J Co2 Util* **2018**, *27*, 283-288. DOI: 10.1016/j.jcou.2018.08.009.

(47) Hauenstein, O.; Reiter, M.; Agarwal, S.; Rieger, B.; Greiner, A. Bio-based polycarbonate from limonene oxide and CO2 with high molecular weight, excellent thermal resistance, hardness and transparency. *Green Chem.* **2016**, *18* (3), 760-770. DOI: 10.1039/c5gc01694k.
(48) Winkler, M.; Romain, C.; Meier, M. A. R.; Williams, C. K. Renewable polycarbonates and polyesters from 1,4-cyclohexadiene. *Green Chem.* **2015**, *17* (1), 300-306. DOI: 10.1039/c4gc01353k.
(49) Yi, N.; Chen, T. T. D.; Unruangsri, J.; Zhu, Y. Q.; Williams, C. K. Orthogonal functionalization of alternating polyesters: selective patterning of (AB)n sequences. *Chem. Sci.* **2019**, *10* (43), 9974-9980. DOI: 10.1039/c9sc03756j.

CHAPTER 3

Controlled Carbon Dioxide Terpolymerisations to Deliver Toughened Yet Recyclable Thermoplastics

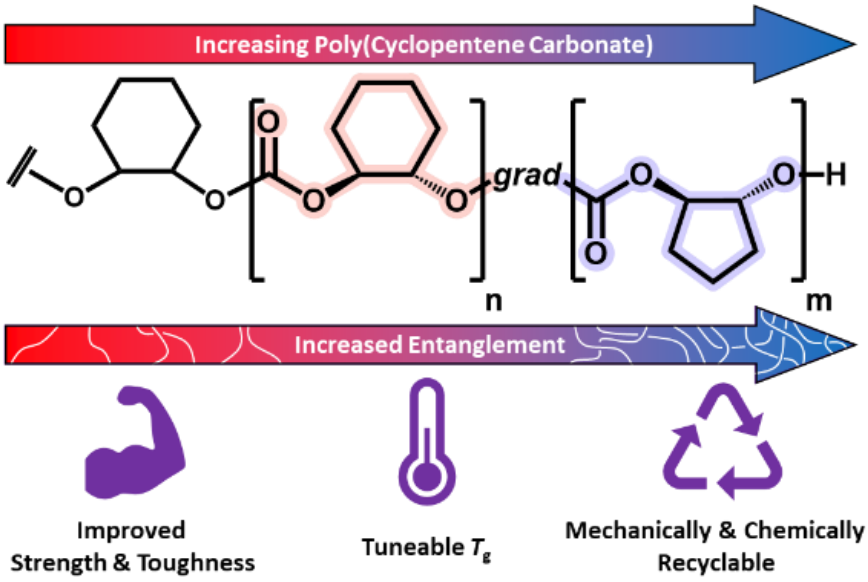

3.1. Introduction

To date, CO_2-derived polymers are almost exclusively explored for uses as low molar mass (M_n) polyols, for example in the production of polyurethanes as foams, elastomers, adhesives and coatings.[1-6] While specialty high molar mass CO_2-derived polycarbonates, such as poly(cyclohexene carbonate) (PCHC), are available commercially, they are employed as sacrificial binders. PCHC could be a useful engineering plastic since it has a high glass transition temperature (T_g = 126 ° C), high tensile strength (40 MPa), and high Young's modulus (2.2 GPa). However, it is very brittle with a very low elongation at break (< 3%) and this limits its effective processing and use.[7, 8] If these materials are to find uses in other applications, their mechanical properties must be better understood, improved, and expanded.

Only a few high molar mass CO_2-derived polycarbonates have been reported and, even in those cases, the mechanical properties were usually not investigated. In 2019, Feng and co-workers synthesised 'ultrahigh' molar mass PCHC (M_n ~ 450 kg mol^{-1}, $Đ_M$ =1.31) through rigorous drying of both CO_2 and CHO, using triisobutylaluminium and triethylborane, respectively.[9] Li and co-workers also produced high molar mass PCHC (M_n ~ 280 kg mol^{-1}, $Đ_M$ =1.59), in a similar manner in 2022.[10] Rieger *et al.* and Greiner *et al.* both reported high molar mass (M_n > 100 kg mol^{-1}), bio-derived poly(limonene) carbonate and terpolymers with PCHC.[11-14] While these reports are synthetically impressive, they do not address the high molar mass PCHC mechanical characterisation.

In 2001, Darensbourg and Koning reported moderate molar mass, high dispersity PCHC (M_n = 42 kg mol^{-1}, $Đ_M$ = 6) which exhibited an ultimate tensile strength of 43 MPa, Young's modulus of 3.3 GPa and strain at break of 2%.[7] The authors predicted the molar mass between entanglements (M_e) to be 16 kg mol^{-1} but noted that the value was likely to be an underestimate. In 2022, Frey and Floudas reported on PCHC chain dynamics through experimental and computational investigations, highlighting these were dominated by the

cyclohexene ring conformational changes.[8] The authors synthesised intermediate molar mass PCHC ($5 < M_n < 33$ kg mol^{-1}) and predicted that the M_e should be far-above 16 kg mol^{-1}, noting that higher molar masses materials are needed to more accurately determine a value of M_e. Williams and co-workers recently reported the synthesis of high M_n, narrowly dispersed CO_2-derived PCHC and poly(cyclopentene carbonate) (PCPC), using a high activity and selectivity [Co(II)Mg(II)] catalyst.[15] The PCHC and PCPC samples, both having M_n ~100 kg mol^{-1}, were investigated using oscillatory rheology to estimate the M_e (from time-temperature superposition (TTS) master-curves, **Equation 3.1**, **Figure 3.1**). The results were striking, with an order of magnitude difference in M_e values between PCHC, M_e = 56 kg mol^{-1}, and PCPC, M_e = 4.0-4.9 kg mol^{-1}. As such, in that study only the PCPC sample was expected to be above the critical molar mass (M_c).

$$G^0{}_N = \frac{4\rho RT}{5M_e} \tag{3.1}$$

Where $G^0{}_N$ is the rubbery plateau modulus (at tan(δ) minimum), ρ is the polymer density (ρ ranges from 800–1100 kg·m^{-3} in most estimates),[16] R is the ideal gas constant, T is the temperature and M_e is the entanglement molar mass.

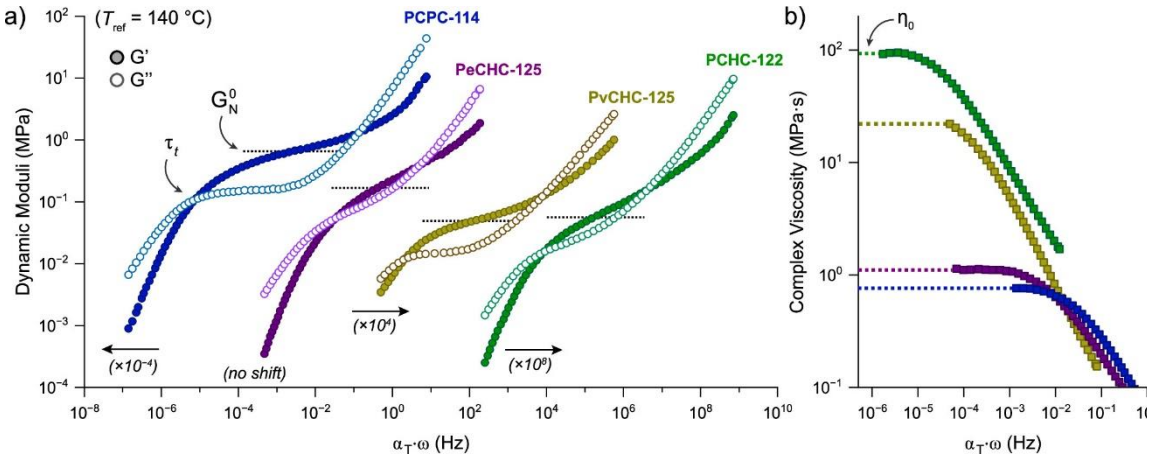

Figure 3.1: a) Time-temperature superposition master-curves for high molar mass polycarbonates b) Plot of shear viscosity vs frequency obtained from TTS master curves and projection of the plateau viscosity to zero-shear. Reproduced from Ref. 15 with permission from the American Chemical Society.[15]

PCPC remains a far less explored polymer than PCHC, with a few reports of its use in catalysis. For example, Wu and co-workers synthesised PCPC with M_n up to 84 kg mol^{-1} and Lu and co-workers have reported the synthesis of semicrystalline, stereo-complex PCPC, with a high melting temperature of 199 °C.[17, 18] Despite these reports, the potential of PCPC as a tough engineering plastic is yet to be fully realised. Comparing PCPC to PCHC reveals it has a slightly higher CO_2 content (34 vs. 31 wt%), a significantly lower zero shear viscosity (0.8 vs. 90 MPa s), higher ultimate tensile strength (59 vs. 40 MPa, respectively) and a slightly higher strain at break (7 and 3%, respectively) resulting in a greater tensile toughness (2.9 and 0.9 MJ m^{-3}, respectively).[15, 18] In fact, only the Young's Modulus and T_g of PCPC are lower than those of PCHC (1.7 vs. 2.2 GPa, 85 vs. 126 °C respectively). Recently, the catalysed chemical recycling of PCHC, and PCPC, to form epoxides and carbon dioxide was reported.[15] This route allows for the synthesis of recycled polymers exhibiting equivalent properties to the virgin materials. For PCPC, Darensbourg and co-workers reported the first depolymerisation catalyst forming CPO and CO_2.[19, 20] Subsequently, other depolymerisation catalysts were reported for both PCHC and PCPC.[17, 18, 21-25] Williams and co-workers reported a very selective solid-state depolymerisation of high molar mass PCHC and PCPC, using a high activity [Mg(II)Co(II)] catalyst.[15]

3.2. Aims

The impressive properties of PCPC motivated the study reported in this chapter. Terpolymerisations incorporating CHO, CPO and carbon dioxide will target higher molar mass polycarbonates in a one-pot synthesis. The objective is to understand how terpolymer compositions and structures might influence chain entanglement and, subsequent, thermomechanical properties with the goal to increase toughness. A series of terpolymers with varying PCHC and PCPC segment content will be produced and the resulting thermomechanical properties will be characterised.

It is anticipated that the PCHC and PCPC segments will be miscible and therefore allow for a reduction in M_e as a result of inter- and intra-chain interactions between the two enchained polycarbonates. It will be critical to determine the reactivity ratios of CHO and CPO with CO_2 to understand the terpolymer microstructure. Moderating the terpolymer composition could be a means to not only improve mechanical performance while maintaining a wide operating window but allow for the tuning of material properties without significant alterations to the synthetic protocol.

The steps taken to achieve these aims will involve: 1) Synthesising a range of high molar mass terpolymers with 25:75, 50:50 and 75:25 mol% PCHC and PCPC respectively; 2) Thermomechanical characterisation of all terpolymers and homopolymers to elucidate the influence segmental composition has on the performance of the materials; 3) Determination of M_e for each material by dynamic mechanical analysis and subsequently, with uniaxial tensile testing, deduce the critical molar mass (M_c); and finally, 4) The terpolymers reported in this chapter should be investigated for both mechanical and chemical recycling and to explore the impact multiple rounds of recycling have on the mechanical performance of the materials.

3.3. Terpolymer Synthesis

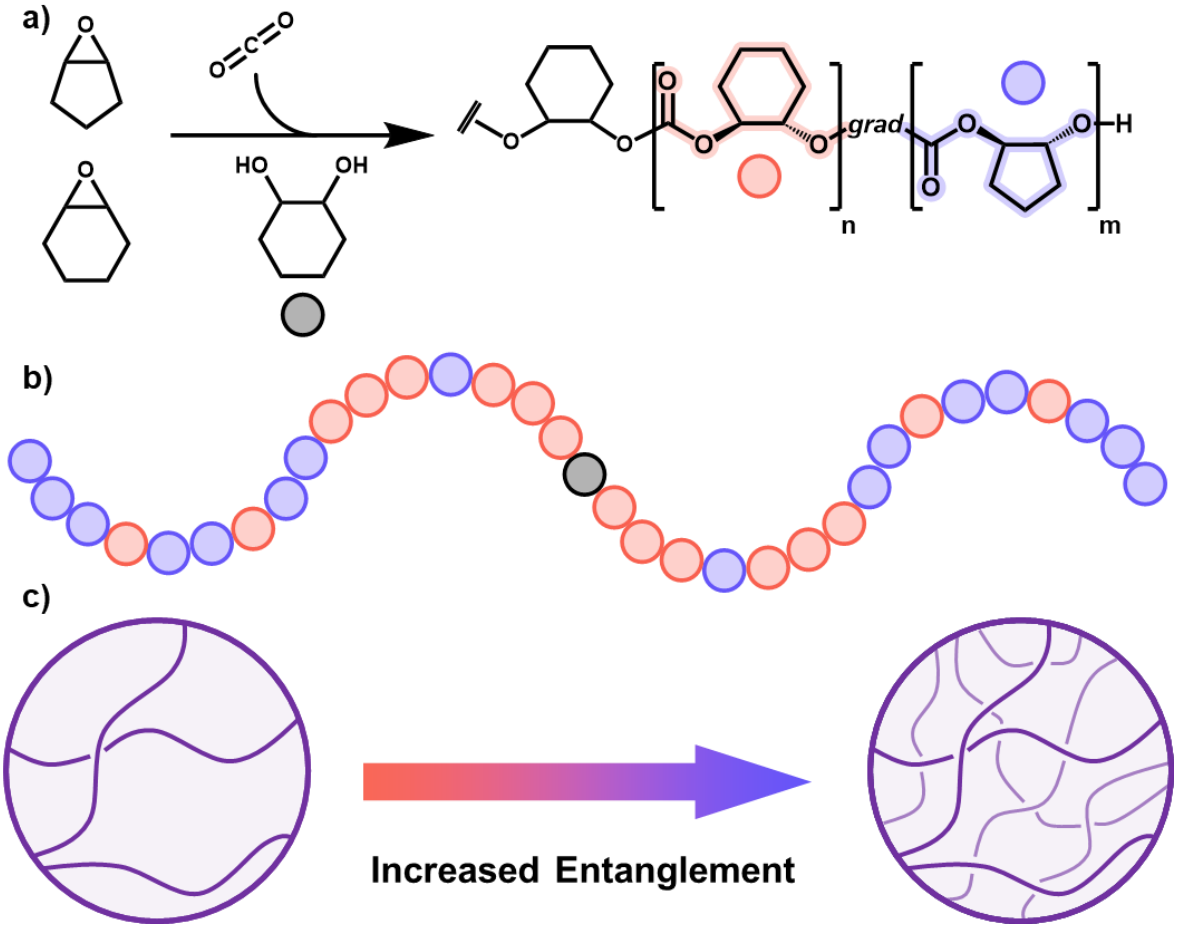

Scheme 3.1: a) Synthesis of PCHC-*grad*-PCPC terpolymers. ROCOP of CO_2, CHO and CPO. Polymerisation conditions: [LZnMg(C_6F_5)$_2$] catalyst, with cyclohexene diol (CHD) as initiator, where $[Cat]_0$:$[CHD]_0$:$[CHO + CPO]_0$ = 1:4:10 000, $[CHO + CPO]_0$ = 4 M, toluene, 80 °C. Schematic representation of b) PCHC-*grad*-PCPC terpolymer and c) increasingly entangled networks.

To make the terpolymers from CHO, CPO and CO_2, we selected the previously reported [LZnMg(C_6F_5)$_2$] catalyst due to its high activity, selectivity, ease of synthesis, end-group selectivity and ability to produce high molar mass, monomodal, low $Đ_M$ polycarbonates.[26] The catalyst features aryl co-ligands which cannot initiate polymerisation, rather they react with an added diol, 1,2-cyclohexane diol (CHD), to form the true initiator *in situ*. This strategy results in the highest levels of initiation control, essential to deliver high molar mass, monodisperse terpolymer samples. To make the terpolymers, the catalyst [LZnMg(C_6F_5)$_2$], cyclohexane diol,

and both monomers CHO and CPO were dissolved in toluene ($[cat.]_0$ = 0.3 mM, $[CHO + CPO]_0$ = 4 M, [cat.]:[CHD]:[CHO + CPO] = 1 : 4 : 10 000). The polymerisations were conducted in a steel Parr reactor, at 80 °C and under a CO_2 atmosphere (40 bar) for 96 hours; conditions were selected to maximise productivity (conversion) (**Scheme 3.1**). Since these are controlled polymerisations, varying the starting monomer feed ratios, i.e. CHO:CPO should result in terpolymers with predictable PCHC:PCPC (**Table 3.1**).

Table 3.1: Summary of Polymerisation Conditions and Results

cat. /mg	CHD /mg	CHO /mL	CPO /mL	Toluene /mL	CO_2 /bar	[a]CHO conv./ %	[a]CPO conv./ %	PCHC :PCPC
5	2.4	2.60	2.18	10	20	86	58	71:29
5	2.4	2.60	2.18	10	40	98	93	51:49
5	2.4	3.89	1.12	10	40	99	91	77:23
5	2.4	1.30	3.36	10	40	96	90	28:72

[a]Determined from ^{1}H NMR spectrum of crude polymer sample

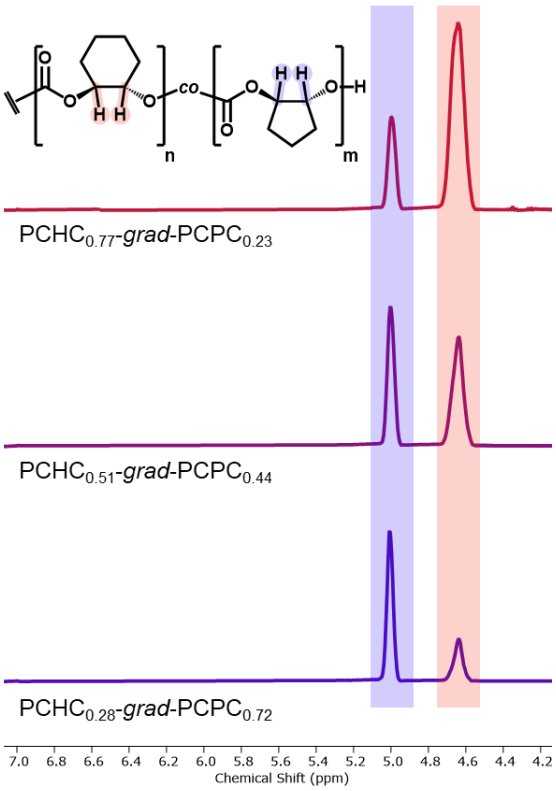

Figure 3.2: ^{1}H NMR (400 MHz, $CDCl_3$) spectra of PCHC-*grad*-PCPC terpolymers with the purple highlighting the PCHC and pink the PCPC resonances used to determine terpolymer composition. (For full spectra, see Figures S7.3.1-S7.3.3)

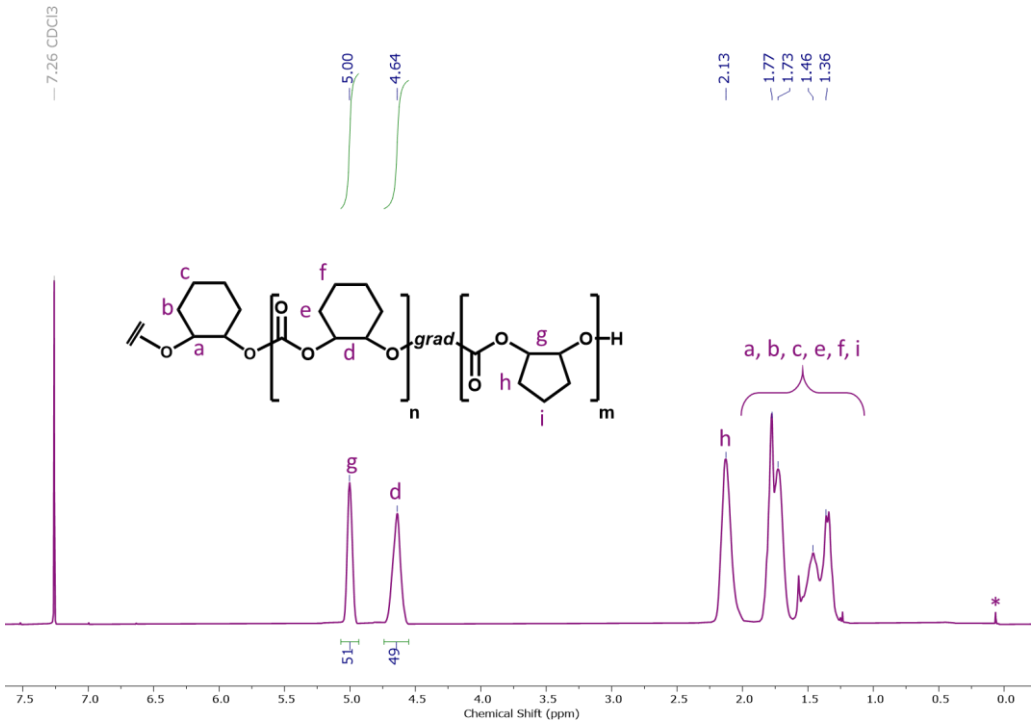

Figure 3.3: Representative ^{1}H NMR spectrum (400 MHz, $CDCl_3$) of PCHC-*grad*-PCPC terpolymer ($PCHC_{0.51}$-*grad*-$PCPC_{0.49}$).

The polymerisations were stopped by reducing the temperature and depressurising the reactors, the crude products were analysed by ^{1}H NMR spectroscopy. For all materials synthesised, >95% epoxide conversion was achieved. The materials were then isolated by precipitation in MeOH. The ^{1}H NMR spectrum of the purified materials established the PCHC and PCPC content in each of the materials, by comparing the integrals of the methine proton signals at δ 4.65 (PCHC) and 5.00 (PCPC), respectively (**Figure 3.2**). The PCHC:PCPC values are 77:23, 51:49 and 28:72. The PCHC-PCPC terpolymers were fully characterised by ^{1}H NMR and ^{13}C NMR spectroscopy (**Figures 3.3** & S7.3.1-S7.3.3). The absence of resonances corresponding to ether linkages (3.45 ppm) or cyclic carbonate (4.00 and 4.68 ppm) indicated there was >99% CO_2 selectivity and >99% polymer selectivity. Size exclusion chromatography (SEC) confirmed the formation of samples showing high molar masses, with M_n > 86 kg mol^{-1}, monomodal distributions with narrow dispersities ($Đ_M$ < 1.22) (**Figure 3.4 & Table 3.2**). The terpolymer structure was also indicated by ^{1}H DOSY NMR spectroscopy with single diffusion coefficient observed for PCHC and PCPC signals (**Figure 3.5**).

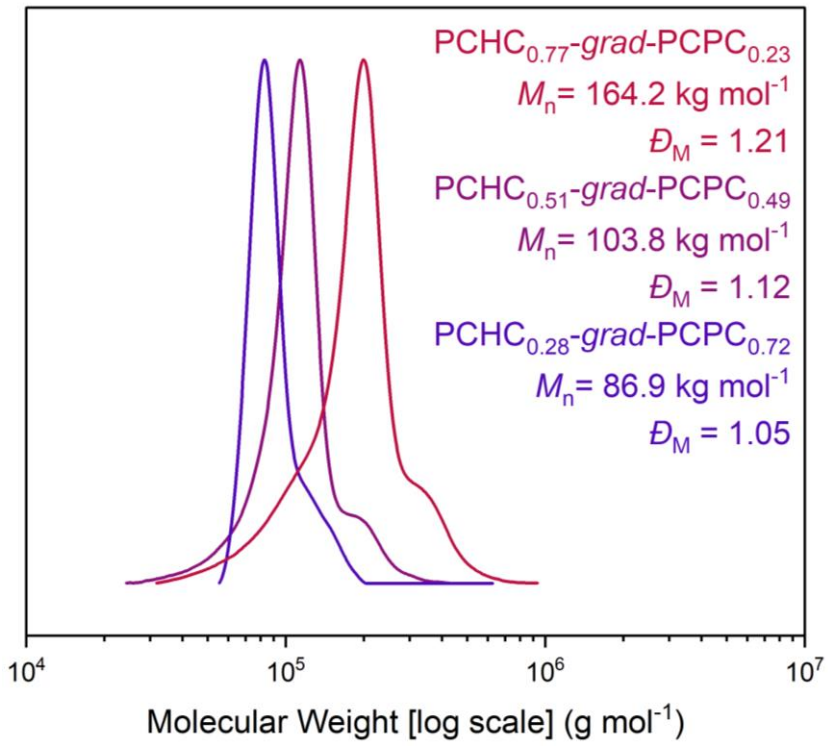

Figure 3.4: SEC (THF, 1 mL min^{-1}) traces for the PCHC-*grad*-PCPC terpolymers. The instrument is calibrated with poly(styrene) standards.

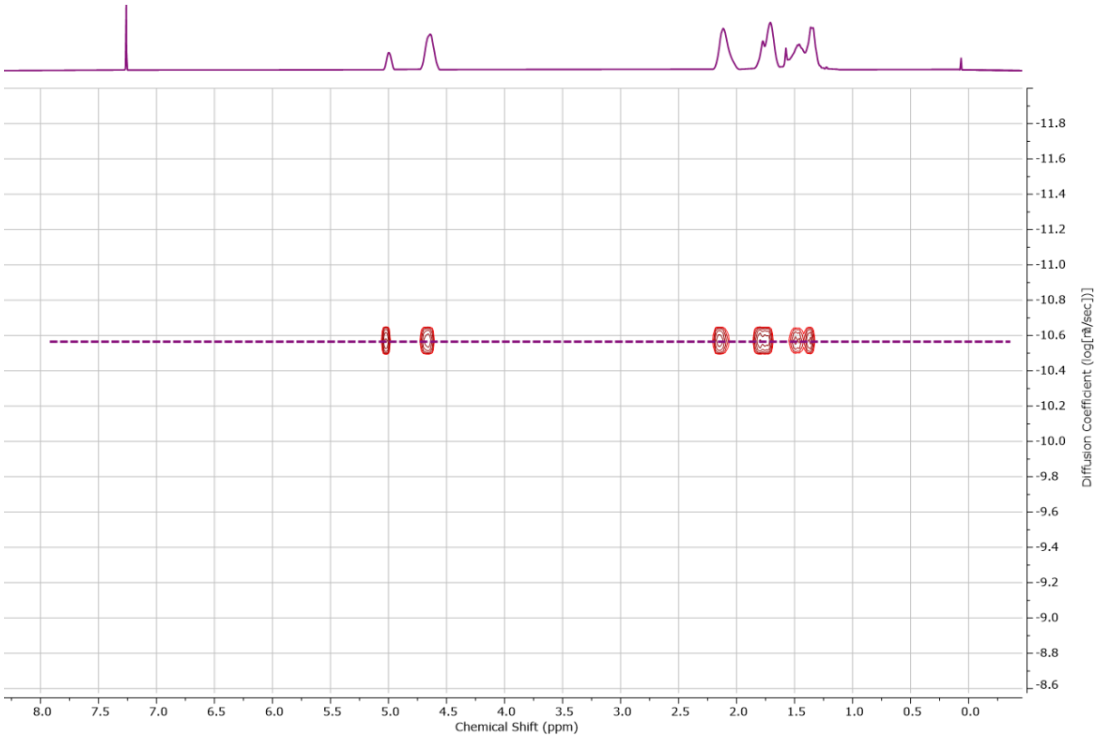

Figure 3.5: Representative ^{1}H DOSY NMR spectrum (500 MHz, $CDCl_3$) of PCHC-*grad*-PCPC terpolymer ($PCHC_{0.51}$-*grad*-$PCPC_{0.49}$).

Table 3.2: Polycarbonate Materials Characterisation Data

Polymer	[a]M_n [b][$Đ_M$] /kg mol^{-1}	[c]$T_{g,DSC}$ / ° C	[d]$T_{d,5\%}$ / ° C	[e]E_Y /GPa	[f]σ /MPa	[g]ε_b /%	[h]U_T /MJ m^{-3}	[i]M_e /kg mol^{-1}
PCHC	121.6 [1.09]	126	265	2.16 ± 0.06	40.0 ± 1.8	3.3 ± 0.3	0.9 ± 0.1	27.6 ± 4.4
$PCHC_{0.77}$ *-grad-* $PCPC_{0.23}$	[†]164.2 [1.21]	108	274	1.48 ± 0.06	50.1 ± 3.2	6.8 ±1.3	2.36 ± 0.5	22.7 ± 3.6
$PCHC_{0.51}$ *-grad-* $PCPC_{0.49}$	103.8 [1.12]	105	250	1.55 ± 0.15	49.4 ± 3.4	6.5 ±0.9	2.34 ± 0.6	10.7 ± 1.7
$PCHC_{0.28}$ *-grad-* $PCPC_{0.72}$	86.9 [1.05]	96	255	1.70 ± 0.24	52.0 ±3.7	7.4 ± 1.3	2.81 ± 0.6	4.3 ± 0.7
PCPC	114.4 [1.06]	85	271	1.7 ± 0.09	58.5 ± 1.7	7.1 ± 1.9	2.9 ± 1.1	3.2 ± 0.5

[a]Determined from SEC analysis (THF); calibrated with narrow polystyrene standards (Figure 3.3). [b]M_w/M_n. [†]Higher M_n a result of higher epoxide conversion and lower residual diol content. All terpolymers above critical molar mass (M_c) [c]Glass transition temperature determined from the mid-point of the 2nd DSC heating cycle. [d]Thermal degradation is the temperature at 5% mass loss, determined by TGA. Specimens suitable for uniaxial tensile testing were solvent cast, dried and compression molded (150 ° C, 1.2 ton m^{-2}, 60 min, Supporting Information). Measurements conducted independently on 10 specimens. [e]Young's modulus. [f]Tensile strength. [g]Strain at break. [h]Tensile toughness (area under the stress-strain curve). Mean values ± std. dev. [i]Entanglement molecular weight determined by DMA temperature ramps, range in values reflect the assumed melt density range of 800 – 1100 kg m^{-3} (**Equation 3.1**, Table S7.3.1, Figures S7.3.4-S7.3.8).

3.3.1. Reactivity Ratios

To better understand the terpolymer structures, Fineman-Ross kinetic analysis was used to determine the epoxides' reactivity ratios in the ROCOP.[27, 28] Terpolymerisations were conducted using the same catalyst and initiator at 1 bar CO_2 pressure, with varying starting quantities of CHO and CPO. By comparing the CHO:CPO feed ratios (F) to the ratio of the monomers enchained in the terpolymer (f) at low conversion (< 15% total epoxide consumption) the Fineman-Ross plot was constructed (**Equation 3.2, Figure 3.6** & Table S7.3.2).

$$\frac{(f-1)}{F} = r_{CPO} - r_{CHO}\frac{f}{F^2} \qquad (3.2)$$

Where f is the ratio of monomers enchained in the terpolymer, F is the feed ratio of monomers, r_{CPO} is the reactivity ratio of CPO and r_{CHO} is the reactivity ratio of CHO.

The relative ratios, F and f, were determined from the ^{1}H NMR spectra of aliquots taken from the terpolymerisations, at t = 0 min and t = 120 min, respectively. Subsequently the reactivity ratios, r_{CHO} and r_{CPO} were determined as 1.53 and 0.08 for the [Zn(II)Mg(II)] catalyst, respectively.[29] As $r_{CHO} > 1 > r_{CPO}$, compositional drift should result in a gradient polycarbonate structure. In the initial stages of the copolymerisation CHO is incorporated faster than CPO, however, as the CHO is depleted increasing quantities of CPO are enchained in the terpolymer. Using a ^{31}P{^{1}H} NMR titration method, the chain end-groups all correspond to PCPC-OH which is fully consistent with the proposed gradient terpolymer structure (**Figure 3.7**). Henceforth terpolymers are abbreviated as $PCHC_{0.x}$-grad-$PCPC_{0.y}$ where x and y are the molar ratios of the two carbonates.

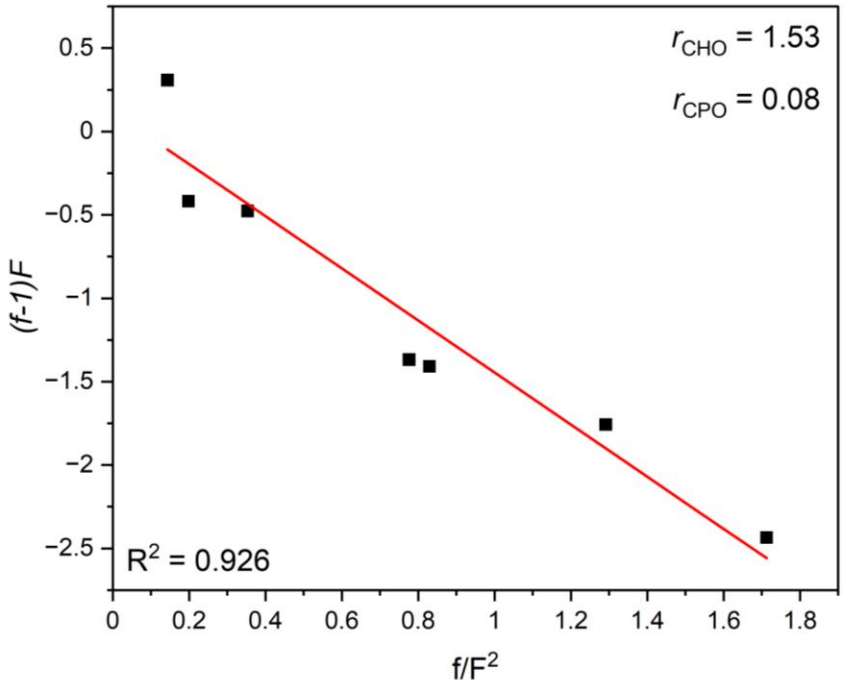

Figure 3.6: Fineman-Ross plots for CHO, CPO and CO_2 terpolymerisations at 80 °C, where the gradient equals -r_{CHO} and the intercept equals r_{CPO}.

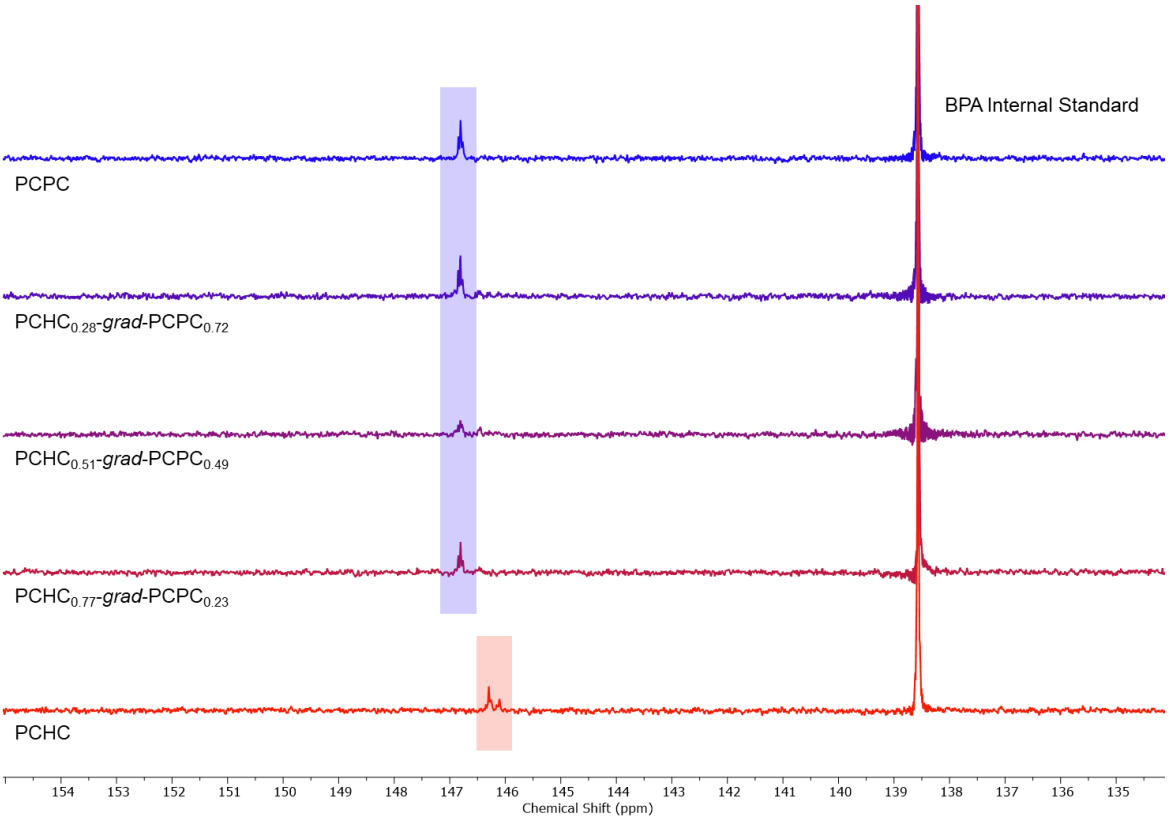

Figure 3.7: $^{31}P\{^{1}H\}$ NMR spectra used for end-group analysis of PCHC, PCHC-*grad*-PCPC terpolymers and PCPC.

3.4. Material Characterisation

3.4.1. Thermal Properties

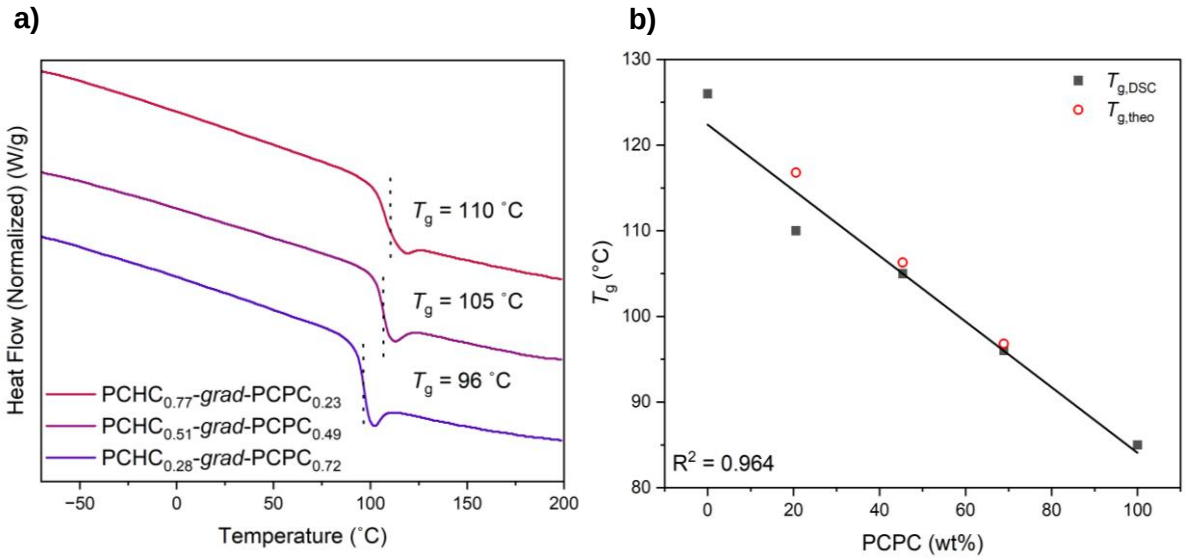

Figure 3.8: a) Differential Scanning Calorimetry (DSC) data for PCHC-*grad*-PCPC terpolymers. b) Plot of the T_g values for PCHC-*grad*-PCPC, from DSC, vs. the PCPC content. The experimental data (black squares) is compared with $T_{g,theo}$ values (red circles) determined using the Fox Flory relationships.

The glass transition temperatures (T_g) of the gradient terpolymers were determined by differential scanning calorimetry (DSC) (**Figure 3.8a & Table 3.2**). All materials are amorphous and a single T_g was observed, its value gradually decreased as the PCPC content increases, falling from 110 °C for PCHC$_{0.77}$-*grad*-PCPC$_{0.23}$ to 96 °C for PCHC$_{0.28}$-*grad*-PCPC$_{0.72}$. The experimental T_g values are fully consistent with the theoretical values ($T_{g,theo}$) predicted by the Flory-Fox equation for each terpolymer (**Equation 3.3, Figure 3.8b**). As such, the PCHC and PCPC segments are expected to be miscible in the terpolymers. This segmental miscibility is proposed to be critical to controlling the chain entanglement, M_e, since it allows for inter-chain PCHC and PCPC interactions. All the terpolymers exhibited good thermal stability, with all $T_{d,5\%}$ values exceeding 250 °C (Figure S7.3.9). Therefore, the material processing temperature range is >143 °C for all the terpolymers.

$$\frac{1}{T_{g,theo}} = \frac{w_{PCHC}}{T_{g,PCHC}} + \frac{w_{PCPC}}{T_{g,PCPC}} \quad (3.3)$$

Where $T_{g,theo}$ is the theoretical T_g of the terpolymer, w_{PCHC} and w_{PCPC} are the weight fractions of PCHC and PCPC respectively, and $T_{g,PCHC}$ and $T_{g,PCPC}$ are the glass transition temperatures for PCHC and PCPC.

3.4.2. Mechanical Properties

To probe the influences of the terpolymer composition on the tensile mechanical properties of the materials, specimens were subjected to uniaxial extension experiments, according to ISO 527 (10 mm min^{-1}) (**Table 3.2, Figure 3.9**). Thin terpolymer films were solvent cast from THF (20 wt% solution) and dried under vacuum to remove all solvent residues (120 °C, 48 h). ^{1}H NMR spectroscopy confirmed the absence of residual THF. The terpolymers were subsequently compression moulded (150 °C, 1.2 tonnes, 60 min) to produce samples suitable for mechanical testing. The $PCHC_{0.77}$-*grad*-$PCPC_{0.23}$, $PCHC_{0.51}$-*grad*-$PCPC_{0.49}$ and $PCHC_{0.28}$-*grad*-$PCPC_{0.72}$ all exhibit high Young's moduli (~1.6 GPa), ultimate tensile strengths (~50 MPa), elongation at break values (~7%), and tensile toughness values (~2.5 MJ m^{-3}) that are within error of each other, despite the varying polycarbonate compositions. All the gradient terpolymers display tensile strengths halfway between those for high M_e PCHC (~40 MPa) and low M_e PCPC (~60 MPa). Critically, even at the lowest levels of PCPC content, the strain at break for the gradient terpolymers is significantly greater than that of PCHC, and, within error, of the 7.1% for PCPC. As a result, the tensile toughness of all these terpolymers is >200% greater than that of PCHC. This improvement in toughness for PCHC, even with the introduction of low quantities of PCPC linkages (23 mol%), results in minimal compromise to the terpolymer glass transition temperatures and, crucially, is easily implemented using the catalysed polymerisation.

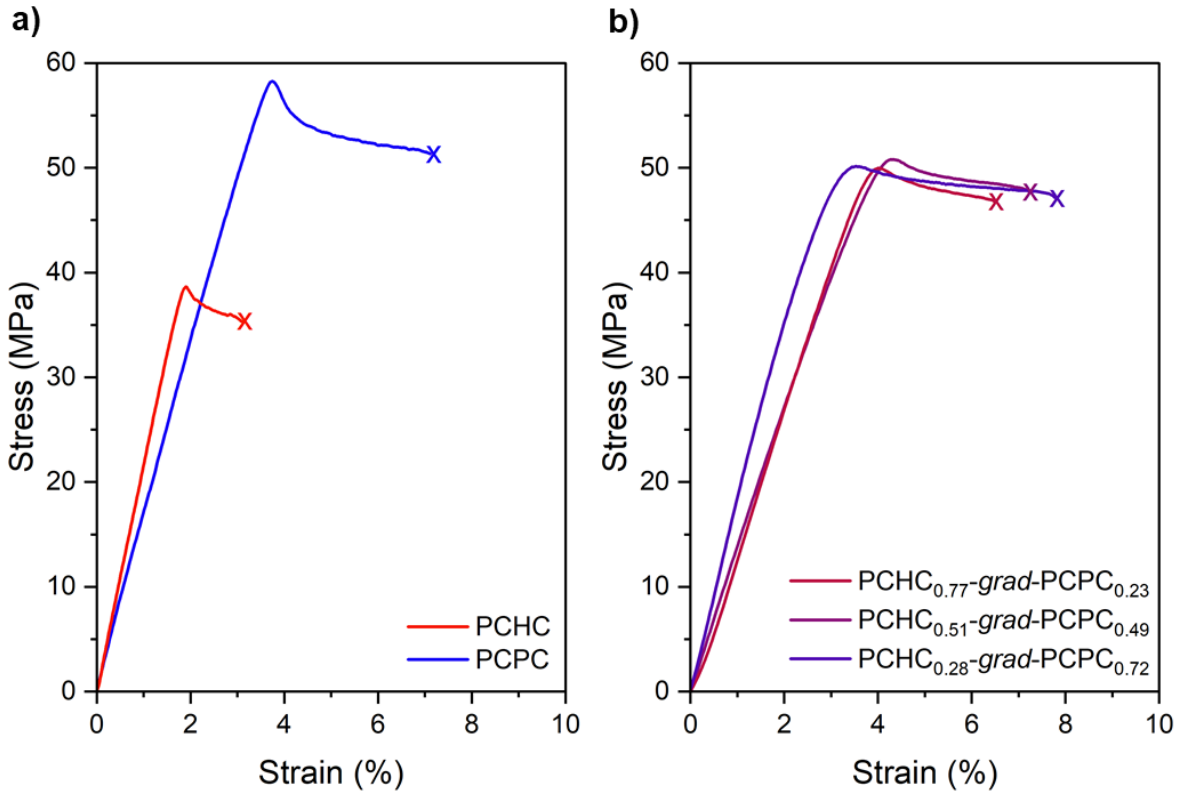

Figure 3.9: Representative stress-strain curves (10 mm min^{-1}) for a) PCHC and PCPC homopolymers and b) PCHC-*grad*-PCPC terpolymers.

3.5. Determining Entanglement Molar Mass (M_e)

To better understand these trends in mechanical performance, all polycarbonates were subjected to dynamic mechanical analysis (DMA) temperature ramps. Thin films were cut using two parallel blades, placed in tension clamps and heated from -80 °C to 250 °C (or until the material deformed beyond the limits of the geometry), at a rate of 3 °C min^{-1}, with a frequency of 1 Hz, 0.1 N pre-load force, and 0.1% strain amplitude (**Figure 3.10**, Figures S7.3.4-S7.3.8). Below the glass transition of each polycarbonate, the storage modulus remains above the loss modulus with both values reaching a plateau despite the increasing temperature. In this region, the terpolymers are glassy and chain movement is severely restricted. As the material passes through its glass transition, the storage modulus decreases while the loss modulus increases (resulting in a peak in the tan(δ)). In this transition region, terpolymer chains start to move with short-range rearrangements dominating and the material transitions from a glassy to rubbery state. Beyond this region, the storage modulus is once again greater than the loss modulus. This is the plateau region where the polymer network is bound by molecular entanglements between the polymer chains. As temperatures increase further, there is sufficient energy for polymer chains to move through any topological restrictions and the network losses mechanical integrity, i.e. the terminal region. By extracting the value of storage modulus at the minimum of tan(δ) in the plateau region, E^0_N was determined. This value was converted to the sheer modulus using **Equation 3.4**. Where ν, the Poisson's ratio of the material, is estimated as 0.36, for all polycarbonates.[30] As such, a value of M_e was estimated using **Equation 3.1** (**Table 3.3**).

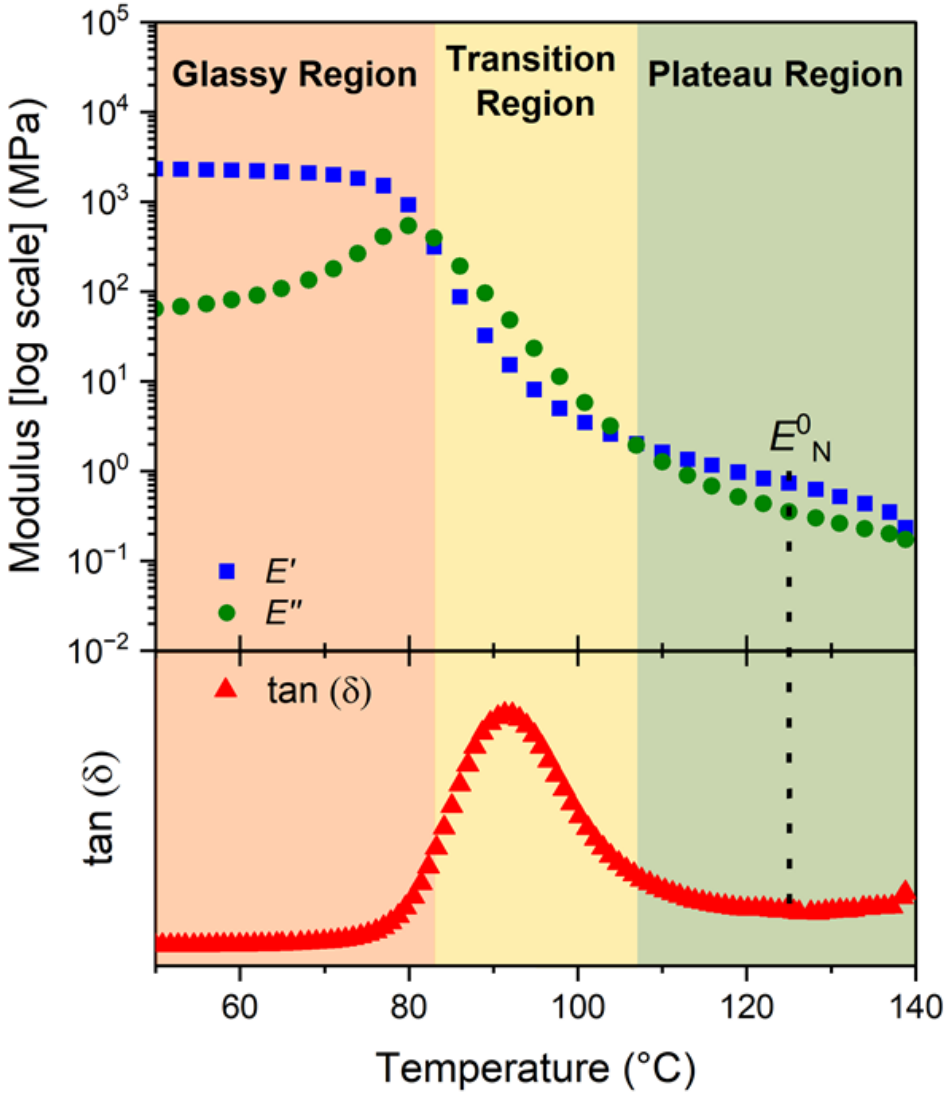

Figure 3.10: Example DMA temperature ramp profile for $PCHC_{0.51}$-*grad*-$PCPC_{0.49}$. Glassy, transition and plateau regions highlighted in orange, yellow and green, respectively. E^0_N is extracted from the rubbery plateau at the minimum of tan (δ).

$$E_N^0 = 2G_N^0(1+\nu) \tag{3.4}$$

Where E^0_N is the elastic modulus, G^0_N is the sheer modulus and ν is the Poisson ratio (assumed to be 0.36 for all materials).[30]

Table 3.3: DMTA Results Used to Determine Entanglement Molecular Weight

Polymer	E^0_N /MPa	T /K
PCHC	0.26933	432.15
$PCHC_{0.77}$-*grad*-$PCPC_{0.23}$	0.32828	434.54
$PCHC_{0.77}$-*grad*-$PCPC_{0.23}$	0.64471	400.46
$PCHC_{0.77}$-*grad*-$PCPC_{0.23}$	1.55958	393.98
PCPC	2.06587	379.62

Values of E^0_N and T taken from the minimum tan (δ) in the plateau region. The value for the density, ρ = 1135 kg·m^{-3} for PCHC.[31] For the terpolymers and PCPC, a density range of 800–1100 kg·m^{-3} was used to provide an estimate.[31]

It is important to note that M_e is often reported from TTS master curves constructed from numerous rheological frequency sweeps at various temperatures. Deducing M_e by DMA is often more challenging as high molar mass materials are required to ensure the plateau region is observed before the material deforms. Here, the high molar masses of these terpolymers obviates this issue. The benefit is that using DMA to determine M_e lies in its simplicity and speed compared with alternative rheological methods and it eliminates the need to fit data to the Williams-Landel-Ferry or Arrhenius equations.

Analysis of the entanglement molar mass for the different samples reveals that as the PCPC content increases, M_e decreases, consistent with increased chain entanglements. This finding is important since it helps fine tune the extent of molecular entanglement within these CO_2-derived polycarbonates. In the same series there was not any marked increase in tensile toughness as the M_e decreases (**Figure 3.11**). Examining materials with steadily increasing PCPC contents from 23 to 72%, the tensile toughness measurements are within error of each other. This suggests that for all these gradient terpolymers, the critical molecular mass (M_c), was exceeded and chains are sufficiently entangled. While estimating the value of M_c as a multiple of M_e is somewhat controversial, most of these polymers show critical molar mass values which appear to be in the range of $4.4M_e < M_c < 7.2M_e$ – such ranges are observed for

many other thermoplastics. Another aspect to emphasise is that despite the pure PCPC sample possessing a value of M_n which is 36 times greater than its M_e, it remains easily processable and reprocessable at 150 °C.

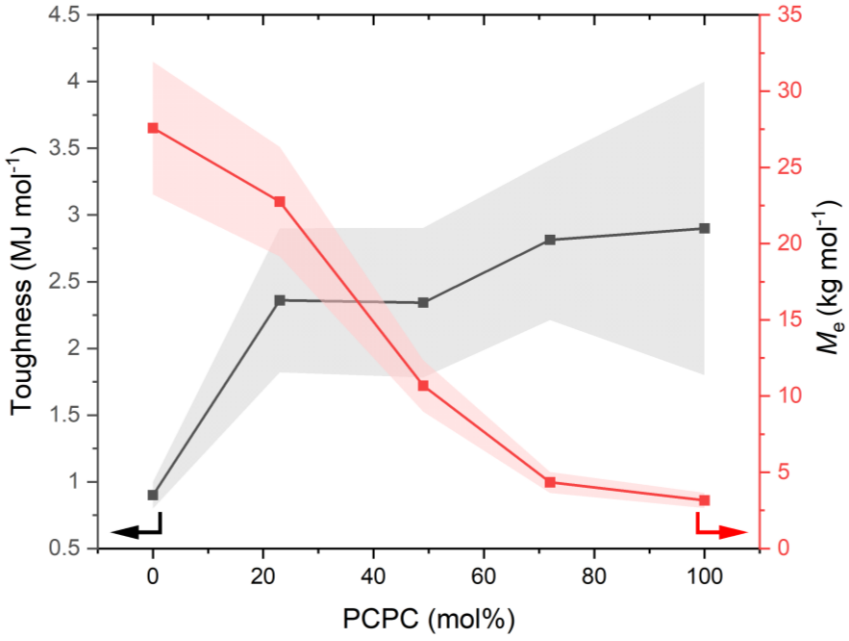

Figure 3.11: Plot showing tensile toughness and entanglement molecular weight of vs. PCPC (mol%) for PCHC-*grad*-PCPC terpolymers.

Literature analysis reveals surprisingly few investigations where polymer structures were modified to control/minimise M_e and hence improve mechanical properties.[32] However, unlike PCHC and PCPC, the previously investigated materials were usually applied at molar masses well above the M_e and the objective was usually to increase M_e to improve processing.[32] For example, Pawlak and co-workers controlled the M_e of poly(propylene) through the regulated slow cooling of a dilute polymer solution.[33] The stress-strain profile for the PP, up to the yield point, was unaffected by the entanglement density but the lower the M_e, the faster the stress increased during the strain hardening stage. Bartczak and co-workers controlled the M_e of ultra-high molar mass poly(ethylene) through high-pressure annealing. Like Pawlak, they observed a greater strain hardening modulus and later onset of strain hardening with increased M_e.[34] Bartczak and co-worker also demonstrated that a lower entanglement density improves

the properties of ultra-high molar mass polypropylene.[35] Hillmyer and co-workers showed that employing low M_e poly(γ-methyl-ε-caprolactone) as a central block in an ABA triblock copolymer is an effective means to produce tough thermoplastic elastomers.[36] The elastomer tensile strength and extensibility were both controlled by the low entanglement molar mass polyester.

In this work, we have demonstrated that through the incorporation of low entanglement molar mass carbonate segments into CO_2-terpolymers, the elasticity of the thermoplastic polycarbonates is improved. It may be that this approach could be applied to toughen other sustainable plastics, many of which are well-known to be highly brittle. Considering the epoxide co-monomers, CPO and CHO are currently petrochemicals,[37] but they can also be prepared by one-pot chemo-enzymatic reactions from triglycerides.[38]

3.6. Recycling

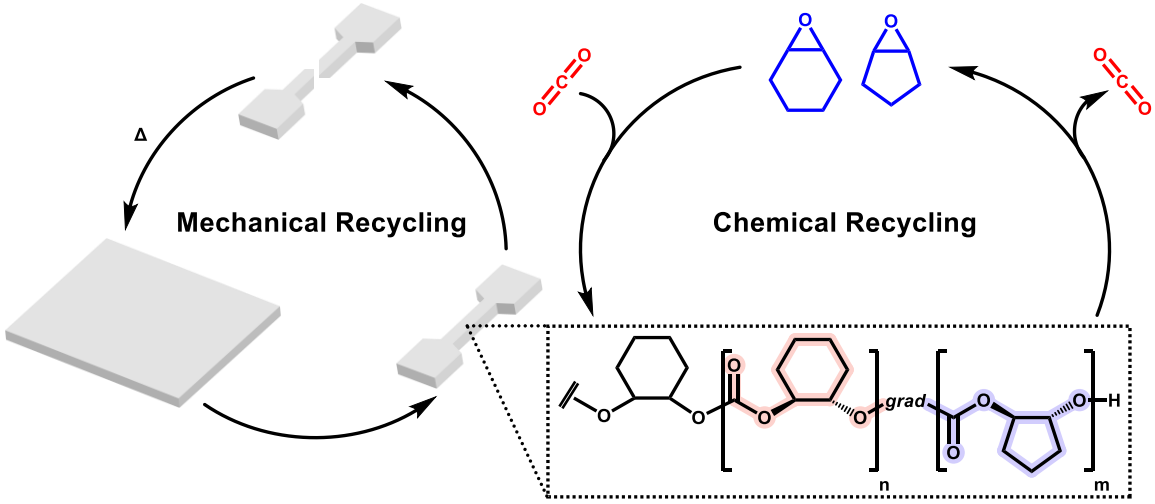

Scheme 3.3: Schematic of the mechanical and chemical recycling of polycarbonate terpolymers.

3.6.1. Mechanical Recycling

The closed loop recycling of thermoplastics is important to minimise end-of-life environmental impacts (**Figure 3.12**).[39, 40] To explore the mechanical recyclability of these gradient terpolymers, $PCHC_{0.51}$-*grad*-$PCPC_{0.49}$ was reprocessed four times by compression moulding at 150 °C, 1.2 tonnes, 60 min. This allowed for the production of films suitable for uniaxial tensile testing (**Figure 3.12**). Throughout the mechanical recycling, the material remained colourless and transparent. SEC analysis, after each reprocessing cycle, revealed no significant change in polycarbonate molecular weight or dispersity, confirming its compatibility with the recycling conditions (**Figure 3.13**). The recycled products showed the same tensile strengths, elongations at break, and tensile toughness, over the four mechanical recycles, compared with virgin polymers (**Figure 3.14**). The slight decrease to the Young's modulus after the first reprocessing is proposed to be the result of minor contamination by

dust/particulate matter into the film, more challenging to exclude on these smaller scales, resulting in defects that slightly reduce the stiffness of the material.

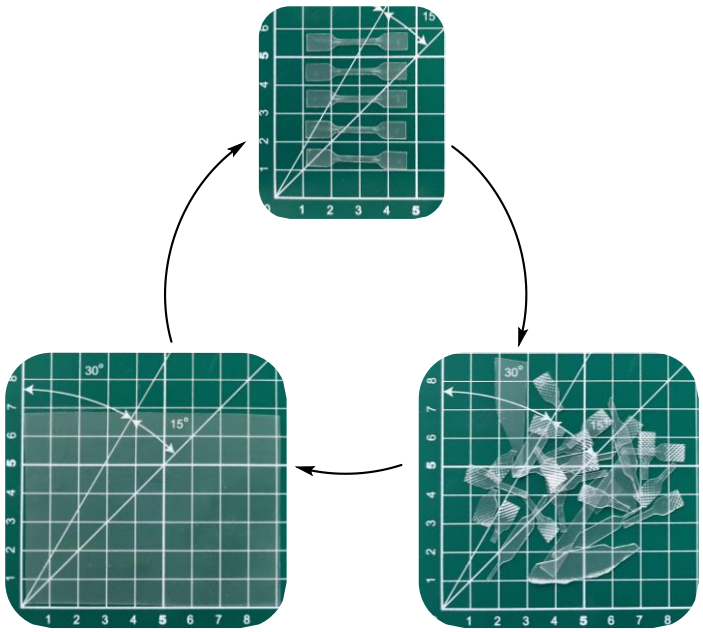

Figure 3.12: Photographs of $PCHC_{0.51}$-*grad*-$PCPC_{0.49}$ throughout the compression moulding and mechanical recycling process. Film thickness ~0.2 mm.

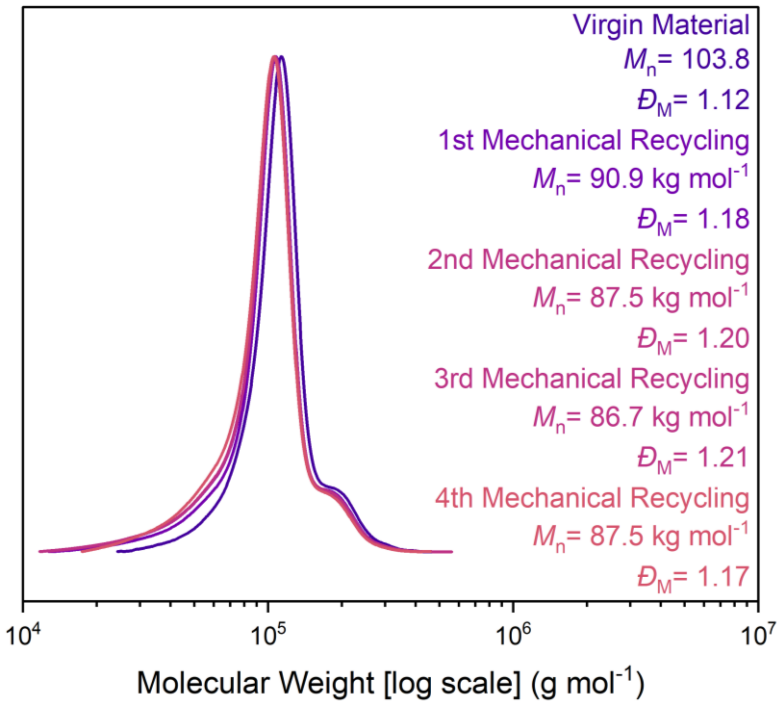

Figure 3.13: SEC (THF, 1 mL min^{-1}) traces for the $PCHC_{0.51}$-*grad*-$PCPC_{0.49}$ after each cycle of mechanical reprocessing. The SEC instrument is calibrated with poly(styrene) standards.

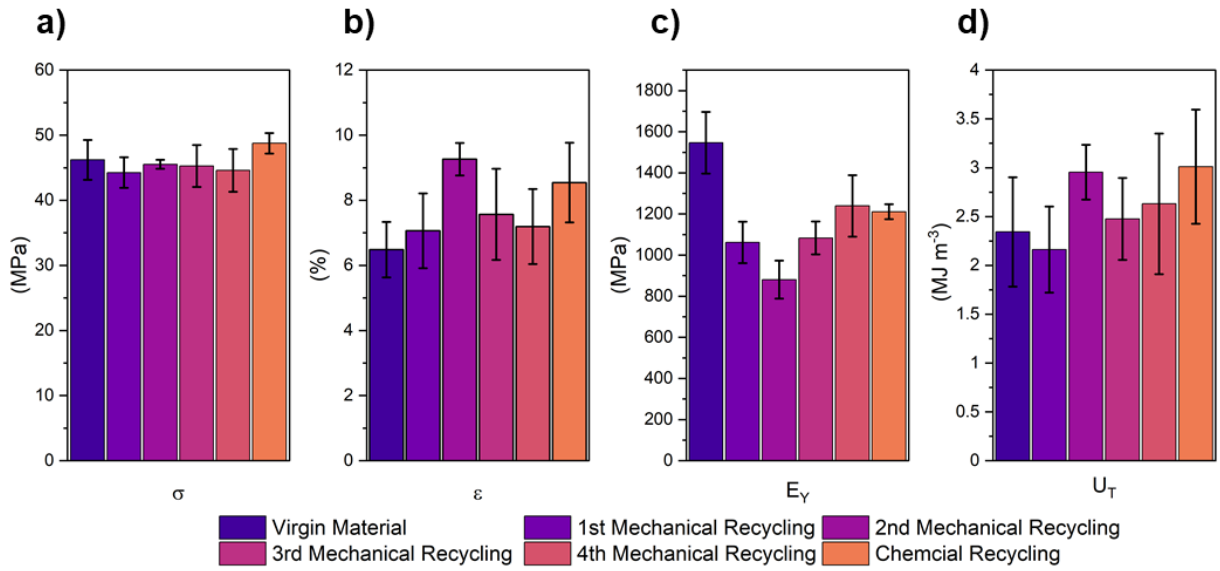

Figure 3.14: a) Tensile strength, b) strain at break, c) Young's modulus and d) tensile toughness for virgin $PCHC_{0.51}$-*grad*-$PCPC_{0.49}$, after four mechanical reprocessing cycles and after chemical recycling to monomer and subsequent repolymerisation. Mean values ± std. dev. From measurements conducted independently on 5 specimens.

3.6.2. Chemical Recycling

Finally, the ability to chemically recycle the gradient terpolymers to the constituent epoxides CHO and CPO, together with CO_2, was explored. A [LCoMg$(OAc)_2$] recycling catalyst was previously reported for the highly efficient and fully selective solid-state PCHC depolymerisation.[25] It was, therefore, selected for investigation in the chemical recycling of the gradient terpolymers and a recently reported TGA experimental method was used to monitor the chemical recycling reaction.[25]

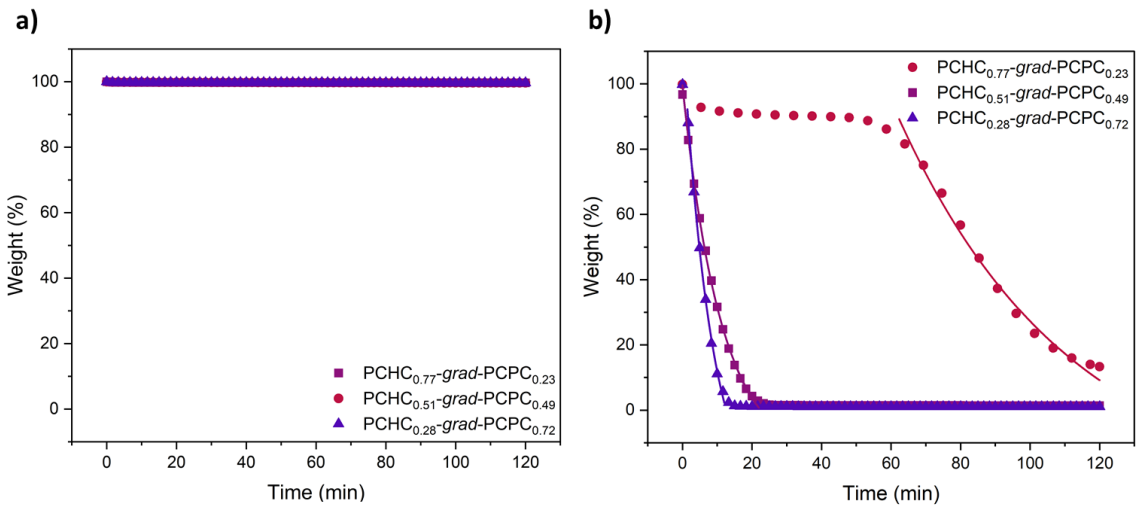

Figure 3.15: Solid-state depolymerisation data for PCHC-*grad*-PCPC terpolymers using a) no catalyst and b) [LCoMg(OAc)$_2$] catalyst (1:300), at 140 °C. Plots show terpolymer mass loss data vs. time. The data is fit to exponentials to determine the pseudo first order rate constants, k_{obs}.

Samples were prepared for these depolymerisation experiments by solvent casting the polymer and catalyst mixtures into TGA crucibles (**Figure 6.10**). In the experiments the relative loadings of [LCoMg(OAc)$_2$] catalyst : polycarbonate repeat unit was 1 : 300. All depolymerisations were performed in triplicate, at 140 °C, with an N_2 flow rate of 25 mL min^{-1}. The complete depolymerisation of PCHC$_{0.51}$-*grad*-PCPC$_{0.49}$ and PCHC$_{0.28}$-*grad*-PCPC$_{0.72}$ was achieved. Plots of the polycarbonate mass loss against time were fit to exponentials, allowing determination of rate constants and, from these, turnover frequencies (TOF) of 926 ± 14 and 1653 ± 201 h^{-1}, respectively (**Figure 3.15**). The depolymerisation of PCHC$_{0.77}$-*grad*-PCPC$_{0.23}$ exhibited an initiation period (1 h) and showed a lower TOF of 270 ± 5 h^{-1}. The lower rate is attributed to the higher absolute molar mass of that sample, compared with others in the series. Previously, chain-end-capping experiments resulted in complete inhibition of the depolymerisation and strongly support a chain-end depolymerisation mechanism.[25] As such, longer chains have a lower chain-end group concentration which reduces their depolymerisation rates relative to shorter chains. Moreover, the restricted chain motion of the

longer polymer chains may reduce the mass transport to the catalyst, which would also slow the depolymerisations and results in the observed initiation period (**Table 3.4**).

Table 3.4: Data for the terpolymer depolymerisations using the [Co(II)Mg(II)] Catalyst

Polymer	[a]k_{obs} / h^{-1}	[b]TOF / h^{-1}
$PCHC_{0.77}$-*grad*-$PCPC_{0.23}$	1.79 ± 0.19	270 ± 5
$PCHC_{0.51}$-*grad*-$PCPC_{0.49}$	5.93 ± 0.99	926 ± 14
$PCHC_{0.28}$-*grad*-$PCPC_{0.72}$	9.40 ± 1.68	1653 ± 201

[a]k_{obs} calculated from exponential fits to plots of terpolymer mass loss vs time. [b]Mass loss rate = mass of PCHC consumed (20−80%conversion)/mass of catalyst/time. Errors are reported from the mean and standard deviations of values determined from three repeat experiments.

The depolymerisation rate constants (k_{obs}) were determined through the exponential fits of the mass loss vs. time data ($R^2 > 0.97$, **Figure 3.15**). The depolymerisation rate constants were 1.8 ± 0.2, 5.9 ± 1.0, 9.4 ± 1.7 h^{-1} for $PCHC_{0.77}$-*grad*-$PCPC_{0.23}$, $PCHC_{0.51}$-*grad*-$PCPC_{0.49}$, and $PCHC_{0.28}$-*grad*-$PCPC_{0.72}$, respectively. These rate data match the TOF data, with $PCHC_{0.51}$-*grad*-$PCPC_{0.49}$ and $PCHC_{0.28}$-*grad*-$PCPC_{0.72}$ showing faster depolymerisation than PCHC but slower than PCPC. The $PCHC_{0.77}$-*grad*-$PCPC_{0.23}$ is slower than either of the homopolymers due to its higher molar mass and lower chain end concentration.

To validate the TGA depolymerisation experiments, a scaled-up depolymerisation of $PCHC_{0.51}$-*grad*-$PCPC_{0.49}$ was conducted using 2.72 g of polymer and standard laboratory glassware. This was carried out by Ms Madeleine L. Smith. The terpolymer and catalyst were cast, as a film, into a glass vessel and the resulting epoxides were collected under a partial

vacuum (40 mbar, N_2). The catalytic recycling resulted in the isolation of 1.41 g of a mixture of CHO:CPO with 3:7 composition, as determined by ^{1}H NMR spectroscopy. The overall recycling occurred with ~ 77% isolated yield of the epoxides (Figure S7.3.10). One aspect to note is that the recycled epoxide ratio does not exactly match the starting terpolymer composition, instead somewhat less CHO was isolated than expected. The difference can be understood by considering the chain end depolymerisation mechanism which is initiated at the PCPC chain ends (see end-group titration experiments, **Figure 3.7**). As the depolymerisation progresses, it is more challenging to ensure chain-catalyst interactions which reduces the recovery of the CHO. Consequently, the overall PCPC and PCHC conversions to epoxide were 95% and 47%, respectively.

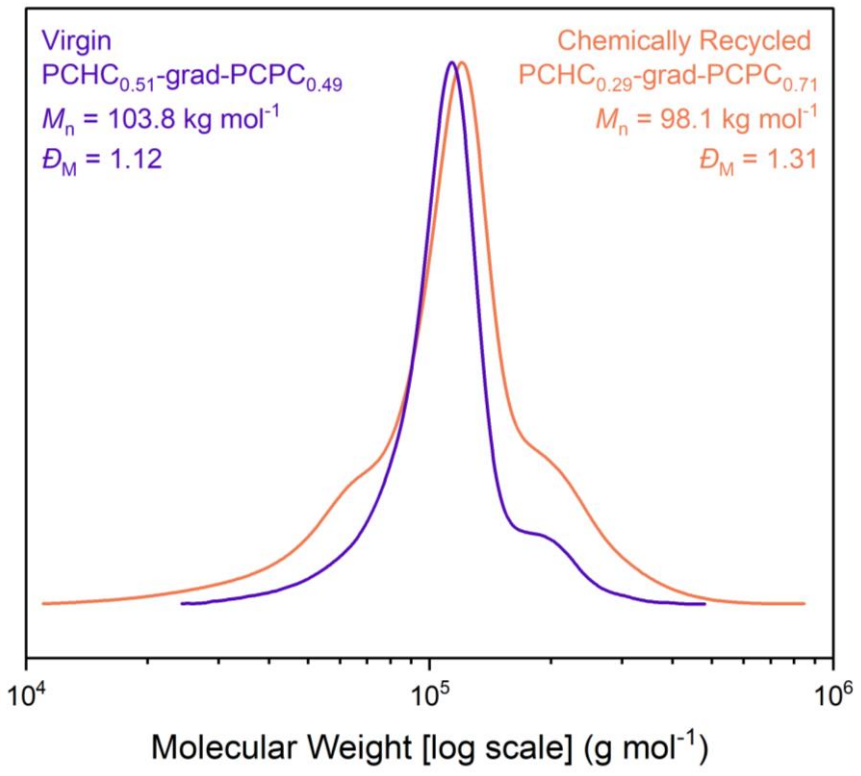

Figure 3.16: SEC (THF, 1 mL min^{-1}) traces for the PCHC$_{0.51}$-*grad*-PCPC$_{0.49}$ and chemically recycled PCHC$_{0.29}$-*grad*-PCPC$_{0.71}$.

To demonstrate that the monomer mixture could be effectively re-polymerised, the CHO and CPO mixture was dried, over CaH_2, distilled and re-polymerised (cat : monomer = 1: 5000, 3 M toluene). The resulting gradient terpolymer, $PCHC_{0.29}$-*grad*-$PCPC_{0.71}$ (M_n = 98.1 kg mol^{-1}, $Đ_M$ = 1.31), had the expected composition and complete epoxide conversions were achieved (1.90 g, Figure S7.3.11). The isolated polycarbonate showed an overall chemical recycling yield of ~70%. The low molar mass shoulder is tentatively attributed to the initiation of trace quantities of acetic acid which result from the acetate co-ligands from the [Co(II)Mg(II)] depolymerisation catalyst (**Figure 3.16**). The high molar mass shoulder, which is also seen in the SEC traces for all terpolymers, is believed to arise from residual cyclopentane diol (CPD) present in the CPO monomer. The slight difference in initiation time between CPD and CHD is responsible for the observed SEC traces. However, it is important to highlight that these protic impurities are only present at trace levels and despite this, the overall molar mass is very high (98 kg mol^{-1}), above M_e, and the chemically recycled material displays equivalent mechanical properties to that of the virgin material. Uniaxial tensile testing of the chemically recycled polycarbonate showed the same mechanical properties as the starting material and to the mechanically recycled polymers (**Figure 3.14,** Figure S7.3.12 & Table S7.3.3). These findings suggest that in future both mechanical and chemical recycling would be feasible for these terpolymers.

3.7. Summary and Future Work

3.7.1. Conclusion

A series of high molar mass, gradient polycarbonates, PCHC-*grad*-PCPC, were produced using carbon dioxide/epoxide ring opening copolymerisations. The materials overcame the brittleness and processing issues associated with prior investigations of poly(cyclohexene carbonate) and exemplify the benefits of cyclopentene carbonate linkage incorporation. The terpolymerisation of cyclohexene oxide, cyclopentene oxide and carbon dioxide, using a high activity and selectivity [Zn(II)Mg(II)] catalyst, formed amorphous gradient polycarbonates in which both carbonate segments were miscible. All terpolymers showed high molar masses (M_n > 86 kg mol^{-1}), glass transition temperatures (T_g > 96 ° C), and wide processing temperature ranges (> 145° C). The gradient terpolymers showed lower entanglement molar masses than PCHC (4 < M_e < 23 kg mol^{-1}) and all samples showed molar mass values that should exceed the critical molar mass. The gradient terpolymers exhibit significantly greater elongation at break and tensile strength than PCHC, resulting in a 200% increase in tensile toughness. The polycarbonates were mechanically recycled via compression molding, at 150 °C, up to four times without any discoloration or loss in mechanical performance. They were also efficiently chemically recycled to epoxide/CO_2, using a solid-state process and [Co(II)Mg(II)] catalyst. The isolated monomers are used to make a recycled polycarbonate showing equivalent properties to the starting materials. The incorporation of some PCPC linkages improves the properties of PCHC. Overall, this work highlights the potential to apply terpolymerisations to improve upon the properties of carbon dioxide-derived thermoplastics. This will enable targeted polycarbonate design where optimal mechanical and thermal properties are achieved and would likely enable the property profile expansion of a range of other sustainable and bio-derived polymers.

3.7.2. Future Work

The ability to increase macromolecular entanglements within a thermoplastic through a terpolymerisation strategy opens up a number of potential opportunities to expand the property space of sustainable and bio-derived polymeric materials.

To develop a better understanding of the importance of terpolymer microstructure on the entanglement molar mass, a number of terpolymers with varying architectures should be synthesised. These should range from diblock, triblock and multiblock copolymers, produced through sequential monomer addition, to those with varying gradient/statistical/random structures, produced by changing the terpolymerisation catalyst and subsequently, the reactivity ratios.[29] This would allow for the influence of the reactivity ratios of the two epoxides in the terpolymerisation to be deconvolved from the final material properties. While this would be academically interesting and help develop a further understanding of sustainable polymer design, it might be less practically valuable as it complicates the existing one-pot synthesis.

This same terpolymerisation approach should be tested with other classes of renewably sourced polymers. For example, the ROCOP of CHO, CPO with a cyclic anhydride (e.g. phthalic anhydride) may also allow for an increase in tensile toughness while maintaining a desirable high T_g for the resulting polyester.[41] The wide range of anhydrides and epoxides would result in a diverse array of polyesters which can be produced by ROCOP. Which give rise to a vast number of terpolymer combinations. This structural variety would likely open up new and previously not accessible property spaces for oxygenated polymers.

Furthermore, terpolymers could also be employed beyond plastics and in an ABA triblock structure to produced tough thermoplastic elastomers (TPEs). Previously reported poly(carbonate-*b*-ester-*b*-carbonate) TPEs have often utilized the physical crosslinking within PCHC blocks to provide structural rigidity and drive elastic recovery.[26, 42, 43] However, as these

blocks typically comprise 30-50 wt% of a triblock copolymer of 50-100 kg mol^{-1}, the PCHC outer blocks are not entangled, let alone above the critical molar mass for the polymer. Utilising PCPC outer blocks would ensure the polycarbonate blocks were entangled and give rise to superior mechanical properties. This would also result in a drop in the upper T_g of the phase separated material and therefore, reduce the operating temperature window. Incorporating a PCHC-*grad*-PCPC terpolymer as the A blocks would yield a TPE with entangled polycarbonate blocks while maintaining a high upper operating temperature.

Finally, as shown in this chapter, PCHC and PCPC are miscible, and it is hypothesised this is critical to ensure intra- and inter-chain interactions which result in a reduction of M_e. Therefore, it may be possible to increase entanglement density by blending the two homopolymers together. This is particularly attractive as PCHC is already produced on a commercial scale. On the other hand, PCPC is currently a specialty polymer. Blending small proportions (<20 wt%) of PCPC into a commercial PCHC matrix may result in the same strengthening and toughening achieved through the terpolymer approach. These tough CO_2-derived thermoplastic blends could simply be produced through the compounding of the two homopolymers. The increased scale of this material production and processing would facilitate additional mechanical testing, such as impact testing (Izod/Charpy), to better understand the potential applications of these new materials and better identify current petrochemical commodity plastics they could replace.

3.8. References

(1) Lee, S. H.; Cyriac, A.; Jeon, J. Y.; Lee, B. Y. Preparation of thermoplastic polyurethanes using generated poly(propylene carbonate)-diols. *Polym. Chem.* **2012**, *3* (5), 1215-1220. DOI: 10.1039/c2py00010e.
(2) Langanke, J.; Wolf, A.; Hofmann, J.; Böhm, K.; Subhani, M. A.; Müller, T. E.; Leitner, W.; Gürtler, C. Carbon dioxide (CO) as sustainable feedstock for polyurethane production. *Green Chem.* **2014**, *16* (4), 1865-1870. DOI: 10.1039/c3gc41788c.
(3) DeBolt, M.; Kiziltas, A.; Mielewski, D.; Waddington, S.; Nagridge, M. J. Flexible polyurethane foams formulated with polyols derived from waste carbon dioxide. *J. Appl. Polym. Sci.* **2016**, *133* (45), 44086. DOI: 10.1002/app.44086.
(4) Stösser, T.; Li, C. L.; Unruangsri, J.; Saini, P. K.; Sablong, R. J.; Meier, M. A. R.; Williams, C. K.; Koning, C. Bio-derived polymers for coating applications: comparing poly(limonene carbonate) and poly (cyclohexadiene carbonate). *Polym. Chem.* **2017**, *8* (39), 6099-6105. DOI: 10.1039/c7py01223c.
(5) Alagi, P.; Ghorpade, R.; Choi, Y. J.; Patil, U.; Kim, I.; Baik, J. H.; Hong, S. C. Carbon Dioxide-Based Polyols as Sustainable Feedstock of Thermoplastic Polyurethane for Corrosion-Resistant Metal Coating. *ACS Sustain. Chem. Eng.* **2017**, *5* (5), 3871-3881. DOI: 10.1021/acssuschemeng.6b03046.
(6) Scharfenberg, M.; Hilf, J.; Frey, H. Functional Polycarbonates from Carbon Dioxide and Tailored Epoxide Monomers: Degradable Materials and Their Application Potential. *Adv. Funct. Mater.* **2018**, *28* (10), 1704302. DOI: 10.1002/adfm.201704302.
(7) Koning, C.; Wildeson, J.; Parton, R.; Plum, B.; Steeman, P.; Darensbourg, D. J. Synthesis and physical characterization of poly(cyclohexane carbonate), synthesized from CO2 and cyclohexene oxide. *Polymer* **2001**, *42* (9), 3995-4004. DOI: Doi 10.1016/S0032-3861(00)00709-6.
(8) Spyridakou, M.; Gardiner, C.; Papamokos, G.; Frey, H.; Floudas, G. Dynamics of Poly(cyclohexene carbonate) as a Function of Molar Mass. *ACS Appl. Polym. Mater.* **2022**, *4* (5), 3833-3843. DOI: 10.1021/acsapm.2c00299.
(9) Jia, M.; Hadjichristidis, N.; Gnanou, Y.; Feng, X. Monomodal Ultrahigh-Molar-Mass Polycarbonate Homopolymers and Diblock Copolymers by Anionic Copolymerization of Epoxides with CO(2). *ACS Macro. Lett.* **2019**, *8* (12), 1594-1598. DOI: 10.1021/acsmacrolett.9b00854.
(10) Zhang, J. B.; Wang, L. B.; Liu, S. F.; Li, Z. B. Synthesis of Diverse Polycarbonates by Organocatalytic Copolymerization of CO and Epoxides: From High Pressure and Temperature to Ambient Conditions. *Angew. Chem., Int. Ed.* **2022**, *61* (4), e202111197. DOI: 10.1002/anie.202111197.
(11) Kernbichl, S.; Rieger, B. Aliphatic polycarbonates derived from epoxides and CO2: A comparative study of poly(cyclohexene carbonate) and poly(limonene carbonate). *Polymer* **2020**, *205*, 122667. DOI: 10.1016/j.polymer.2020.122667.
(12) Hauenstein, O.; Reiter, M.; Agarwal, S.; Rieger, B.; Greiner, A. Bio-based polycarbonate from limonene oxide and CO2 with high molecular weight, excellent thermal resistance, hardness and transparency. *Green Chem.* **2016**, *18* (3), 760-770. DOI: 10.1039/c5gc01694k.
(13) Hauenstein, O.; Agarwal, S.; Greiner, A. Bio-based polycarbonate as synthetic toolbox. *Nat. Commun.* **2016**, *7*, 11862. DOI: 10.1038/ncomms11862.
(14) Bailer, J.; Feth, S.; Bretschneider, F.; Rosenfeldt, S.; Drechsler, M.; Abetz, V.; Schmalz, H.; Greiner, A. Synthesis and self-assembly of biobased poly(limonene carbonate)-block-poly(cyclohexene carbonate) diblock copolymers prepared by sequential ring-opening copolymerization. *Green Chem.* **2019**, *21* (9), 2266-2272. DOI: 10.1039/c9gc00250b.

(15) Rosetto, G.; Vidal, F.; Mcguire, T. M.; Kerr, R. W. F.; Williams, C. K. High Molar Mass Polycarbonates as Closed-Loop Recyclable Thermoplastics. *J. Am. Chem. Soc.* **2024**, *146* (12), 8381-8393. DOI: 10.1021/jacs.3c14170.
(16) Fetters, L. J.; Lohse, D. J.; Richter, D.; Witten, T. A.; Zirkel, A. Connection between Polymer Molecular-Weight, Density, Chain Dimensions, and Melt Viscoelastic Properties. *Macromolecules* **1994**, *27* (17), 4639-4647. DOI: DOI 10.1021/ma00095a001.
(17) Liu, Y.; Zhou, H.; Guo, J. Z.; Ren, W. M.; Lu, X. B. Completely Recyclable Monomers and Polycarbonate: Approach to Sustainable Polymers. *Angew. Chem., Int. Ed.* **2017**, *56* (17), 4862-4866. DOI: 10.1002/anie.201701438.
(18) Yang, G. W.; Wang, Y. H.; Qi, H.; Zhang, Y. Y.; Zhu, X. F.; Lu, C. J.; Yang, L.; Wu, G. P. Highly Selective Preparation and Depolymerization of Chemically Recyclable Poly(cyclopentene carbonate) Enabled by Organoboron Catalysts. *Angew. Chem., Int. Ed.* **2022**, *61* (46), e202210243. DOI: 10.1002/anie.202210243.
(19) Darensbourg, D. J.; Wei, S. H.; Yeung, A. D.; Ellis, W. C. An Efficient Method of Depolymerization of Poly(cyclopentene carbonate) to Its Comonomers: Cyclopentene Oxide and Carbon Dioxide. *Macromolecules* **2013**, *46* (15), 5850-5855. DOI: 10.1021/ma401286x.
(20) Darensbourg, D. J.; Yeung, A. D.; Wei, S. H. Base initiated depolymerization of polycarbonates to epoxide and carbon dioxide co-monomers: a computational study. *Green Chem.* **2013**, *15* (6), 1578-1583. DOI: 10.1039/c3gc40475g.
(21) Li, C. L.; Sablong, R. J.; van Benthem, R. A. T. M.; Koning, C. E. Unique Base-Initiated Depolymerization of Limonene-Derived Polycarbonates. *ACS Macro. Lett.* **2017**, *6* (7), 684-688. DOI: 10.1021/acsmacrolett.7b00310.
(22) Yu, Y.; Fang, L. M.; Liu, Y.; Lu, X. B. Chemical Synthesis of CO2-Based Polymers with Enhanced Thermal Stability and Unexpected Recyclability from Biosourced Monomers. *ACS Catal.* **2021**, *11* (13), 8349-8357. DOI: 10.1021/acscatal.1c01376.
(23) Yu, Y.; Gao, B.; Liu, Y.; Lu, X. B. Efficient and Selective Chemical Recycling of CO2-Based Alicyclic Polycarbonates via Catalytic Pyrolysis. *Angew. Chem., Int. Ed.* **2022**, *61* (34), e202204492. DOI: 10.1002/anie.202204492.
(24) Singer, F. N.; Deacy, A. C.; McGuire, T. M.; Williams, C. K.; Buchard, A. Chemical Recycling of Poly(Cyclohexene Carbonate) Using a Di-Mg Catalyst. *Angew. Chem., Int. Ed.* **2022**, *61* (26), e202201785. DOI: 10.1002/anie.202201785.
(25) McGuire, T. M.; Deacy, A. C.; Buchard, A.; Williams, C. K. Solid-State Chemical Recycling of Polycarbonates to Epoxides and Carbon Dioxide Using a Heterodinuclear Mg(II)Co(II) Catalyst. *J. Am. Chem. Soc.* **2022**. DOI: 10.1021/jacs.2c06937.
(26) Sulley, G. S.; Gregory, G. L.; Chen, T. T. D.; Carrodeguas, L. P.; Trott, G.; Santmarti, A.; Lee, K. Y.; Terrill, N. J.; Williams, C. K. Switchable Catalysis Improves the Properties of CO2-Derived Polymers: Poly(cyclohexene carbonate-b-epsilon-decalactone-b-cyclohexene carbonate) Adhesives, Elastomers, and Toughened Plastics. *J. Am. Chem. Soc* **2020**, *142* (9), 4367-4378. DOI: 10.1021/jacs.9b13106.
(27) Fineman, M.; Ross, S. D. Linear Method for Determining Monomer Reactivity Ratios in Copolymerization. *J. Polym. Sci.* **1950**, *5* (2), 259-262. DOI: DOI 10.1002/pol.1950.120050210.
(28) Sengoden, M.; Bhat, G. A.; Darensbourg, D. J. Sustainable Synthesis of CO2-Derived Polycarbonates from the Natural Product, Eugenol: Terpolymerization with Propylene Oxide. *Macromolecules* **2023**, *56* (6), 2362-2369. DOI: 10.1021/acs.macromol.3c00079.
(29) Darensbourg, D. J.; Chung, W. C. Relative basicities of cyclic ethers and esters. Chemistry of importance to ring-opening co- and terpolymerization reactions. *Polyhedron* **2013**, *58*, 139-143. DOI: 10.1016/j.poly.2012.08.076.
(30) *Modern Plastics: Encyclopedia' 96 with Buyers' Guide*; McGraw-Hill, 1995.
(31) Koning, C.; Wildeson, J.; Parton, R.; Plum, B.; Steeman, P.; Darensbourg, D. J. Synthesis and physical characterization of poly(cyclohexane carbonate), synthesized from CO and

cyclohexene oxide. *Polymer* **2001**, *42* (9), 3995-4004. DOI: Doi 10.1016/S0032-3861(00)00709-6.
(32) Kong, D. C.; Yang, M. H.; Zhang, X. S.; Du, Z. C.; Fu, Q.; Gao, X. Q.; Gong, J. W. Control of Polymer Properties by Entanglement: A Review. *Macromol. Mater. Eng.* **2021**, *306* (12), 2100536. DOI: 10.1002/mame.202100536.
(33) Pawlak, A.; Krajenta, J.; Galeski, A. Cavitation phenomenon and mechanical properties of partially disentangled polypropylene. *Polymer* **2018**, *151*, 15-26. DOI: 10.1016/j.polymer.2018.07.033.
(34) Bartczak, Z. Effect of Chain Entanglements on Plastic Deformation Behavior of Ultra-High Molecular Weight Polyethylene. *J. Polym. Sci. Pol. Phys.* **2010**, *48* (3), 276-285. DOI: 10.1002/polb.21873.
(35) Bartczak, Z.; Beris, P. F. M.; Wasilewski, K.; Galeski, A.; Lemstra, P. J. Deformation of the ultra-high molecular weight polyethylene melt in the plane-strain compression. *J. Appl. Polym. Sci.* **2012**, *125* (6), 4155-4168. DOI: 10.1002/app.36595.
(36) Watts, A.; Kurokawa, N.; Hillmyer, M. A. Strong, Resilient, and Sustainable Aliphatic Polyester Thermoplastic Elastomers. *Biomacromolecules* **2017**, *18* (6), 1845-1854. DOI: 10.1021/acs.biomac.7b00283.
(37) Claus, M.; Claus, E.; Claus, P.; Hönicke, D.; Födisch, R.; Olson, M. Cyclopentadiene and Cyclopentene. In *Ullmann's Encyclopedia of Industrial Chemistry*, pp 1-16.
(38) Wu, S. K.; Zhou, Y.; Gerngross, D.; Jeschek, M.; Ward, T. R. Chemo-enzymatic cascades to produce cycloalkenes from bio-based resources. *Nat. Commun.* **2019**, *10*. DOI: 10.1038/s41467-019-13071-y.
(39) Bachmann, M.; Zibunas, C.; Hartmann, J.; Tulus, V.; Suh, S.; Guillén-Gosálbez, G.; Bardow, A. Towards circular plastics within planetary boundaries. *Nat. Sustain.* **2023**, *6* (5), 599. DOI: 10.1038/s41893-022-01054-9.
(40) Zheng, J. J.; Suh, S. Strategies to reduce the global carbon footprint of plastics. *Nat. Clim. Change* **2019**, *9* (5), 374. DOI: 10.1038/s41558-019-0459-z.
(41) Diment, W. T.; Williams, C. K. Chain end-group selectivity using an organometallic Al(iii)/K(i) ring-opening copolymerization catalyst delivers high molar mass, monodisperse polyesters. *Chem. Sci.* **2022**, *13* (29), 8543-8549. DOI: 10.1039/d2sc02752f.
(42) Yang, G. W.; Wu, G. P. High-Efficiency Construction of CO2-Based Healable Thermoplastic Elastomers via a Tandem Synthetic Strategy. *ACS Sustain. Chem. Eng.* **2019**, *7* (1), 1372-1380. DOI: 10.1021/acssuschemeng.8b05084.
(43) Jia, M. C.; Zhang, D. Y.; de Kort, G. W.; Wilsens, C. H. R. M.; Rastogi, S.; Hadjichristidis, N.; Gnanou, Y.; Feng, X. S. All-Polycarbonate Thermoplastic Elastomers Based on Triblock Copolymers Derived from Triethylborane-Mediated Sequential Copolymerization of CO2 with Various Epoxides. *Macromolecules* **2020**, *53* (13), 5297-5307. DOI: 10.1021/acs.macromol.0c01068.

CHAPTER 4

Digital Light Processing to Afford High Resolution and Degradable CO_2-Derived Copolymer Elastomers

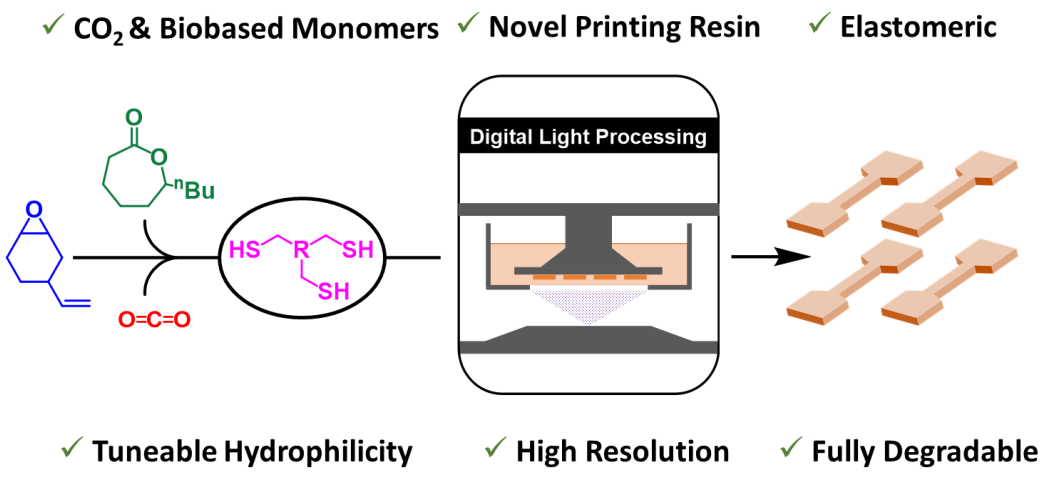

4.1 Introduction

The additive manufacturing (commonly known as 3D printing) of polymers is a powerful means to quickly produce complex geometries and shapes which would otherwise be very challenging to fabricate through traditional manufacturing techniques like compression or injection molding.[1-4] In 3D printing, a layer-by-layer build approach may be achieved through various methods including material extrusion, binder jetting or powder bed fusion. However, these techniques often result in poor resolution.[5] On the other hand, vat photopolymerisation techniques, such as digital light processing (DLP) allow for fast build speeds, high resolution and smooth finishes.[6, 7]

Additive manufacturing is useful for improving process sustainability since it is energy efficient, reduces material loses, and allows for part customisation.[8] The use of DLP to print highly customisable parts from oxygenated, degradable polymers is a promising strategy for tissue engineering and regenerative medicine.[9-11] Beyond biomedical applications, DLP could be useful in other high growth fields like electronics and robotics.[12, 13]

DLP is a bottom-up printing technique that uses projected UV light to cross-link photoreactive resins with spatiotemporal control. DLP features a build tray which rises after the formation of each layer to allow uncured resin to refill the vat, resulting in a layer-by-layer printing process.[14] To date, the vast majority of DLP resins are either polyacrylates, poly(methacrylate)s or poly(propylene fumarate)s.[5, 15] The rather narrow range of printable resins constrains the property profiles of the printed materials. There is an urgent need to develop new resins and, subsequently, to broaden the thermomechanical properties of the printed materials to unlock new applications.

Low M_n and hydroxyl end-capped polymeric materials, polyols, are interesting for printing as they offer low viscosities and high reactivities.[16-22] Therefore, developing routes to cross-link polyol resins can improve thermomechanical properties and allow for the formation of

functional materials without complicating processing. Furthermore, the production of polyols by ROP and ROCOP minimises the extensive purification required for high molar mass polymers. Recent developments in additive manufacturing have shown how oxygenated block copolymers, prepared by ROCOP, can be printed to produce materials with a wide range of properties.[23-25] The precise control of molar mass, end-group fidelity, and architecture ROCOP provides makes these materials highly tunable.[26] Not only does ROCOP provide great control over the polymers produced, but it also allows for a wide monomer scope, which can be expanded even further when coupled with heterocyclic ROP in switch catalysis.[27] Utilisation of these methods should be prioritised to tune properties of 3D printed materials. For example, Wang and co-workers recently reported the thiol-ene based DLP printing of cytocompatible elastomers, where the ROCOP of *cis*-5-norbornene-endo-2,3-dicarboxylicanhydride and propylene oxide (PO) afforded a functionalisable A block in an ABA block copolymer.[25]

Extensive studies into the use of poly(propylene fumarate) (PPF), prepared from the ROCOP of maleic anhydride and PO, have underlined the potential of oxygenated polymers in printing resins.[23-25] The unsaturated alkenes can undergo photochemical cross-linking, allowing its use in DLP as a homopolymer, random copolymer and block copolymer, in both linear and star architectures.[23, 24, 26, 28-31] The 3D printing of PPF and biocompatible composites has made it a promising candidate for tissue engineering and regenerative medicine.[26] Recent developments have harnessed a thiol-ene crosslinking to produce fully degradable elastomers, while eliminating the use of toxic solvents.[23, 24, 31] By controlling the alkene to thiol ratio, the cross-linking density can be tuned and subsequently, so too the mechanical properties.[23, 24]

To date, there have been relatively few studies into the use of aliphatic polycarbonates for additive manufacturing.[5] In 2022, Pentzer and Darensbourg reported the extrusion-based printing of high molar mass (M_n = 20.2-53.9 kg mol^{-1}) poly(vinyl cyclohexene carbonate-*b*-butylene carbonate-*b*-vinyl cyclohexene carbonate).[32] The porous structures printed were easily modified by UV-initiated thiol-ene functionalisation; however, lower print resolutions were

achieved (nozzle diameter = 838 μm) and *N*,*N*-dimethyl formamide was needed in the formulation.

Vat photopolymerisation may help to obviate these limitations (*vide supra*). Grijpma and Eglin employed end-group functionalised poly(trimethylene carbonate) (PTMC) for stereolithography, in combination with hydroxyapatite, to produce high resolution composite scaffolds for bone repair.[33-35] Dove and co-workers used an alkene functionalised TMC, in thiol-ene stereolithography, to make tissue engineering scaffolds.[36-38] Finally, Simpson and Jin reported the thiol-yne DLP printing of degradable alkyne functionlised TMC.[39]

4.2 Aims

It is imperative that new and sustainable DLP resins are developed while the mass adoption of the additive manufacturing technology is in its infancy. This will ensure that this rapidly growing manufacturing sector develops with sustainability integral to its foundations. This ambition motivated the work in this chapter and this investigation was carried out in collaboration with Prof. Matthew L. Becker at Duke University, N.C., U.S.A. Here, we target the synthesis of a low molar mass ABA triblock copolymer with CO_2-derived polycarbonate outer blocks flanking a central bio-derived poly(ε-decalactone) (PDL) block, low molar mass analogue of the triblock copolymer reported in Chapter 2. The pendent vinyl group on each repeat unit of the polycarbonate blocks can then be utilised in thiol-ene based DLP printing.

The steps taken to achieve the successful high resolution 3D printing of elastomer and development of new bio- and CO_2-derived material will involve: 1) The optimization of printing conditions and a resin formulation with a range of trifunctional thiols with varying chain lengths and poly(ethylene glycol) (PEG) contents; 2) Full thermomechanical characterization to understand the influence of the thiol crosslinker on the performance of the material; 3) Exploring the change in hydrophilicity on the degradation profile and cytotoxicity as PEG content increases.

The goals are to employ sustainable feedstocks in additive manufacturing to produce functional, degradable, and biocompatible materials, which can be printed at high resolutions. It is anticipated that this series of materials will demonstrate the wide array of bio-derived and sustainable monomers available for use in additive manufacturing. Furthermore, they will elucidate design principles key to guiding the development of new 3D printed materials for high value applications in biomedicine, robotics, and electronics.

4.3 Triblock Copolymer Synthesis

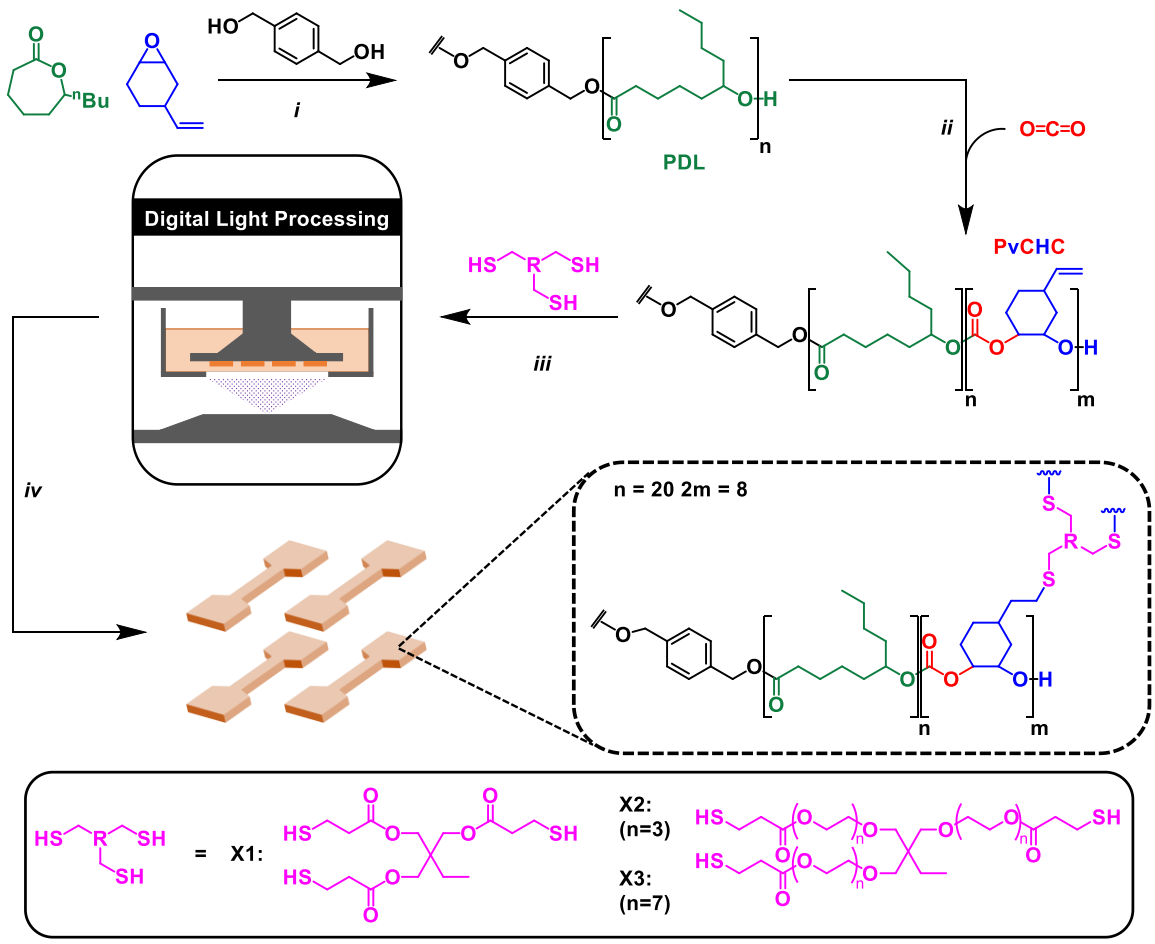

Scheme 4.1: Synthesis of poly(carbonate-ester-carbonate) **P1** for DLP thiol-ene 3D printing. (i) ε-DL ROP, 80˚C, [LCoMg(OAc)$_2$] (Supporting Information for synthetic protocol) with BDM as the initiator, where [Cat.]$_0$:[BDM]$_0$:[vCHO]$_0$:[ε-DL]$_0$ = 1:150:1486:4405, [LCoMg(OAc)$_2$]$_0$ = 0.35 mM, toluene. (ii) CO_2/vCHO ROCOP, CO_2 (1 bar), 80 ˚C. PvCHC-PDL-PvCHC (**P1**): $M_{n,\ SEC}$ = 6.3 kg mol^{-1} ($Đ_M$ = 1.26), 30 wt% PvCHC by ^{1}H NMR spectroscopy. (iii) DLP of **P1** with trimethylolpropane tris(3-mercaptopropionate) (**X1**) and ethoxylated trimethylolpropane tris(3-mercaptopropionate) (**X2, X3**), [alkene]$_0$:[thiol]$_0$ = 5:1, λ = 385 nm, 30 wt% ethyl acetate, 0.6 wt% BAPO photoinitiator, 0.4 wt% oxybenzone photoinhibitor, 0.1 wt% Sudan I dye. (iv) Printed parts washed in ethyl acetate, isopropyl alcohol, and water. Post-cured at λ = 385 nm for 15 min and dried at 60 ˚C, *in vacuo*, for 6 days.

The triblock copolymer, poly(vinyl cyclohexene carbonate-*b*-ε-decalactone-*b*-vinyl cyclohexene carbonate) (PvCHC-PDL-PvCHC) was prepared on a 204 g scale using switchable catalysis.[40] The one-pot process utilised a heterodinuclear [LCoMg(OAc)$_2$] catalyst, with 1,4-benzenedimethanol (BDM) as both the bifunctional initiator and chain transfer agent (CTA), to yield ABA triblock polymer architectures (**Scheme 2.1**).[41] The catalyst [LCoMg(OAc)$_2$] was selected for its high turnover frequencies (TOF) for both lactone ROP and CO_2/epoxide ROCOP, tolerance to high monomer loadings, and end-group fidelity.[41]

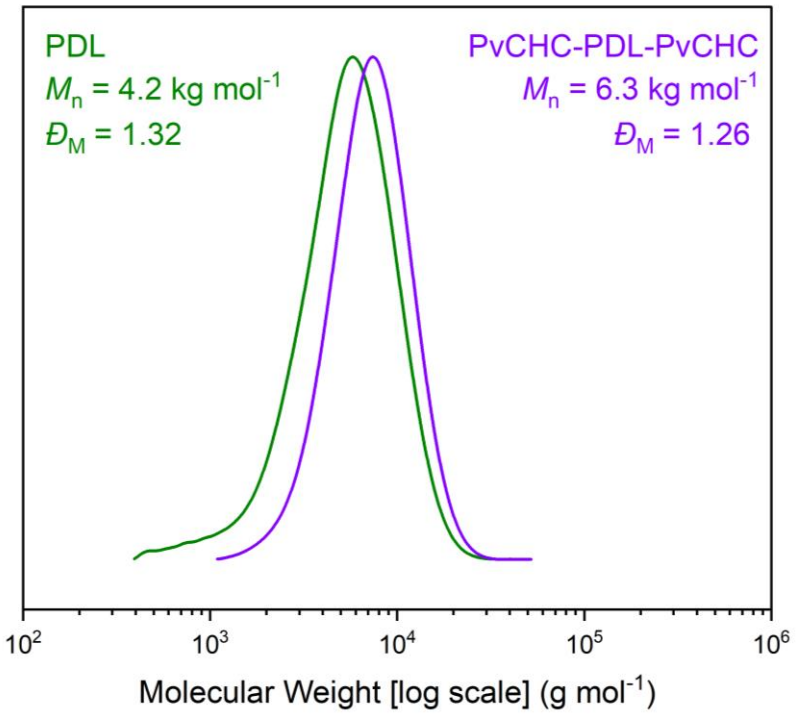

Figure 4.1: SEC (THF, 1 mL min^{-1}) data for the PDL block (B block) and the purified PvCHC-PDL-PvCHC (**P1**).

In the scaled-up synthesis, the catalyst and CTA were dissolved in the monomer mixture of ε-decalactone (ε-DL), 4-vinyl-cyclohexene oxide (vCHO), and toluene ([LCoMg(OAc)$_2$]$_0$ = 0.35 mM, [LCoMg(OAc)$_2$]$_0$:[BDM]$_0$:[vCHO]$_0$:[ε-DL]$_0$ = 1:150:1486:4405). The reaction was heated to 80 °C, resulting in efficient ROP of ε-DL to produce the central PDL block, in high conversion and rate (98%, TOF = 1439 h^{-1}). Removal of a reaction aliquot allowed for characterisation by ^{1}H NMR spectroscopy showing only PDL formation and by size exclusion

chromatography (SEC) analysis, a molar mass of 4.2 kg mol^{-1} with a monomodal distribution ($Đ_M$ = 1.32) (**Figure 4.1**). At this point, the reaction gas was changed from N_2 to CO_2 (1 bar) to switch the reaction to vCHO and CO_2 ROCOP, forming the flanking PvCHC end blocks in high epoxide conversions (>99%, >99% CO_2 selectivity, >99% polymer selectivity, TOF = 21 h^{-1}). The triblock copolymer was isolated and purified by dilution in THF, stirring with Amberchrom™ 50WX8 (hydrogen form, 100-200 mesh) overnight and filtration (twice, through silica) to remove the used catalyst and any diol. Following concentration *in vacuo*, the colorless polymer was collected with 85% yield (**P1**) (Figure S7.4.1).

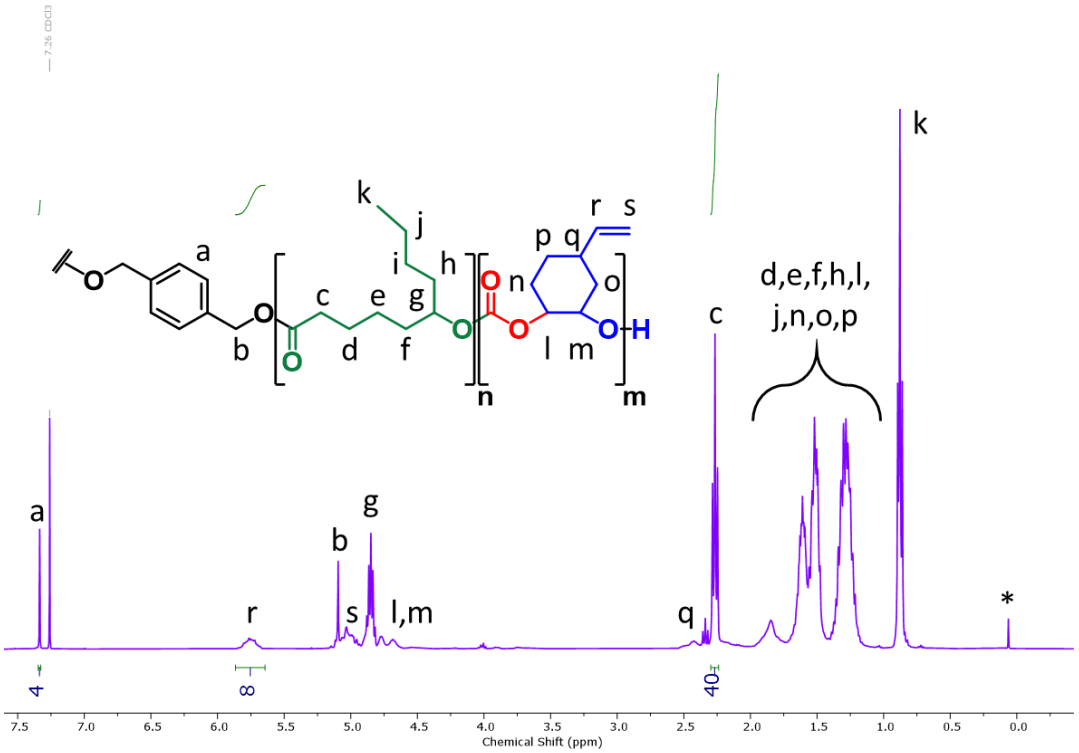

Figure 4.2: ^{1}H NMR (400 MHz, $CDCl_3$) spectrum of PvCHC-PDL-PvCHC triblock copolymer (**P1**).

The purified triblock copolymer (**P1**) showed a molar mass of 6.3 kg mol^{-1} ($Đ_M$ = 1.26) by SEC (**Figure 1**). The residual initiating acetate groups on the catalyst resulted in ~1% diblock content. The residual diblock content (1.3%) is a theoretical determination based on the molar ratio of difunctional benzene dimethanol (BDM) and monofunctional acetate ligands present on the catalyst. Both species can act as initiators and chain transfer agents. There are two

acetate co-ligands per catalyst and 150 equivalents of BDM. Therefore, the maximum number of possible diblock copolymer chains initiated from the acetate coligands is 2/(150+2) = 1.3%. The real diblock content is likely significantly lower because residual diols present in the vCHO act as a bifunctional initiator (these diols form from any water that the epoxide is exposed to, including from carbon dioxide). Experimentally, ^{1}H NMR spectroscopy is used to characterise the polymers and the only initiator signals observed are for BDM, signals corresponding to acetate end-groups are not seen. These results indicate the diblock copolymer content in **P1** is too low to be detected by NMR spectroscopy but nonetheless it is expected to be present.

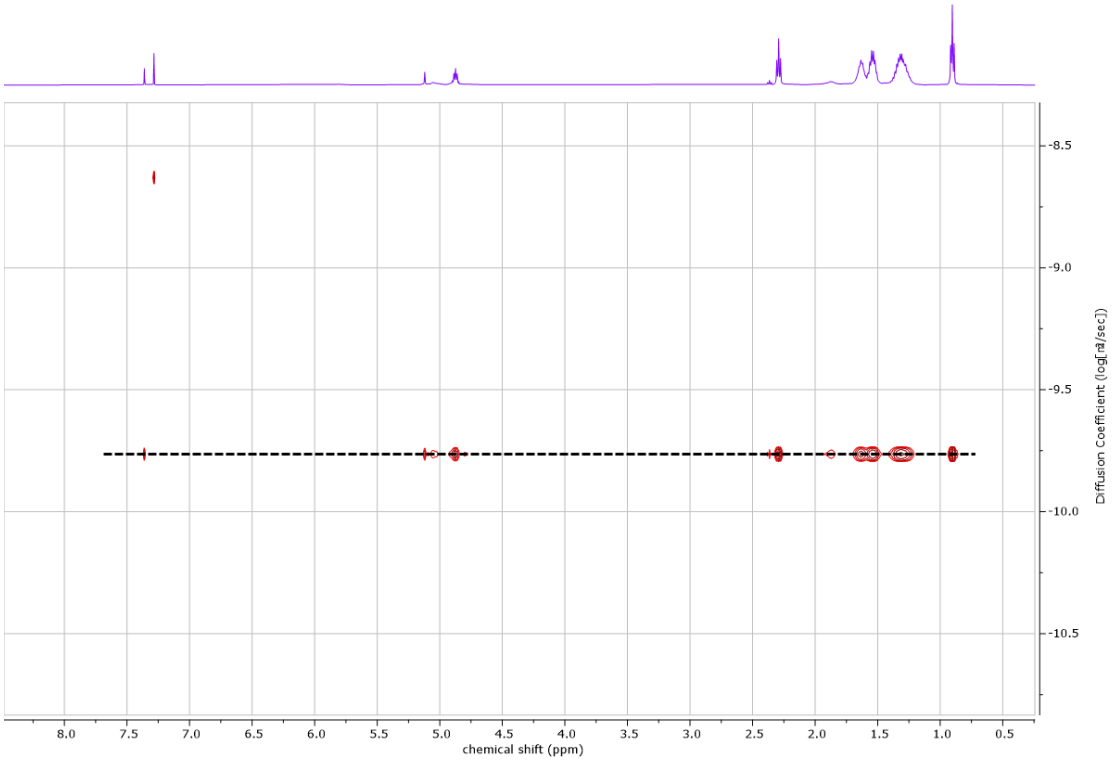

Figure 4.3: ^{1}H DOSY NMR (400 MHz, $CDCl_3$) spectrum of PvCHC-PDL-PvCHC triblock copolymer (**P1**).

Given the high loadings of benzenedimethanol and the overall low molar mass of **P1**, a monomodal mass distribution was obtained by SEC. The molar mass (SEC) agreed well with both the theoretical value (5 kg mol^{-1}) and the value determined by ^{1}H NMR spectroscopy (**Figure 4.2** & Figures S7.4.2-S7.4.4). By comparing the integrals of the initiator (BDM) aromatic resonances, at 7.34 ppm, with those at 2.27 and 5.76 ppm (PDL main-chain -C*H*$_2$-

and PvCHC -C*H*=CH$_2$ respectively), $M_{n,\,NMR}$ was calculated as 4.8 kg mol^{-1} and the average DPs for the blocks were 4:20:4 (PvCHC-PDL-PvCHC). Furthermore, a PvCHC (A-block) content of 30 wt% was determined, matching the range targeted for elastomeric properties.[42]

^{1}H DOSY NMR spectroscopy of the triblock polymer showed only a single diffusion coefficient for all resonances consistent with its copolymer structure (**Figure 4.3**). The addition of a phospholane reagent to the triblock polymer, followed by ^{31}P{^{1}H} NMR spectroscopy, allowed for the analysis of the chain end-groups (**Figure 4.4**).[43] This experiment revealed almost complete PvCHC end-group formation (97%). A very small proportion of PDL end-groups was attributed to the slower diffusion of CO_2 through the viscous reaction mixture at 1 bar. Nonetheless, the presence of low quantities of PDL should not hinder the use of **P1** in additive manufacturing.

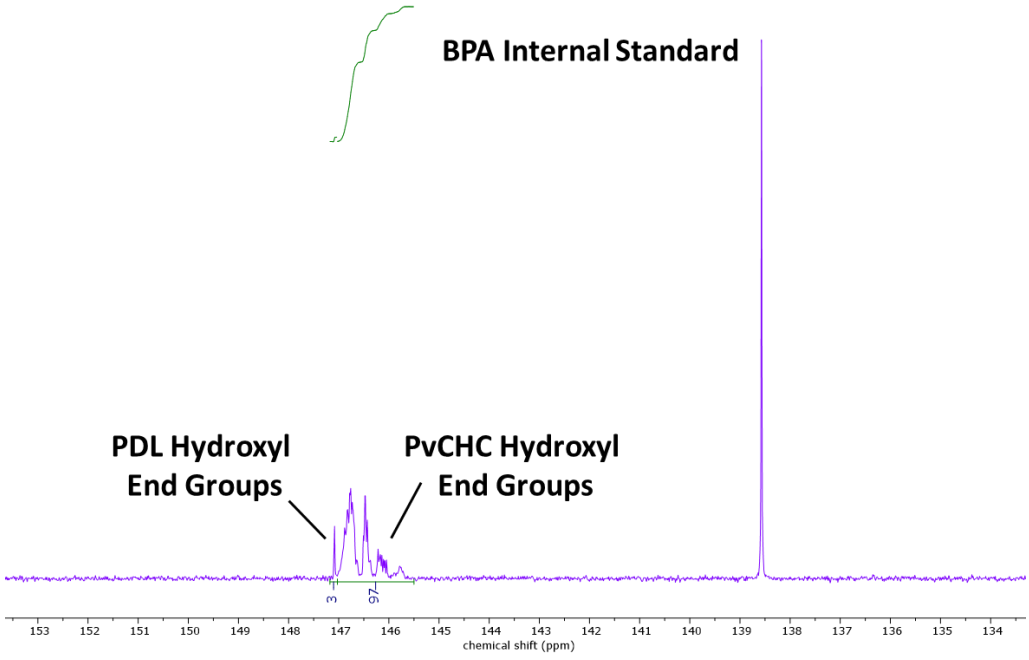

Figure 4.4: ^{31}P{^{1}H} NMR end-group analysis of PvCHC-PDL-PvCHC triblock copolymer (**P1**).

Inductively Coupled Plasma Mass Spectrometry (ICP-MS) analysis on **P1** revealed that the residual cobalt from spent catalyst in the polymer is 1.36 μg/g or 1.36 mg/kg (1.36 ppm).

Therefore 97.2% of the spent cobalt from the catalyst was removed during purification. For context the LD_{50} for soluble cobalt salts is between 150 and 500 mg/kg.[44] Subsequently, for a 100 kg person, the LD_{50} of **P1** would be over 14,000 kg or 14 tonnes. Subsequently, we believe that these extremely low cobalt concentrations in **P1** pose minimal toxicity risk but further testing is needed to fully understand the long-term *in vitro* health impacts of these materials.

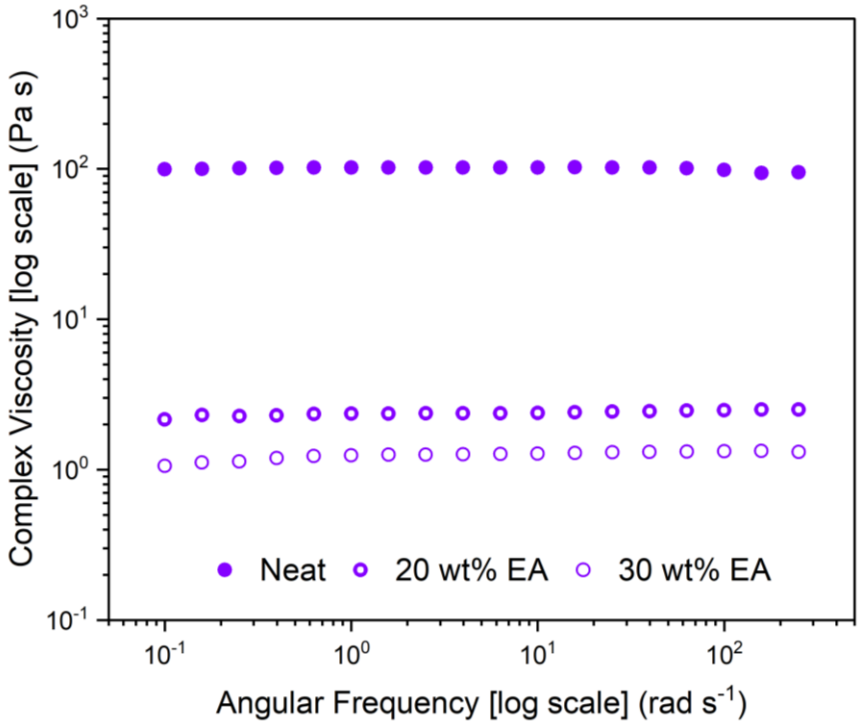

Figure 4.5: Complex viscosity of **P1** triblock copolymer with varied dilutions in ethyl acetate (EA).

Differential scanning calorimetry (DSC) showed a single glass transition temperature (T_g) for **P1** of -39 °C, which indicates that the blocks are miscible as expected given its low molar mass (**Table 4.1** & Figures S7.4.5-S7.4.6). Critically, the T_g of **P1** is below room temperature and it is a viscous liquid under ambient conditions. A rheological frequency sweep was used to determine its complex viscosity, which was 102 Pa s, significantly greater than the 10 Pa s empirical limit for DLP 3D printing **(Figure 4.4)**.[45] The addition of 20 and 30 wt% ethyl acetate decreased the complex viscosity to 2.4 and 1.3 Pa S, respectively. The printing resin

was subsequently formulated with 30 wt% ethyl acetate which resulted in a viscosity closest to 1 Pa s, where optimal printing performance is generally observed.[24]

4.4 Resin Formulation

The 3-arm trithiol, trimethylolpropane tris(3-mercaptopropionate) (**X1**), was initially employed for the thiol-ene based printing (alkene:thiol = 5:1) and produced 3D printed thermosets capable of complete hydrolytic degradation. Controlled thiol-ene cross-linking was achieved by adding 0.6 wt% phenylbis(2,4,6-trimethylbenzoyl)phosphine oxide (BAPO, photoinitiator) and 0.4 wt% oxybenzone (photoinhibitor) to the printing resin.[39] Finally, to eliminate lateral overcuring and allow for spatiotemporal control of the thiol-ene cross-linking during the print, 0.1 wt% Sudan I orange dye was added to the resin (**Figure 4.6**). UV-vis spectroscopy was used to titrate the amount of dye and match the absorbance profile of the novel resin to well-established poly(propylene fumarate) based resins known to successfully print via DLP (Figure S7.4.7).

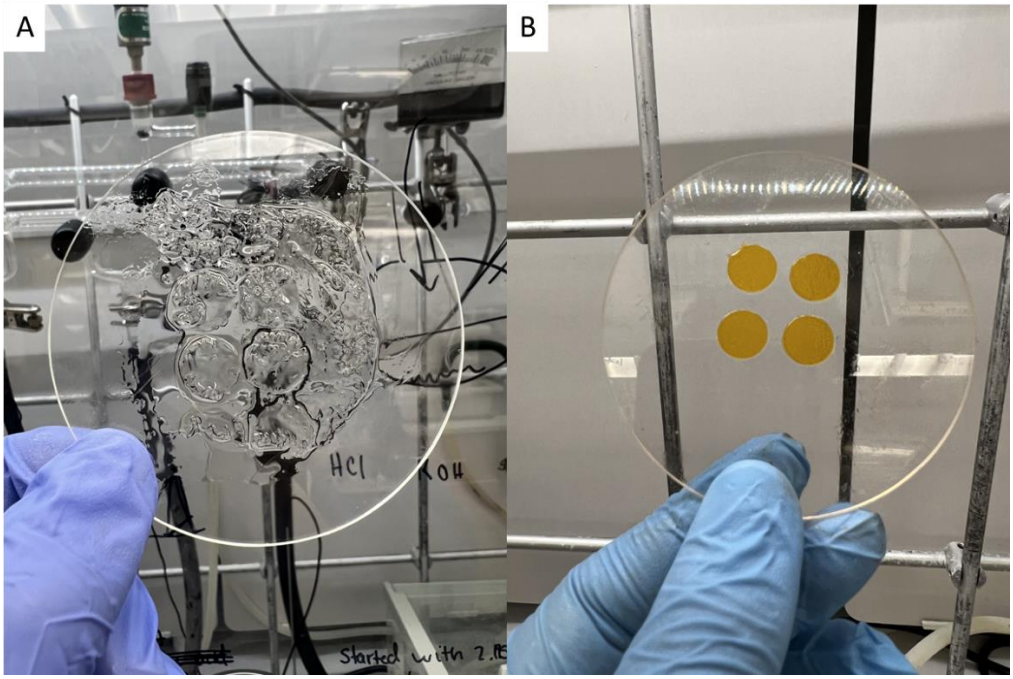

Figure 4.6: Digital photographs of cure testing of **P1** and **X1** A) without and B) with 0.1 wt% Sudan I dye.

4.5 DLP Printing

The resin was successfully printed by DLP using an EnvisionTech D4K Pro 3D printer (λ = 385 nm) to form a novel thermoset (**P1X1**). A series of dumbbell-shaped, cuboid, and cylindrical specimens were 3D printed, then washed sequentially with ethyl acetate, isopropyl alcohol, ethyl acetate, and finally water (**Figures 4.7-4.8**). The printed parts were then cured in a UV oven (λ = 390-420 nm) for 15 minutes, followed by drying *in vacuo* at 60 °C for 6 days. Following the successful printing of **P1** with **X1**, the printing process was repeated with two additional 3-arm thiol cross-linkers, with varying oligoethylene glycol units (n = 3 and n = 7 per arm for **X2** and **X3**, respectively, **Scheme 4.1**). The use of different cross-linkers allows investigation of their length on thermomechanical properties and the effect of increased hydrophilicity upon degradation rates in relation to PEG content. Both **P1X2** and **P1X3** were successfully printed and a series of three thermosets were obtained.

Figure 4.7: Digital photograph of **P1X1** printed parts on built plate (before workup).

The small defects which can be observed in **Figure 4.7**, likely result from a slightly over-crowded build plate design. In this central area, it is harder for the resin to refill because of the surrounding parts and its viscosity. Because the resin isn't as efficiently refilled in these areas, the same sections of resin are repeatedly experiencing UV exposure, resulting in slight gelation. In future, such effects may be eliminated by either: 1) a greater degree of dilution to further reduce the viscosity of the resin or 2) optimization of the build plate layout to ensure efficient resin refilling. The lightly crosslinked regions of the excess resin are not attached to the parts and hence were removed from the build plate when the printed parts were washed and purified. No trimming was required.

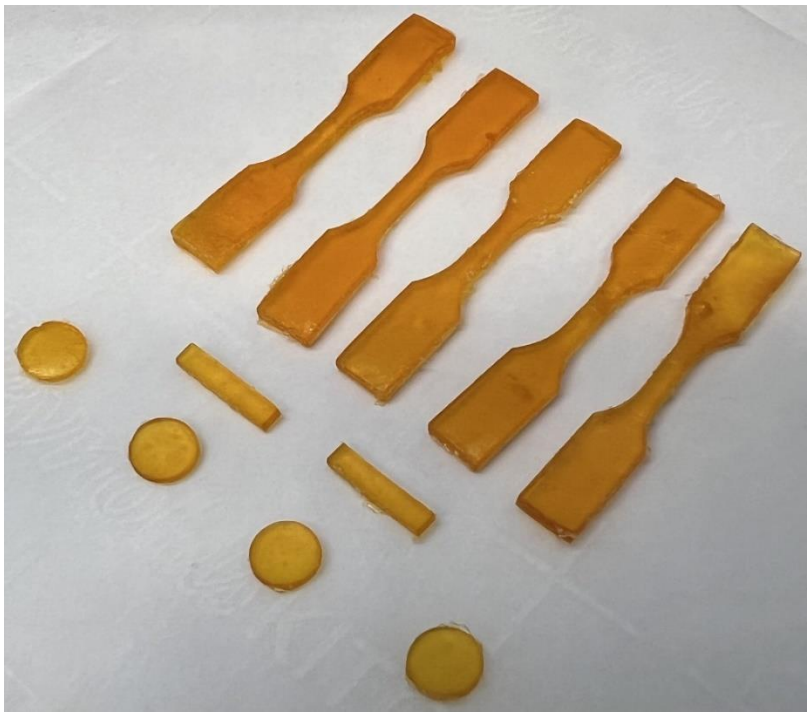

Figure 4.8: Digital photograph of **P1X1** printed parts after washes and drying.

Once dry, the cuboids from each print were measured and compared to the expected dimensions of the print as specified by the STL file. All three materials exhibited similar and low isotropic part shrinkage (~10%) (**Figure 4.9**).

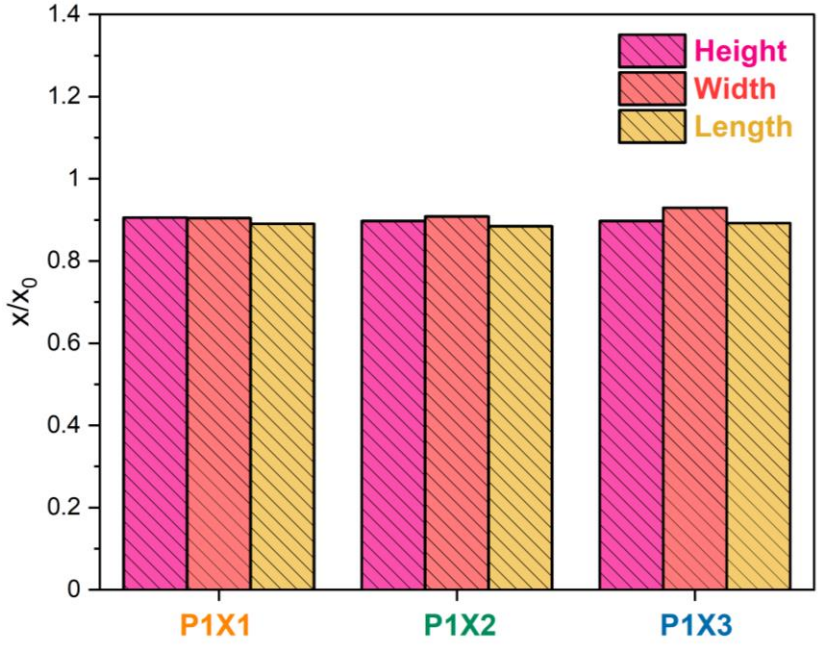

Figure 4.9: Part shrinkage of printed parts after drying. Isotropic part shrinkage observed for all materials.

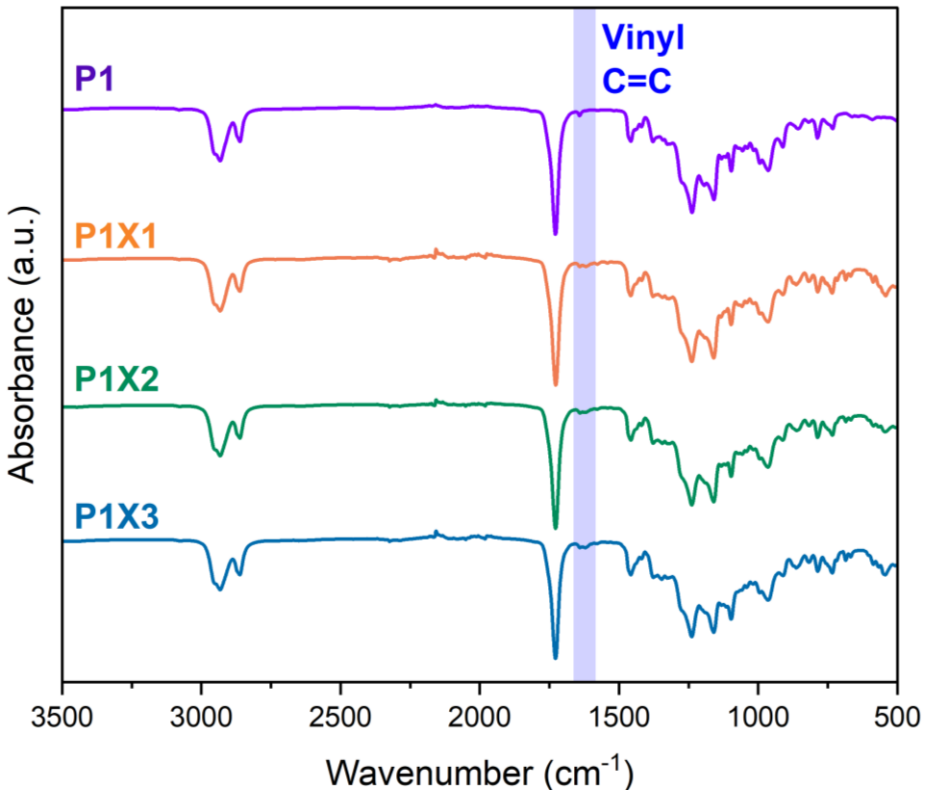

Figure 4.10: FTIR spectra of **P1**, **P1X1**, **P1X2** and **P1X3**.

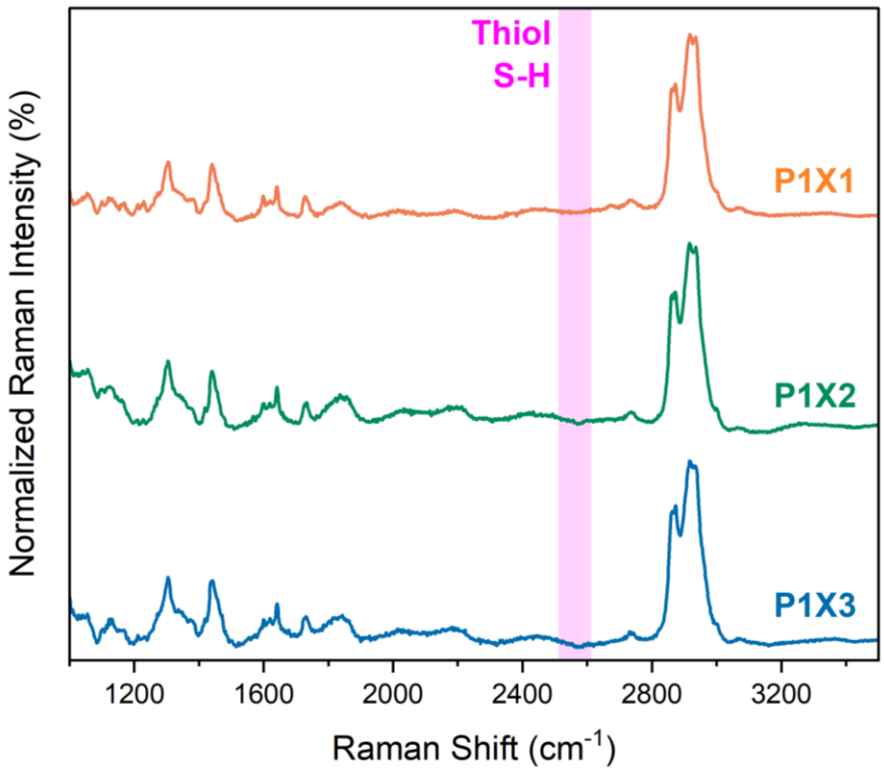

Figure 4.11: Raman spectra of **P1X1**, **P1X2** and **P1X3**.

Fourier transform infrared spectroscopy (FTIR) showed the **P1** vinyl group, C=C stretch at 1641 cm^{-1}, was present in all materials suggesting that total alkene functionalisation did not occur (**Figure 4.10** & Figure S7.4.8). This is to be expected since an alkene:S-H ratio of 5:1 was used for all prints, but it does suggest an insignificant amount of alkene-alkene overcuring took place. Raman spectroscopy of the 3D printed materials revealed the absence of sharp peaks from 2530 to 2610 cm^{-1}, which correspond to the free thiol S-H groups (**Figure 4.11**). This finding indicates quantitative consumption of the thiols and that **P1X1**, **P1X2** and **P1X3** are similarly cross-linked.

4.6 Material Characterisation

Table 4.1. Summary of thermal and mechanical properties of CO_2- and bio-derived 3D printed copolymer elastomers.

Polymer	[a]$T_{g,DSC}$ [˚C]	$T_{g,\,DMTA}$ [˚C]	[c]$T_{d,5\%}$ [˚C]	[d]E_y [kPa]	[e]σ [kPa]	[f]ε_b [%]	[g]U_T [kJ m^{-3}]
P1	-39	-29	295	-	-	-	-
P1X1	-35	-6, 19	287	120.4 ± 49.1	144.9 ± 14.7	113 ± 10	92.4 ± 18.3
P1X2	-37	-12, 11	290	93.0 ± 9.2	139.0 ± 6.0	115 ± 12	82.3 ± 12.2
P1X3	-39	-14, 9	288	68.5 ± 27.5	127.0 ± 15.8	115 ± 12	81.4 ± 16.2

Glass transition temperature from [a]DSC (2[nd] heating cycle) and from peak in tan(δ) in [b]DMTA. [c]Thermal degradation behavior reported as temperature at 5% mass loss, determined by TGA. [d]Young's modulus. [e]Tensile strength. [f]Strain at break. [g]Tensile toughness (area under the stress strain curve). Mean values ± std. dev. from measurements conducted independently on 5 specimens.

4.6.1 Thermal Properties

Thermogravimetric analysis (TGA) showed that all three thermosets displayed high thermal stability ($T_{d,5\%}$ > 250 ˚C, **Table 4.1** & Figures S7.4.9-S7.4.14). DSC analysis revealed that the printed materials are completely amorphous, without any crystallinity even with the longest PEG chains in **X3** (**Table 4.1** & Figures S7.4.5-S7.4.6). Glass transition temperatures of -35, -37 and -39 ˚C were determined for **P1X1**, **P1X2** and **P1X3**, respectively. The minor decrease in the T_g value with increasing cross-linker length is attributed to the increased segmental motion as the flexibility and degrees of freedom of the cross-linker increases.

4.6.2 Mechanical Properties

To examine the mechanical performance of the printed materials, the dumbbell-shaped specimens were subjected to uniaxial extension experiments, according to ISO 527 (10 mm min^{-1}) (**Table 4.1** & **Figure 4.12**). All three materials showed purely elastic behavior with no evidence of yielding or plastic deformation. The ultimate tensile strength, Young's modulus, strain at break, and tensile toughness values were not statistically different across the series (Table S7.4.1). These observations are consistent with the similar cross-linking density within the materials.

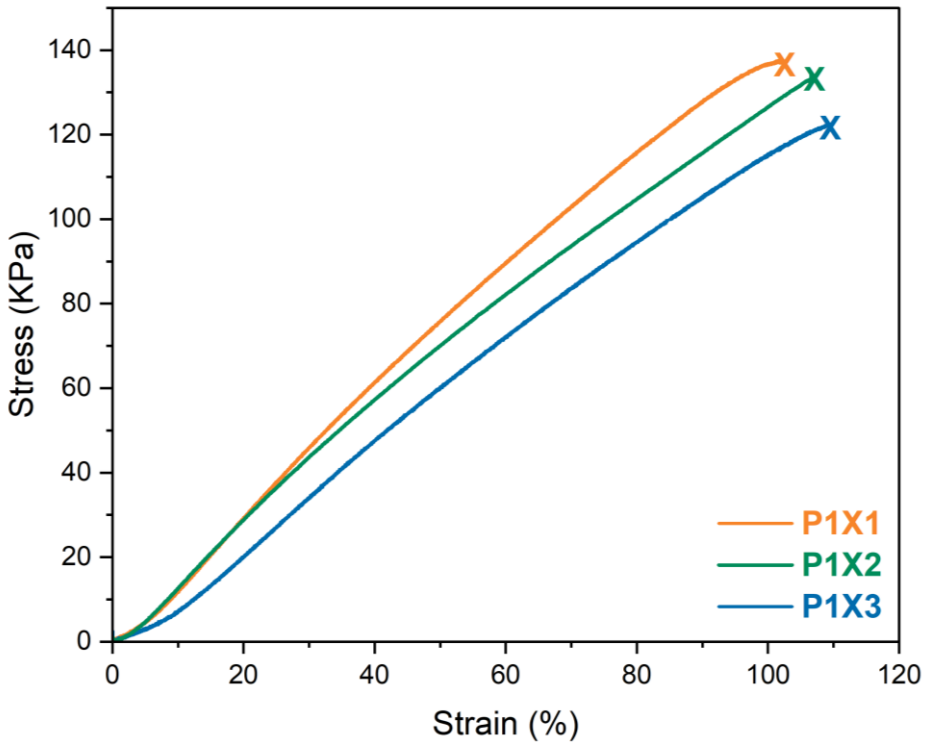

Figure 4.12: Representative stress-strain curves for **P1X1**, **P1X2**, and **P1X3** (10 mm min^{-1} extension rate).

Specimens were also subjected to cyclic uniaxial tensile testing to study their elastomeric properties and critically their ability to recover after deformation (**Figure 4.13**). Specimens were cycled between 0 and 20% tensile strain for thirty cycles. All three materials exhibited >80% elastic recovery over the cycles (Figure S7.4.15). The increased size and flexibility of the

cross-linkers did have a significant effect on the mechanical performance of the materials. The maximum stress on the 30th cycle of **P1X1** decreased 57% from that of the first, whereas this drop was 84% for **P1X3**. This rapid decay in strength is ascribed to the increased degrees of freedom of the longer cross-linkers and the reduced chain restriction they impart, which in turn results in increased hysteresis and reduced elastic recovery.

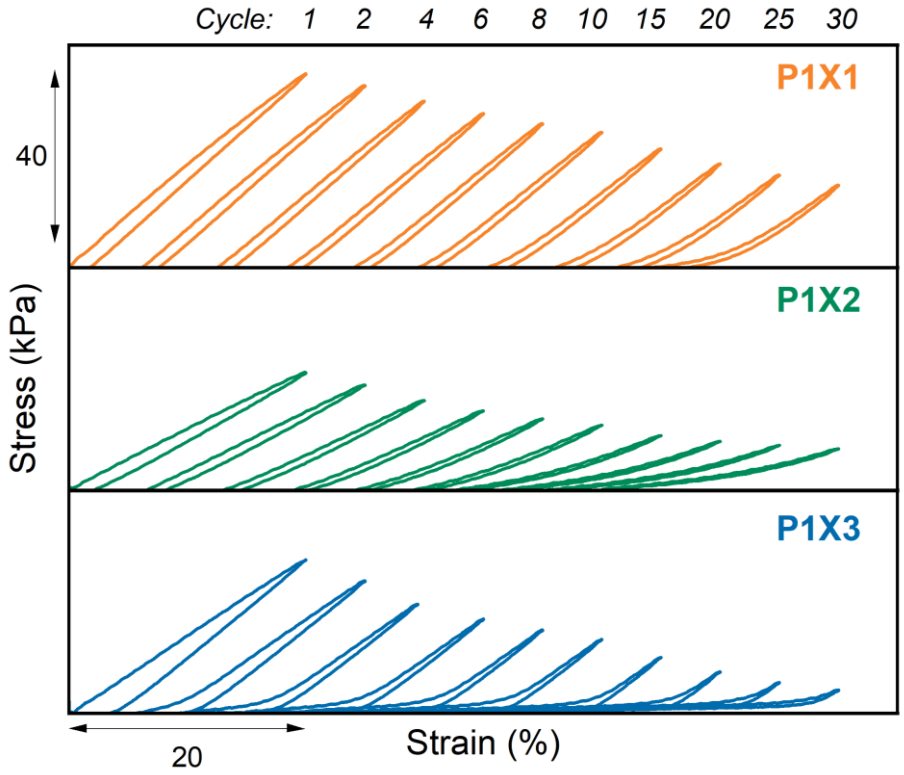

Figure 4.13: Uniaxial cyclic tensile testing (20% strain).

4.7 Printing Induced Phase Separation

To further probe the thermomechanical properties of these printed materials, specimens were subjected to dynamic mechanical thermal analysis (DMTA) under tension (**Figure 4.14** & Figures S7.4.16-S7.4.17). The tan(δ) profiles for all printed materials displayed bimodal peaks, indicative of two separate thermal transitions taking place: the T_g for PDL and the T_g for PvCHC.

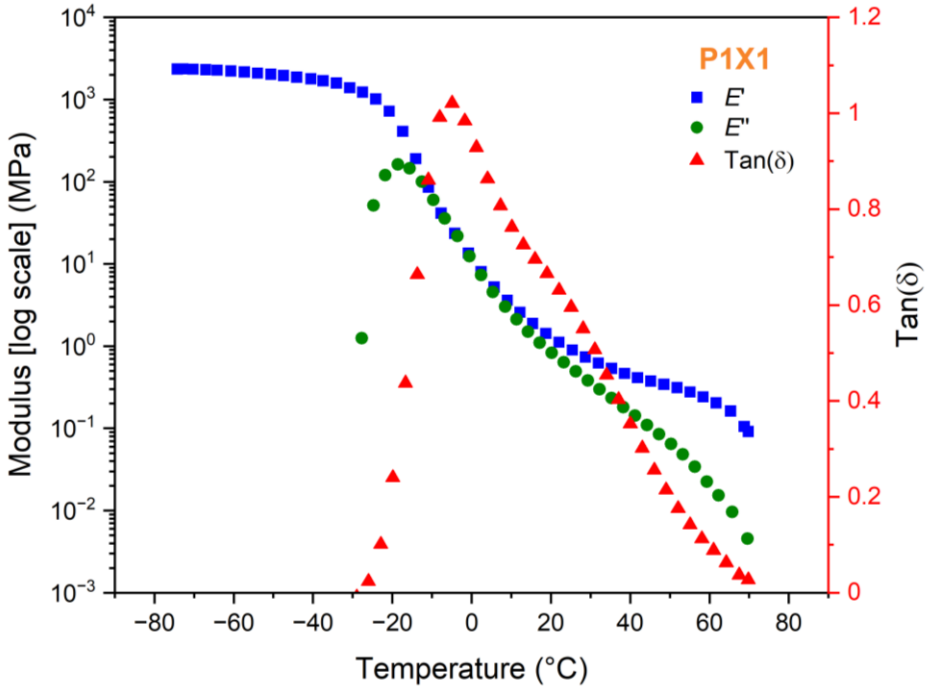

Figure 4.14: Dynamic mechanical thermal analysis (DMTA) temperature sweep for **P1X1**.

By deconvoluting these tan(δ) peaks, the values for these transitions were determined (**Table 4.1** & **Figure 4.15**). In all cases, the lower transition is sharper and attributed to PDL, whereas the upper transition is much broader, occurring over a wide temperature range and attributed to the cross-linked PvCHC. The broad upper T_g is a result of the variety of cross-linking architectures present in the material, each resulting in varying degrees of chain segmental motion. The difference in temperature between these transitions remains approximately the same. However, as with the DSC analysis, the absolute T_g values decrease

with increasing cross-linker length. This is likely due to increasing chain mobility for thermosets featuring longer cross-linkers.

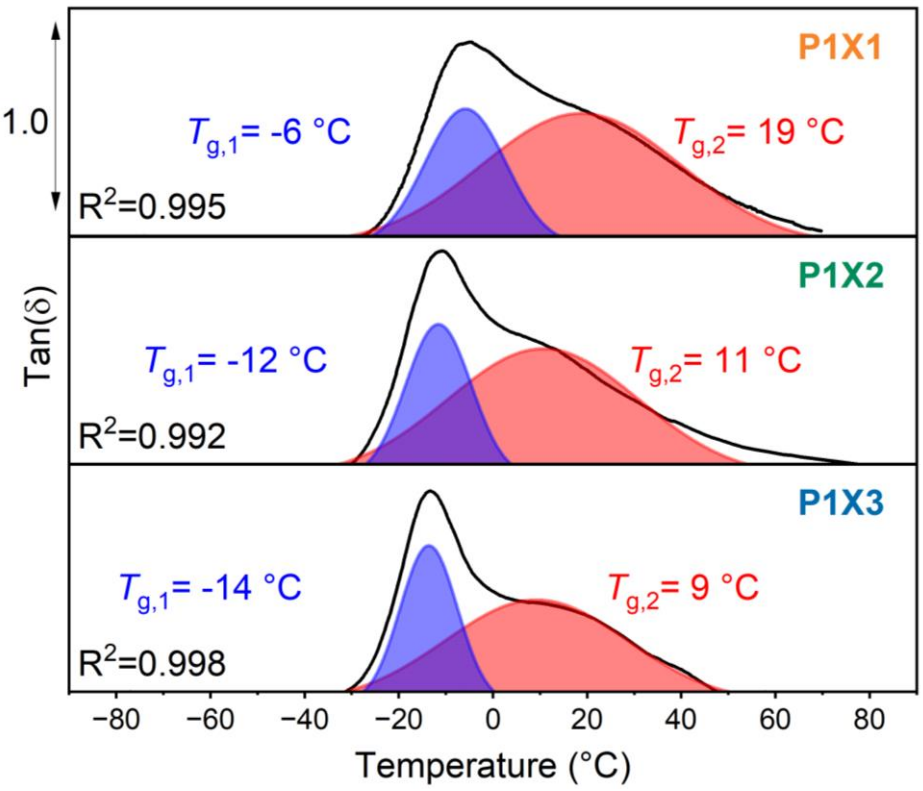

Figure 4.15: Deconvoluted tan(δ) profiles of **P1X1**, **P1X2** and **P1X3**.

It is hypothesised that the cross-linking of only the outer (A) blocks in the triblock copolymers and the subsequent higher temperature drying may enable block microphase separation within the thermosets. Microphase separation is usually only observed for these polymers at high M_n values (M_n > 50 kg mol^{-1}) but is expected to enhance the desired elastomeric properties.[42, 46] The observation that the thermosets show two T_g values suggests some microphase separation which is highly unusual for a low molar mass material. The T_g values are far from the expected values for the individual homopolymers, indicating they are not fully phase separated but rather are only partially miscible. To investigate whether the partial microphase separation might be printing induced, the **P1** starting material was pasted between two steel plates and subjected to a three-point-bend DMTA temperature ramp

(Figures S7.4.18-S7.4.19). The data showed a clear, sharp, monomodal glass transition, at -29 °C, indicating the starting block polymer is fully miscible and providing further evidence for printing induced microphase separation (**Figure 4.16**).

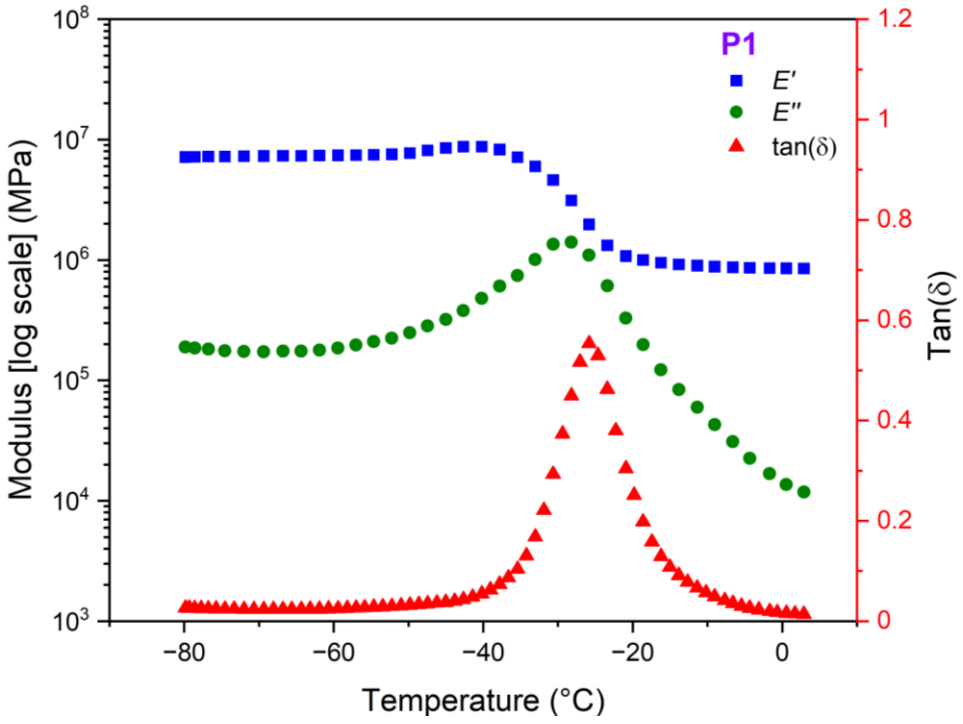

Figure 4.16: Dynamic mechanical thermal analysis (DMTA) temperature sweep for **P1** between steel plates in 3-point bend geometry.

To probe the microphase separation of the thermosets further, small-angle X-ray scattering (SAXS) was conducted on the series of printed samples (**Figure 4.17** & **Table 4.2**). Principle scattering peaks were observed for all materials, but no higher order scattering peaks were observed suggesting there is only short-range ordering in all materials (d = 9.3 – 12.1 nm). This ability to induce some microphase separation in low molar mass materials may prove useful for expanding the property profile of vat photopolymerisation printed materials and to help to broaden the applications of low M_n CO_2- and bio-derived polymers in the future.

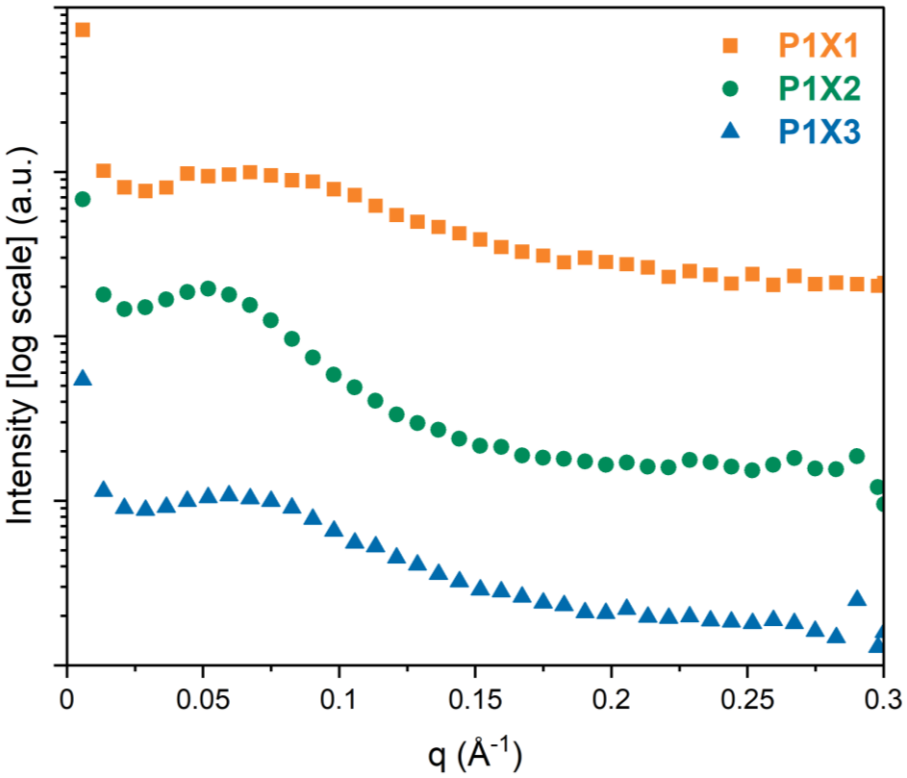

Figure 4.17: Room temperature SAXS profiles of **P1X1**, **P1X2** and **P1X3**.

Table 4.2: Summary of SAXS Data.

Material	q*/ Å^{-1}	d/nm
P1X1	0.067	9.3
P1X2	0.052	12.1
P1X3	0.060	10.5

Where q* = principle scattering peak (d=2π/q*).

4.8 Hydrophilicity and Aqueous Stability

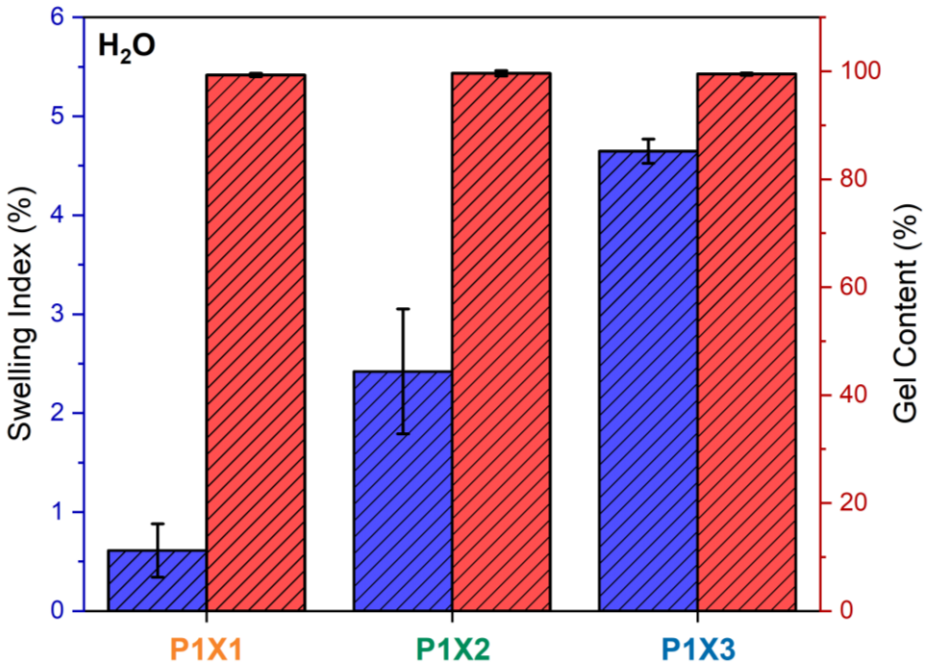

Figure 4.18: Swelling index and gel content after swelling the polymer samples in water, for 48 hours.

To examine any differences in hydrophilicity across the series of printed thermosets, samples were subjected to water swelling experiments. Uniform disks (10 mm diameter, 2 mm thick) were submerged in water for 24 h, dried (vacuum oven, 48 h) and weighed both swollen and dried to determine the swelling index and gel content, respectively (**Figure 4.18**). It was hypothesised that that the increasing PEG content from **X1** to **X2** to **X3** might control the extent of swelling in aqueous environments. Such swelling is particularly important for *in vivo* applications, such as regenerative medicine, and may provide a means to enhance sample hydrolytic degradation.[47] All printed materials have gel contents >99% indicating good chemical resistance to water and indicative of equivalent cross-linking density across the series. The swelling index for **P1X1** is only 0.6%; however, the values rise significantly to 2.4% and 4.6% for **P1X2** and **P1X3**, respectively due to the longer crosslinker lengths. While these values are in absolute terms low, the increase signifies a change in hydrophilicity, as the major

component of the material is hydrophobic PDL. The increase in swelling index arises from the increase in hydrophilic PEG content within the thermosets. The effect is coupled with the increasingly long and flexible cross-linkers providing a greater swellable volume within the material.

To deconvolute these two effects, surplus resin from each print was spin-coated onto glass slides, cured in a UV oven (390-420 nm, 15 min), dried in vacuo, and water contact angle measurements were conducted (**Figure 4.19** & Figure S7.4.20). The experiments revealed a marked change in hydrophilicity. The water contact angle for **P1X1** was >90° (93°) while those for **P1X2** and **P1X3** were 85 and 68°, respectively. This significant increase in surface wetting underlines the ability to tune the hydrophilicity/hydrophobicity of additively manufactured materials through the simple substitution of the cross-linker employed. Differences in swelling index and water contact angles are statisticly significant (Table S7.4.2).

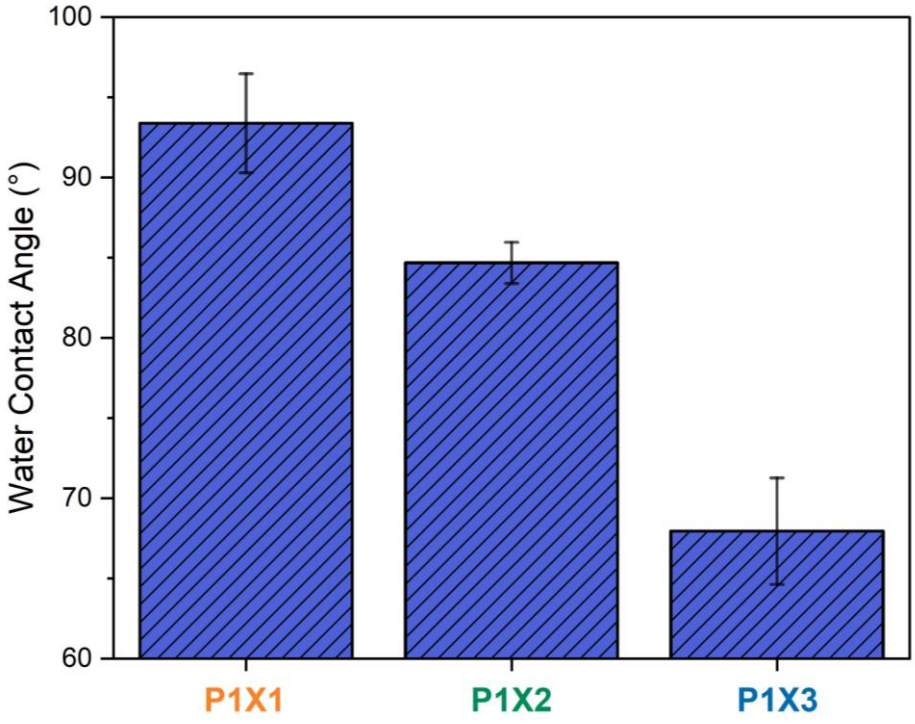

Figure 4.19: Water contact angle for **P1X1**, **P1X2**, and **P1X3** resins dissolved in ethyl acetate, spin coated and cured on glass slides.

It was predicted that the increasing swelling index with water across the series should result in enhanced rates of hydrolytic degradation. As a proof-of-concept, an accelerated degradation study was performed. Cuboids (10 x 10 x 2 mm) of **P1X1**, **P1X2** and **P1X3** were submerged in basic aqueous solutions (4 M NaOH) at room temperature, and the sample mass loss was measured over time (**Figure 4.20**). The **P1X3** samples, exhibited complete hydrolytic degradation within 65 days while **P1X2** and **P1X1** has only lost 75 and 49% mass, respectively, after 85 days. The ability to control the rate of degradation in this manner could be relevant for biomedical applications, where the rate of *in vivo* degradation should be matched to the specific application.

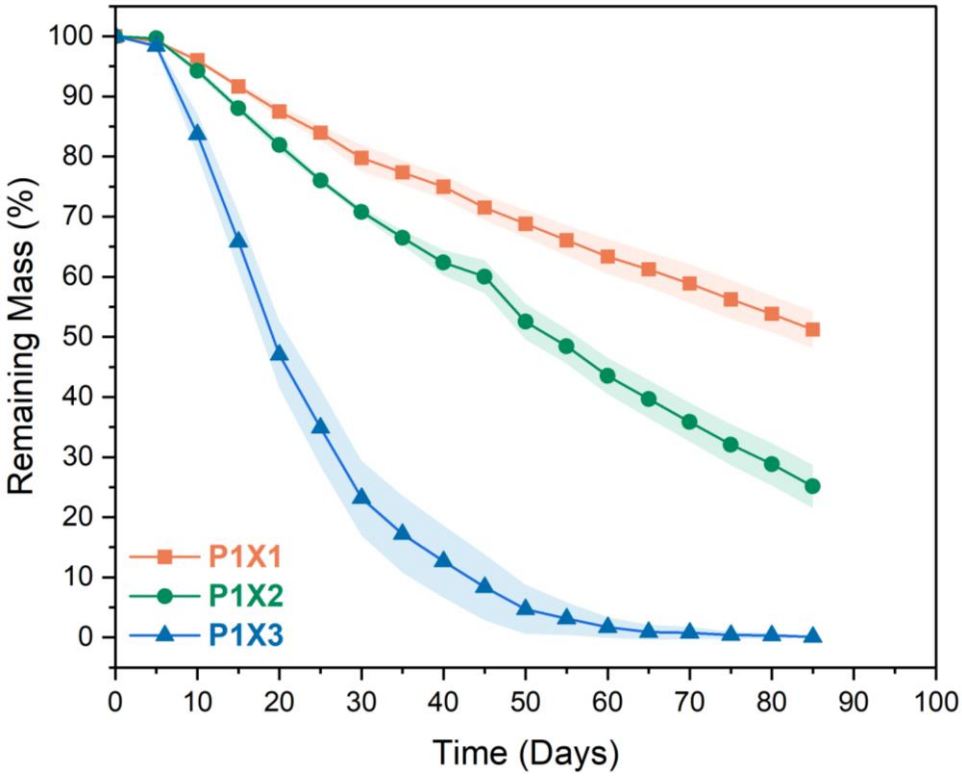

Figure 4.20: Degradation study in aqueous media, (4 M NaOH, pH = 14.6, room temperature).

4.9 Cytotoxicity

To explore the biocompatibility of the printed thermosets **P1X1**, **P1X2** and **P1X3**, mouse Schwann cells were seeded on thin films of each cured material with a poly-L-lysine (PLL) and laminin coating. This was carried out by Ms Yin Mei Chan. Schwann cells were selected for their high sensitivity and, therefore, to investigate any cytotoxic response. After 24 h, the films were stained with a live/dead assay (**Figure 4.21**). Live and healthy cells were observed on films of all three printed materials, suggesting there was no initial cytotoxicity from **P1X1**, **P1X2** and **P1X3**. Therefore, the CO_2- and bio-derived elastomers could be further explored for a range of biomedical applications.

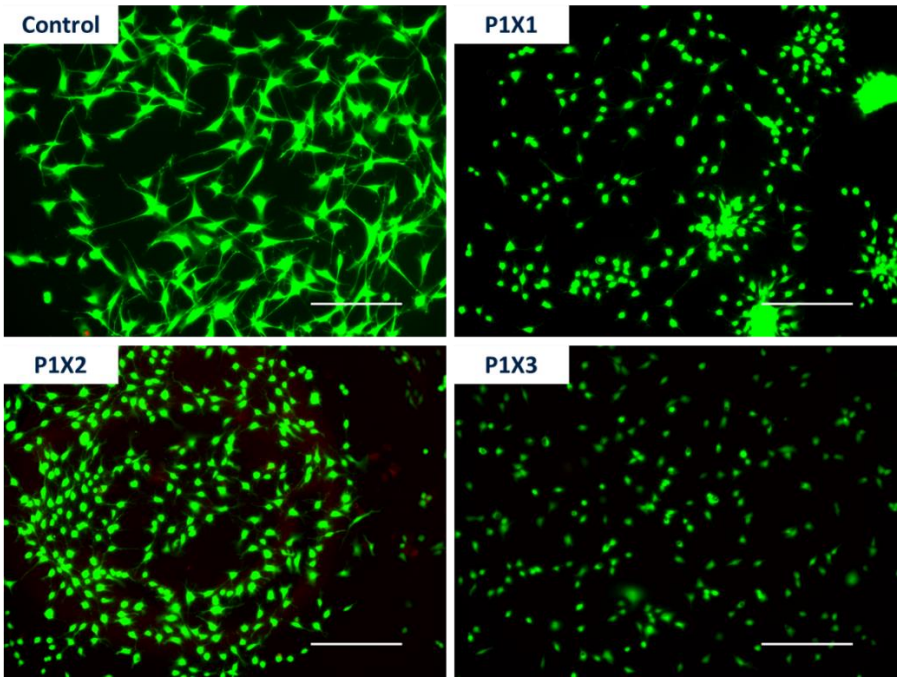

Figure 4.21: Mouse Schwann cells seeded on thin films of **P1X1**, **P1X2** and **P1X3** and stained with live/dead assay (scale bar: 300 μm). Live cells appear green while dead cells appear red.

4.10 3D Printing of Gyroids

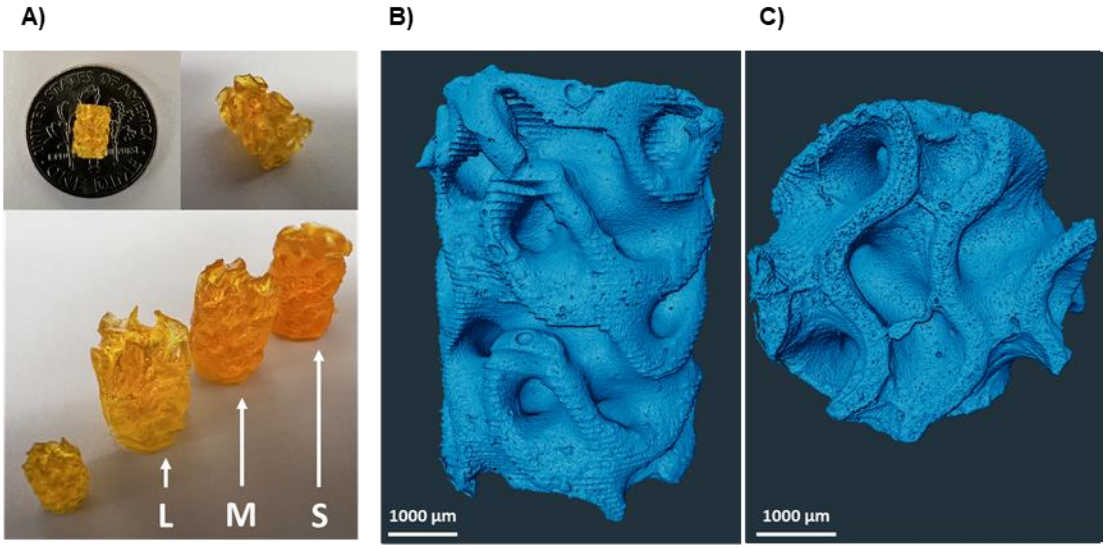

Figure 4.22: A) Digital photographs of small gyroid (5.9 mm tall) and large gyroids (10.6 mm tall) with small, medium and large holes. Micro CT scan of small gyroid showing B) XZ and C) XY planes.

Finally, to determine the printing resolution possible with the **P1** resins, **P1X1** was used to print a series of gyroids. These structures are triply periodic minimal surfaces with zero mean curvature and have shown promise in regenerative medicine, impact absorption, heat exchange, and acoustic management.[48] The structure's complex topology, with hollow tunnels and internal cavities, were selected to test whether high resolution structures could be printed with the polymer **P1**. Four series of different sized gyroids were all successfully printed. Three sets of samples (10.6 mm tall) with large (L), medium (M) and small (S) interpenetrating holes and one set of smaller samples (5.9 mm tall) with large (L) interpenetrating holes were printed (**Figure 4.22a**). Micro computed tomography (CT) scans on the small 5.9 mm gyroid showed the high resolution achievable using **P1** for DLP printing, with the smallest features (holes < 700 µm in diameter) and hollow structures present (**Figure 4.22b, 4.22c** & Figure S7.4.21). The results highlight the lack of lateral overcuring during printing and the ability to use bio-

and CO_2-derived materials to produce complex structures which would be hard to make using traditional fabrication methods.

Some very small pores and bubbles are observed by micro CT (**Figure 4.22b & c**), we believe these arise from the post-processing conditions. These gyroids were placed in a vacuum oven immediately after washing and curing. Leaving them to dry more slowly might help to eliminate the formation of these pores and bubbles. However, even so, the majority of these pores are smaller than the layer thickness/printing resolution (< 200 μm) and not visible to the naked eye. As seen in Figure S7.4.21, these are only present on the surface of the printed structure and not evenly distributed throughout.

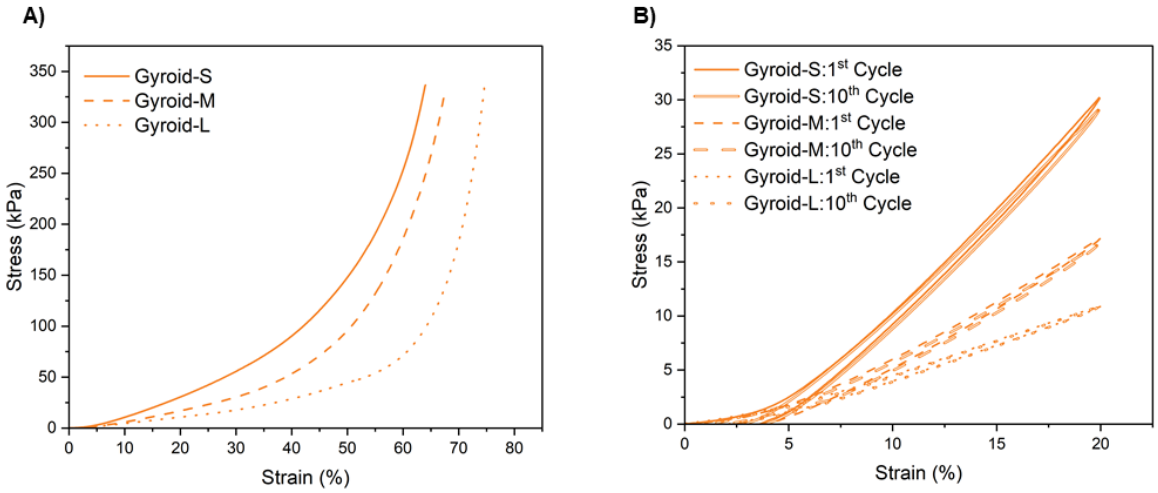

Figure 4.23: . A) Uniaxial compression testing and B) cyclic compression testing (20% strain) of large gyroids.

The L, M, and S series of gyroids were subjected to compression testing to study their mechanical performance under crushing loads (**Figure 4.23a** & Figure S7.4.22). All three structures displayed purely elastic behaviour with no yield or plastic behaviour and were all able to withstand relatively high compressive strain (>60%) before reaching the limit of the load cell. All three gyroid structures also exhibited excellent elastic recovery, over 10 cycles of loading and unloading, to 20% compressive strain, with negligible hysteresis or compressive strength loss (**Figure 4.23b**). The compressive mechanical properties of **P1X1** are simply

modified through changing the design of the printed part, allowing for a further option to tune the material properties without the need for new moulds or reoptimised fabrication procedures.

4.11 Summary and Future Work

4.11.1 Conclusion

A series of poly(carbonate-ester-carbonate) elastomers were 3D printed with three different trifunctional thiol crosslinkers having varying lengths and PEG contents. The low molar mass, amorphous, CO_2- and bio-derived triblock copolymer was synthesised using a highly active and selective [Co(II)Mg(II)] dinuclear catalyst on a large scale. Each repeat unit in the outer polycarbonate blocks contained one pendent vinyl group to afford post-polymerisation functionalisation. Following the optimisation of the resin formulation, digital light processing was employed to produce elastomeric thermosets via a spatiotemporally controlled thiol-ene crosslinking. The additive manufacturing of gyroid structures with internal voids and cavities underlined the high resolution achieved through the printing process. Dynamic mechanical analysis and SAXS experiments also revealed the presence of short-range printing-induced microphase separation of the constituent blocks contributing to the observed elastomeric properties. Significantly, no cytotoxic response was observed for any of the 3D printed materials. Overall, this work demonstrates how DLP can be utilised to produce sustainable, functional materials from low molar mass polyols and how properties can be controlled through choice of cross-linker. In the future, the continued development of sustainable polymers will help enable the rapid production of 3D printed plastics and elastomers capable of replacing current petrochemical options.

4.11.2 Future Work

Having established an understanding of the thermomechanical, degradation and hydrophilic properties of these novel 3D printed materials, future work should start with the additive manufacturing of implantable devices. For example, the production of printed parts for the use as stents, wound dressings, nerve conduits, and for cartilage repair would establish the

potential of these **P1** based materials for biomedical applications.[5] This would further test the printing resolution achievable with these resins as these products often poses complex geometries. The ability to rapidly customise part design to an individual patient opens up enormous potential for tailored healthcare. Take stents for example, soft and flexible materials which can be rapidly printed are needed in a spectrum of sizes given the patient, ailment, and considering any case specific complications.[49] Animal studies would be essential to access how the material behaves once implanted. Regularly testing specimens that have been in an *in vivo* environment at different time points would reveal how the material degrades and the mechanical performance alters over time, critical to for any long-term applications.[50] This would also facilitate a histological study on long-term cytotoxicity implications for the material.

For applications which require higher tensile strengths, such as bone scaffolds, the composition of the triblock copolymer could be fine-tuned. By increasing the content of polycarbonate to polyester, the T_g of the polyol would increase and likely result in stronger materials after printing, as a result of increased covalent and physical crosslinking. However, this would likely result in an increased viscosity. The use of solvent, as seen in this chapter would likely help overcome this. Furthermore, as part shrinkage is isotropic, additional solvent in the print should not impede part production.

Finally, the bio-based content of the polyol employed in the printing process would be further increased through the replacement of vCHO with limonene oxide. A poly(limonene carbonate-*b*-ε-decalactone-*b*-limonene carbonate) precursor should behave similarly to **P1** with respect to printing condition, thermomechanical properties and degradation profile. The ROCOP of CO_2 with epoxides could be employed with a range of other alkene containing epoxides to produce new DLP printing resins. Ally glycidyl ether or 1,4-cyclohexadiene oxide could be employed as a homopolymer or in a block architecture to give a range of sustainable printed material with new and unique properties.[51]

4.12 References

(1) Capel, A. J.; Rimington, R. P.; Lewis, M. P.; Christie, S. D. R. 3D printing for chemical, pharmaceutical and biological applications. *Nat. Rev. Chem.* **2018**, *2* (12), 422-436. DOI: 10.1038/s41570-018-0058-y.
(2) Hartings, M. R.; Ahmed, Z. Chemistry from 3D printed objects. *Nat. Rev. Chem.* **2019**, *3* (5), 305-314. DOI: 10.1038/s41570-019-0097-z.
(3) Ragelle, H.; Tibbitt, M. W.; Wu, S. Y.; Castillo, M. A.; Cheng, G. Z.; Gangadharan, S. P.; Anderson, D. G.; Cima, M. J.; Langer, R. Surface tension-assisted additive manufacturing. *Nat. Commum.* **2018**, *9*, 1184. DOI: 10.1038/s41467-018-03391-w.
(4) Tumbleston, J. R.; Shirvanyants, D.; Ermoshkin, N.; Janusziewicz, R.; Johnson, A. R.; Kelly, D.; Chen, K.; Pinschmidt, R.; Rolland, J. P.; Ermoshkin, A.; et al. Continuous liquid interface production of 3D objects. *Science* **2015**, *347* (6228), 1349-1352. DOI: 10.1126/science.aaa2397.
(5) Kirillova, A.; Yeazel, T. R.; Asheghali, D.; Petersen, S. R.; Dort, S.; Gall, K.; Becker, M. L. Fabrication of Biomedical Scaffolds Using Biodegradable Polymers. *Chem Rev* **2021**, *121* (18), 11238-11304. DOI: 10.1021/acs.chemrev.0c01200.
(6) Chaudhary, R.; Fabbri, P.; Leoni, E.; Mazzanti, F.; Akbari, R.; Antonini, C. Additive manufacturing by digital light processing: a review. *Prog. Addit. Manuf.* **2023**, *8* (2), 331-351. DOI: 10.1007/s40964-022-00336-0.
(7) Ligon, S. C.; Liska, R.; Stampfl, J.; Gurr, M.; Mülhaupt, R. Polymers for 3D Printing and Customized Additive Manufacturing. *Chem Rev* **2017**, *117* (15), 10212-10290. DOI: 10.1021/acs.chemrev.7b00074.
(8) Chyr, G.; DeSimone, J. M. Review of high-performance sustainable polymers in additive manufacturing. *Green Chem.* **2023**, *25* (2), 453-466. DOI: 10.1039/d2gc03474c.
(9) Langer, R. Perspectives and Challenges in Tissue Engineering and Regenerative Medicine. *Adv. Mater.* **2009**, *21* (32-33), 3235-3236. DOI: 10.1002/adma.200902589.
(10) Murphy, S. V.; De Coppi, P.; Atala, A. Opportunities and challenges of translational 3D bioprinting. *Nat. Biomed. Eng.* **2020**, *4* (4), 370-380. DOI: 10.1038/s41551-019-0471-7.
(11) Bao, Y. Y.; Paunovic, N.; Leroux, J. C. Challenges and Opportunities in 3D Printing of Biodegradable Medical Devices by Emerging Photopolymerization Techniques. *Adv. Funct. Mater.* **2022**, *32* (15), 2109864. DOI: 10.1002/adfm.202109864.
(12) Gul, J. Z.; Sajid, M.; Rehman, M. M.; Siddiqui, G. U.; Shah, I.; Kim, K. H.; Lee, J. W.; Choi, K. H. 3D printing for soft robotics - a review. *Sci. Technol. Adv. Mat.* **2018**, *19* (1), 243-262. DOI: 10.1080/14686996.2018.1431862.
(13) Wallin, T. J.; Pikul, J.; Shepherd, R. F. 3D printing of soft robotic systems. *Nat. Rev. Mater.* **2018**, *3* (6), 84-100. DOI: 10.1038/s41578-018-0002-2.
(14) Zhao, Z.; Tian, X. X.; Song, X. Y. Engineering materials with light: recent progress in digital light processing based 3D printing. *J. Mater. Chem. C* **2020**, *8* (40), 13896-13917. DOI: 10.1039/d0tc03548c.
(15) Cai, Z. Y.; Wan, Y.; Becker, M. L.; Long, Y. Z.; Dean, D. Poly(propylene fumarate)-based materials: Synthesis, functionalization, properties, device fabrication and biomedical applications. *Biomater.* **2019**, *208*, 45-71. DOI: 10.1016/j.biomaterials.2019.03.038.
(16) Lee, S. H.; Cyriac, A.; Jeon, J. Y.; Lee, B. Y. Preparation of thermoplastic polyurethanes using in situ generated poly(propylene carbonate)-diols. *Polym. Chem.* **2012**, *3* (5), 1215-1220. DOI: 10.1039/c2py00010e.
(17) Langanke, J.; Wolf, A.; Hofmann, J.; Böhm, K.; Subhani, M. A.; Müller, T. E.; Leitner, W.; Gürtler, C. Carbon dioxide (CO2) as sustainable feedstock for polyurethane production. *Green Chem.* **2014**, *16* (4), 1865-1870. DOI: 10.1039/c3gc41788c.
(18) Hauenstein, O.; Agarwal, S.; Greiner, A. Bio-based polycarbonate as synthetic toolbox. *Nat. Commun.* **2016**, *7*, 11862. DOI: 10.1038/ncomms11862.

(19) DeBolt, M.; Kiziltas, A.; Mielewski, D.; Waddington, S.; Nagridge, M. J. Flexible polyurethane foams formulated with polyols derived from waste carbon dioxide. *J. Appl. Polym. Sci.* **2016**, *133* (45), 44086. DOI: 10.1002/app.44086.
(20) Stösser, T.; Li, C. L.; Unruangsri, J.; Saini, P. K.; Sablong, R. J.; Meier, M. A. R.; Williams, C. K.; Koning, C. Bio-derived polymers for coating applications: comparing poly(limonene carbonate) and poly (cyclohexadiene carbonate). *Polym. Chem.* **2017**, *8* (39), 6099-6105. DOI: 10.1039/c7py01223c.
(21) Scharfenberg, M.; Hilf, J.; Frey, H. Functional Polycarbonates from Carbon Dioxide and Tailored Epoxide Monomers: Degradable Materials and Their Application Potential. *Adv. Funct. Mater.* **2018**, *28* (10), 1704302. DOI: 10.1002/adfm.201704302.
(22) Alagi, P.; Ghorpade, R.; Choi, Y. J.; Patil, U.; Kim, I.; Baik, J. H.; Hong, S. C. Carbon Dioxide-Based Polyols as Sustainable Feedstock of Thermoplastic Polyurethane for Corrosion-Resistant Metal Coating. *ACS Sustain. Chem. Eng.* **2017**, *5* (5), 3871-3881. DOI: 10.1021/acssuschemeng.6b03046.
(23) Petersen, S. R.; Yu, J. Y.; Yeazel, T. R.; Bass, G.; Alamdari, A.; Becker, M. L. Degradable, Photochemically Printable Poly(propylene fumarate)-Based ABA Triblock Elastomers. *Biomacromolecules* **2022**, *23* (6), 2388-2395. DOI: 10.1021/acs.biomac.2c00151.
(24) Yeazel-Klein, T. R.; Davis, A. G.; Becker, M. L. Thiol-ene-Based 3D Printing of Bioresorbable Fumarate-Based ABA Triblock Copolyester Elastomers. *Adv. Mater. Technol.* **2023**, *8* (23), 2201904. DOI: 10.1002/admt.202201904.
(25) Ma, W. R.; Miller, P. G.; Wang, Y. D. ABA Block Copolyester Thiol-Ene Resin From Triethylborane-Assisted Ring-Opening Copolymerization. *ACS Appl. Polym. Mater.* **2024**, *6* (2), 1503-1513. DOI: 10.1021/acsapm.3c02745.
(26) Klein, T. R.; Kirillova, A.; Gall, K.; Becker, M. L. Influence of post-processing on the properties of 3D-printed poly(propylene fumarate) star polymer hydroxyapatite nanocomposites. *RSC Appl. Polym.* **2023**, *1* (1), 73-81, 10.1039/D3LP00013C. DOI: 10.1039/D3LP00013C.
(27) Deacy, A. C.; Gregory, G. L.; Sulley, G. S.; Chen, T. T. D.; Williams, C. K. Sequence Control from Mixtures: Switchable Polymerization Catalysis and Future Materials Applications. *J. Am. Chem. Soc.* **2021**, *143* (27), 10021-10040. DOI: 10.1021/jacs.1c03250.
(28) Le Fer, G.; Luo, Y. Y.; Becker, M. L. Poly(propylene fumarate) stars, using architecture to reduce the viscosity of 3D printable resins. *Polym. Chem.* **2019**, *10* (34), 4655-4664. DOI: 10.1039/c9py00738e.
(29) Luo, Y. Y.; Dolder, C. K.; Walker, J. M.; Mishra, R.; Dean, D.; Becker, M. L. Synthesis and Biological Evaluation of Well-Defined Poly(propylene fumarate) Oligomers and Their Use in 3D Printed Scaffolds. *Biomacromolecules* **2016**, *17* (2), 690-697. DOI: 10.1021/acs.biomac.6b00014.
(30) Luo, Y. Y.; Le Fer, G.; Dean, D.; Becker, M. L. 3D Printing of Poly(propylene fumarate) Oligomers: Evaluation of Resin Viscosity, Printing Characteristics and Mechanical Properties. *Biomacromolecules* **2019**, *20* (4), 1699-1708. DOI: 10.1021/acs.biomac.9b00076.
(31) Kirillova, A.; Yeazel, T. R.; Gall, K.; Becker, M. L. Thiol-Based Three-Dimensional Printing of Fully Degradable Poly(propylene fumarate) Star Polymers. *ACS Appl. Mater. Inter.* **2022**, *14* (34), 38436-38447. DOI: 10.1021/acsami.2c06553.
(32) Wei, P. R.; Bhat, G. A.; Cipriani, C. E.; Mohammad, H.; Schoonover, K.; Pentzer, E. B.; Darensbourg, D. J. 3D Printed CO2-Based Triblock Copolymers and Post-Printing Modification. *Angew. Chem. Int. Edit.* **2022**, *61* (37), e202208355. DOI: 10.1002/anie.202208355.
(33) Schüller-Ravoo, S.; Zant, E.; Feijen, J.; Grijpma, D. W. Preparation of a Designed Poly(trimethylene carbonate) Microvascular Network by Stereolithography. *Adv. Healthc. Mater.* **2014**, *3* (12), 2004-2011. DOI: 10.1002/adhm.201400363.

(34) Geven, M. A.; Varjas, V.; Kamer, L.; Wang, X. J.; Peng, J.; Eglin, D.; Grijpma, D. W. Fabrication of patient specific composite orbital floor implants by stereolithography. *Polym. Advan. Technol.* **2015**, *26* (12), 1433-1438. DOI: 10.1002/pat.3589.
(35) Guillaume, O.; Geven, M. A.; Grijpma, D. W.; Tang, T. T.; Qin, L.; Lai, Y. X.; Yuan, H.; Richards, R. G.; Eglin, D. Poly(trimethylene carbonate) and nano-hydroxyapatite porous scaffolds manufactured by stereolithography. *Polym. Advan. Technol.* **2017**, *28* (10), 1219-1225. DOI: 10.1002/pat.3892.
(36) Barker, I. A.; Ablett, M. P.; Gilbert, H. T. J.; Leigh, S. J.; Covington, J. A.; Hoyland, J. A.; Richardson, S. M.; Dove, A. P. A microstereolithography resin based on thiol-ene chemistry: towards biocompatible 3D extracellular constructs for tissue engineering. *Biomater. Sci.* **2014**, *2* (4), 472-475. DOI: 10.1039/c3bm60290g.
(37) Weems, A. C.; Arno, M. C.; Yu, W.; Huckstepp, R. T. R.; Dove, A. P. 4D polycarbonates via stereolithography as scaffolds for soft tissue repair. *Nat. Commun.* **2021**, *12* (1), 3771. DOI: 10.1038/s41467-021-23956-6.
(38) Brooks, S. L.; Arno, M. C.; Dove, A. P.; Weems, A. C. Postfabrication Functionalization of 4D-Printed Polycarbonate Photopolymer Scaffolds. *ACS Appl. Polym. Mater.* **2022**, *4* (8), 5670-5679. DOI: 10.1021/acsapm.2c00648.
(39) Wu, Y. M.; Simpson, M. C.; Jin, J. Y. Fast Hydrolytically Degradable 3D Printed Object Based on Aliphatic Polycarbonate Thiol-Yne Photoresins. *Macromol. Chem. Phys.* **2021**, *222* (6), 2000435. DOI: 10.1002/macp.202000435.
(40) Sulley, G. S.; Gregory, G. L.; Chen, T. T. D.; Carrodeguas, L. P.; Trott, G.; Santmarti, A.; Lee, K. Y.; Terrill, N. J.; Williams, C. K. Switchable Catalysis Improves the Properties of CO2-Derived Polymers: Poly(cyclohexene carbonate-b-ε-decalactone-b-cyclohexene carbonate) Adhesives, Elastomers, and Toughened Plastics. *J. Am. Chem. Soc.* **2020**, *142* (9), 4367-4378. DOI: 10.1021/jacs.9b13106.
(41) Deacy, A. C.; Kilpatrick, A. F. R.; Regoutz, A.; Williams, C. K. Understanding metal synergy in heterodinuclear catalysts for the copolymerization of CO2 and epoxides. *Nat. Chem.* **2020**, *12* (4), 372-380. DOI: 10.1038/s41557-020-0450-3.
(42) Poon, K. C.; Gregory, G. L.; Sulley, G. S.; Vidal, F.; Williams, C. K. Toughening CO2-Derived Copolymer Elastomers Through Ionomer Networking. *Adv. Mater.* **2023**, *35* (36), 2302825. DOI: 10.1002/adma.202302825.
(43) Spyros, A.; Argyropoulos, D. S.; Marchessault, R. H. A study of poly(hydroxyalkanoate)s by quantitative P-31 NMR spectroscopy: Molecular weight and chain cleavage. *Macromolecules* **1997**, *30* (2), 327-329. DOI: DOI 10.1021/ma9601979.
(44) Donaldson, J. D.; Beyersmann, D. Cobalt and Cobalt Compounds. In *Ullmann's Encyclopedia of Industrial Chemistry*.
(45) Bass, G. F.; Shin, Y.; Becker, M. L. Regio-Random Clemmensen Reduction of Biodegradable Polyesters for Photochemically Triggered 3D Printing. *Macromolecules* **2021**, *54* (3), 1273-1280. DOI: 10.1021/acs.macromol.0c02729.
(46) Bates, F. S.; Hillmyer, M. A.; Lodge, T. P.; Bates, C. M.; Delaney, K. T.; Fredrickson, G. H. Multiblock Polymers: Panacea or Pandora's Box? *Science* **2012**, *336* (6080), 434-440. DOI: 10.1126/science.1215368.
(47) Fuoco, T.; Cuartero, M.; Parrilla, M.; García-Guzmán, J. J.; Crespo, G. A.; Finne-Wistrand, A. Capturing the Real-Time Hydrolytic Degradation of a Library of Biomedical Polymers by Combining Traditional Assessment and Electrochemical Sensors. *Biomacromolecules* **2021**, *22* (2), 949-960. DOI: 10.1021/acs.biomac.0c01621.
(48) Ramos, H.; Santiago, R.; Soe, S.; Theobald, P.; Alves, M. Response of gyroid lattice structures to impact loads. *Int. J. Impact. Eng.* **2022**, *164*, 104202. DOI: 10.1016/j.ijimpeng.2022.104202.
(49) Yeazel, T. R.; Becker, M. L. Advancing Toward 3D Printing of oresorbable Shape Memory Polymer Stents. *Biomacromolecules* **2020**, *21* (10), 3957-3965. DOI: 10.1021/acs.biomac.0c01082.

(50) Dreger, N. Z.; Wandel, M. B.; Robinson, L. L.; Luong, D.; Sondergaard, C. S.; Hiles, M.; Premanandan, C.; Becker, M. L. Preclinical in Vitro and in Vivo Assessment of Linear and Branched L-Valine-Based Poly(ester urea)s for Soft Tissue Applications. *ACS Biomater. Sci. Eng.* **2018**, *4* (4), 1346-1356. DOI: 10.1021/acsbiomaterials.7b00920.
(51) Winkler, M.; Romain, C.; Meier, M. A. R.; Williams, C. K. Renewable polycarbonates and polyesters from 1,4-cyclohexadiene. *Green Chem.* **2015**, *17* (1), 300-306. DOI: 10.1039/c4gc01353k.

CHAPTER 5

Outlook

5.1 Thesis Summary

This thesis has detailed the synthesis and characterisation of series of CO_2-derived polycarbonates and the employment of these in poly(carbonate-*b*-ester-*b*-carbonate) thermoplastic elastomers. Networking through the introduction of metal-ligand interactions, increased macromolecular entanglement density, and thiol-ene based 3D printing have all been explored. The development of new plastics and elastomers has not only expanded the property profile of CO_2- and bio-derived materials reported but provides an insight into how new sustainable materials should be designed to compete with petrochemical incumbents. Critically, in each investigation, end-of-life options have been studied. The propensity of a material to degrade and/or undergo mechanical and chemical recycling is essential to take a holistic approach to the design of new materials with a minimal environmental footprint.

In Chapter 2, a series of ionomeric elastomers are reported with varying metal-carboxylate (M= Na(I), Ca(II), Mg(II), Zn(II), Al(III)) interactions in the hard domains.[1] These interactions act to reinforce physical cross-linking in the glassy domains and prevent chain pull out and subsequent mechanical failure. This resulted in a up to 52-fold and 21-fold increase in Young's modulus and ultimate tensile strength respectively. Moreover, the formation of ionomeric cross-linking improved creep resistance while maintaining high elasticity and elastic recovery. The loading of metal into the materials facilitated the further regulation of thermomechanical properties (<1 wt% metal). Unlike covalent cross-linking, the reversible metal-ligand interactions introduced allow for mechanical reprocessing/recycling.

In Chapter 3, a series of poly(cyclohexene carbonate-*grad*-cyclopentene carbonate) (PCHC-*grad*-PCPC) terpolymers were produced.[2] The enchainment of small quantities of PCPC with PCHC acted to reduce the entanglement molar mass (M_e) and produced plastics with a 200% improvement in toughness relative to PCHC. Furthermore, this resulted in a minimal reduction in T_g, ensuring the terpolymers had a wide operating temperature window.

The terpolymers were shown to undergo both mechanical and chemical recycling to monomer without compromise to the thermomechanical properties.

In Chapter 4, a low molar mass poly(carbonate-*b*-ester-*b*-carbonate) triblock copolymer was produced on a 200g scale and was used in the formulation of a novel digital light processing resin.[3] Using a thiol-ene based 3D printing process, a series of degradable thermosets were produced with cross-linkers containing increasing poly(ethylene glycol) (PEG) content. These materials display printing-induced microphase separation and behave as soft elastomers. The thermomechanical properties, the hydrophilicity, and the degradation profile of the elastomers was controlled through the selection of the cross-linker used. No initial cytotoxic response was observed, indicating their potential in regenerative medicine and tissue engineering applications.

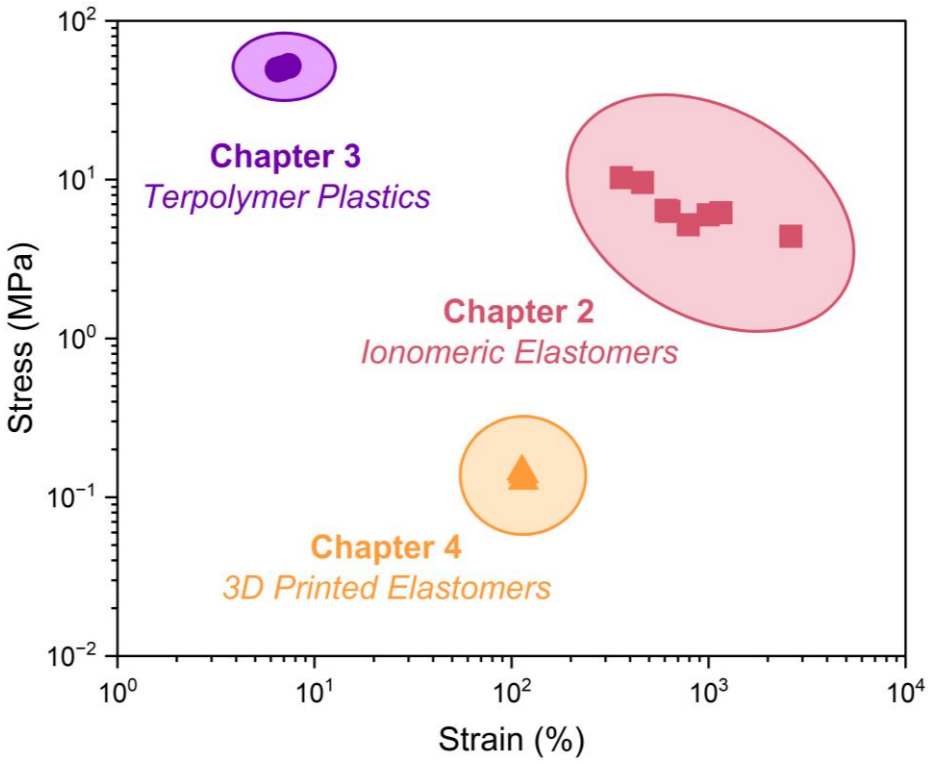

Figure 5.1: Ashby plot summarising the mechanical properties of materials reported in this thesis.

The materials reported in this thesis cover a wide area of property space, toughened elastomers, toughened plastics, and soft elastomers (**Figure 5.1**). This highlights the potential of CO_2- and bio-derived polymers to be used in a wide array of applications. However, further development is required to enable this and to further expand the properties accessible by oxygenated polymers.

5.2 Outlook

As outlined in Chapters 2, 3 and 4, there are numerous avenues of future exploration and materials development following the results reported in this thesis. There are two key areas currently under investigation which build on the work of this thesis. These are the introduction of metal-carboxylate cross-linking in the central block of a TPE and the chain extension of low molar mass triblock copolymers through the formation of halatopolymers.

5.3 Ionomeric Cross-Linking in TPE Central Block

The introduction of reversible metal-ligand and hydrogen bonding cross-linking within the outer blocks/'hard' domains of a TPE has proven an effective means to toughen and tune the thermomechanical properties (Chapter 2). However, as these reversible cross-links exist within a high T_g (above room temperature) domain, they are not dynamic and can only undergo exchange reactions at elevated temperatures and pressures. On the other hand, if the same interactions were incorporated into the central 'soft' block of a TPE, they should be reversible and dynamic.[4] This dynamism should arise from the segmental motion of the low T_g block at room temperature. It is anticipated that these interactions will give rise to tougher elastomers as the reversible bonds can repeatedly break and reform under tension to relieve stress.[5] Furthermore, these dynamic interactions should improve strain hardening and give rise to strain rate dependent behaviour.[6]

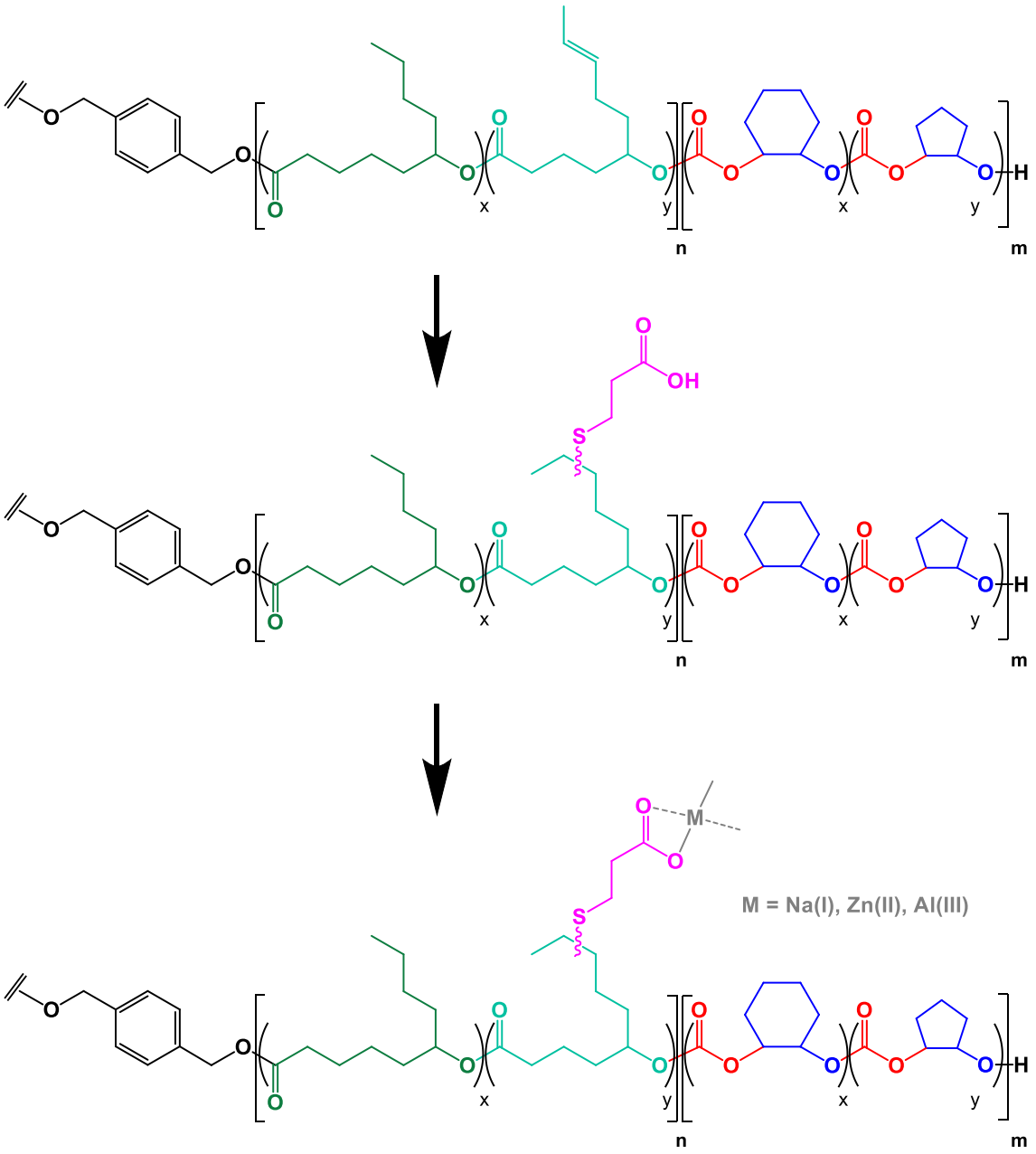

Scheme 5.1: Synthesis of poly(carbonate-*b*-ester-*b*-carbonate) ionomers with metal-ligand cross-linking in the central low T_g block.

To achieve this, a ABA triblock copolymer was synthesised, with a poly(ε-decalactone-*co*-δ-jasmine lactone) central block with poly(cyclohexene carbonate-*grad*-cyclopentene carbonate) outer blocks (**Scheme 5.1**). Jasmine lactone is a bio-derived lactone which is commonly used in fragrances but has received minimal investigation as a monomer for ROP.[7-9] It features alkene functionality in the side chain which can be modified via thiol-ene

functionalisation to install carboxylate ligands to every poly(δ-jasmine lactone) (PJL) repeat unit. The carboxylates can then be co-ordinated to the metal cations to produce an ionomeric networks. The terpolymer polycarbonate outer block was targeted for its low M_e and high T_g (Chapter 3).[2]

P1-vinyl was synthesised on a 12.8 g scale, with an overall molar mass (M_n) of 67.2 kg mol^{-1} ($Đ_M$ = 1.16) from SEC (Figure S7.5.1), with a PDL:PJL content of 9:1, and with 33 wt% polycarbonate content (PCHC: PCPC = 58:42), determined by ^{1}H NMR spectroscopy (Figure S7.5.2). The UV-initiated thiol-ene functionalisation with 3-mercaptopropionic acid was conducted to produce 8.4 g of **P1**-COOH. Full alkene functionalisation was confirmed by ^{1}H NMR spectroscopy (Figure S7.5.3). To form a zinc ionomer, **P1**-Zn, half an equivalent of diethyl zinc with respect to carboxylate ligands was added in solution (5 wt% THF), solvent cast, dried *in vacuo* and compression moulded into thin films.

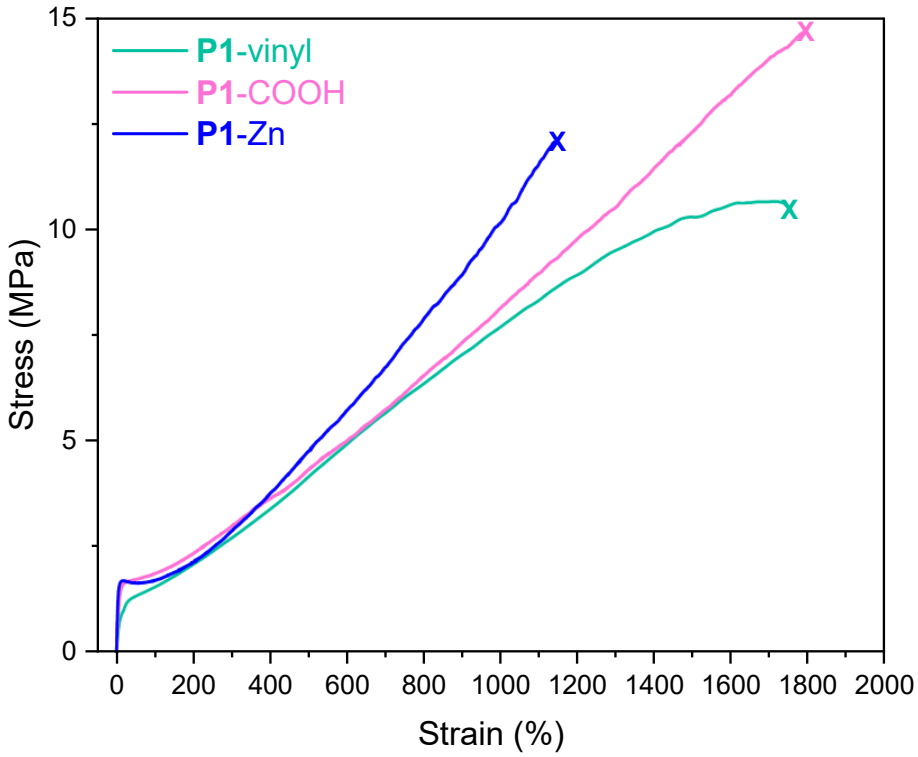

Scheme 5.2: Representative stress–strain curves (10 mm min^{-1} extension rate) for **P1**-vinyl, **P1**-COOH and **P1**-Zn.

The upper T_g for the polycarbonate blocks did not significantly change with functionalisation. DSC analysis revealed an upper T_g of 100, 102 and 103 °C for **P1**-vinyl, **P1**-COOH and **P1**-Zn respectively (Figure S7.5.4). Surprisingly, the lower T_g, corresponding to the central polyester block also didn't change significantly. It was anticipated that the ionomeric cross-linking would raise the T_g of the central block however it was observed to be -49, -42 and -43 °C for **P1**-vinyl, **P1**-COOH and **P1**-Zn respectively (Figure S7.5.4). This is an early indication of the dynamic nature of the cross-linking as segmental motion is minimally impeded.

Table 5.1: Summary of mechanical properties of ionomeric elastomers.

Polymer	[a] E_y (MPa)	[b] σ (MPa)	[c] ε_b (%)	[d] U_T (MJ m^{-3})
P1-vinyl	33.3 ± 9.5	10.7 ± 0.8	1754 ± 81	134 ± 7.4
P1-COOH	30.1 ± 7.6	13.7 ± 0.7	1781 ± 88	126 ± 9
P1-Na	t.b.d.	t.b.d.	t.b.d.	t.b.d.
P1-Zn	68.7 ± 1.6	12.2 ± 0.3	1157 ± 33	60 ± 7
P1-Al	t.b.d.	t.b.d.	t.b.d.	t.b.d.

a) Young's modulus; b) Tensile strength; c) Strain at break; d) Tensile toughness (area under the stress–strain curve).Mean values ± standard deviation from measurements conducted independently on 5 specimens

Uniaxial tensile testing was conducted on **P1**-vinyl, **P1**-COOH and **P1**-Zn to evaluate the mechanical performance of the ABA triblock copolymers (**Figure 5.2** and **Table 5.1**). **P1**-

vinyl behaves as an elastomer, displaying good elastic recovery, despite exhibiting a relatively pronounced yield point. The unfuctionalised material displayed an ultimate tensile strength of 11.2 MPa and an elongation at break of 2447%. The ultimate tensile strength increased to 13.7 MPa upon installation of the carboxylate ligands in **P1**-COOH. This came at the expense of a small reduction in elongation at break, which dropped to 1781%. Coordination to zinc, to form **P1**-Zn, resulted in a decrease in both tensile strength and elongation at break, 12.2 MPa and 1137% respectively. However, the rate of strain hardening observed increases from **P1**-vinyl to **P1**-COOH to **P1**-Zn. This is attributed to increased inter-chain interactions within the elastomers. The yield point observed for **P1**-vinyl became more diffuse for **P1**-COOH and **P1**-Zn, which is tentatively attributed to the reversible interactions which act to limit molecular separation and the disentanglement of the central block under tension.

Future work will build on these preliminary results. In particular, a sodium and aluminium ionomer will be produced through the addition of sodium cyclopentadienide and triethyl aluminium. This will allow for the exploration of how valency of the metal employed changes the bulk thermomechanical properties. Furthermore, the metals are light, cheap, Earth-abundant, usually of low toxicity, and should result in the formation of a colourless network. Uniaxial and cyclic tensile testing will be conducted to interrogate how strain rate influences the mechanical performance and elasticity of the ABA triblock copolymers. The time scale of the ionomeric interactions will be probed through the construction of a time-temperature superposition master curve; the environmental stability will be studied though the use of relative humidity DMA experiments; and any changes to mechanical performance will be explored through repeated thermal reprocessing.

5.4 Ionomeric Chain Extension Through Halatopolymer Formation

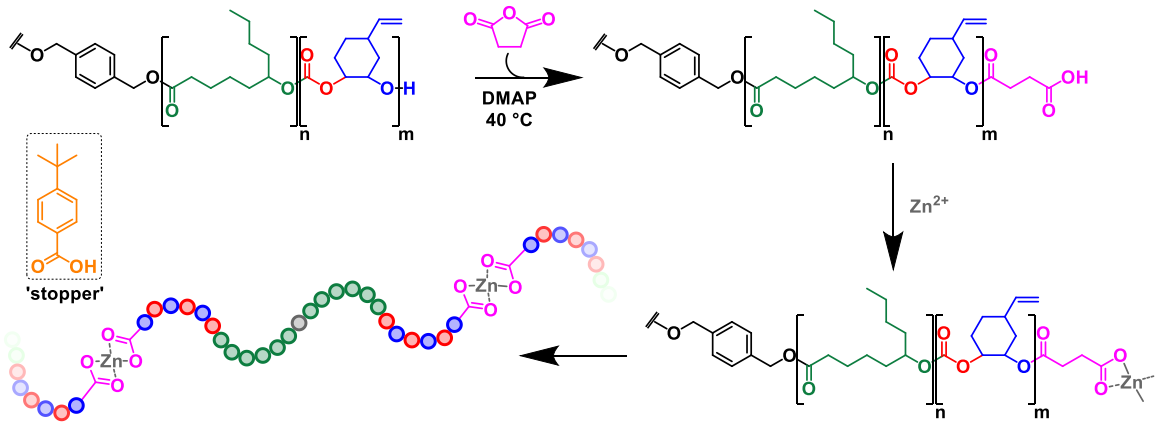

Scheme 5.2: Synthesis of halatopolymers through carboxylic acid end-group functionalization of a poly(carbonate-*b*-ester-*b*-carbonate) followed by the incorporation of Zn(II) and a monocarboxylic acid 'stopper'.

Halatopolymers are formed of linear polymers (halato-telechelic polymers) coupled by carboxylate end-groups with divalent metal cations.[10] The influence of metal-carboxylate interactions have been and are being explored in the outer and central blocks of a ABA triblock copolymer TPEs. Ongoing work now aims to explore how the installation of carboxylate end-group on a low molar mass (M_n < 10 kg mol^{-1}) poly(vinyl cyclohexene carbonate-*b*-ε-decalactone-*b*-vinyl cyclohexene carbonate) (**P1**, Chapter 4) can be used as a means to produce higher molar mass multi-block copolymers (**Scheme 5.2**). It is anticipated that by controlling the ratio of diethyl zinc and a monocarboxylic acid 'stopper', 4-*tert*-butylbenzoic acid, the molar mass of the resulting halatopolymer may be controlled. It is anticipated this synthetic approach will allow for the transformation of a low molar mass viscous liquid into a functional, freestanding, elastomer. Furthermore, microphase separation may be induced through the increase in the molar mass of the polymer chains paired with the ionic functionality in the polycarbonate blocks. As the metal-carboxylate interactions are known to be reversible, under

elevated temperatures, the halatopolymer materials should exhibit low viscosities in the melt, enabling facile reprocessing.

The end-group functionalisation of **P1** was successfully carried out through the base-catalysed ring-opening of succinic anhydride (SA) by the hydroxy telechelic end groups in the presence of 4-dimethylaminopyridine (DMAP). The reaction progress was followed through the end-group titration of aliquots with 2-chloro-4,4,5,5-tetra-methyldioxaphospholane (Figure S7.5.5).[11] Complete end-group functionalisation was achieved, with a complete loss of signals corresponding to the PvCHC hydroxy end-groups and the observation of only succinic acid end-groups (**Figure 5.3**).

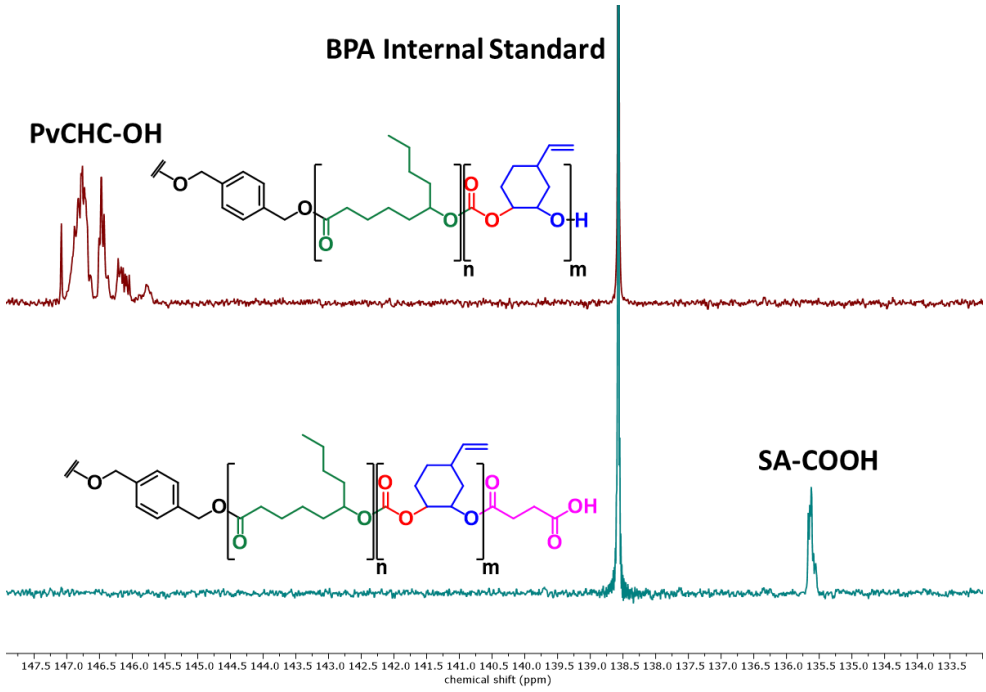

Figure 5.3: $^{31}P\{^{1}H\}$ NMR spectra used for end-group analysis of HO-**P1**-OH and HOOC-**P1**-COOH.

Work will now continue to explore the impact of metal-carboxylate coordination and subsequent chain-end coupling on complex viscosity (at room temperature and at elevated temperatures, molar mass (by SEC), block miscibility (by DSC), and microphase separation (by DMTA and SAXS).

5.5 Conclusion

This thesis has aimed to synthesise a range of new functional and oxygenated polymers, formed through the polymerisation of CO_2 and bio-derived monomers. It has also aimed to devise strategies to improve and tune the thermomechanical properties of the resulting materials. However, the development of new and sustainable materials is only one element to tackling a complex, multifaceted, global challenge. Alongside new materials, we need improved recycling, a conscientious approach to material selection, and a societal shift from decision makers to enact increasingly urgent change.

5.6 References

(1) Poon, K. C.; Gregory, G. L.; Sulley, G. S.; Vidal, F.; Williams, C. K. Toughening CO2-Derived Copolymer Elastomers Through Ionomer Networking. *Adv. Mater.* **2023**, *35* (36), 2302825. DOI: 10.1002/adma.202302825.
(2) Poon, K. C.; Smith, M. L.; Williams, C. K. Controlled Carbon Dioxide Terpolymerizations to Deliver Toughened yet Recyclable Thermoplastics. *Macromolecules* **2024**, *57* (9), 4199-4207. DOI: 10.1021/acs.macromol.4c00455.
(3) Poon, K. C.; Segal, M.; Bahnick, A. J.; Chan, Y. M.; Gao, C.; Becker, M. L.; Williams, C. K. Digital Light Processing to Afford High Resolution and Degradable CO2-Derived Copolymer Elastomers. *Angew. Chem. Int. Edit.* **2024**, e202407794 DOI: 10.1002/anie.202407794.
(4) Khare, E.; Holten-Andersen, N.; Buehler, M. J. Transition-metal coordinate bonds for bioinspired macromolecules with tunable mechanical properties. *Nat. Rev. Mater.* **2021**, *6* (5), 421-436. DOI: 10.1038/s41578-020-00270-z.
(5) Wang, S.; Hu, Y.; Kouznetsova, T. B.; Sapir, L.; Chen, D.; Herzog-Arbeitman, A.; Johnson, J. A.; Rubinstein, M.; Craig, S. L. Facile mechanochemical cycloreversion of polymer cross-linkers enhances tear resistance. *Science* **2023**, *380* (6651), 1248-1252. DOI: doi:10.1126/science.adg3229.
(6) Petersen, S. R.; Prydderch, H.; Worch, J. C.; Stubbs, C. J.; Wang, Z.; Yu, J.; Arno, M. C.; Dobrynin, A. V.; Becker, M. L.; Dove, A. P. Ultra-Tough Elastomers from Stereochemistry-Directed Hydrogen Bonding in Isosorbide-Based Polymers. *Angew. Chem. Int. Edit.* **2022**, *61* (17), e202115904. DOI: 10.1002/anie.202115904.
(7) Zeng, L.; Zhou, Y.; Fu, X.; Liao, Y.; Yuan, Y.; Jia, Y.; Dong, F.; Yang, Z. Biosynthesis of Jasmine Lactone in Tea (Camellia sinensis) Leaves and Its Formation in Response to Multiple Stresses. *J. Agric. Food Chem.* **2018**, *66* (15), 3899-3909. DOI: 10.1021/acs.jafc.8b00515.
(8) Bansal, K. K.; Özliseli, E.; Rosling, A.; Rosenholm, J. M. Synthesis and Evaluation of Novel Functional Polymers Derived from Renewable Jasmine Lactone for Stimuli-Responsive Drug Delivery. *Adv. Funct. Mater.* **2021**, *31* (33), 2101998. DOI: 10.1002/adfm.202101998.
(9) Ali, A.; Bhadane, R.; Asl, A. A.; Wilén, C.-E.; Salo-Ahen, O.; Rosenholm, J. M.; Bansal, K. K. Functional block copolymer micelles based on poly (jasmine lactone) for improving the loading efficiency of weakly basic drugs. *RSC Adv.* **2022**, *12* (41), 26763-26775, 10.1039/D2RA03962A. DOI: 10.1039/D2RA03962A.
(10) halato-telechelic polymer. 3.0.1 ed.; International Union of Pure and Applied Chemistry (IUPAC), 2019.
(11) Spyros, A.; Argyropoulos, D. S.; Marchessault, R. H. A Study of Poly(hydroxyalkanoate)s by Quantitative 31P NMR Spectroscopy: Molecular Weight and Chain Cleavage. *Macromolecules* **1997**, *30* (2), 327-329. DOI: 10.1021/ma9601979.

CHAPTER 6

Experimental

6.1 General

Catalysis synthesis, polymerisations, and post-polymerisation functionalisations were performed using either a dual manifold nitrogen-vacuum Schlenk line or a nitrogen-filled glovebox.

Materials. All reagents and solvents were purchased and used as obtained from commercial sources (Sigma Aldrich) unless stated otherwise. The macrocyclic ligand, H_2L, was synthesised following a previously reported procedure.[1] Magnesium bis(1,1,1,3,3,3-hexamethyldisilazan-2-ide) (97%) and bis(pentafluorophenyl)zinc (97%) were purchased from Sigma-Aldrich. Bis(pentafluorophenyl)zinc was used as received and magnesium bis(1,1,1,3,3,3-hexamethyldisilazan-2-ide) was recrystallised from hexane.

Solvents used for synthesis and polymerisation were collected from a solvent purification system (SPS), degassed with three freeze-pump-thaw cycles, and stored over 4 Å molecular sieves, under an inert atmosphere. 4-Vinyl-1-cyclohenxene 1,2-epoxide (98%) (vCHO) was purchased from Sigma-Aldrich, dried by stirring over CaH_2, followed by fractional distillation at 60 °C and 18 mbar. Cyclohexene 1,2-epoxide (98%) (CHO) was purchased from Alfa Aesar, dried by stirring over CaH_2, followed by fractional distillation at 60 °C, 50 mbar. *n*-Butyl lithium was then added and the CHO distilled twice more. Cyclopentene 1,2-epoxide (98%) (CPO) was purchased from Sigma-Aldrich, dried by stirring over CaH_2, followed by fractional distillation at 60 °C, 55 mbar. ε-Decalactone (ε-DL) was dried over CaH_2, followed by fractional distillation, at 115 °C, under reduced pressure, and kept under a nitrogen atmosphere. Epoxide and lactone monomers were stored under a nitrogen atmosphere. 1,4-Benzenedimethanol (BDM) was crystallised from toluene and stored under inert atmosphere. Research-grade carbon dioxide was dried through a Drierite column and two additional drying columns (Micro Torr, Model number: MC1-804FV) in series before use.

3-Mercaptopropionic acid was purchased from Sigma-Aldrich and degassed by bubbling through nitrogen. Sodium triflate, magnesium triflate, calcium triflate, zinc triflate and aluminium triflate were purchased from Fluorochem and used as received.

Sudan I dye was purchased from AmBeed and used as received. Trimethylolpropane tris(3-mercaptopropionate) (**X1**) was purchased from Sigma-Aldrich and ethoxylated trimethylolpropane tris(3-mercaptopropionate) (**X2** and **X3**) were donated by Bruno Bock (Thiocure®). All thiols were used as received.

6.2 Experimental Procedures

Synthesis of 4-*tert*-butly-2,6-diformyl phenol[1]

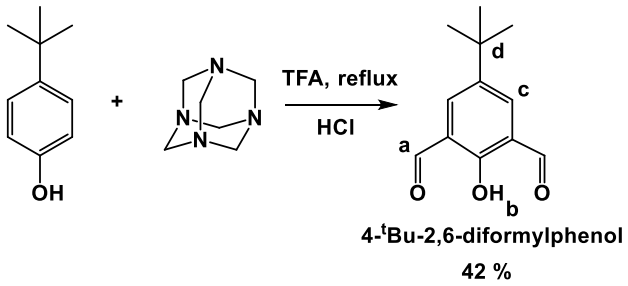

Figure 6.1: Structure and synthesis of 4-*tert*-butly-2,6-diformyl phenol, with labelling corresponding to the ^{1}H NMR spectra assignment.[1]

4-*tert*-butlyphenol (25 g, 166.5 mmol) and hexamethylenetetramine (37.35 g, 266.5 mmol) were dissolved in trifluoroacetic acid (130 mL) under slow stirring. The reaction mixture was refluxed (125 °C) overnight. A Dean-Stark apparatus was added and the reaction mixture was refluxed at 150 °C for 2.5 hours. The reaction mixture was cooled to 100 °C and HCl (3M) was added slowly. The reaction mixture was cooled to room temperature and then cooled in the freezer overnight. The resulting solid product was filtered, washed with cool methanol (-78 °C) and dried. Yield: 14.4357 g (42%). ^{1}H NMR (400 MHz, $CDCl_3$) δ 11.47 (s, 1H, *C**H**O*, a), 10.23 (s, 2H, -*O**H***, b), 7.97 (s, 2H, *Ar-**H***, c), 1.34 (s, 11H, *C**H**$_3$*, d).

Synthesis of $[H_4L](ClO_4)_2$[1]

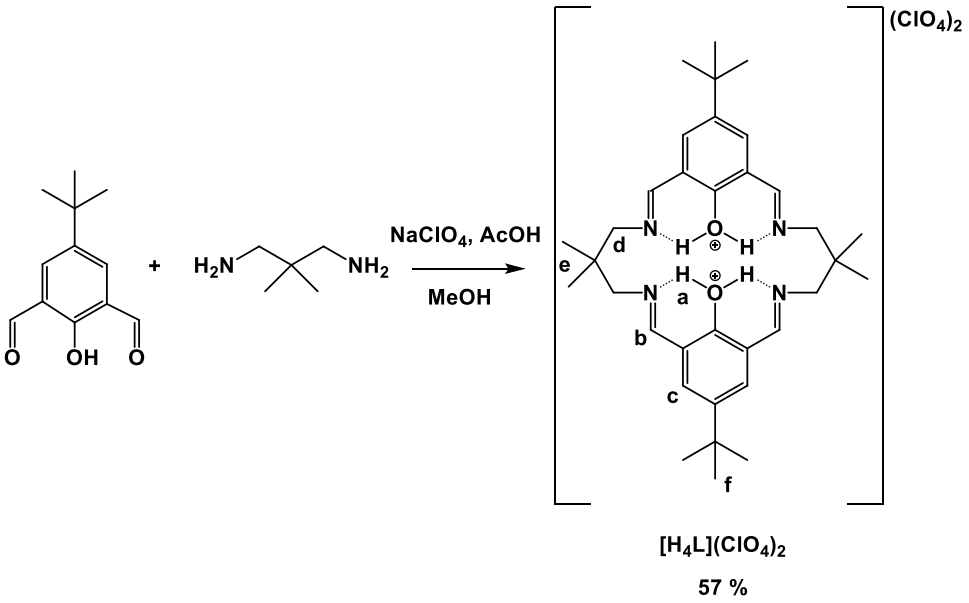

Figure 6.2: Structure and synthesis of $[H_4L](ClO_4)_2$, with labelling corresponding to the ^1H NMR spectra assignment.[1]

4-*tert*-Butyl-2,6-diformylphenol (6.00 g, 206.24 mmol), $NaClO_4$ and acetic acid (3.32 mL, 60.05 mmol) were dissolved in methanol (450 mL). The reaction mixture was heated to 70 °C and a solution of 2,2-dimethyl-1,3-propandiamine (3.48 mL in 150 mL of methanol) was added slowly to the reaction mixture. The reaction was cooled to room temperature and stirred for 72 hours. The solid precipitate was filtered under gravity and dried. The filtrate was concentrated under reduced pressure and a second crop of product was collected and dried. The filtrate was allowed to slowly evaporate at room temperature and a third and fourth crop of product was collected and dried. A fifth and final crop was collected by allowing the reaction mixture to evaporate to dryness at room temperature and pressure. Yield: 12.4557 g (57%). ^1H NMR (400 MHz, DMSO) δ 13.61 (br s, 4H, -O***H***N-, a), 8.68 (d, 4H, *J* = 13.5 Hz, imine *C**H***, b), 7.65 (s, 4H, *Ar-**H***, c), 3.87 (d, 8H, *J* = 6.0 Hz, =N*C**H**₂*-, d), 1.28 (s, 12H, *C(C**H**₃)₂*, e), 1.14 (s, 18H, *C(C**H**₃)₃*, f).

Synthesis of H_2L^1

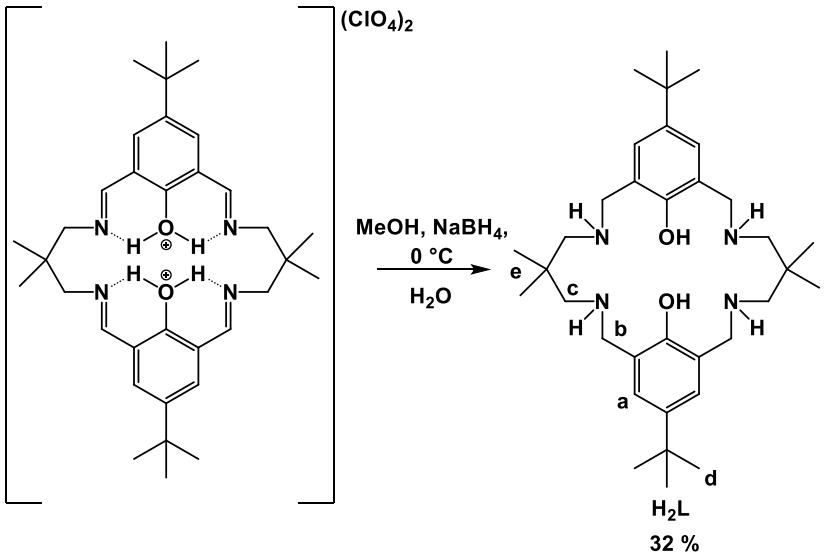

Figure 6.3: Structure and synthesis of H_4L, with labelling corresponding to the ^{1}H NMR spectra assignment.[1]

$[H_4L](ClO_4)_2$ (3.00 g, 4.01 mmol) was suspended in methanol (300 mL) and cooled to 0 °C. $NaBH_4$ (3.94 g, 104 mmol) was added slowly to the reaction mixture and stirred for 1 hour at room temperature. The stiring was stopped water (600 mL) was rapidly added to the reaction mixture and left to sit overnight. The solution was filtered under reduced pressure and crystallised in methanol. Yield: 0.9976 g (45%). ^{1}H NMR (400 MHz, $CDCl_3$) δ 6.93 (s, 4H, *Ar-**H***, a), 3.74 (s, 8H, *-CHCC**H**$_2$N-*, b), 2.51 (s, 8H, *-CH$_3$CC**H**$_2$N-*, c), 1.25 (s, 18H, *-C(C**H**$_3$)$_3$,* d), 1.01 (s, 12H, *C(C**H**$_3$)$_2$*, e).

Synthesis of [LZnMg(C_6F_5)$_2$] Catalyst[2]

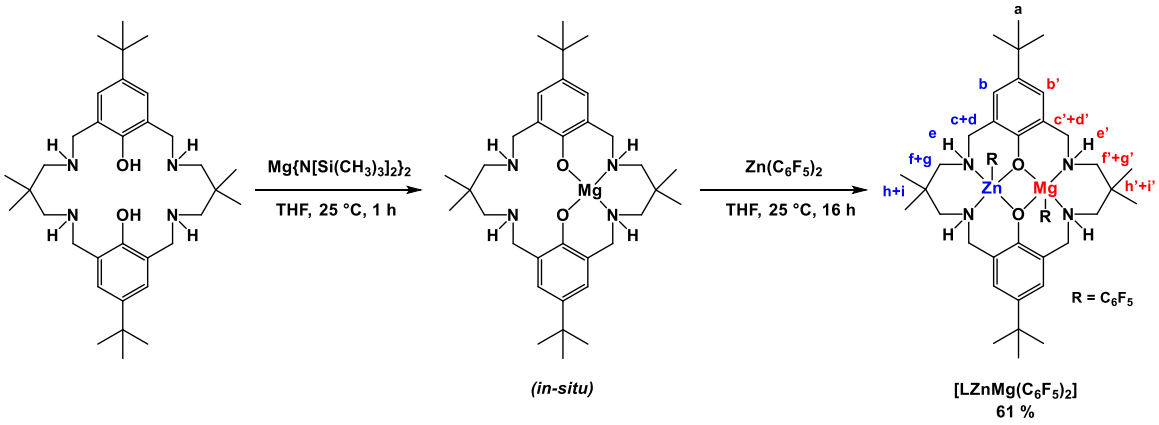

Figure 6.4: Structure and synthesis of [LZnMg(C_6F_5)$_2$], with labelling corresponding to the ^{1}H NMR spectra assignment.[2]

The catalyst was synthesised following a previously reported procedure.[2] Under inert conditions, the macrocyclic ligand (H_2L) (0.50 g, 0.90 mmol) and recrystallised Mg{N[Si(CH_3)$_3$]$_2$}$_2$ (0.31 g, 0.90 mmol) were dissolved in THF (10 mL), at 25 °C, for 1 hour. Zn(C_6F_5)$_2$ was dissolved in THF (5 mL) and added dropwise to the reaction mixture. The dark orange solution was stirred overnight, at 25 °C. The pale orange reaction mixture was then cooled to -29 °C and the supernatant solvent was removed. The solid product was washed (hexane) and the product (precipitate) dried under reduced pressure. Yield: 0.54 g (61%). ^{1}H NMR (400 MHz, $CDCl_3$) δ 6.81 (s, 2H, b), 6.76 (s, 2H, b'), 4.42 – 4.25 (m, 4H, c+c'), 3.40 (d, J = 13.7 Hz, 2H, d), 3.26 (d, J = 13.3 Hz, 2H, d'), 3.14 – 2.94 (m, 4H, f+f'), 2.68 (m, 6H, g+g'+e), 2.11 – 2.00 (m, 2H, e'), 1.27 (s, 3H, h), 1.20 (s, 18H, a), 1.17 (s, 3H, h'), 1.06 – 1.01 (m, 6H, i+i').

Synthesis of [LCoMg(OAc)$_2$] Catalyst[3]

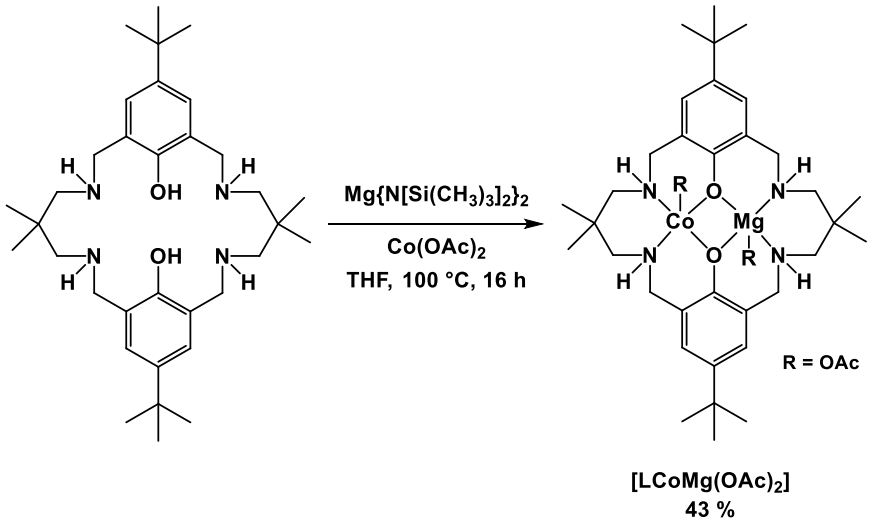

Figure 6.5: Structure and synthesis of [LCoMg(OAc)$_2$], with labelling corresponding to the ^{1}H NMR spectra assignment.[3]

Mg(N(SiMe$_3$)$_2$)$_2$ (0.44 g, 0.13 mmol) and Co(OAc)$_2$ (0.23 g, 0.13 mmol) was added to a solution of H_2L (0.70 g, 0.13 mmol) in THF (6 mL) and heated to 100 °C in a sealed Schlenk tube for 16 h. The solvent was removed, in vacuo, and the solid washed with pentane (3 x 10 mL) to afford the product as a pale pink solid. Yield: 0.41 g (43%). MS (MALDI-ToF): m/z 692.31 [LMgCo(OAC)]$^+$.

General Synthesis of PvCHC-PDL-PvCHC Triblock Copolymers

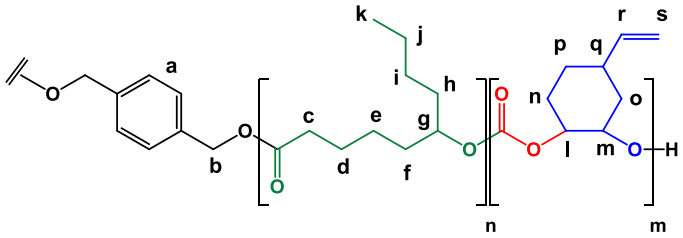

Figure 6.6: Structure of PvCHC-PDL-PvCHC (**1**-vinyl and **2**-vinyl), with labelling corresponding to the ^{1}H NMR spectra assignment.

[LZnMg(C_6F_5)$_2$] (10 mg, 0.01 mmol), 1,4-benzenedimethanol (5.7 mg, 0.04 mmol), 4-vinyl-1-cyclohexene 1,2-epoxide (0.94 mL, 7.32 mmol) and ε-decalactone (2.94 mL, 16.87 mmol) were dissolved in toluene (10 mL) and heated to 80 °C. The progress of the reaction was monitored by ^{1}H NMR spectroscopy. After 16 min of heating, 90% conversion was achieved. The reaction mixture was placed under 20 bar of CO_2 in a high-pressure reactor, heated to 80 °C and left to stir overnight. The reaction mixture was quenched by exposure to air. The polymer was precipitated in methanol twice and dried under reduced pressure. ^{1}H NMR (400 MHz, $CDCl_3$) δ 7.34 (s, 4H, a), 5.76 (m, 1H, r), 5.04 (m. 5H, b+s), 4.85 (m, 1H, g), 4.77 (br s, 2H, l+m), 2.43 (br s, 1H, q), 2.27 (t, 2H, c), 1.85-1.29 (br m, 20H, d+e+f+g+h+i+j+n+o+p), 0.88 (t, 3H, k). Integrals given are for a single repeat unit of each block.

Table 6.1: Summary of Polymerisation Conditions for **1**-vinyl and **2**-vinyl.

Entry	cat. /mg	BDM /mg	ε-DL /mL	vCHO /mL	PhMe /mL	CO_2 /bar	[a]PDL :PvCHC
1-vinyl	10	5.7	2.94	0.94	10	20	71:29
2-vinyl	40	22.7	11.77	2.34	40	20	79:21

[a]Determined from ^{1}H NMR spectrum of purified samples

General Procedure for Carboxylic Acid Functionalisation

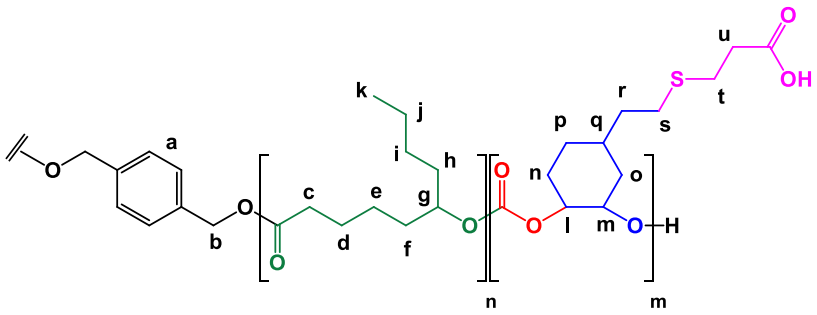

Figure 6.7: Structure of $PvCHC_{COOH}$-PDL-$PvCHC_{COOH}$ (**2**-COOH), with labelling corresponding to the ^1H NMR spectra assignment.

2-Vinyl (1.00 g, 1.1 mmol PvCHC), 3-mercaptopropionic acid (0.37 mL, 4.4 mmol) and 2,2-dimethoxy-2-phenylacetophenone (110 mg, 0.44 mmol) was dissolved in THF (10 mL). The reaction mixture was stirred at room temperature and irradiated with UV light (365 nm) for 60 min. The reaction mixture was quenched by exposure to air, precipitated in methanol twice and dried under reduced pressure. ^1H NMR (400 MHz, $CDCl_3$) δ 7.34 (s, 4H, a), 5.10 (s. 4H, b), 4.85 (m, 1H, g), 4.77 (br s, 2H, l+m), 2.78 (br s, 2H, u), 2.66 (br s, 2H, t), 2.57 (br s, 2H, s), 2.27 (t, 2H, c), 1.61-1.29 (br m, 20H, d+e+f+g+h+i+j+n+o+p+q+r), 0.88 (t, 3H, k). Integrals given are for a single repeat unit of each block.

General Procedure for Ionomer Formation

2-COOH (0.8 g, 0.9 mmol $PvCHC_{COOH}$) was dissolved in THF (16 mL). The reaction mixture was stirred at room temperature and an $Al(OTf)_3$ solution (50 mM, 1.8 mL) was added drop-wise. The reaction mixture was stirred for 10 min, then concentrated under reduced pressure, precipitated in methanol, washed with water and dried under reduced pressure.

General Procedure for CHO, CPO, CO_2 Terpolymerisation

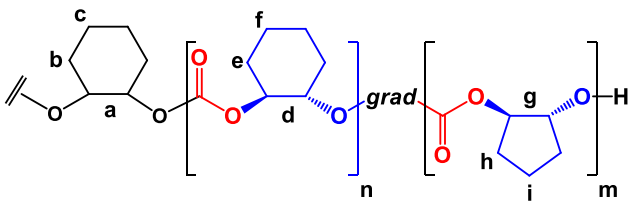

Figure 6.8: Structure of PCHC-*grad*-PCPC, with labelling corresponding to the ^{1}H NMR spectra assignment.

[LZnMg(C_6F_5)$_2$] (5 mg, 0.01 mmol), cyclohexane-1,2-diol (2.4 mg, 0.02 mmol), cyclohexane oxide (2.60 mL, 25 mmol) and cyclopentene oxide (2.18 mL, 25 mmol) were dissolved in toluene (10 mL). The solution was added into a high-pressure Steel reactor which was placed under 40 bar of CO_2 (using a triple manifold line), heated to 80 °C and stirred for 96 h. The reaction mixture was quenched by exposed to air and the polymer was precipitated in methanol (3x) and dried under reduced pressure. ^{1}H NMR (400 MHz, $CDCl_3$) δ 5.00 (br s, 2H, g), 4.64 (br s, 2H, d), 2.13 (br s, 4H, h), 1.77-1.36 (br m, 20H, a+b+c+e+f+i).

Table 6.2: Summary of Polymerisation Conditions and Results.

cat. /mg	CHD /mg	CHO /mL	CPO /mL	PhMe /mL	CO_2 /bar	[a]CHO conv./ %	[a]CPO conv./ %	[b]PCHC :PCPC
5	2.4	2.60	2.18	10	20	86	58	71:29
5	2.4	2.60	2.18	10	40	98	93	51:49
5	2.4	3.89	1.12	10	40	99	91	77:23
5	2.4	1.30	3.36	10	40	96	90	28:72

[a]Determined from ^{1}H NMR spectrum of crude polymer samples. [b]Determined from ^{1}H NMR spectrum of purified samples

Procedure for P1 Synthesis

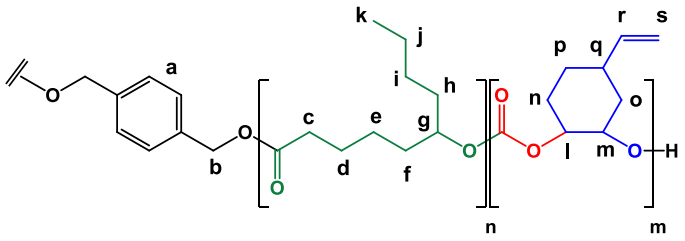

Figure 6.9: Structure of PvCHC-PDL-PvCHC (**P1**), with labelling corresponding to the ^{1}H NMR spectra assignment.

[LCoMg(OAc)$_2$] (250 mg, 0.33 mmol), benzene dimethanol (6.89 g, 50 mmol), 4-vinyl-1-cyclohenxene 1,2-epoxide (46 g, 371 mmol) and ε-decalactone (187 g, 1098 mmol) were dissolved in toluene (157 mL) and stirred at 80 °C for 3 h (98% PDL conversion). Next, the reaction was placed under 1 bar of CO_2, heated to 80 °C and stirred for 96 h (>99% PvCHC conversion). The reaction mixture was quenched by exposure to air. The triblock copolymer was isolated and purified by dilution in THF, stirring with Amberchrom™ 50WX8 (hydrogen form, 100-200 mesh) overnight, filtration (twice, through silica) to remove residual catalyst and any diol. Following concentration in vacuo, the colourless polymer was collected (**P1**). Yield: 85% . ^{1}H NMR (400 MHz, $CDCl_3$) δ 7.34 (s, 4H, a), 5.76 (m, 1H, r), 5.04 (m. 5H, b+s), 4.85 (m, 1H, g), 4.77 (br s, 2H, l+m), 2.43 (br s, 1H, q), 2.27 (t, 2H, c), 1.85-1.29 (br m, 20H, d+e+f+g+h+i+j+n+o+p), 0.88 (t, 3H, k). Integrals given are for a single repeat unit of each block.

6.3 Analytical Techniques

Procedures described were used across all results chapters unless stated otherwise.

NMR Spectroscopy. ^{1}H and $^{31}P\{^{1}H\}$ NMR spectra were obtained using a Bruker AVIII HD 400 NMR spectrometer. $^{13}C\ \{^{1}H\}$ NMR spectra were obtained using a Bruker Avance III AVD500 NMR spectrometer. ^{1}H DOSY spectra were obtained using a Bruker NEO600 NMR spectrometer.

Size Exclusion Chromatography (SEC). Polymers (2-5 mg) dissolved in THF. Samples were passed through 0.2 μm PTFE filters prior to analysis. Analysis was carried out on a Shimadzu LC-20AD instrument, equipped with a Refractive Index (RI) detector and two PSS SDV 5 μm linear M columns. HPLC grade THF was used as the eluent at 1.0 mL/min at 30 °C. Monodisperse polystyrene standards were used for calibration.

Phosphorus End-Group Tests. Following literature procedure.[4] Polymer samples (40 mg) were dissolved in $CDCl_3$ (0.5 mL) and a solution (40 μL) containing $Cr(acac)_3$ (5.5 mg) and internal standard, bisphenol A (400 mg) in pyridine (10 mL) followed by 40 μL of 2-chloro-4,4,5,5-tetramethyl dioxaphospholane.

Differential Scanning Calorimetry (DSC). Recorded for purified polymer samples of triblock copolymers and ionomers were measured using a DSC25 (TA Instruments). A sealed, empty crucible was used as a reference, and the DSC was calibrated using sapphire and indium. Samples were heated from -80 °C to 150 °C, at a rate of 10 °C min^{-1} under N_2 flow (80 mL min^{-1}) followed by a 5-minute isotherm at 150 °C to erase thermal history. Samples were subsequently cooled to -80 °C, at a rate of 10 °C min^{-1}, and kept at -80 °C for a further 5 minutes, followed by a heating-cooling procedure from -80 °C to 150 °C, at a rate of 10 °C min^{-1}. Each sample was analysed over two heating-cooling cycles. Glass transition

temperatures (T_g) are reported as the midpoint of the transition taken from the second heating cycle.

Thermogravimetric Analysis (TGA). Measured using a TGA5500 system (TA Instruments). Samples were heated from 30 °C to 600 °C, at a rate of 5 °C min^{-1}, under N_2 flow (100 cm^3 min^{-1}).

Film Preparation. Transparent films were prepared by solvent casting into Teflon moulds from THF. Films were dried in a vacuum oven for at least 48 hours. Samples were then compression moulded using a Carver mini CH CE Press (5420CE.4040C00) with heated plates and hydraulic compression press. Polymers were placed between two metal sheets lined with Teflon, heated to 120 °C, 15 min, no pressure, then a further 15 min under 1 ton m^{-2}.

Fourier-Transform Infrared Spectroscopy (FTIR). Chapter 2: Spectra were obtained on a Shimadzu IRSpirit spectrometer, fitted with a KBr window and DLATGS detector with temperature control. FT-IR spectra were recorded inside a glove box using a single reflection ATR accessory and measured in transmission scanning mode. Solid polymer films were scanned from 4700-340 cm^{-1} (100 scans, 4 cm^{-1} resolution). Chapter 4: Spectra were obtained on a Thermo Electron Nicolet 8700 FTIR spectrometer with a built-in iS50 diamond ATR. Resolution of 0.09 cm^{-1}. 64 scans were used for both background and sample collection.

UV-Vis Spectroscopy. Spectra of diluted resins (10 wt% in ethyl acetate) were obtained on a BioTek Synergy™ Mx Microplate Reader (Agilent, California) using Gen 5™ reader control and data analysis software (λabs = 240-700 nm).

Raman Spectroscopy. Raman spectra were recorded on a LabRAM ARAMIS spectrometer with an Andor CCD detector from Horiba Jobin Yvon Ltd. using a He-Ne Laser (633 nm), a 1800 gr/mm grating, and 50x objective microscope. Spectral resolution of 0.6 cm^{-1}.

Tensile Testing. Chapter 2: Tests were carried out using an EZ-LX Universal Testing Instrument (Shimadzu). Chapter 3 and 4: Tests were carried out using an Instron 8600 series universal testing system, using a 50 N load cell and 250 N pneumatic grips. Chapter 2 and 3: Dumbbell-shaped specimens were cut using a Zwick ZCP020 cutting press equipped with a cutting device for ISO 527-2 type 5B. Uniaxial extension experiments (10 mm min^{-1} cross-head speed) were run according to ISO 527.

Zero Force/Stress Recovery. Dumbbell-shaped specimens were extended to 0.3 x elongation at break (determined from uniaxial tensile testing). Specimens were then allowed to relax at 10 mm min^{-1} until zero force/stress was recorded. Zero force/stress was subsequently maintained for 30 min as the material continued to relax. Elastic recovery was determined as: (Final length of specimen/Original length of specimen) x 100%.

Dynamic Mechanical Analysis (DMA). Chapter 2 and 3: Thermal analysis (DMTA) was carried out using a DMA850 (TA Instruments), using an ACS III cooling system. Specimens of uniform width (5.3 mm) were cut using two parallel blades. Samples were heated from -80 °C to 250 °C (or until the material deformed beyond the limits of the geometry employed) at a rate of 3 °C min^{-1}, with a frequency of 1 Hz, 0.1 N pre-load force and 0.1% strain amplitude. Glass transition temperatures (T_g) are reported as the peak maxima in tan (δ). Relative humidity analysis (RH DMA) was carried out with a DMA-RH accessory. Samples were heated from 30 °C to 90 °C at a rate of 1 °C min^{-1}, with a frequency of 1 Hz, 0.1 N pre-load force and 20.0 μm strain amplitude. Relative humidity was increased from 0% at a rate of 2% min^{-1}. Chapter 4: Thermal analysis (DMTA) was carried out using a DMA850 (TA Instruments), using an GCA cooling system. Specimens of uniform width (5.3 mm) were cut using two parallel blades. Temperature ramps for **P1X1**, **P1X2** and **P1X3** conducted in tension geometry. Temperature ramps for **P1** conducted in 3-point bend geometry. Samples were heated from -80 °C to 100 °C (or until the material deformed beyond the limits of the geometry employed) at a rate of 3

°C min^{-1}, with a frequency of 1 Hz, 0.1 N pre-load force and 0.1% strain amplitude. Compression testing carried out at room temperature, 0.01 N pre-load force, 1.0 mm min^{-1}. The diameter of each gyroid was taken in triplicate and the average value was used to calculate the cross-sectional area.

Rheology. Chapter 2: Creep-recovery experiments were conducted on an ARES-G2 (TA Instruments) using polymer samples between 8 mm stainless steel plates. Stress control conditioning experiments were conducted at 30 °C in the linear viscoelastic region as determined by amplitude sweeps. 5 kPa of stress was applied to the samples for 100 s followed by a period of 0 kPa for 100 s and the stain (creep) exhibited monitored, this was repeated a further 3 times. Chapter 4: The complex viscosity of each resin formulation was measured (not including the thiol) using a Discovery HR-3 (TA Instrument, DE, USA). The resin (1 mL) was placed on the 20 mm parallel plate geometry with a 0.2 mm gap. The results collected were from a frequency sweep of 0.1 rad s^{-1} to 500 rad s^{-1} at 10% strain at a constant temperature of 25 °C.

Solvent Swelling. Chapter 2: Uniform disks of the ionomers (8 mm diameter, ≈200 μm thick) were submerged in THF for 72 h, dried (vacuum oven, 72 h) and weighed both swollen and dried to determine the swelling index and gel content respectively. Chapter 4: Uniform disks of **P1X1**, **P1X2** and **P1X3** (10 mm diameter, 2 mm thick) were submerged in water for 24 h, dried (vacuum oven, 48 h) and weighed both swollen and dried to determine the swelling index and gel content respectively. Measurements performed in triplicate.

Swelling Index (SW) % = $[(W_s - W_o)/W_o)]$ x 100

Gel Content (GC) % = (W_d/W_o) x 100

W_o = Original Weight of Polymer

W_s = Weight of Swollen Polymer

W_d = Weight of Dried Polymer

Small-angle X-ray Scattering (SAXS). Chapter 2: Polymer films (prepared as for mechanical testing as described above) were submitted to Harwell Diamond Light Source in a solid sample grid for SAXS analysis (DL-SAXS, P38 instrument). Scans (3 × 5 min) were conducted at camera lengths of 4.5 and 1 m, beam energy = 9.2 keV (using the Ga MetalJet). SAXS data reported are an average of the 3 scans measured from data collected at 1 m. Samples were not annealed prior to testing to reflect the experimental conditions of tensile testing. 2D scattering patterns were reduced to 1D using Dawn software developed at the Diamond Light Source. Chapter 4: Measurements were performed on a SAXS Lab Ganesha system with a Cu 50 kV Xenocs Genix ULD SL X-ray point source and a 170 μm pixel-spaced, single-photon counting Dectris Pilatus 300 k 20 Hz detector. The measurements were performed using a 2 slit configuration where the distance between the sample and the detector was approximately 1041 mm for SAXS. One dimensional (1D) averaging of SAXS data was carried out by averaging across all azimuths with linear x axis binning. Spectra-by spectra reduction and corrections for sample transmission, sample thickness and absolute intensity factor were all included as part of 1D averaging using saxsgui software v2.23.33.

Solid-State PCHC Depolymerisation. The chemical recycling experiments were conducted using the previously reported procedure, conducted in a TGA instrument.[5] The sample was prepared as followed: in the glovebox, PCHC-*grad*-PCPC (1.00 mmol) was dissolved in THF (1 mL). The [Mg(II)Co(II)] catalyst (0.3 mmol) was added to the vial. The catalyst:polymer stock-solution (40 μL) was transferred to an aluminium TGA crucible. The crucible was placed under vacuum, for 30 minutes, before being crimped in the glovebox with a hermetic seal. The crucible was then transferred to a TGA instrument for solid-state depolymerisation using the method outlined below.

1. N_2 flow of 25.0 mL min^{-1}
2. Equilibrate at 30 °C

3. Heat to 140 °C

4. Isotherm at 140 °C, whilst monitoring mass loss

5. After 3 h (> 95% mass loss in all cases), sample was cooled to 30 °C

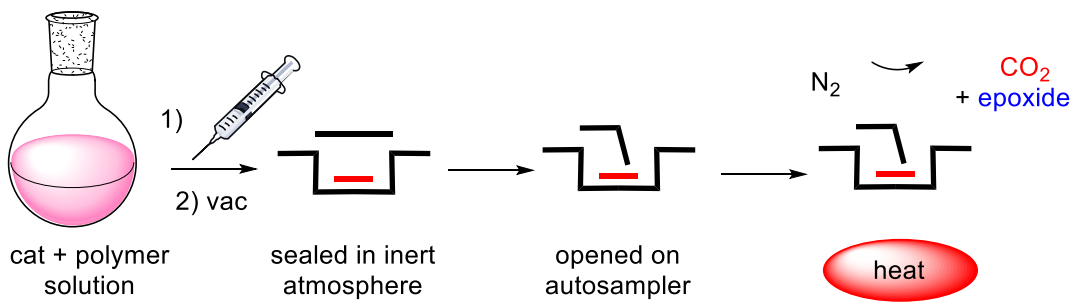

Figure 6.10: Solid-state PCHC-*grad*-PCPC depolymerisation set up for TGA.[5]

Laboratory-Scale Chemical Recycling. Under an N_2 atmosphere, PCHC-*grad*-PCPC (2.72 g, 20 mmol), dissolved in THF (3 mL), was added to a Schlenk tube containing the [Mg(II)Co(II)] catalyst (51 mg, 0.07 mmol). The Schlenk tube was placed under dynamic vacuum, overnight, to remove the THF and form a film on the glass walls of the vessel. A distillation glassware apparatus (short-path) was attached to it, with the collection flask being cooled. The apparatus was placed under vacuum (~40 mbar) and the Schlenk tube heated to 140 °C for 8 h, after which atmospheric pressure was re-established in the system using N_2.

The collected epoxide (1.51 g, 85% yield) was distilled over CaH_2 and then repolymerised with a [LZnMg(C_6F_5)$_2$] catalyst, (catalyst:epoxides = 1:5000, 3 M epoxide solution in toluene, 80 °C, 40 bar CO_2, 5 days).

Digital Light Processing Vat Photopolymerisation 3D Printing. Tensile bars (ASTM D638 type V, 63.5 x 9.5 x 3.2 mm), discs (10 mm diameter, 2 mm height), DMA rectangular bars (2 × 3 × 15 mm), and porous gyroid scaffolds were printed from resin with an EnvisionTech D4K Pro 3D printer (λ = 385 nm). Layer cure time = 35 s for **P1X1** and 37.5 s for **P1X2** and **P1X3**. Layer thinness = 100 µm. Separation velocity = 200 µm. Structures were

washed post-printing with ethyl acetate, isopropyl alcohol and subsequently submerged in deionised water for post-curing in a B9 Model Cure UV oven (B9Creations, 70 W, 55 Hz, λ = 390–420 nm) for 15 minutes. Samples were dried under vacuum at 60 °C for 6 days using a Thermo Scientific Lindberg/Blue M Vacuum Oven.

Water Contact Angle Measurements. A Ramé-Hart instrument co. contact angle goniometer was used with DROPimage Pro software to calculate and image the contact angles of 5 μL of water on the polymer films. DROPimage Pro fits the shape of the droplet on the polymer film and measures the tangent angle between the solid-liquid interface. Five repeat measurements taken for each material.

Cytotoxicity Testing. Schwann cells were seeded at a density of 12,500 cells cm^{-2} per film sample and placed in the incubator. Controls were done using laminin-coated coverglass. After 24 h, cells were stained using the LIVE/DEAD™ Viability/Cytotoxicity Assay Kit for mammalian cells from Invitrogen (following the manufacturer protocol). Briefly, 5 μL of calcein AM and 20 μL ethidium homodimer-1 (EthD-1) were added to 10 mL Dulbecco's phosphate buffer solution (DPBS). The cells were then submerged in staining solution and incubated for 30 mins. Live (green) and dead (red) cells were observed and imaged using a Keyence BZ-X710 microscope**.**

Micro Computed Tomography (CT). The small **P1X1** gyroids (5.9 mm tall) were scanned using a micro x-ray computed tomography scanner (Micro-CT) to visualise the 3D-printed scaffolds versus the original design. Micro-CT scans were carried out on a Nikon XTH 225 ST instrument. Voxel size was 11.8 μm. The source to object distance was 43.9 mm. The source to detector distance was 744 mm. X-ray projections (n = 2629 projections) were taken in a 360° scan with an angular step between projections of 0.137 degrees. The x-ray energy was 120 kilovolts (kV). The x-ray flux was 97 microamps (μA). Scans were reconstructed in Avizo software.

Inductively Coupled Plasma Mass Spectrometry (ICP-MS). Residual cobalt content from catalyst: 1.36 μg/g. Measurements were conducted using the PerkinElmer NexION 350D ICP-MS with ESI PrepFAST M5 auto diluter. Calibration was achieved using a custom-bought multi element standard (VWR) and accuracy confirmed from the measurement of NRC Canada SLRS-6 and a custom-bought QC standard (QMx Laboratories). Cobalt was measured using helium collision cell (kinetic energy discrimination) to minimise interferences from polyatomic moleculars. Rhodium was added to all blanks, standards, QC's and samples as an internal standard, to manage any plasma suppression/ instrument drift.

Statistical Analysis. Statistical analysis was performed using GraphPad Prism 6.0 (GraphPad Software). Data from tensile testing, swelling experiments, and water contact angle measurements were analysed via one-way ANOVA with Tukey's multiple comparisons test. Statistical significance was defined as follows: *$p<0.05$, **$p<0.01$, ***$p<0.001$, ****$p<0.0001$.

6.4 References

(1) Kember, M. R.; Knight, P. D.; Reung, P. T. R.; Williams, C. K. Highly Active Dizinc Catalyst for the Copolymerization of Carbon Dioxide and Cyclohexene Oxide at One Atmosphere Pressure. *Angew Chem Int Edit* **2009**, *48* (5), 931-933. DOI: 10.1002/anie.200803896.
(2) Sulley, G. S.; Gregory, G. L.; Chen, T. T. D.; Peña Carrodeguas, L.; Trott, G.; Santmarti, A.; Lee, K. Y.; Terrill, N. J.; Williams, C. K. Switchable Catalysis Improves the Properties of CO2-Derived Polymers: Poly(cyclohexene carbonate- b-ϵ-decalactone- b-cyclohexene carbonate) Adhesives, Elastomers, and Toughened Plastics. *J. Am. Chem. Soc.* **2020**, *142* (9), 4367-4378. DOI: 10.1021/jacs.9b13106.
(3) Deacy, A. C.; Kilpatrick, A. F. R.; Regoutz, A.; Williams, C. K. Understanding metal synergy in heterodinuclear catalysts for the copolymerization of CO and epoxides. *Nat. Chem.* **2020**, *12* (4), 372-380. DOI: 10.1038/s41557-020-0450-3.
(4) Spyros, A.; Argyropoulos, D. S.; Marchessault, R. H. A study of poly(hydroxyalkanoate)s by quantitative P-31 NMR spectroscopy: Molecular weight and chain cleavage. *Macromolecules* **1997**, *30* (2), 327-329. DOI: DOI 10.1021/ma9601979.
(5) McGuire, T. M.; Deacy, A. C.; Buchard, A.; Williams, C. K. Solid-State Chemical Recycling of Polycarbonates to Epoxides and Carbon Dioxide Using a Heterodinuclear Mg(II)Co(II) Catalyst. *J. Am. Chem. Soc.* **2022**, *144* (40), 18444-18449. DOI: 10.1021/jacs.2c06937.

CHAPTER 7

Appendices & Supporting Information

7.1. Chapter 2

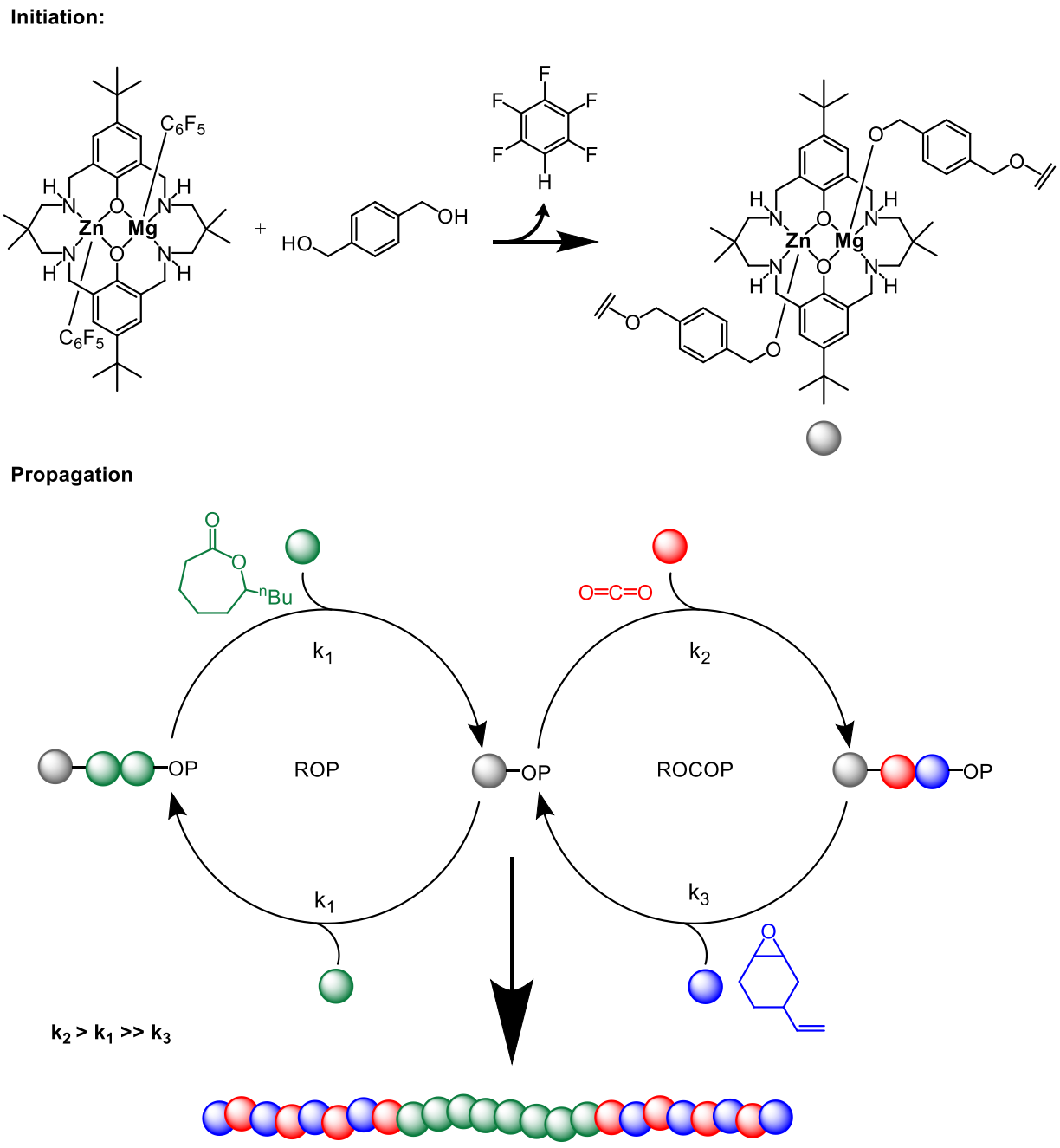

Scheme S7.2.1: Schematic representation of the switch catalysis strategy employed to produce the PvCHC-PDL-PvCHC triblock copolymers.

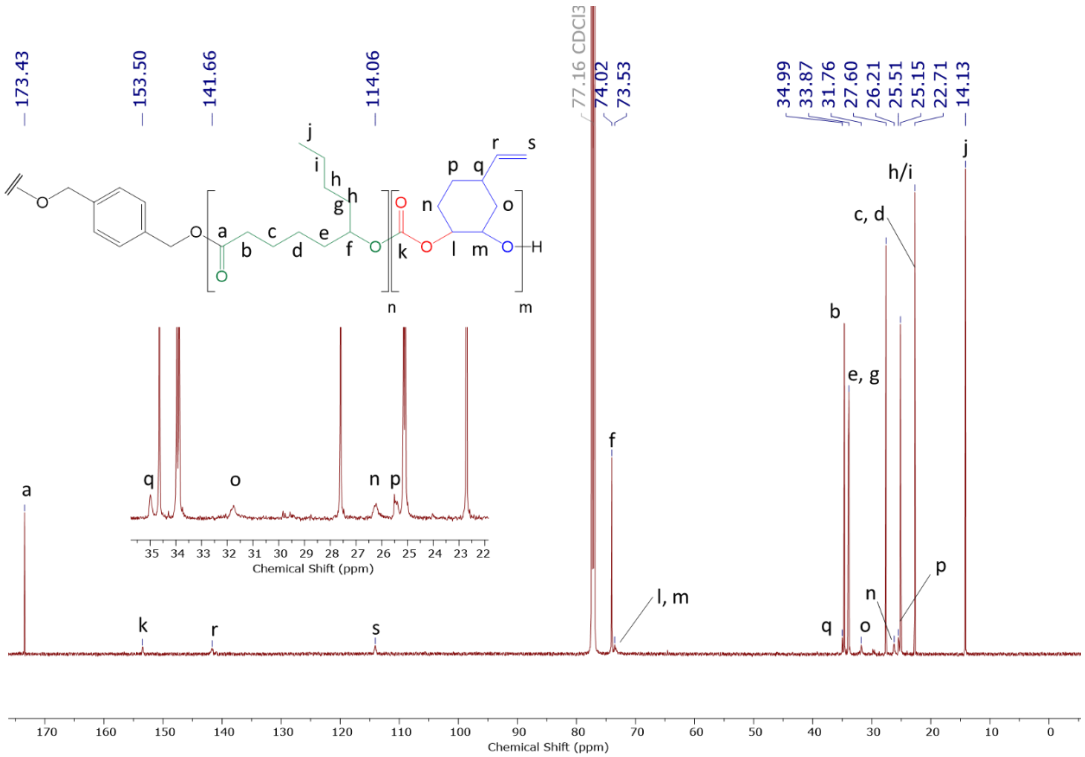

Figure S7.2.2: ^{13}C NMR (100.58 MHz, $CDCl_3$) spectrum of **1**-vinyl poly(vinylcyclohexene carbonate-*b*-ε-decalactone-*b*-vinylcyclohexene carbonate) triblock copolymer.

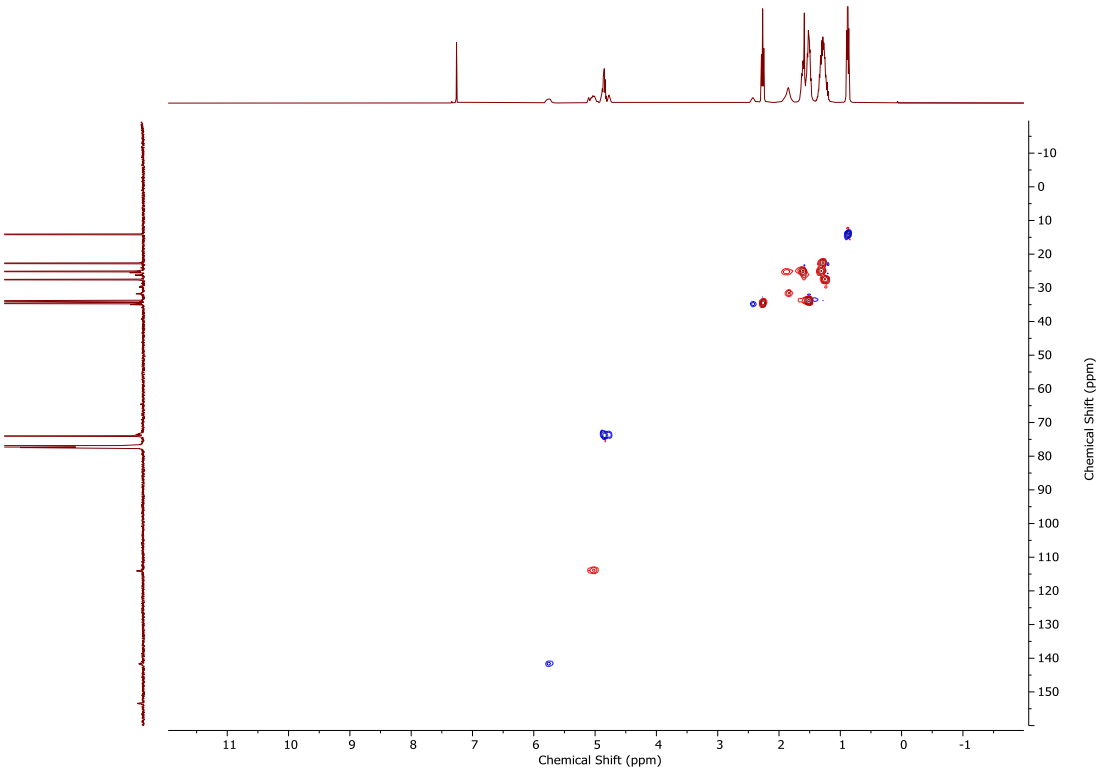

Figure S7.2.3: ^{1}H - ^{13}C HSQC NMR (400 MHz, $CDCl_3$) spectrum of **1**-vinyl poly(vinylcyclohexene carbonate-*b*-ε-decalactone-*b*-vinylcyclohexene carbonate) triblock copolymer.

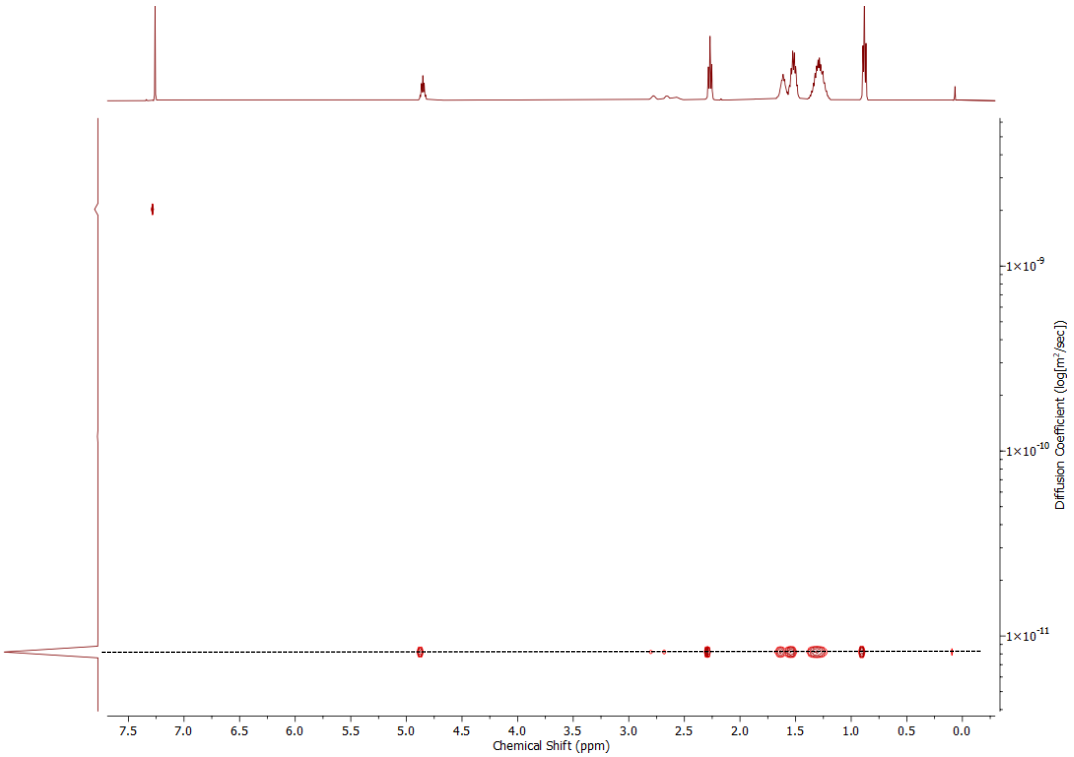

Figure S7.2.4: ^{1}H DOSY NMR (500 MHz, $CDCl_3$) spectrum of functionalized P_{COOH}CHC-PDL- P_{COOH}CHC (**2**-COOH).

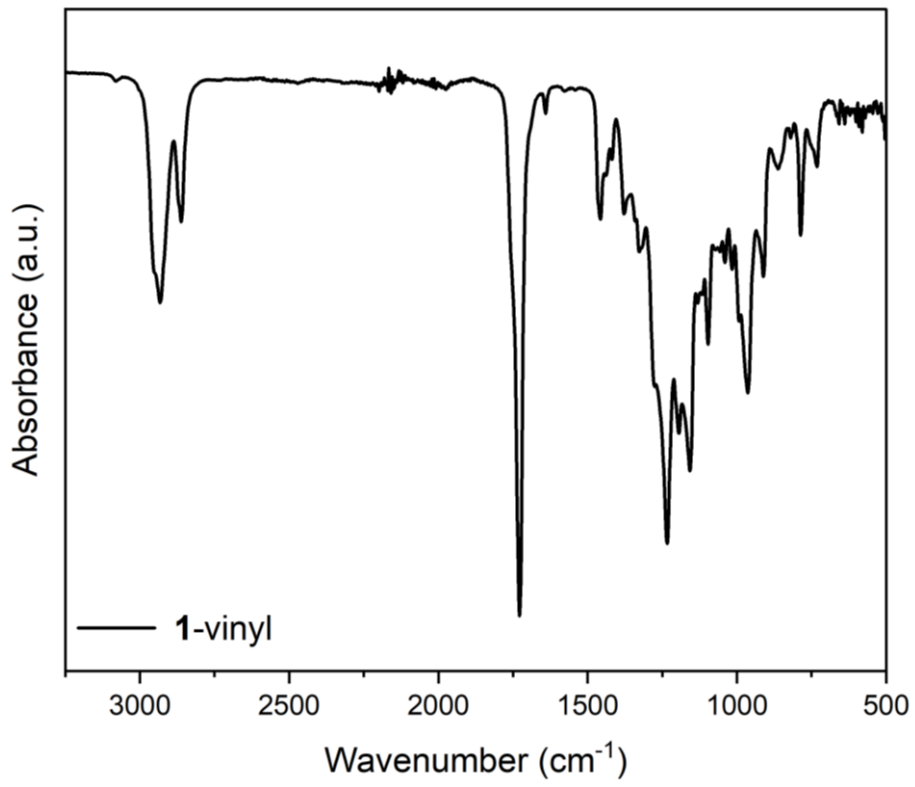

Figure S7.2.5: FTIR spectrum of **1**-vinyl polymer film.

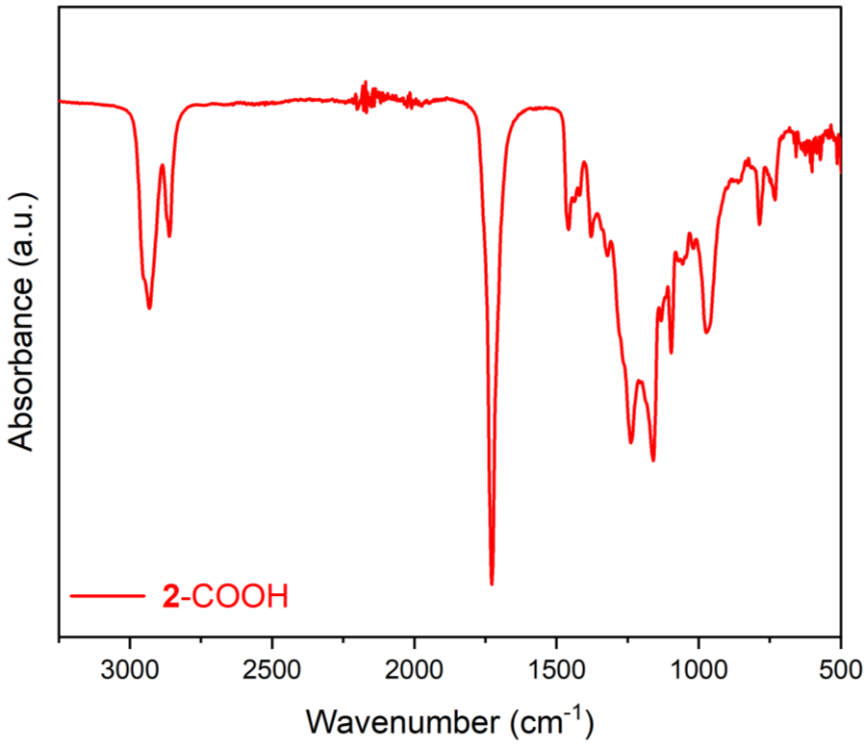

Figure S7.2.6: FTIR spectrum of **2**-COOH polymer film.

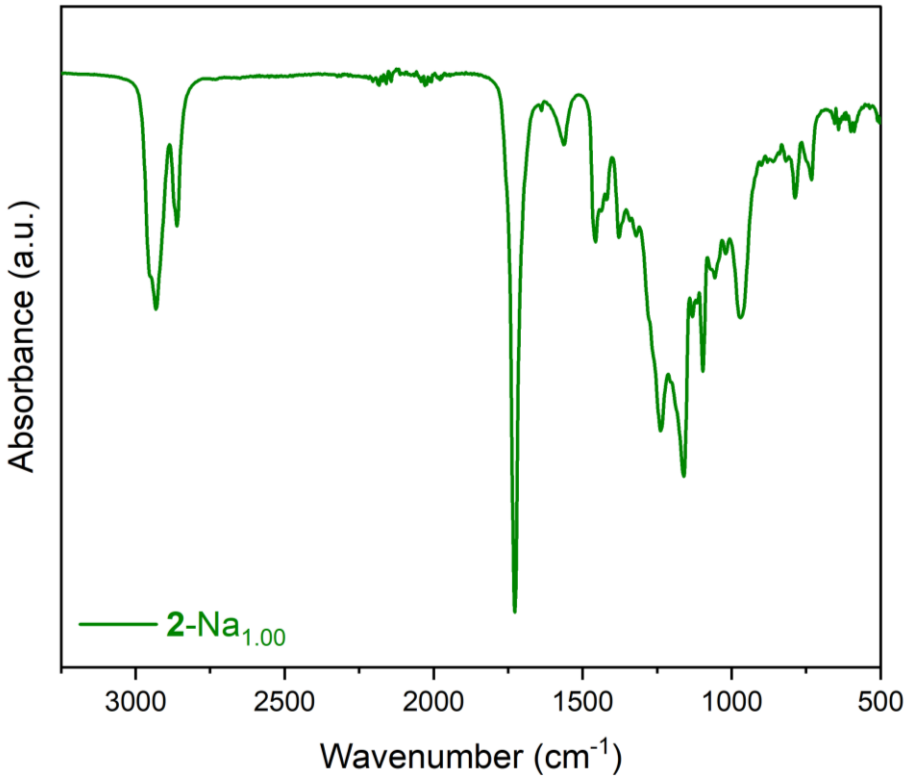

Figure S7.2.7: FTIR spectrum of **2**-$Na_{1.00}$ polymer film.

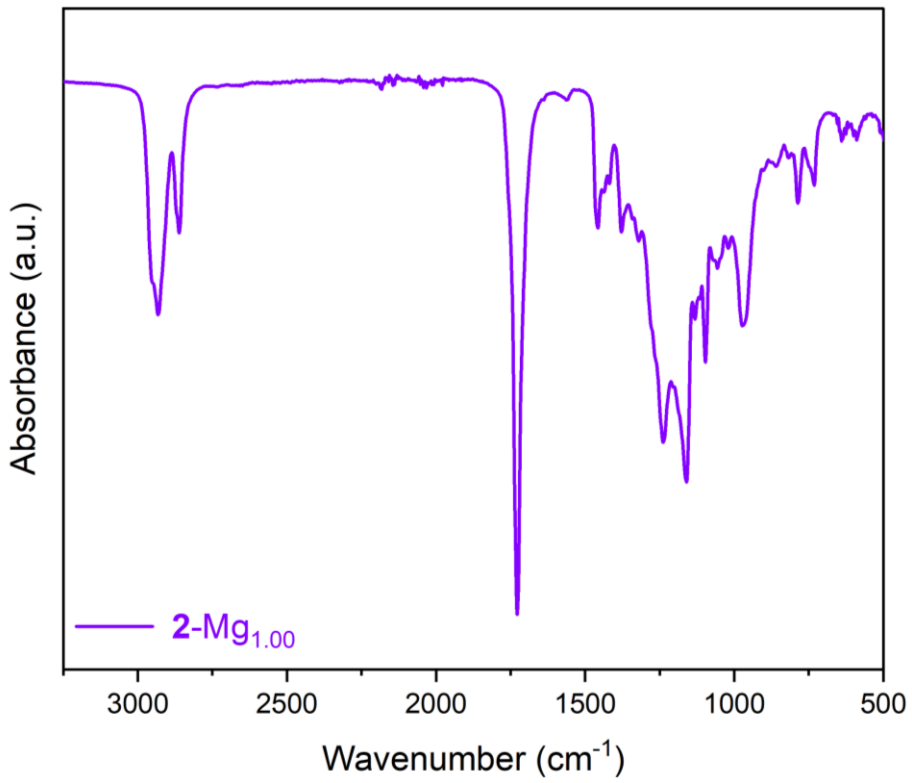

Figure S7.2.8: FTIR spectrum of **2**-$Mg_{1.00}$ polymer film.

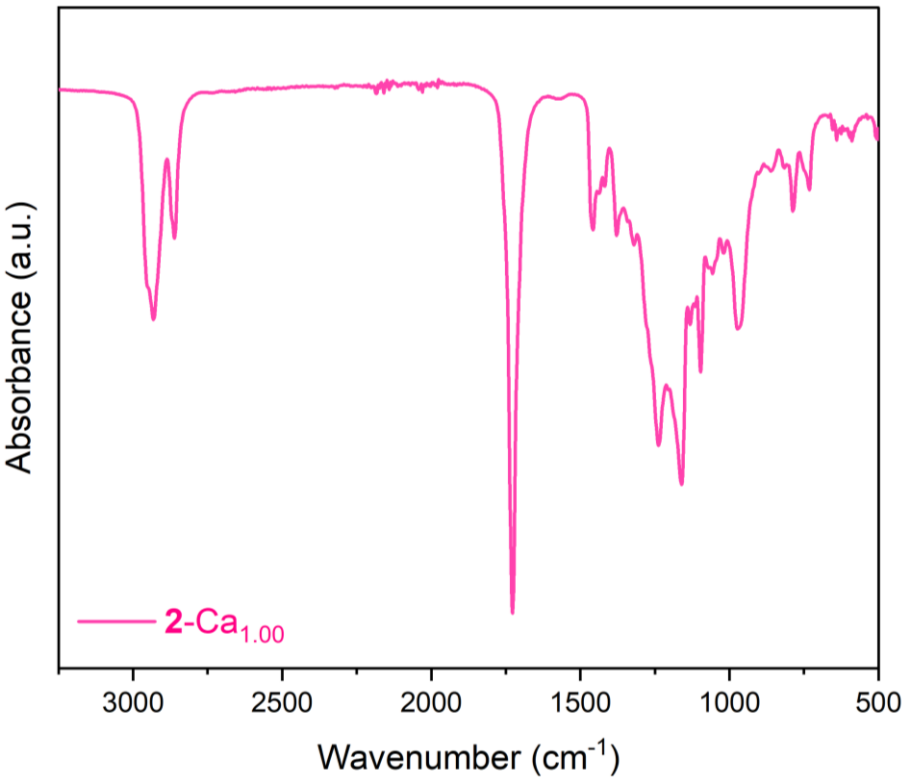

Figure S7.2.9: FTIR spectrum of **2**-$Ca_{1.00}$ polymer film.

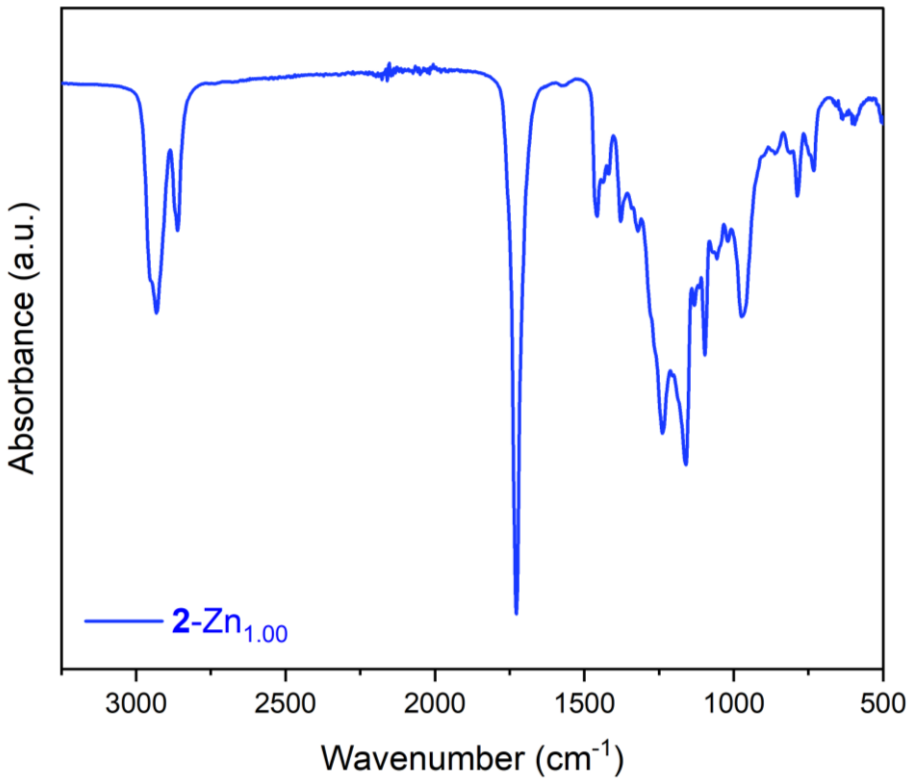

Figure S7.2.10: FTIR spectrum of **2**-$Zn_{1.00}$ polymer film.

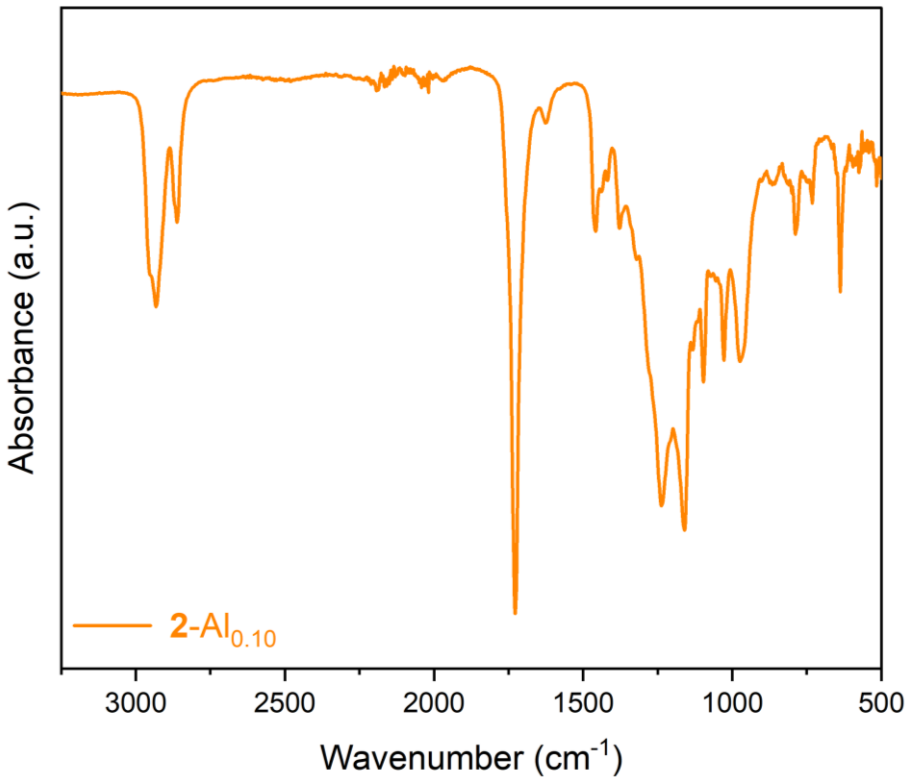

Figure S7.2.11: FTIR spectrum of **2**-$Al_{0.10}$ polymer film.

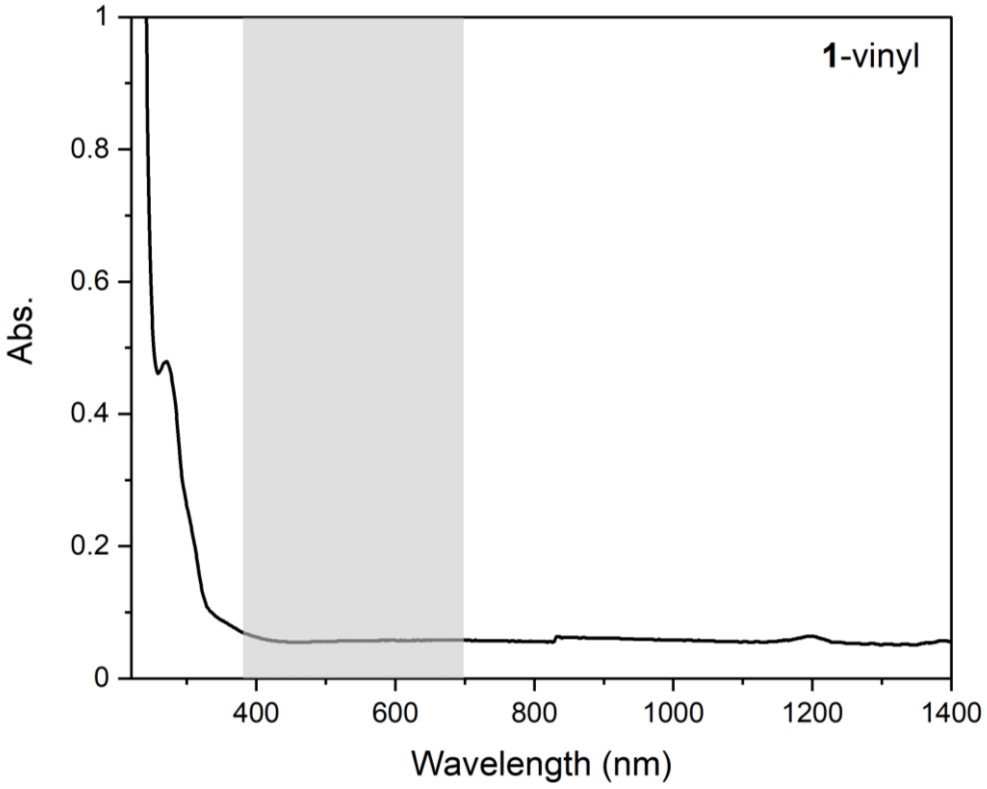

Figure S7.2.12: UV-vis spectrum of **1**-vinyl polymer film. Visible region highlighted in grey.

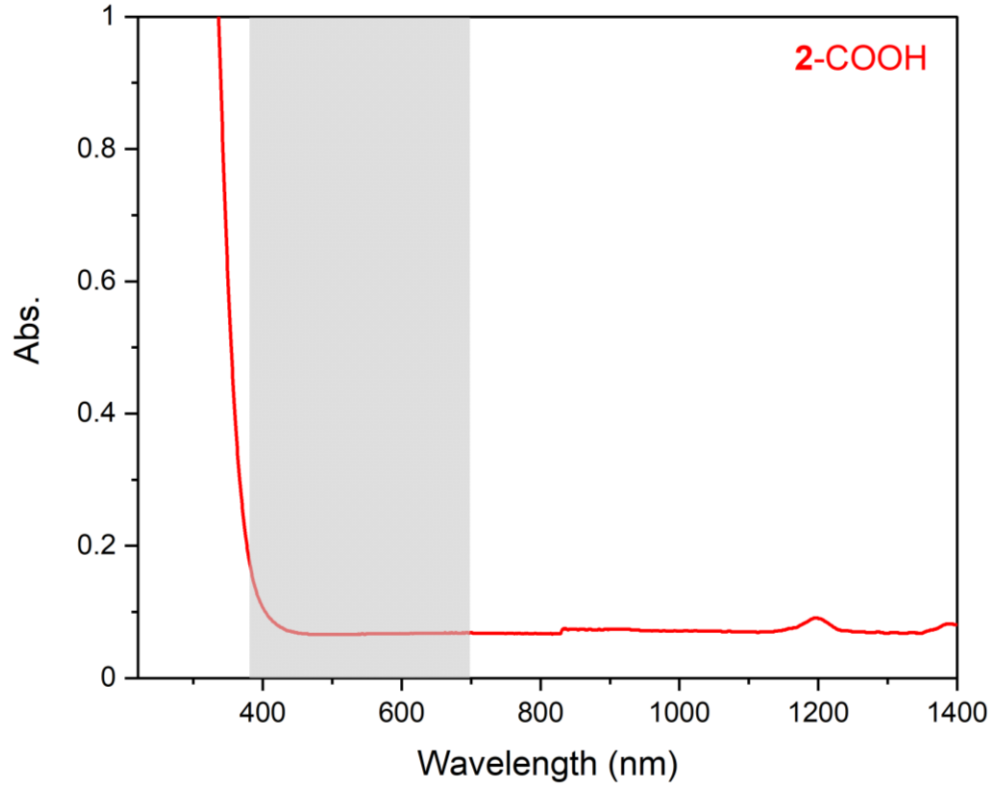

Figure S7.2.13: UV-vis spectrum of **2**-COOH polymer film. Visible region highlighted in grey.

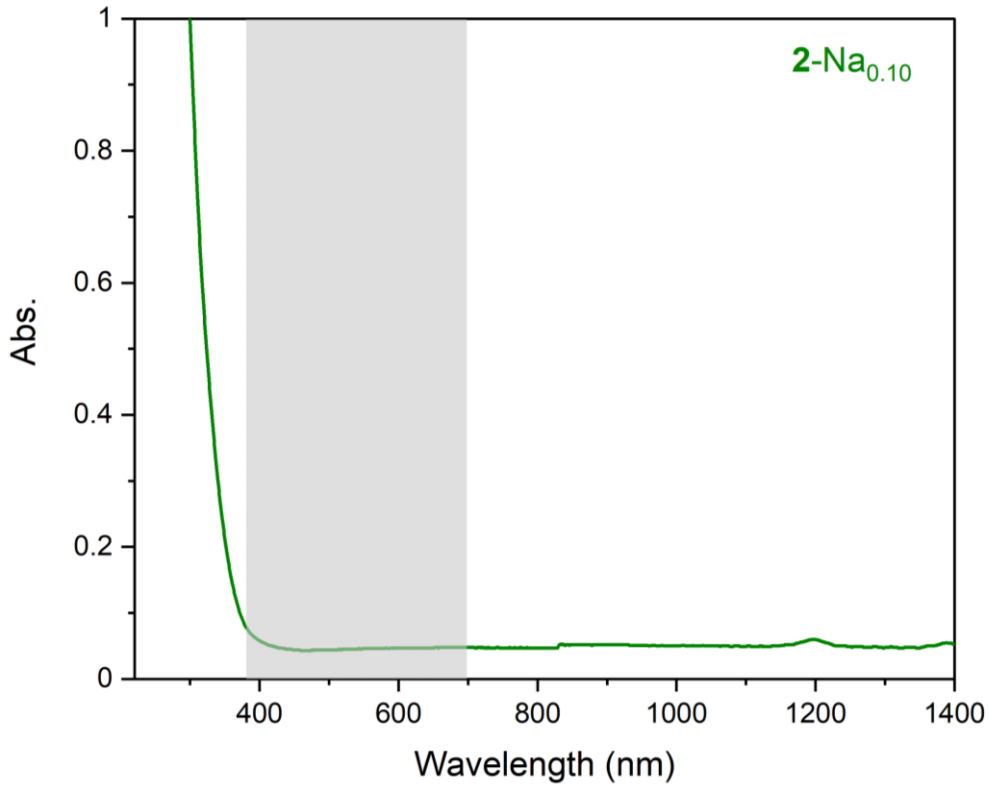

Figure S7.2.14: UV-vis spectrum of **2**-$Na_{0.10}$ polymer film. Visible region highlighted in grey.

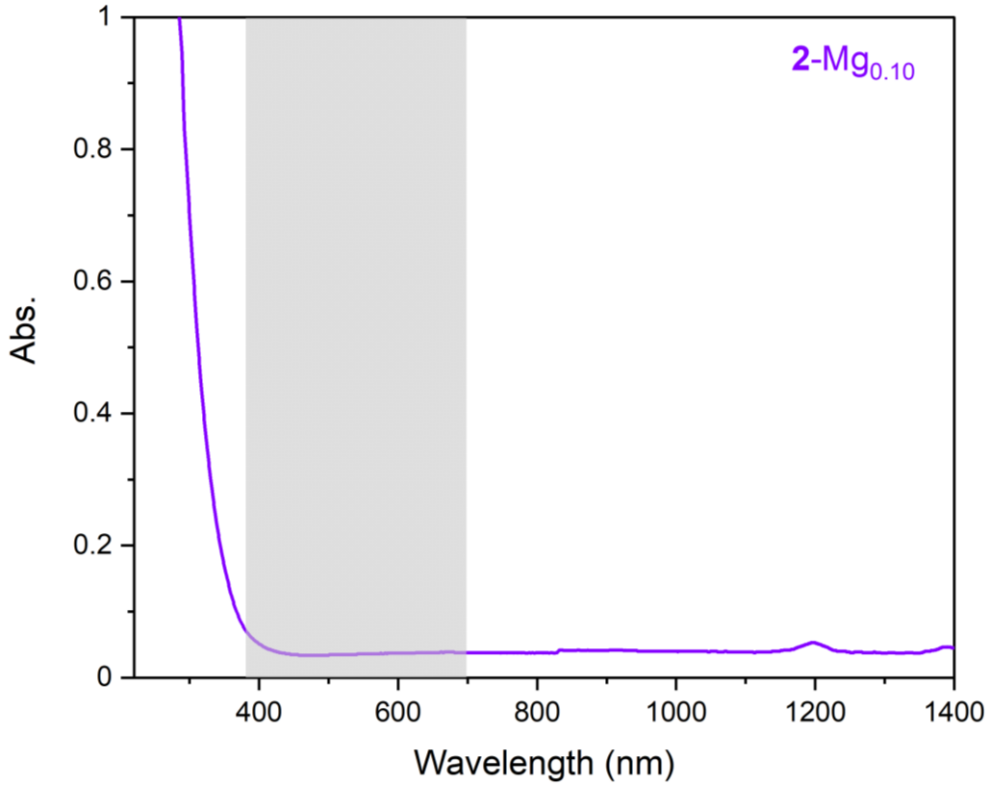

Figure S7.2.15: UV-vis spectrum of **2**-$Mg_{0.10}$ polymer film. Visible region highlighted in grey.

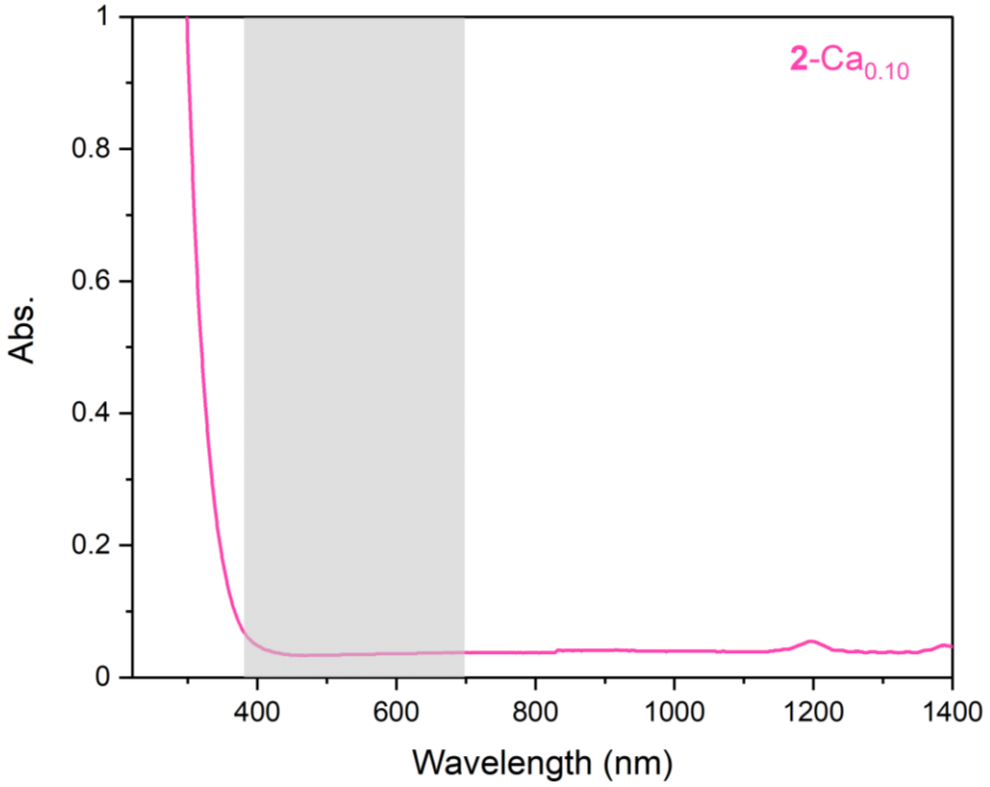

Figure S7.2.16: UV-vis spectrum of **2**-$Ca_{0.10}$ polymer film. Visible region highlighted in grey.

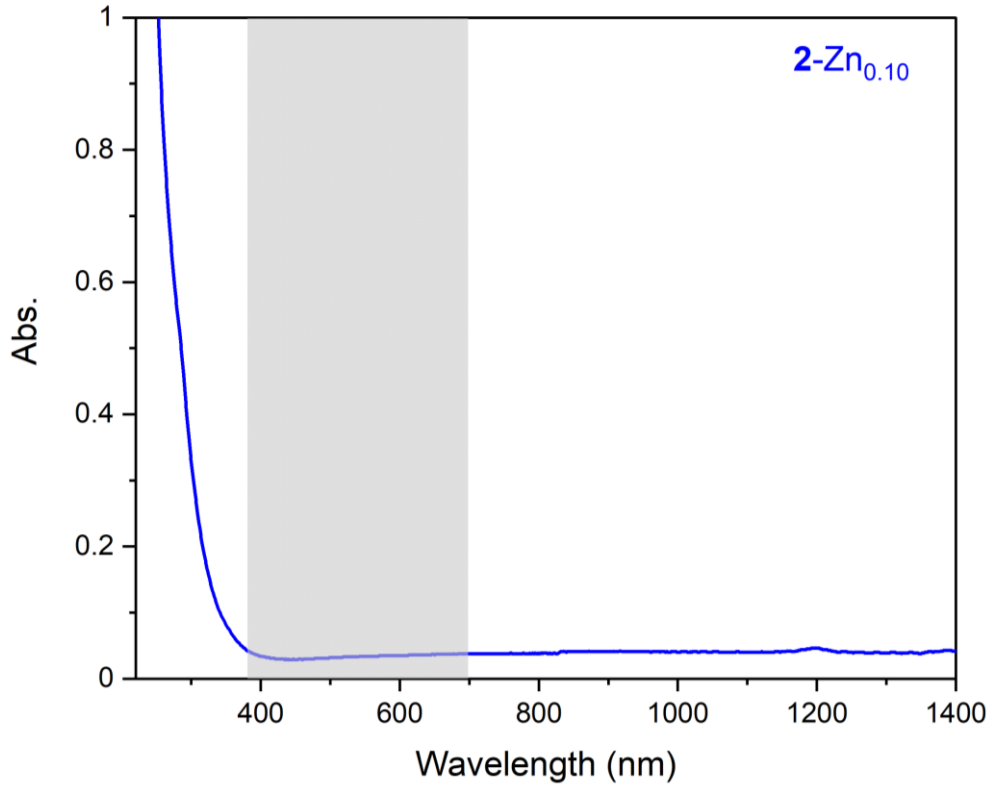

Figure S7.2.17: UV-vis spectrum of **2**-$Zn_{0.10}$ polymer film. Visible region highlighted in grey.

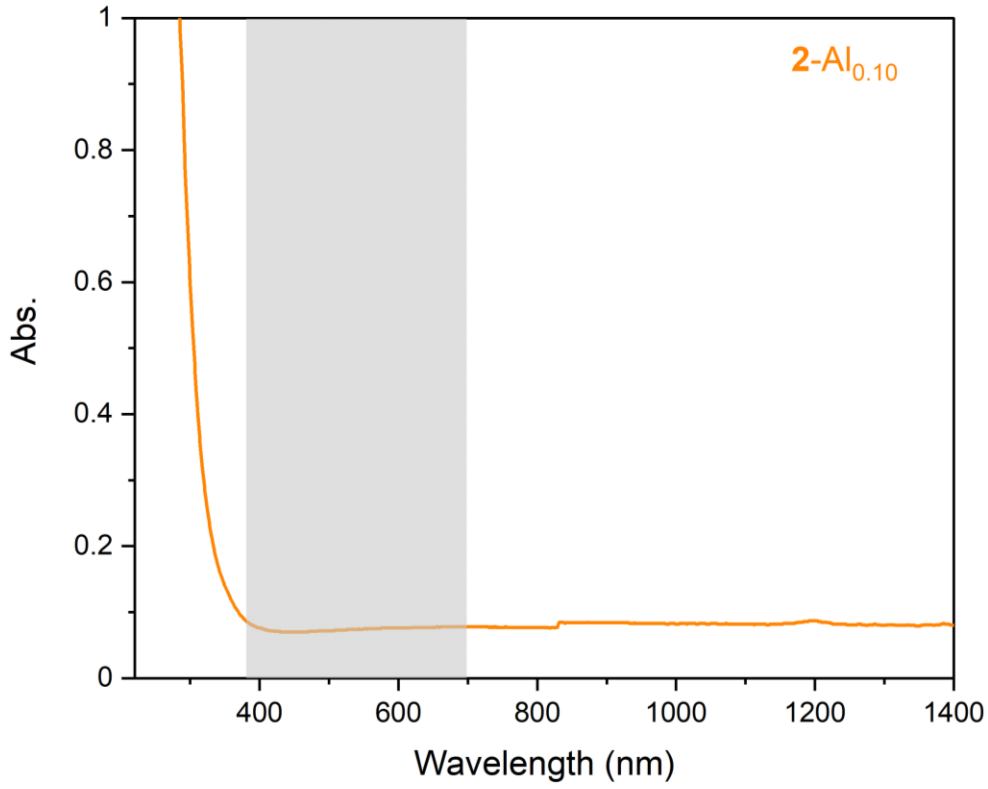

Figure S7.2.18: UV-vis spectrum of **2**-$Al_{0.10}$ polymer film. Visible region highlighted in grey.

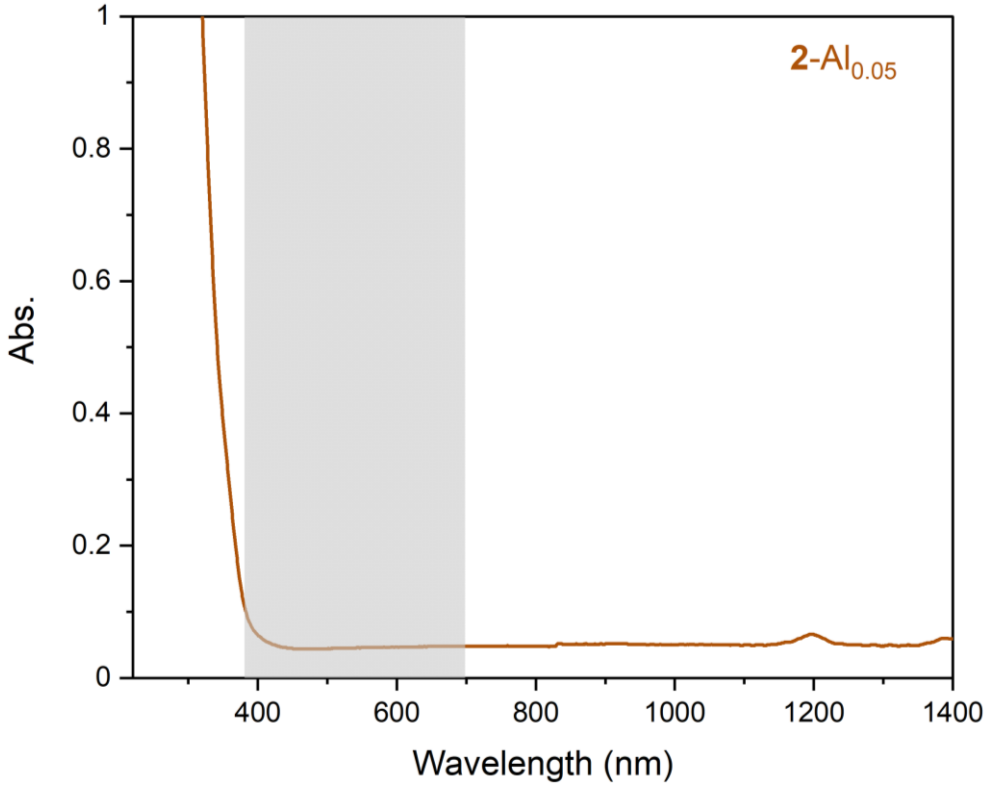

Figure S7.2.19: UV-vis spectrum of **2**-$Al_{0.05}$ polymer film. Visible region highlighted in grey.

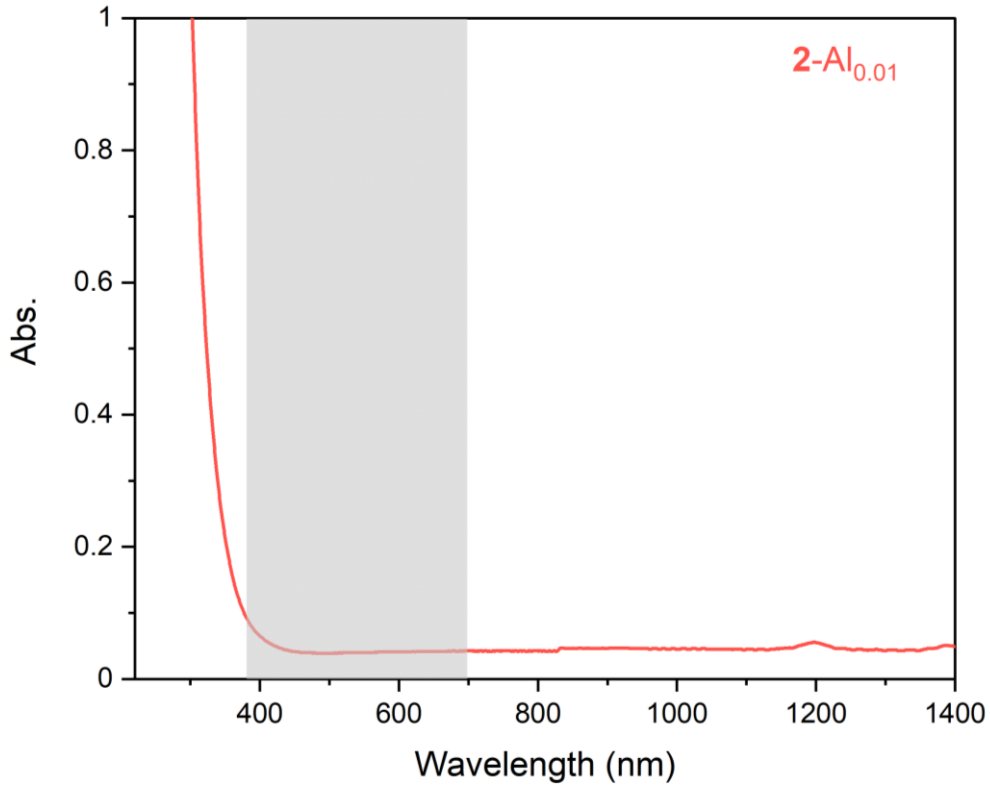

Figure S7.2.20: UV-vis spectrum of **2**-$Al_{0.01}$ polymer film. Visible region highlighted in grey.

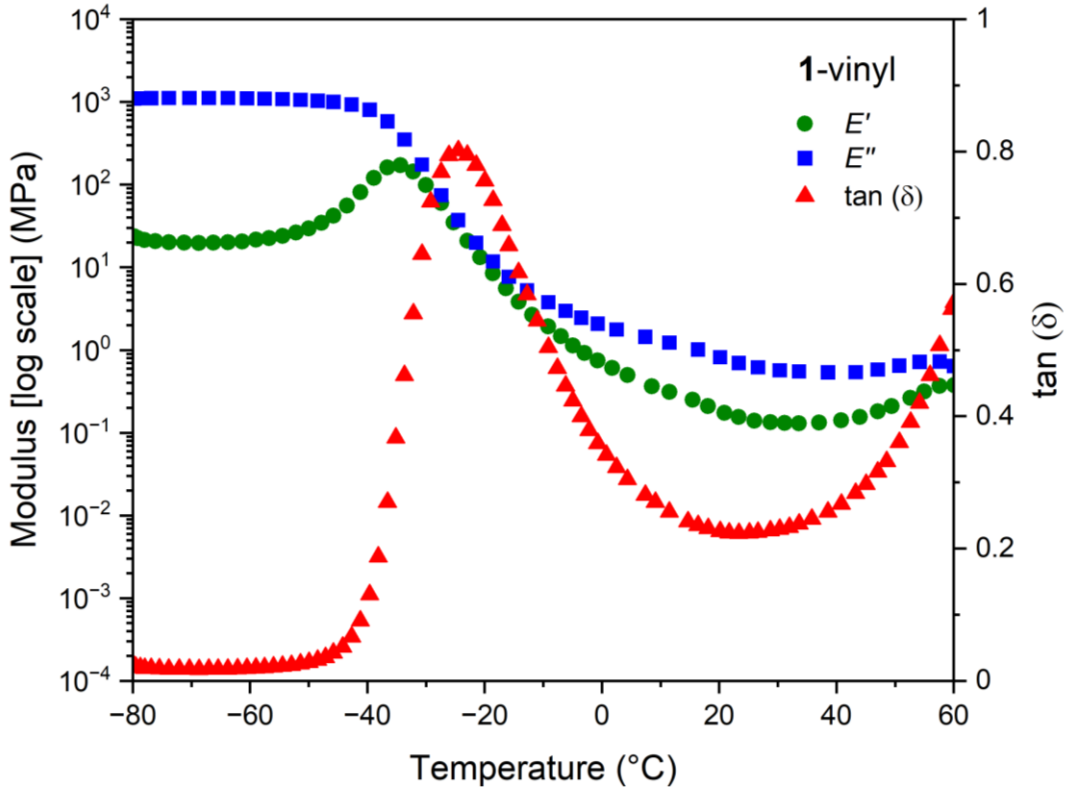

Figure S7.2.21 Dynamic mechanical temperature analysis (DMTA) temperature sweeps for **1**-vinyl.

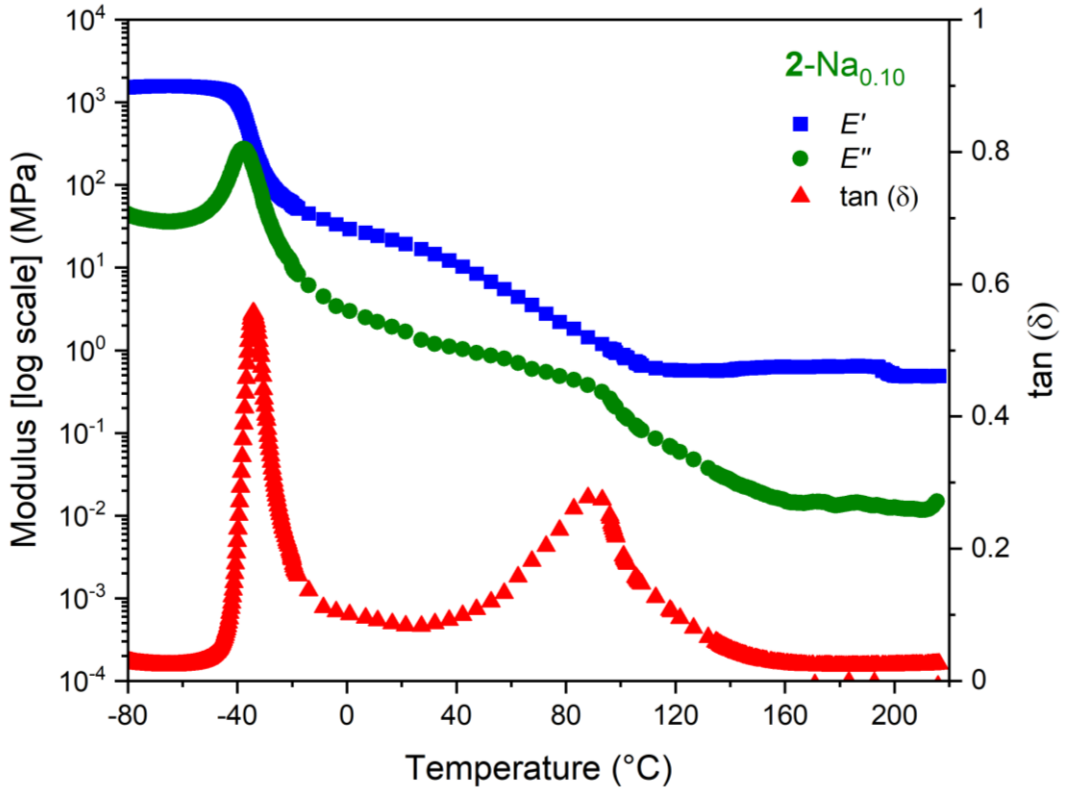

Figure S7.2.22: Dynamic mechanical temperature analysis (DMTA) temperature sweeps for **2**-$Na_{0.10}$.

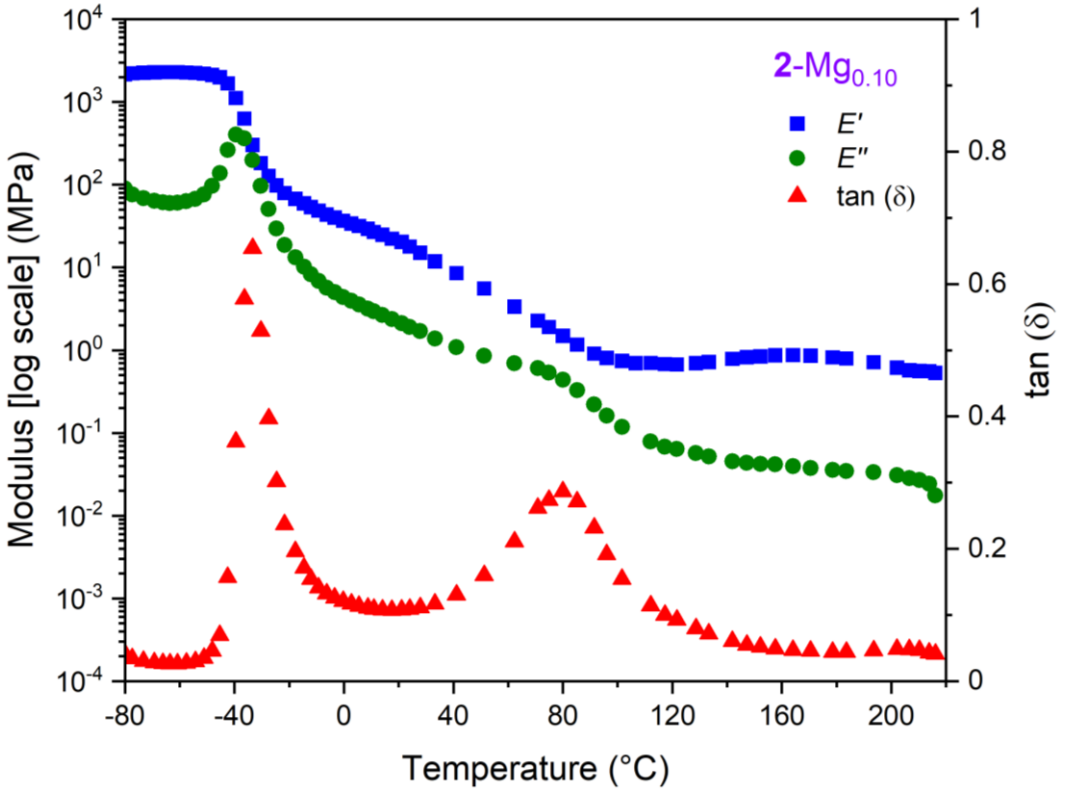

Figure S7.2.23: Dynamic mechanical temperature analysis (DMTA) temperature sweeps for **2**-$Mg_{0.10}$.

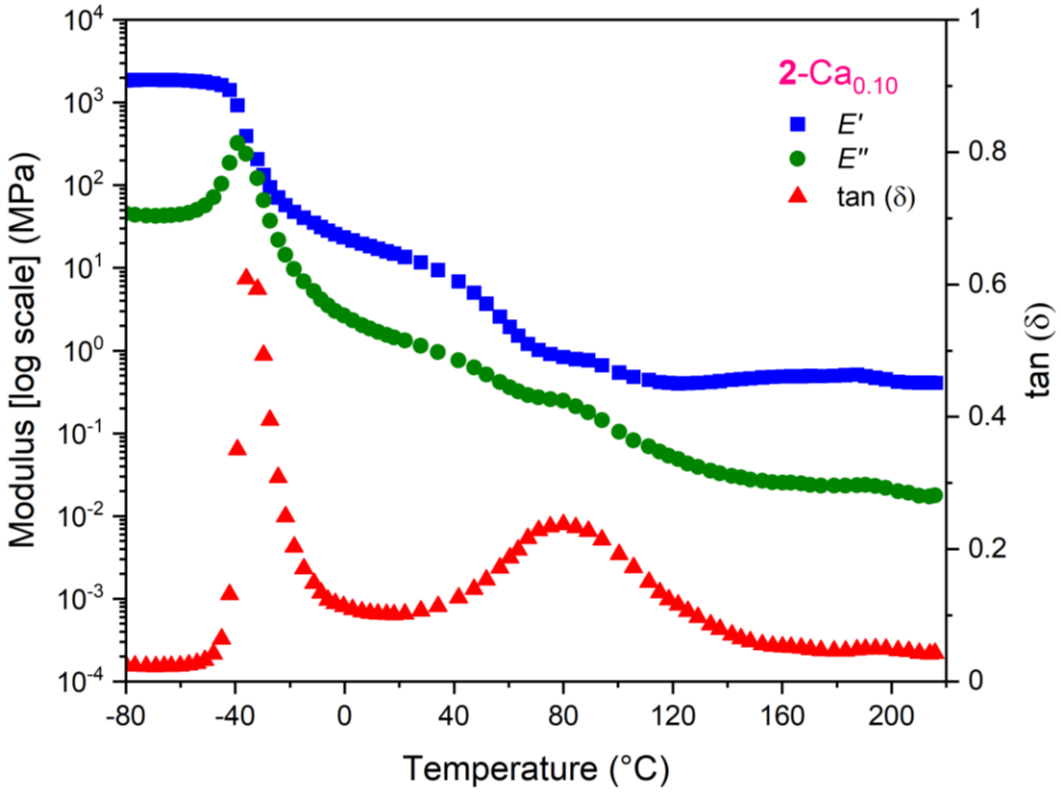

Figure S7.2.24: Dynamic mechanical temperature analysis (DMTA) temperature sweeps for **2**-$Ca_{0.10}$.

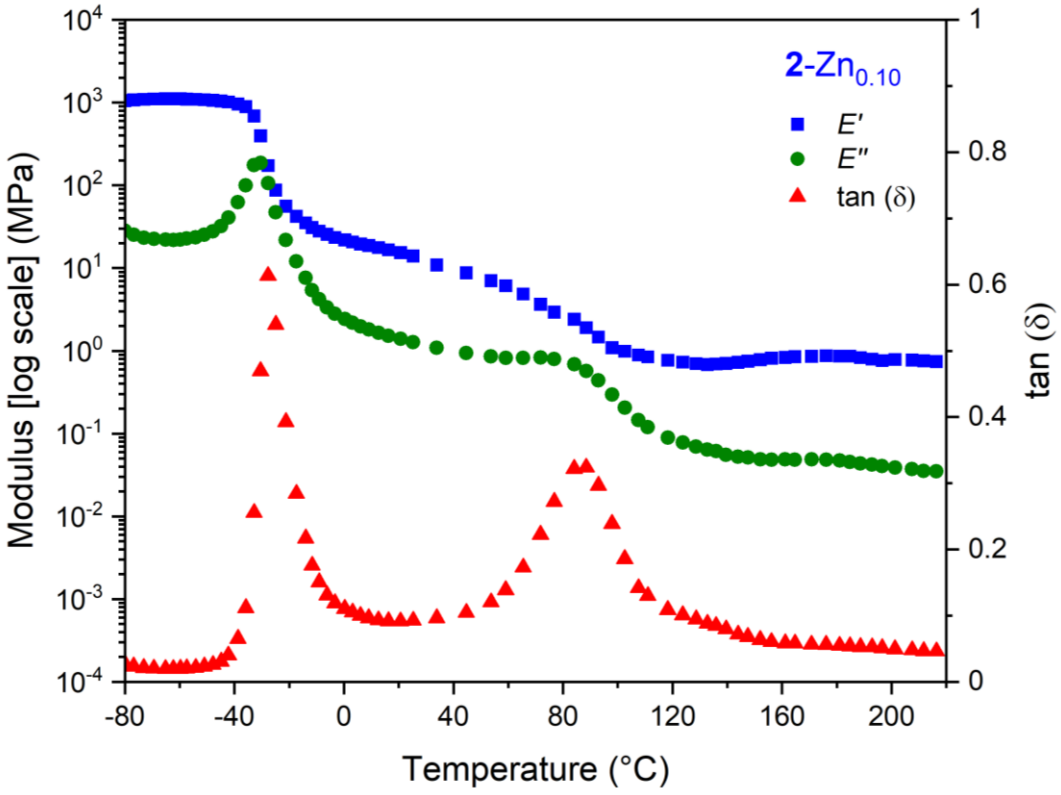

Figure S7.2.25: Dynamic mechanical temperature analysis (DMTA) temperature sweeps for **2**-$Zn_{0.10}$.

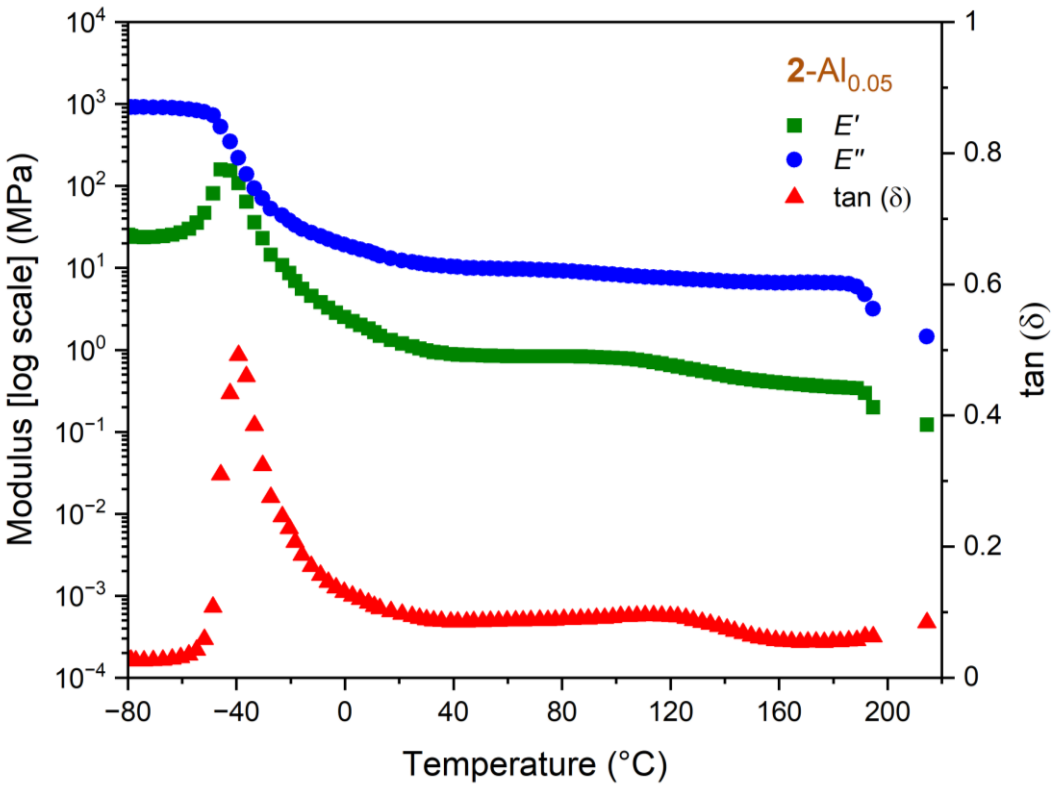

Figure S7.2.26: Dynamic mechanical temperature analysis (DMTA) temperature sweeps for **2**-$Al_{0.05}$.

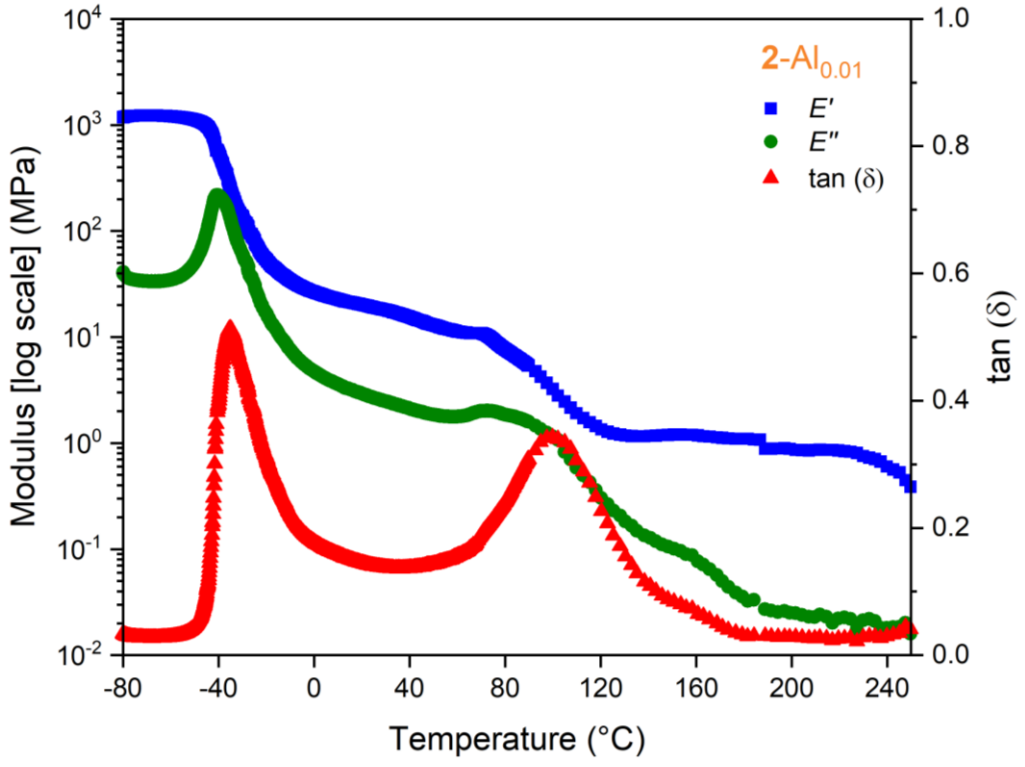

Figure S7.2.27: Dynamic mechanical temperature analysis (DMTA) temperature sweeps for **2**-$Al_{0.05}$.

Table S7.2.1. Lower T_g of polymer films from peak in tan (δ) in DMTA profile.

Material	$T_{g,DMTA}$ / ˚C
1-vinyl	-25
2-COOH	-35
2-$Na_{0.10}$	-34
2-$Mg_{0.10}$	-33
2-$Ca_{0.10}$	-36
2-$Zn_{0.10}$	-28
2-$Al_{0.10}$	-38
2-$Al_{0.05}$	-39
2-$Al_{0.01}$	-35

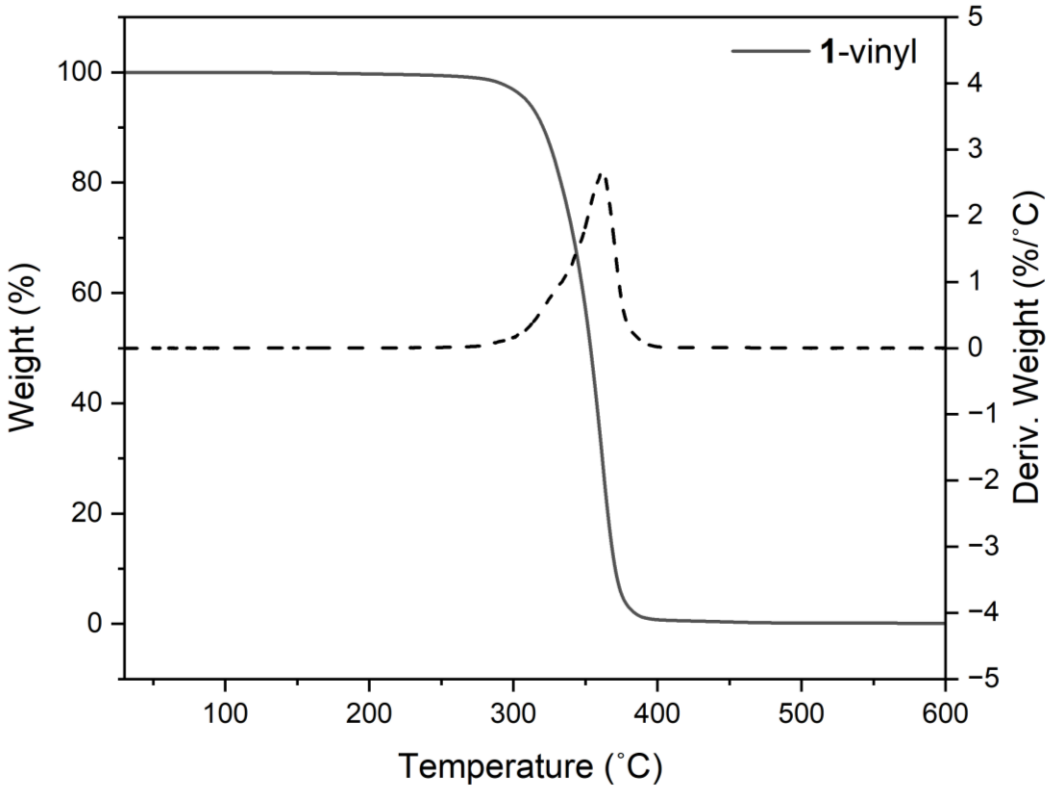

Figure S7.2.28: Thermogravimetric Analysis (TGA) data for **1**-vinyl.

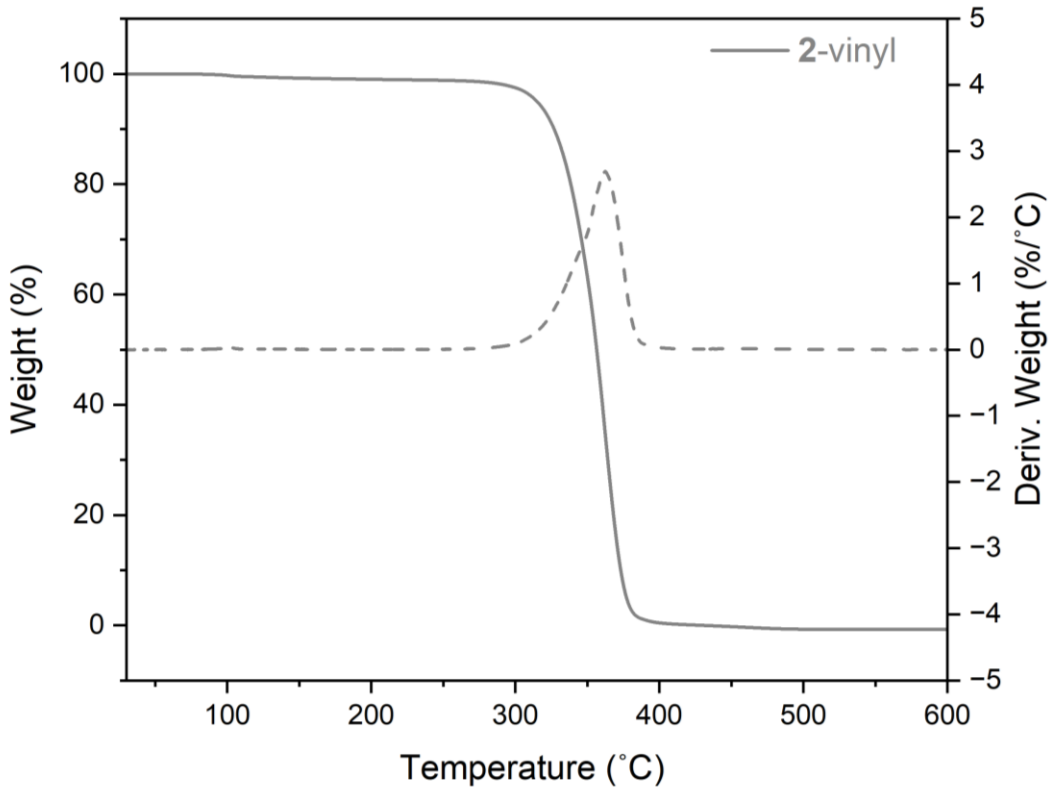

Figure S7.2.29: Thermogravimetric Analysis (TGA) data for **2**-vinyl.

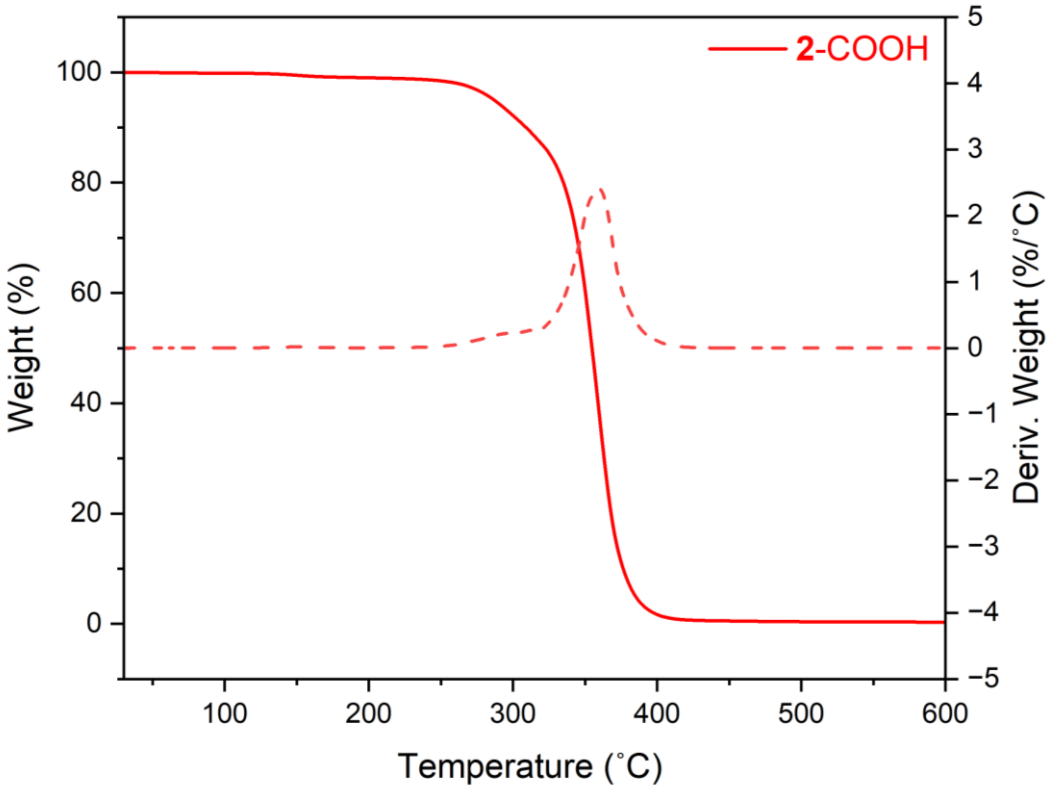

Figure S7.2.30: Thermogravimetric Analysis (TGA) data for **2**-COOH.

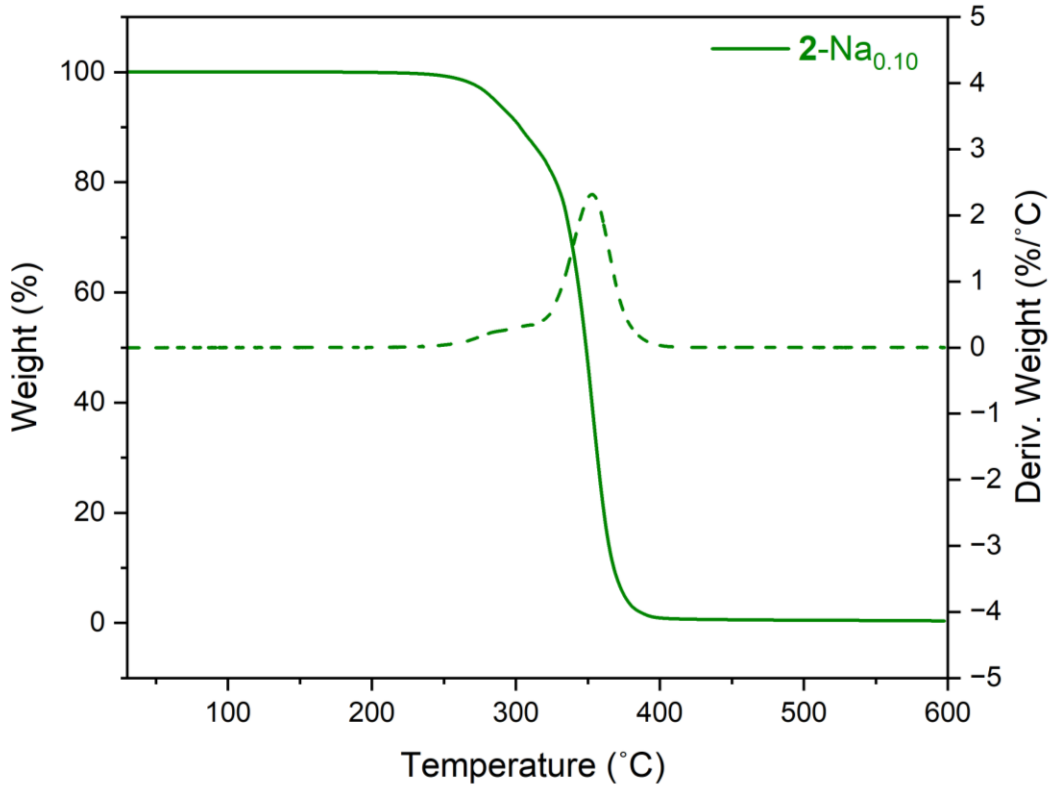

Figure S7.2.31: Thermogravimetric Analysis (TGA) data for **2**-$Na_{0.10}$.

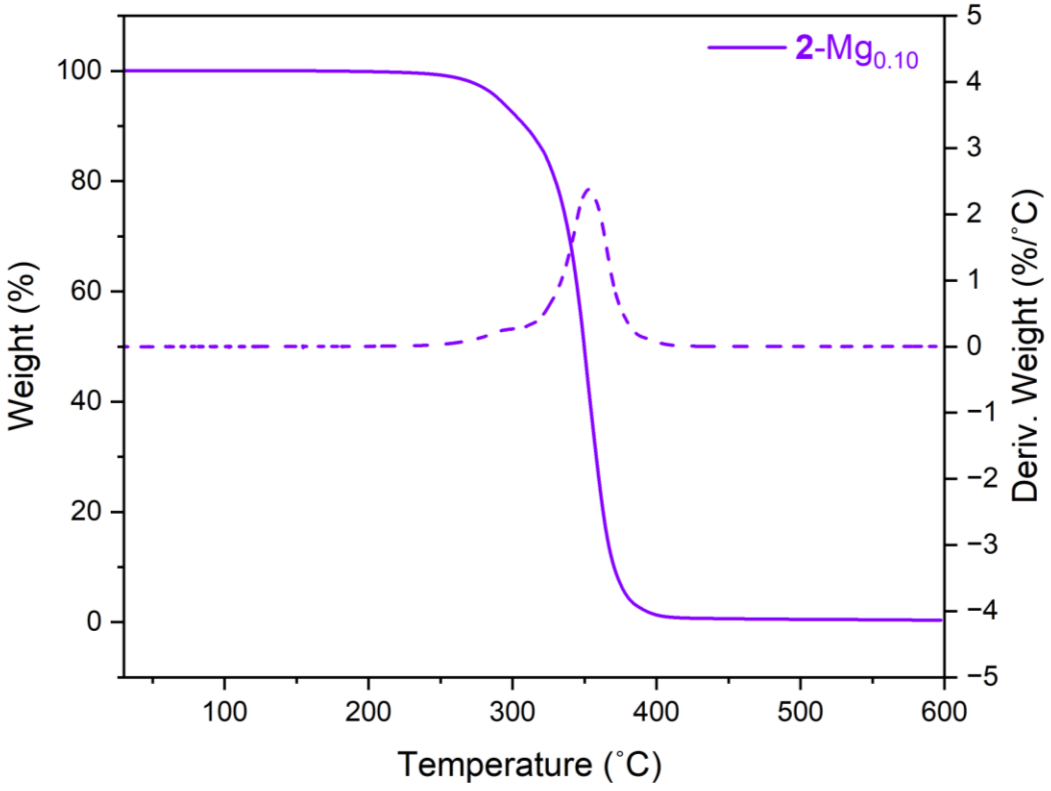

Figure S7.2.32: Thermogravimetric Analysis (TGA) data for **2**-$Mg_{0.10}$.

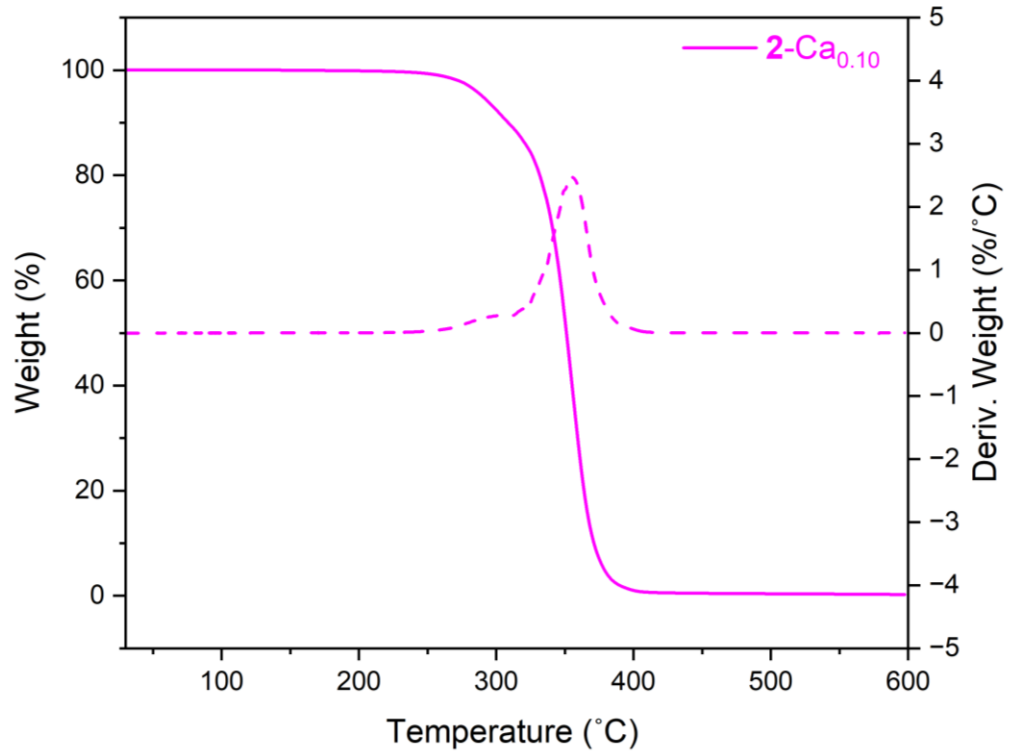

Figure S7.2.33: Thermogravimetric Analysis (TGA) data for **2**-$Ca_{0.10}$.

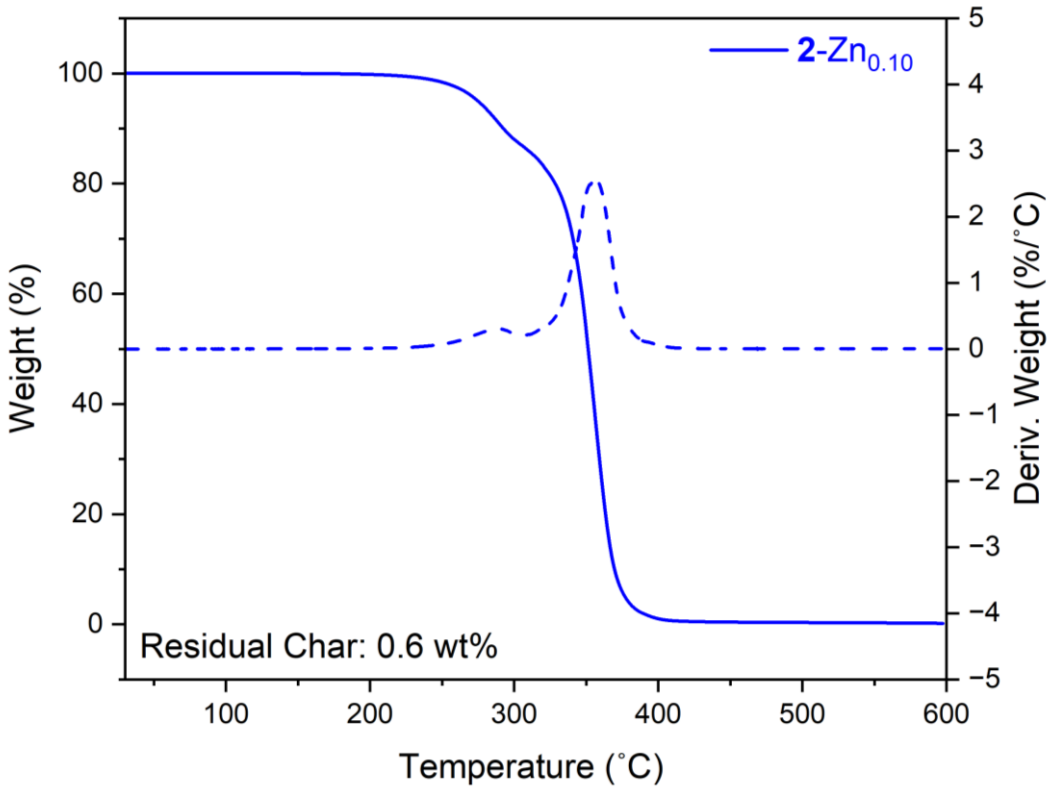

Figure S7.2.34: Thermogravimetric Analysis (TGA) data for **2**-$Zn_{0.10}$.

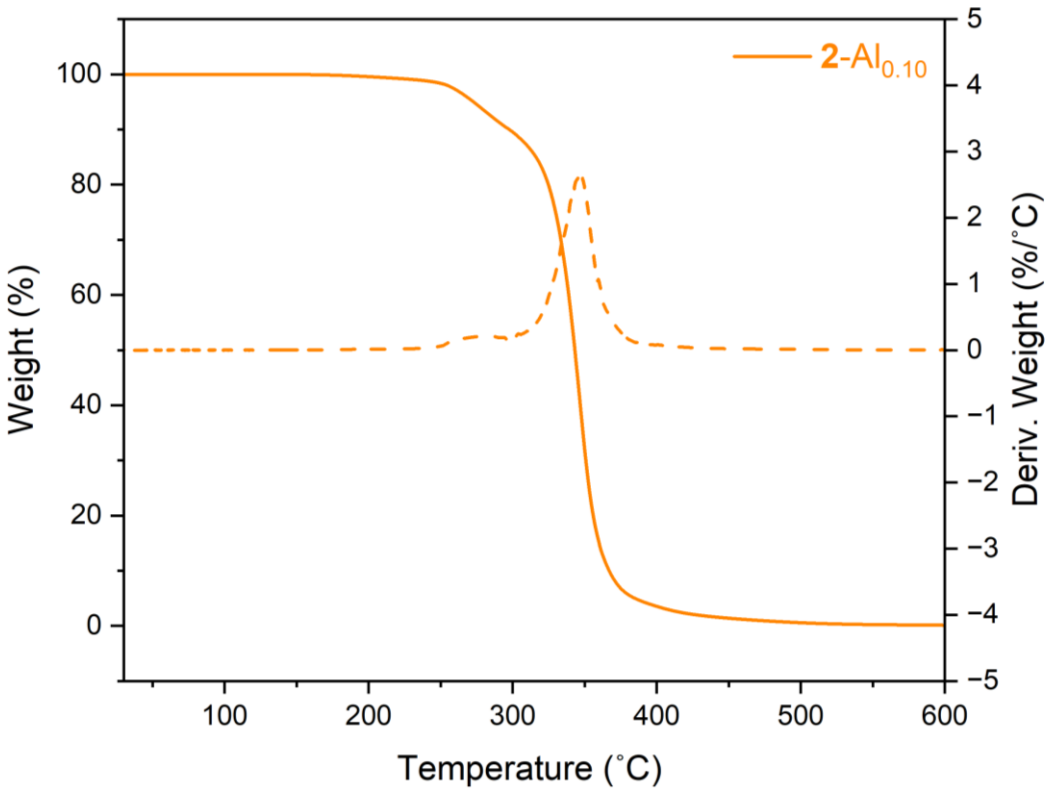

Figure S7.2.35: Thermogravimetric Analysis (TGA) data for **2**-$Al_{0.10}$.

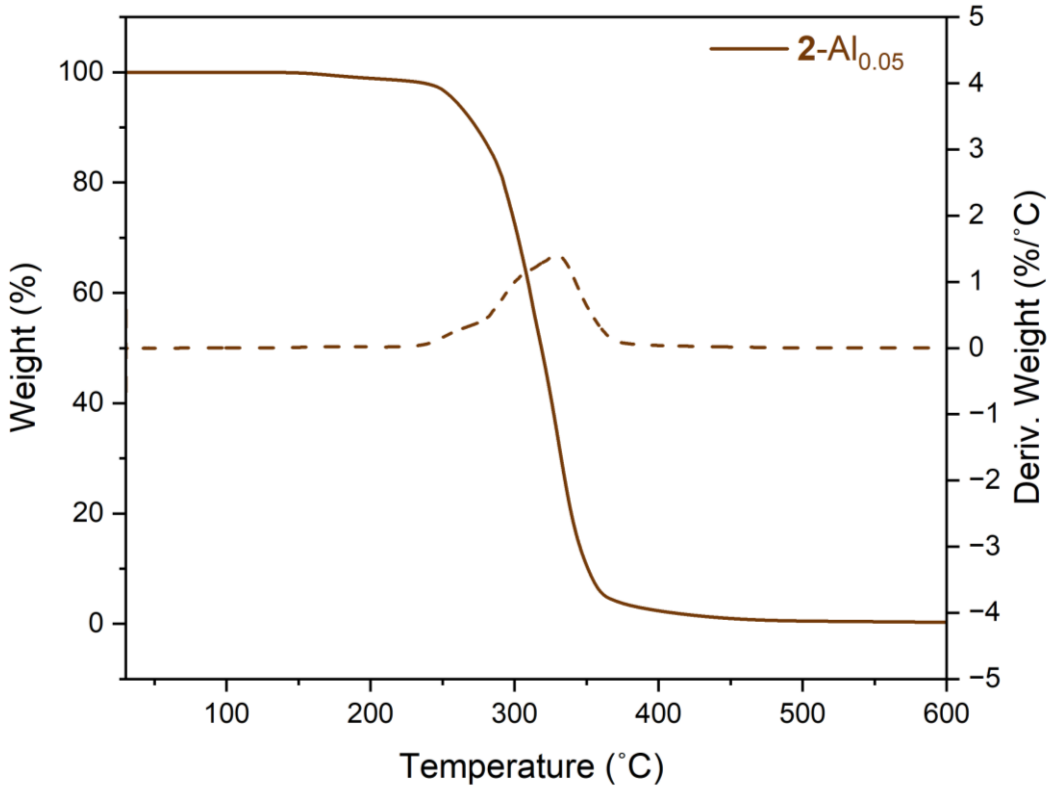

Figure S7.2.36: Thermogravimetric Analysis (TGA) data for **2**-$Al_{0.05}$.

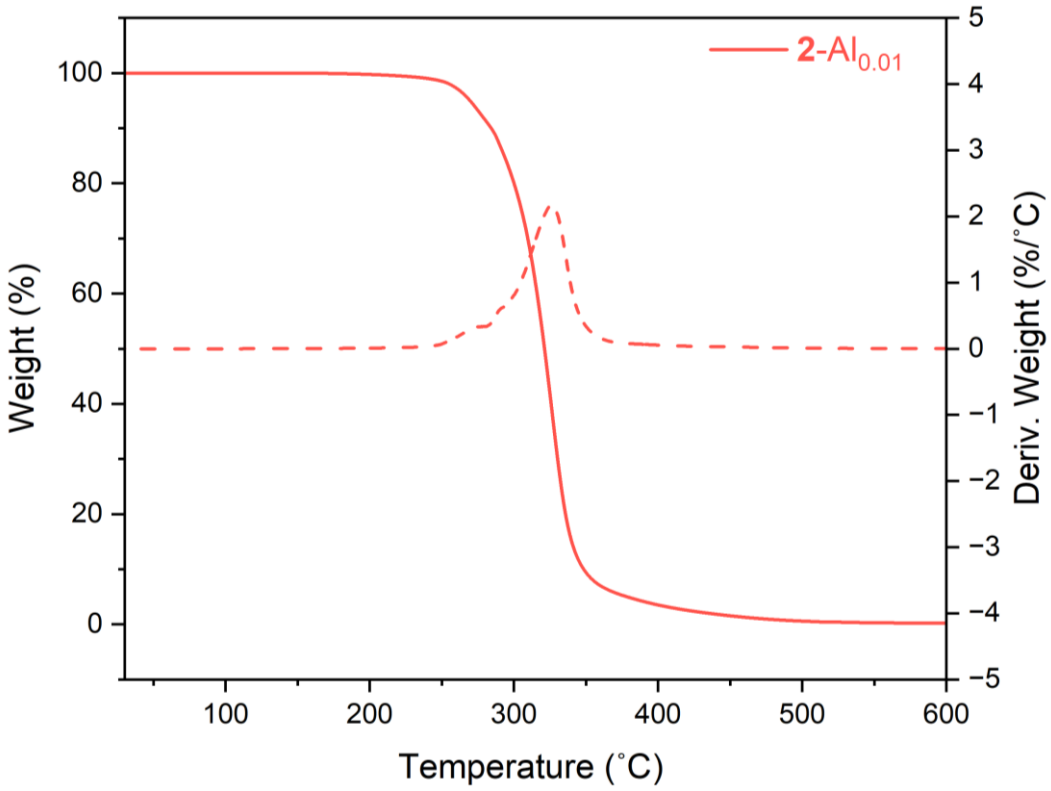

Figure S7.2.37: Thermogravimetric Analysis (TGA) data for **2**-$Al_{0.01}$.

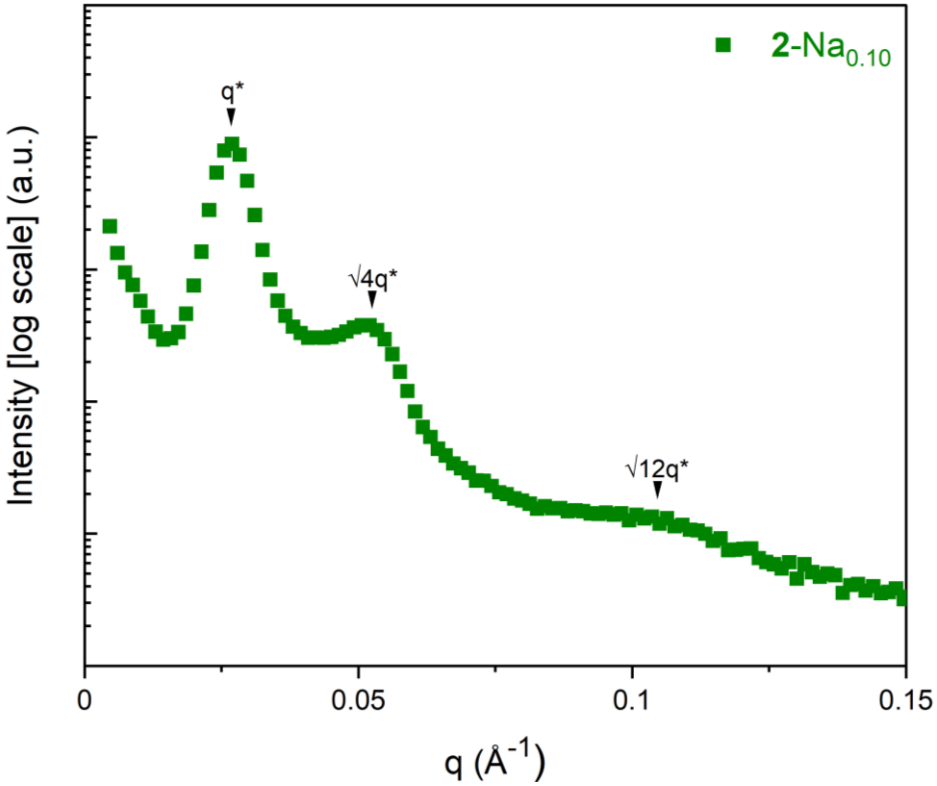

Figure S7.2.38: Room temperature SAXS data for **2**-$Na_{0.10}$.

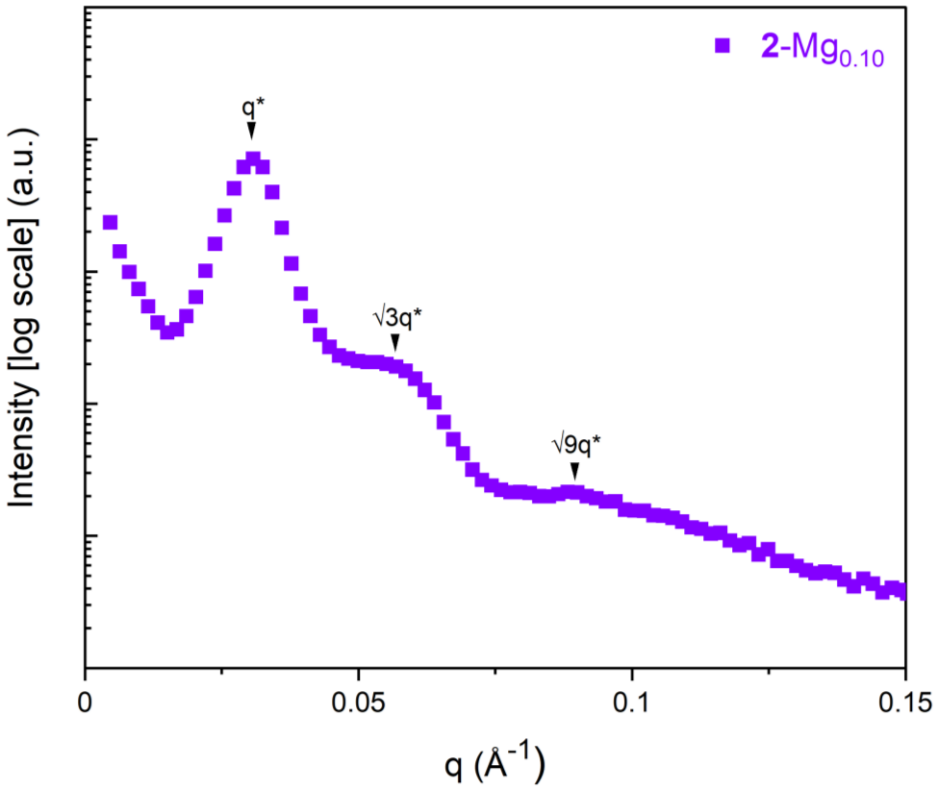

Figure S7.2.39: Room temperature SAXS data for **2**-$Mg_{0.10.}$

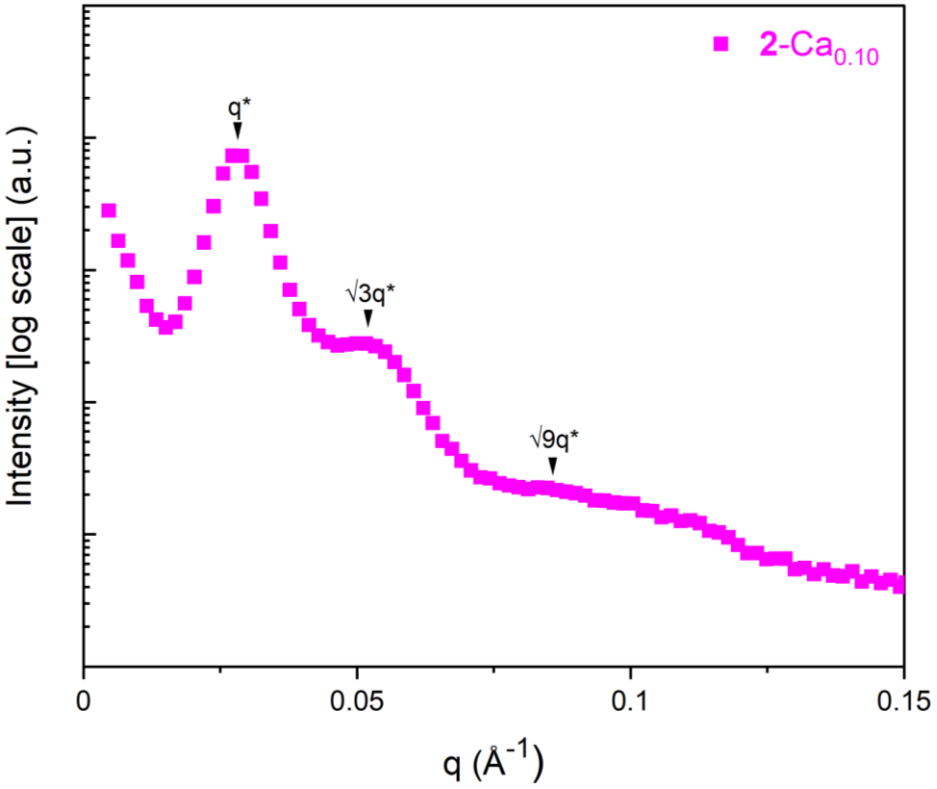

Figure S7.2.40 Room temperature SAXS data for **2**-$Ca_{0.10.}$

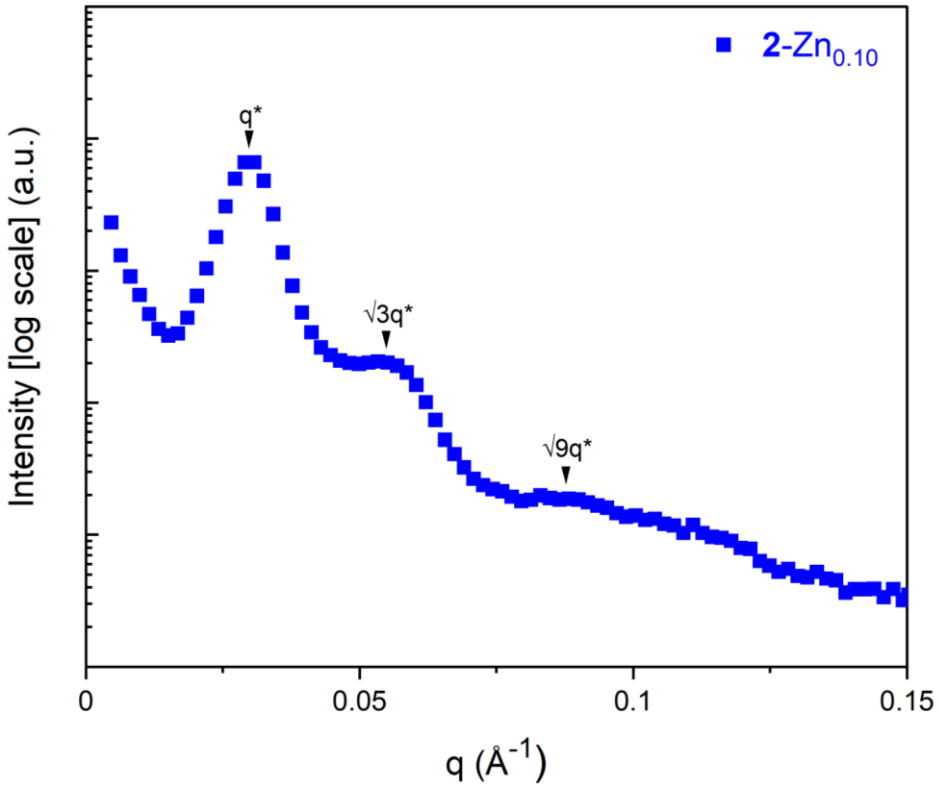

Figure S7.2.41: Room temperature SAXS data for **2**-$Zn_{0.10.}$

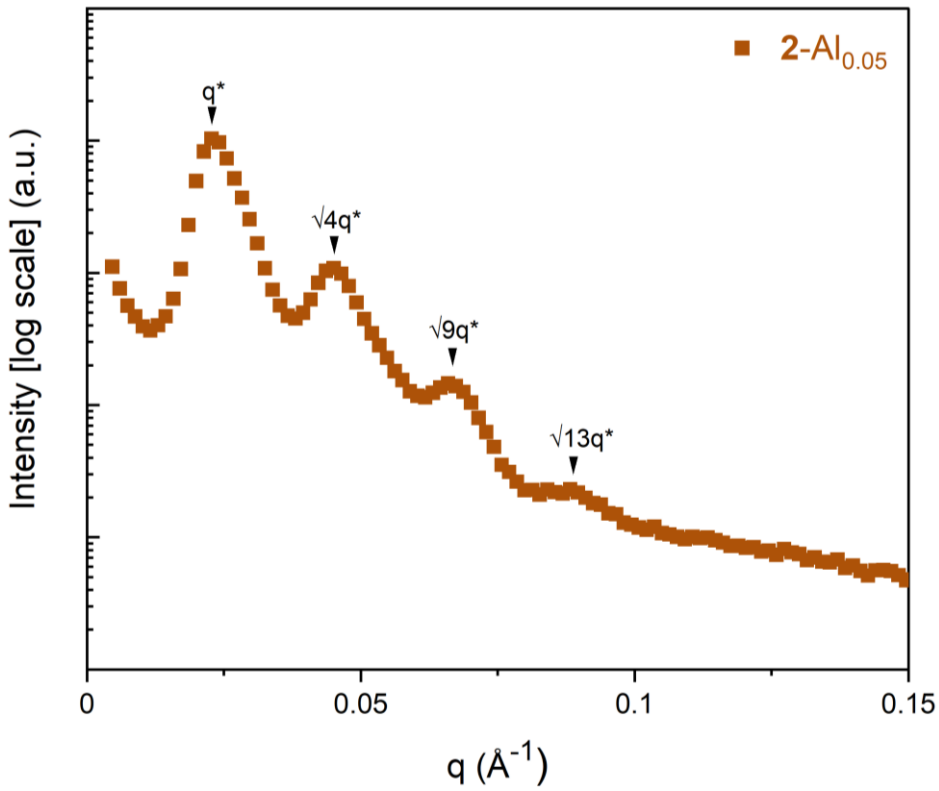

Figure S7.2.42: Room temperature SAXS data for **2**-$Al_{0.05.}$

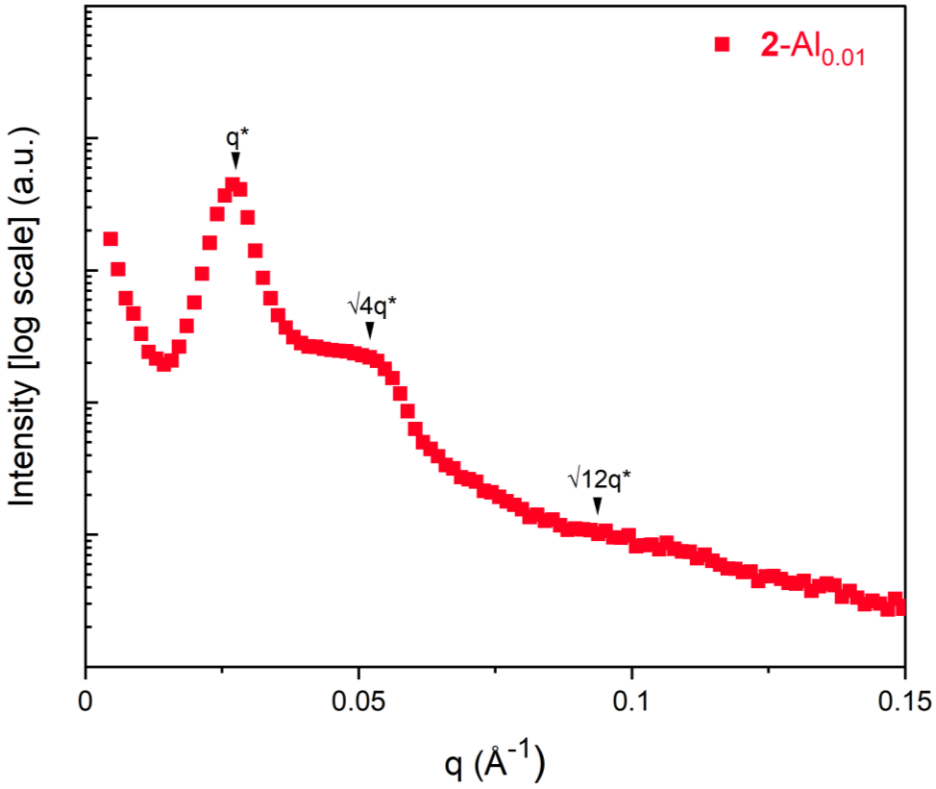

Figure S7.2.43: Room temperature SAXS data for **2**-$Al_{0.01}$.

Table S7.2.2. Gel Content and swelling index of ionomer films.

Material	Gel Content /%	Swelling Index /%
2-$Na_{0.10}$	97	411
2-$Mg_{0.10}$	92	668
2-$Ca_{0.10}$	94	599
2-$Zn_{0.10}$	95	730
2-$Al_{0.10}$	99	276
2-$Al_{0.05}$	99	294
2-$Al_{0.01}$	96	426

Swelling Index (SW) % = $[(W_s - W_o)/W_o)] \times 100$

Gel Content (GC) % = $(W_d/W_o) \times 100$

W_o = Original Weight of Polymer

W_s = Weight of Swollen Polymer

W_d = Weight of Dried Polymer

Table S7.2.3. Resulting improvement of strategy relative to unfunctionalized material.

	Young's Modulus Increase (%)	Ultimate Tensile Strength Increase (%)
[a]Increased Entanglement	767	157
[b]Stereocomplexation	273	0
[c]Hydrogen Bonding	913	5607
Ionomers (this work)	5100	1900

Comparisons made between triblock copolymer TPEs with ~30 wt% A-block.

[a]Comparison of PLLA-ϒMCL-PLLA and PLLA-PM-PLLA. Where ϒMCL and PM are poly(ϒ-methyl-ε-caprolactone) and poly(menthide) respectively.[1]

[b]Comparison of PLLA-PM-PLLA and PDLA-PM-PDLA with PLLA-PM-PLLA/PDLA-PM-PDLA blend.[2]

[c]Comparison of 2-vinyl and 2-COOH.[3, 4]

7.2. Chapter 3

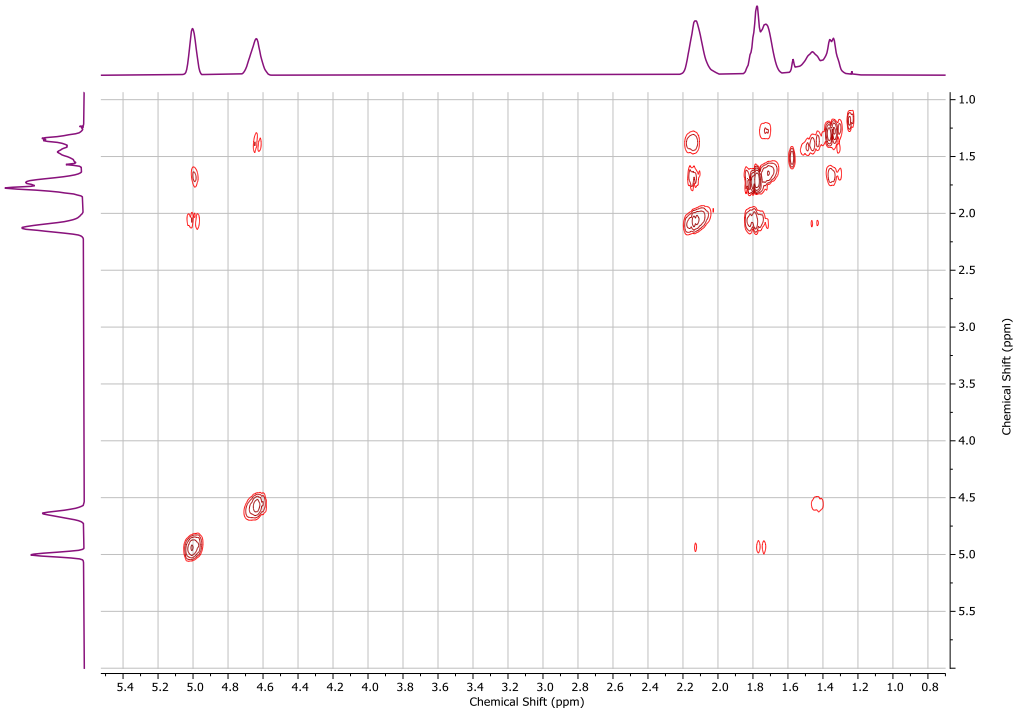

Figure S7.3.1: Representative ^{1}H COSY NMR spectrum (400 MHz, $CDCl_3$) of PCHC-*grad*-PCPC terpolymer ($PCHC_{0.51}$-*grad*-$PCPC_{0.49}$).

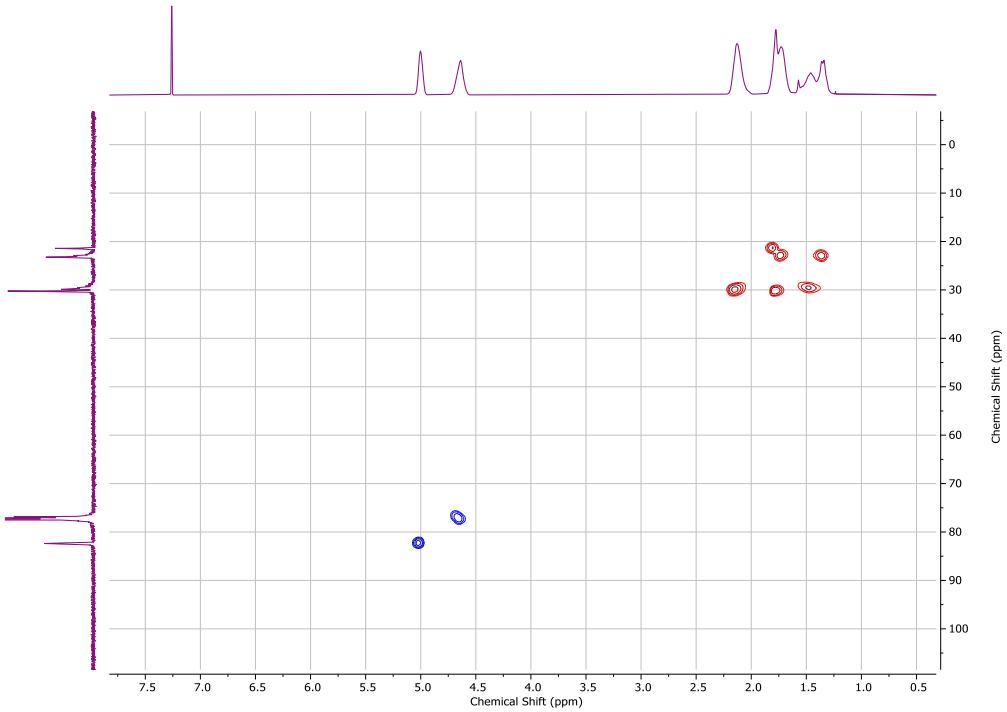

Figure S7.3.2: Representative ^{1}H – ^{13}C HSQC NMR spectrum (400 MHz, $CDCl_3$) of PCHC-*grad*-PCPC terpolymer ($PCHC_{0.51}$-*grad*-$PCPC_{0.49}$).

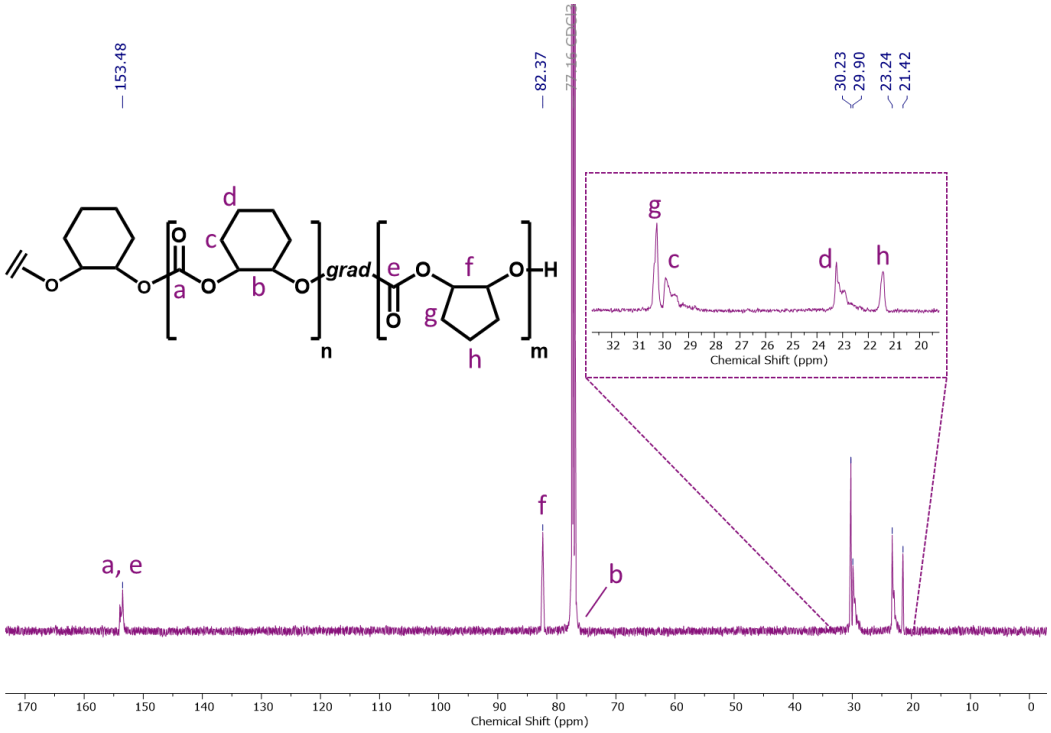

Figure S7.3.3: Representative $^{13}C\{^{1}H\}$ HSQC NMR spectrum (100.58 MHz, $CDCl_3$) of PCHC-*grad*-PCPC terpolymer ($PCHC_{0.51}$-*grad*-$PCPC_{0.49}$).

Table S7.3.1: DMTA Results Used to Determine Entanglement Molecular Weight

Polymer	E^0_N /MPa	T /K
PCHC	0.26933	432.15
$PCHC_{0.77}$-*grad*-$PCPC_{0.23}$	0.32828	434.54
$PCHC_{0.77}$-*grad*-$PCPC_{0.23}$	0.64471	400.46
$PCHC_{0.77}$-*grad*-$PCPC_{0.23}$	1.55958	393.98
PCPC	2.06587	379.62

Values of E^0_N and T taken from the minimum tan (δ) in the plateau region. The value for the density, ϱ = 1135 kg·m^{-3} for PCHC.[7] For the terpolymers and PCPC, a density range of 800–1100 kg·m^{-3} was used to provide an estimate.[7]

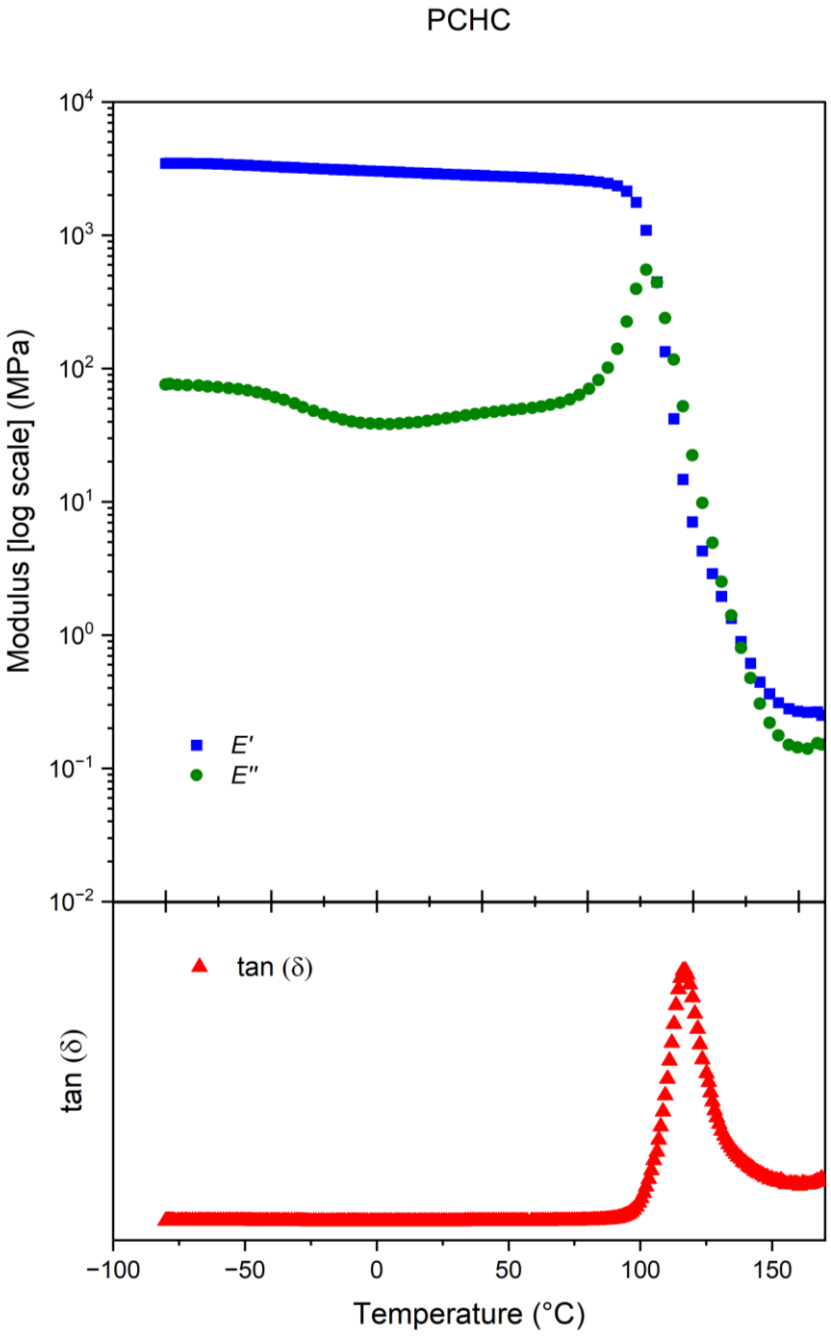

Figure S7.3.4: Dynamic mechanical temperature analysis (DMTA) temperature sweeps for PCHC (**Table S7.3.1**).

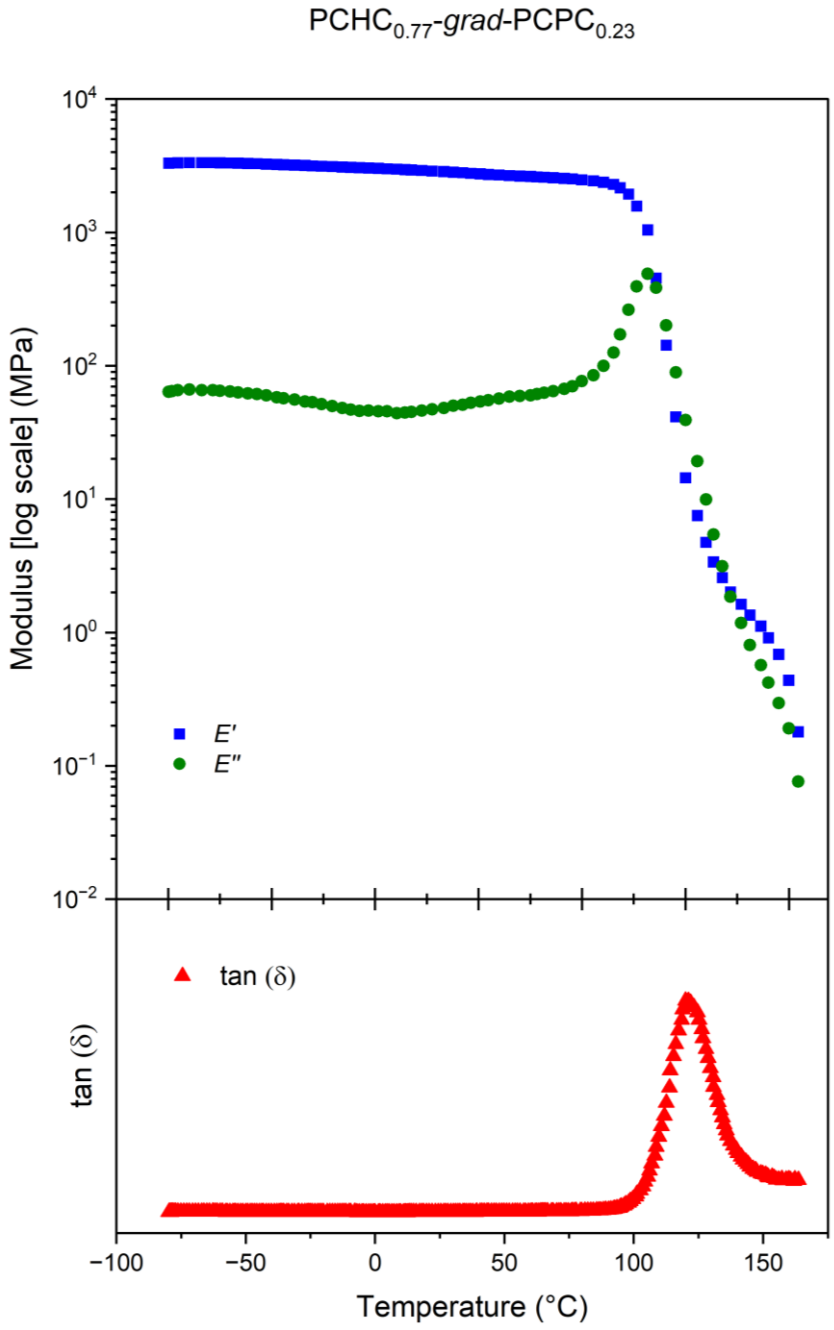

Figure S7.3.5: Dynamic mechanical temperature analysis (DMTA) temperature sweeps for PCHC$_{0.77}$-*grad*-PCPC$_{0.23}$ (**Table S7.3.1**).

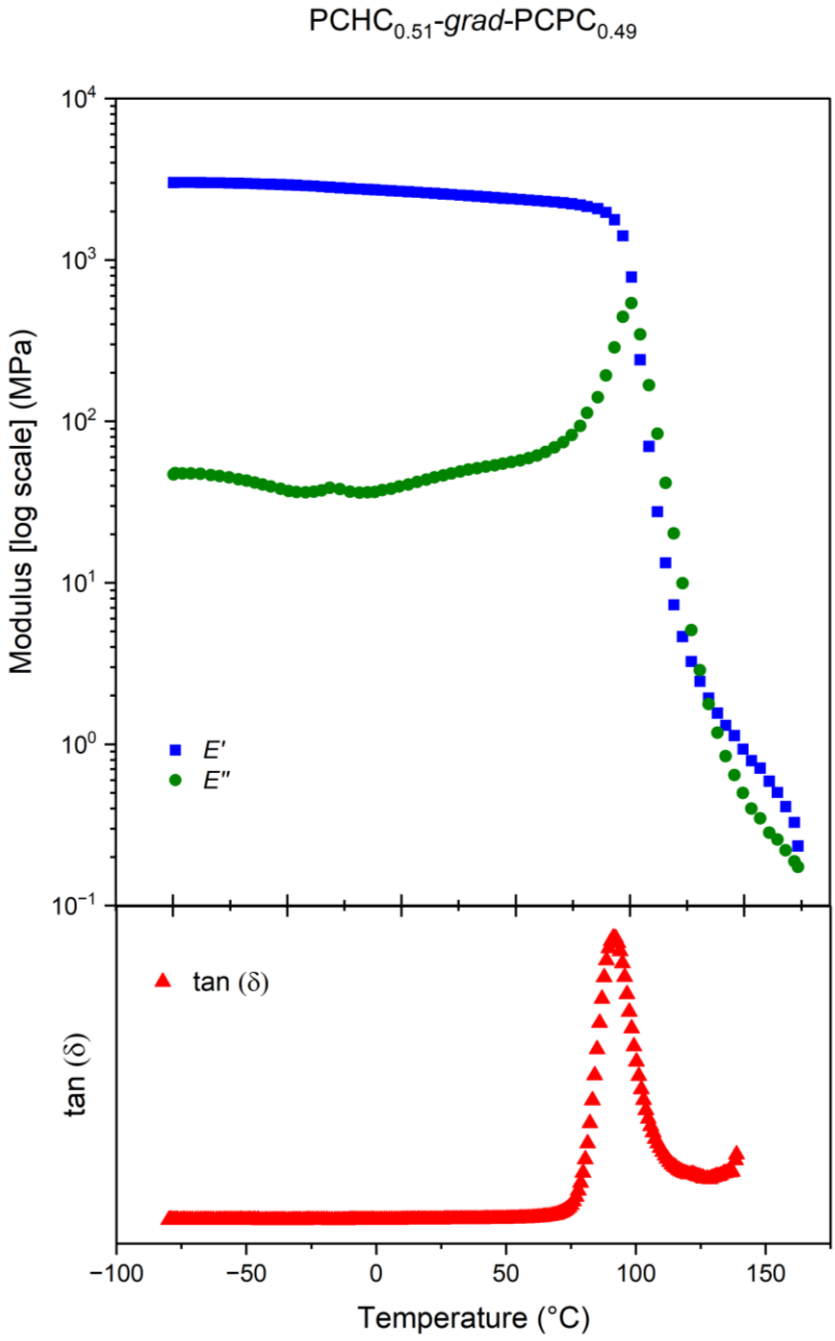

Figure S7.3.6: Dynamic mechanical temperature analysis (DMTA) temperature sweeps for PCHC$_{0.51}$-*grad*-PCPC$_{0.49}$ (**Table S7.3.1**).

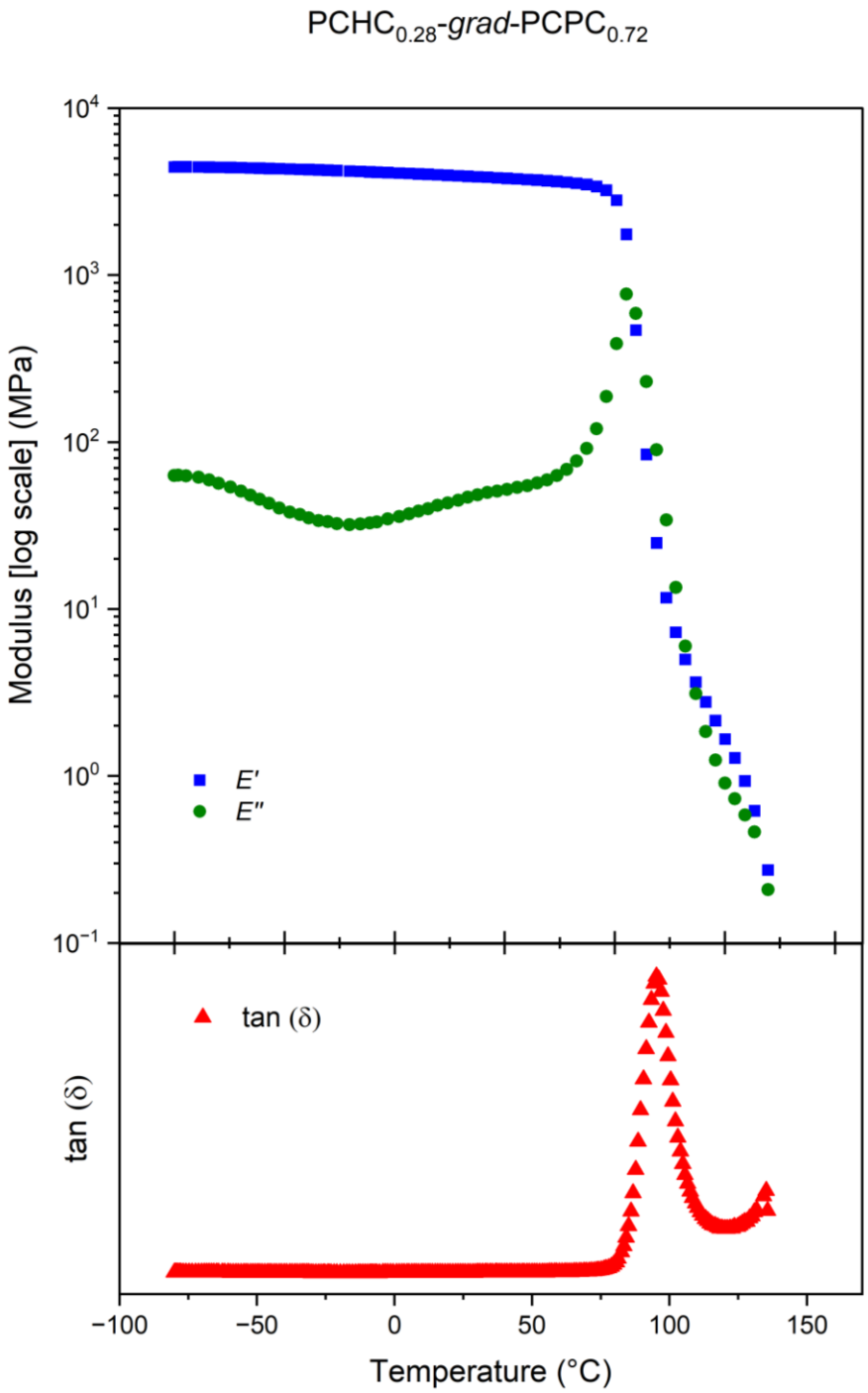

Figure S7.3.7: Dynamic mechanical temperature analysis (DMTA) temperature sweeps for $PCHC_{0.28}$-*grad*-$PCPC_{0.72}$ (**Table S7.3.1**).

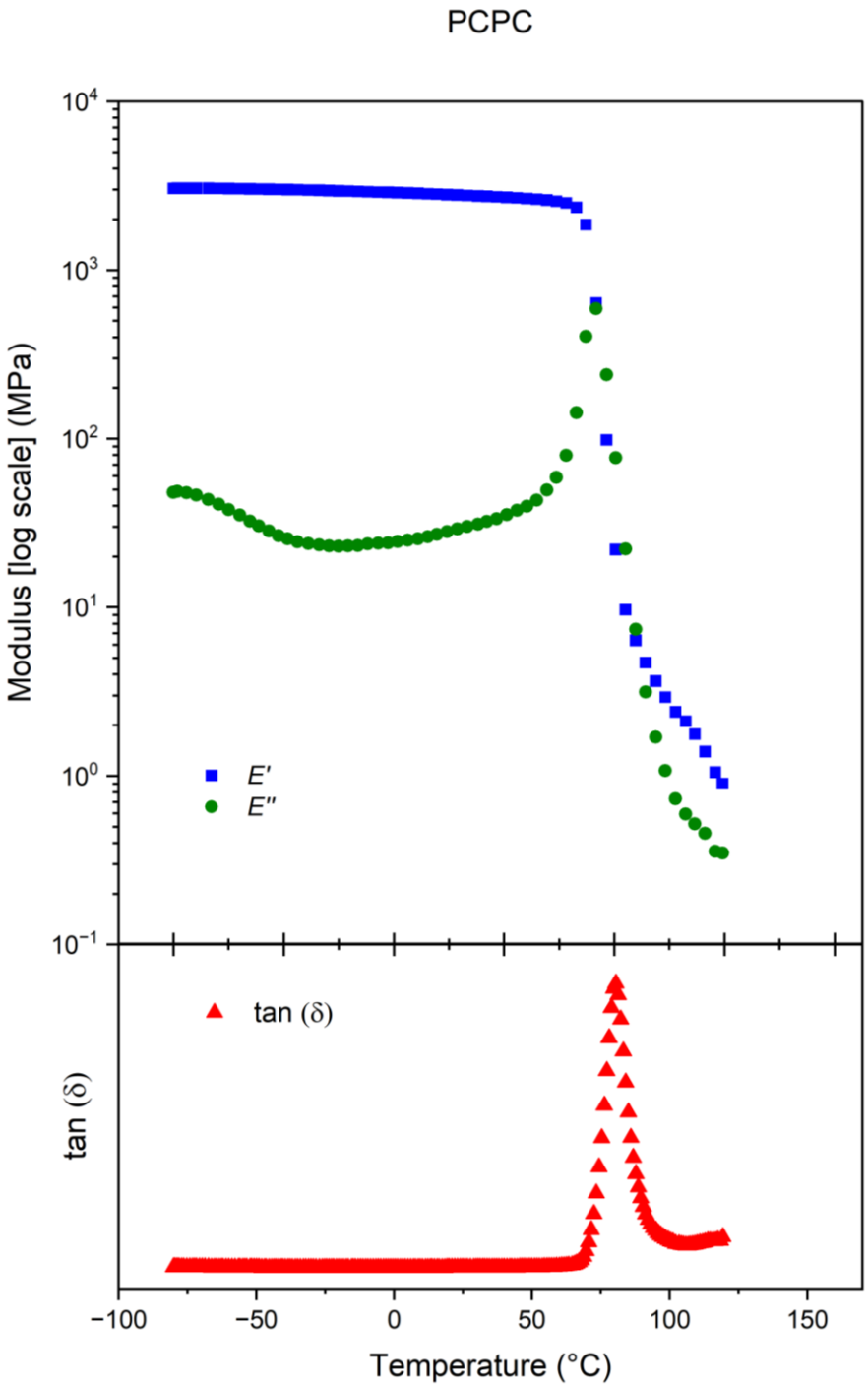

Figure S7.3.8: Dynamic mechanical temperature analysis (DMTA) temperature sweeps for PCPC (**Table S7.3.1**).

Table S7.3.2: Fineman-Ross Analysis Results of CPO/CHO with CO_2 Terpolymerization

Entry	F(CPO/CHO) in feed	f(CPO/CHO) in polymer	f/F^2	(f-1)/F
1	0.56	0.24	0.77	-1.36
2	1.43	0.40	0.20	-0.42
3	1.14	0.46	0.35	-0.47
4	3.93	2.21	0.14	0.31
5	0.33	0.19	1.74	-2.45
6	0.54	0.24	0.82	-1.41
7	0.43	0.24	1.30	-1.77

Reactions were performed at 80 °C, 1 bar CO_2, [cat.]:[CHD]:[CPO+CHO] = 1:4:1000, [CPO+CHO] = 5 M toluene and stopped after 2 h.

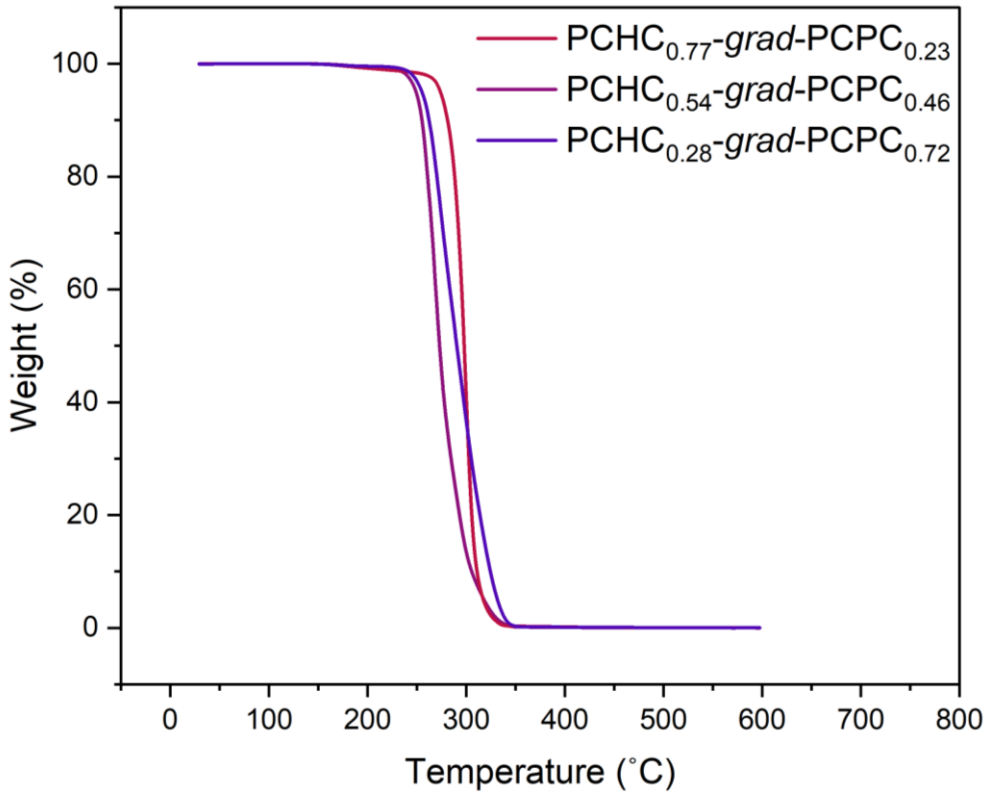

Figure S7.3.9: Thermogravimetric Analysis (TGA) data for PCHC-*grad*-PCPC terpolymers.

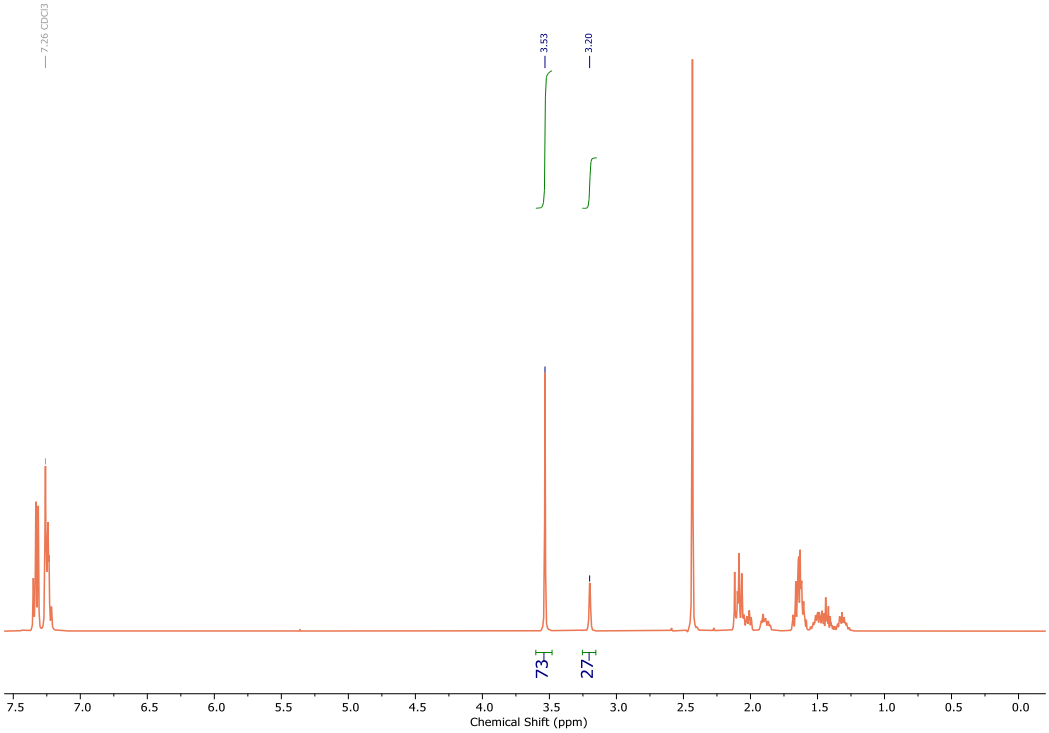

Figure S7.3.10: ^{1}H NMR spectrum (400 MHz, $CDCl_3$) of the CHO and CPO isolated from the depolymerization. The relative ratio, indicated by the integrals, is CHO:CPO = 73 : 27.

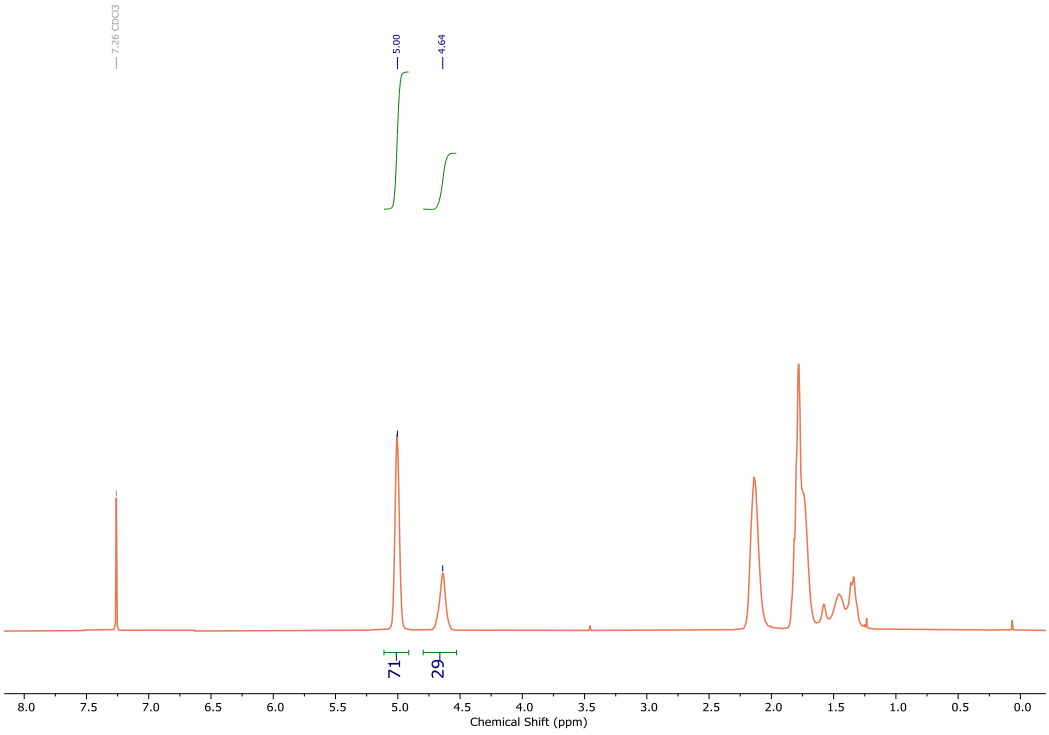

Figure S7.3.11: ^{1}H NMR spectrum (400 MHz, $CDCl_3$) of the chemically recycled (i.e. re-polymerized) PCHC-*grad*-PCPC terpolymer.

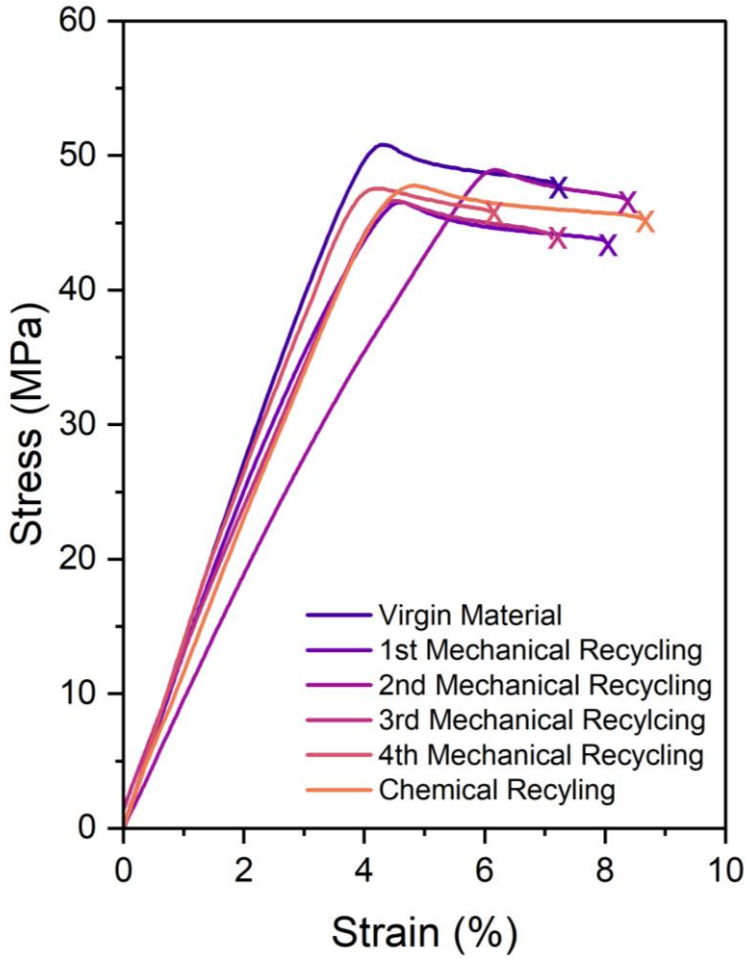

Figure S7.3.12: Representative stress-strain data (10 mL min^{-1}) for $PCHC_{0.51}$-*grad*-$PCPC_{0.49}$ after repeated cycles of mechanical reprocessing and chemical recycling.

Table S7.3.3: Data for the Chemically Recycled PCHC-*grad*-PCPC Terpolymers

Polymer	[a]E_Y /GPa	[b]σ /MPa	[c]ε_b /%	[d]U_T /MJ m^{-3}
$PCHC_{0.51}$-*grad*-$PCPC_{0.49}$ (Virgin Material)	1.54 ± 0.15	46.2 ± 3.1	6.5 ± 0.9	2.34 ± 0.56
1st Mechanical Recycling	1.06 ± 0.1	44.2 ± 2.4	7.1 ± 1.2	2.16 ± 0.44
2nd Mechanical Recycling	0.88 ± 0.09	45.5 ± 0.7	9.3 ± 0.5	2.95 ±0.28
3rd Mechanical Recycling	1.08 ± 0.08	45.2 ± 3.2	4.6 ± 1.4	2.48 ± 0.42
4th Mechanical Recycling	1.24 ± 0.15	44.6 ± 3.3	7.2 ± 1.2	2.63 ± 0.72
$PCHC_{0.29}$-*grad*-$PCPC_{0.71}$ (Chemically Recycled)	1.21 ± 0.04	48.8 ±7.6	8.5 ± 1.2	3.01 ± 0.58

Specimens suitable for uniaxial tensile testing were solvent cast, dried and compression moulded (150 ° C, 1.2 ton m^{-2}, 60 min). Measurements were conducted independently on 10 specimens and values are reported as the mean and standard deviation from those experiments. [a]Young's modulus. [b]Tensile strength. [c]Strain at break. [d]Tensile toughness (area under the stress-strain curve).

7.3. Chapter 4

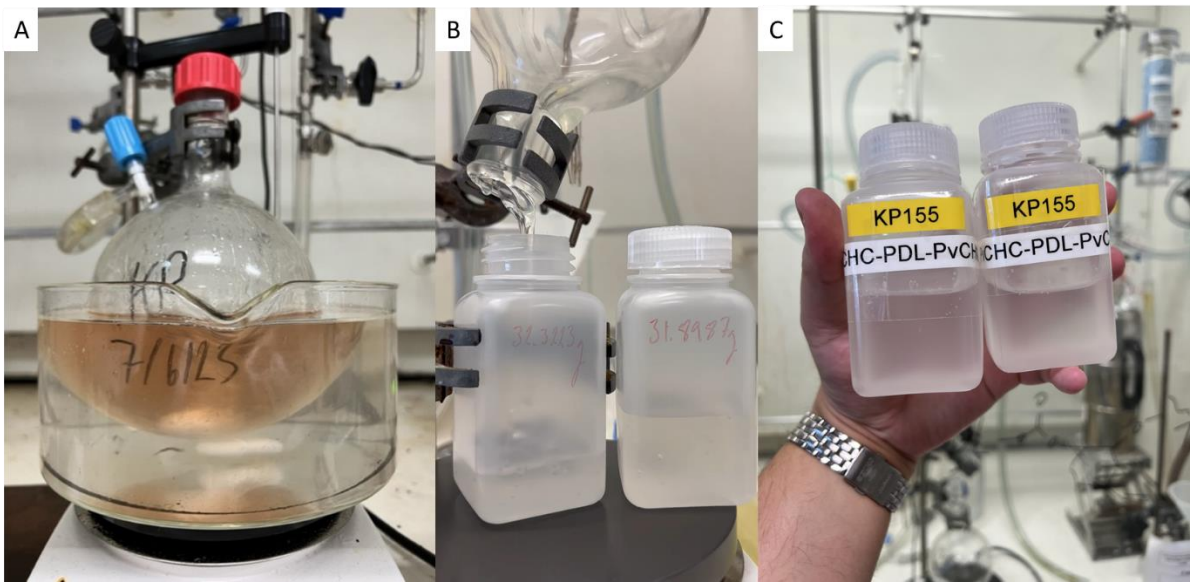

Figure S7.4.1: Digital photographs of A) **P1** polymerization under 1 bar CO_2 atmosphere B) Purified **P1** C) Total 204 g of **P1** triblock copolymer.

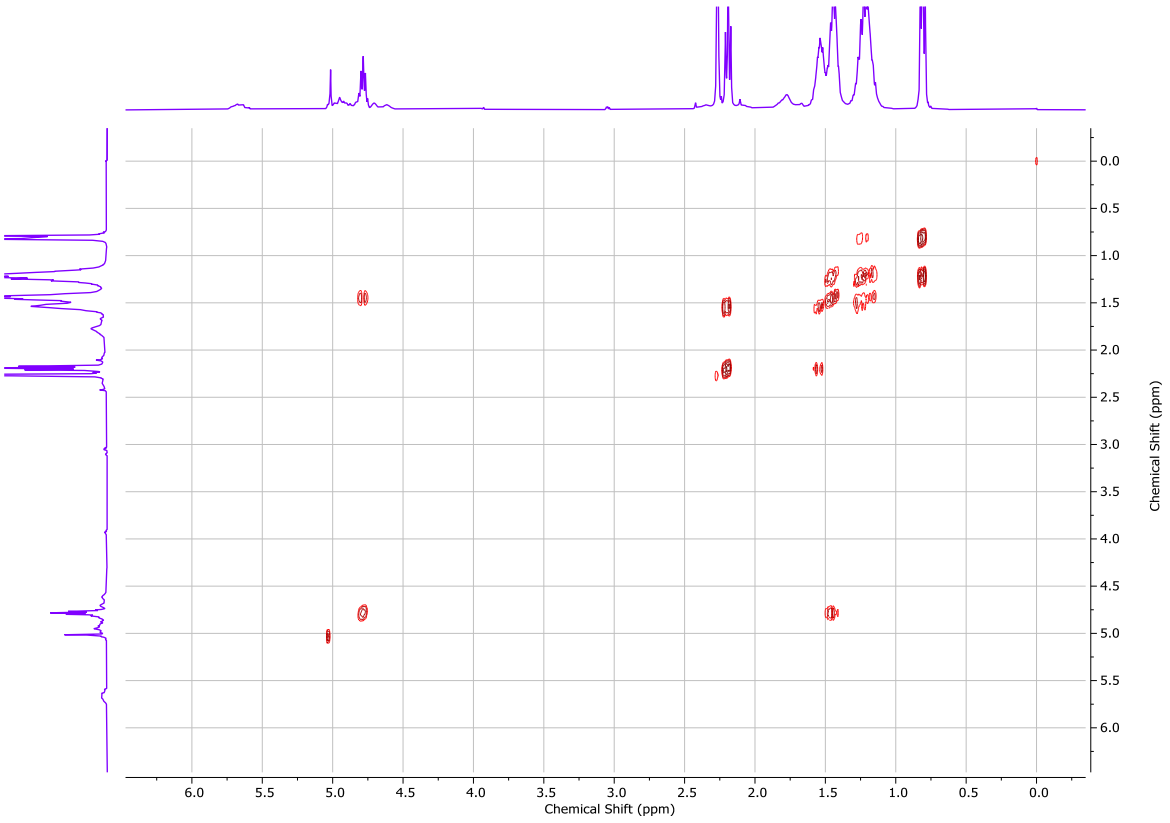

Figure S7.4.2: ^{1}H COSY NMR (400 MHz, $CDCl_3$) spectrum of PvCHC-PDL-PvCHC triblock copolymer (**P1**).

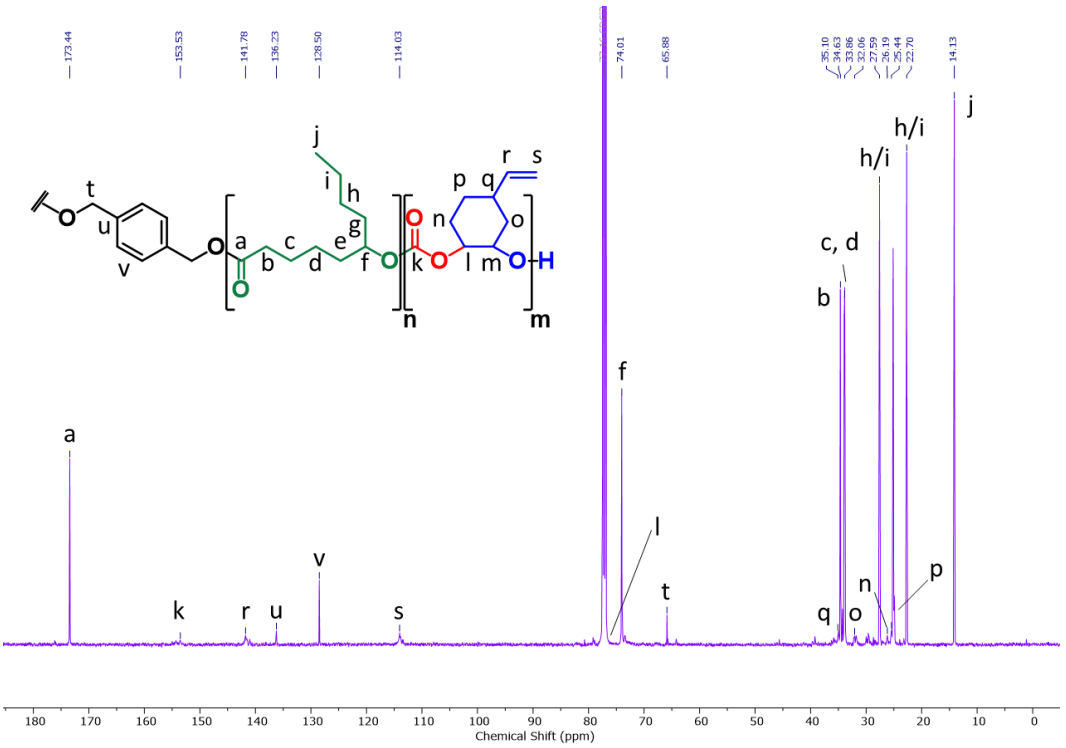

Figure S7.4.3: ^{13}C {^{1}H} NMR (100.58 MHz, $CDCl_3$) spectrum of PvCHC-PDL-PvCHC triblock copolymer (**P1**).

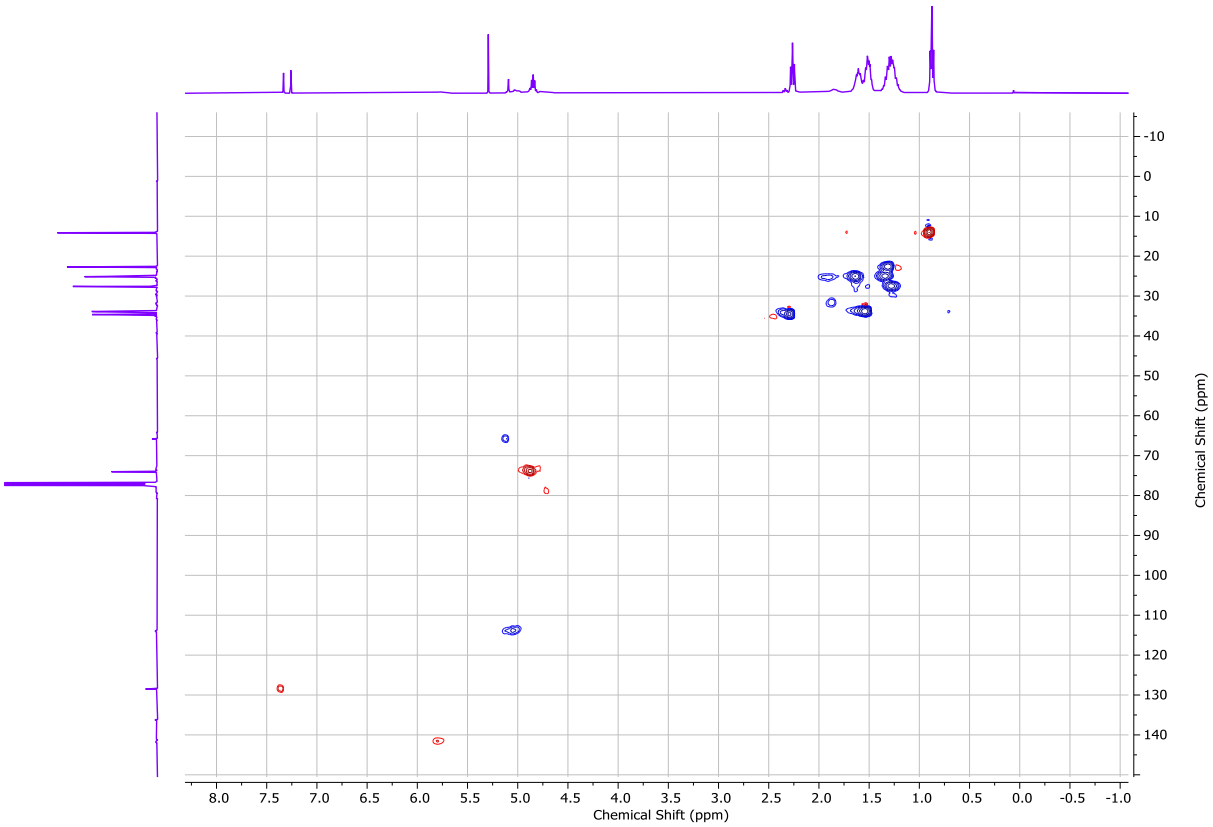

Figure S7.4.4: ^{1}H – ^{13} HSQC NMR (400 MHz, $CDCl_3$) spectrum of PvCHC-PDL-PvCHC triblock copolymer (**P1**).

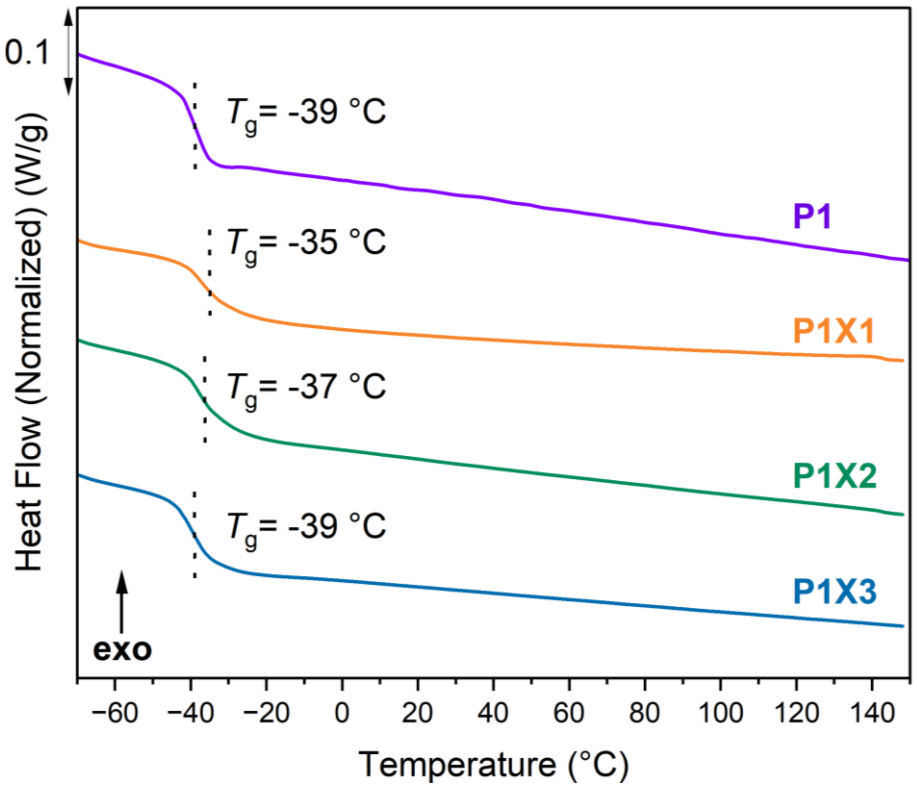

Figure S7.4.5 Differential Scanning Calorimetry (DSC) traces of **P1** resin and printed materials.

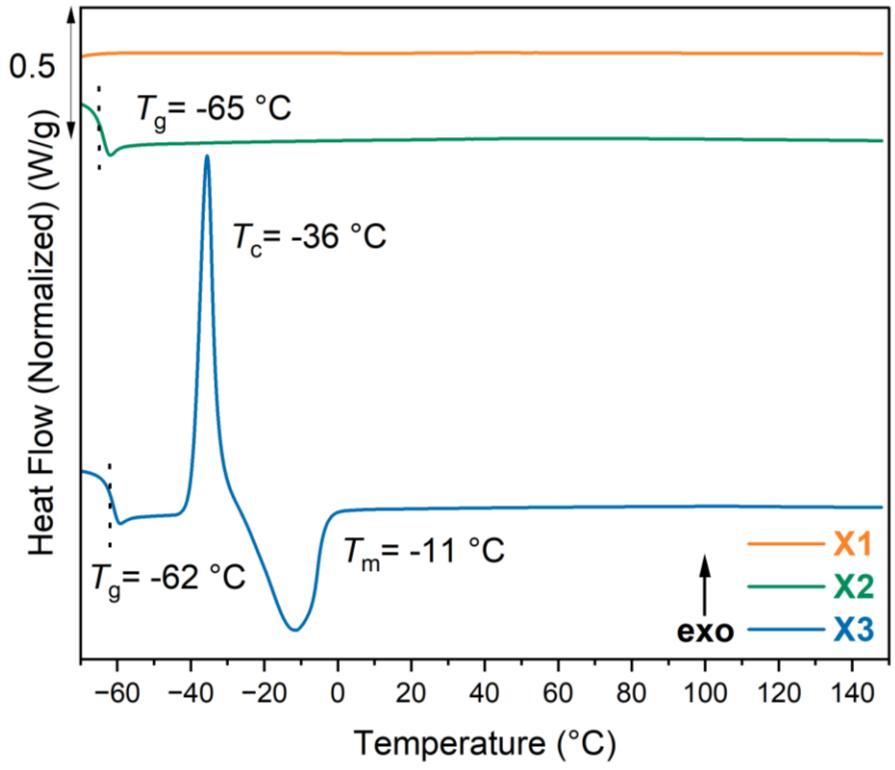

Figure S7.4.6: Differential Scanning Calorimetry (DSC) traces of **X1**, **X2** and **X3** crosslinkers.

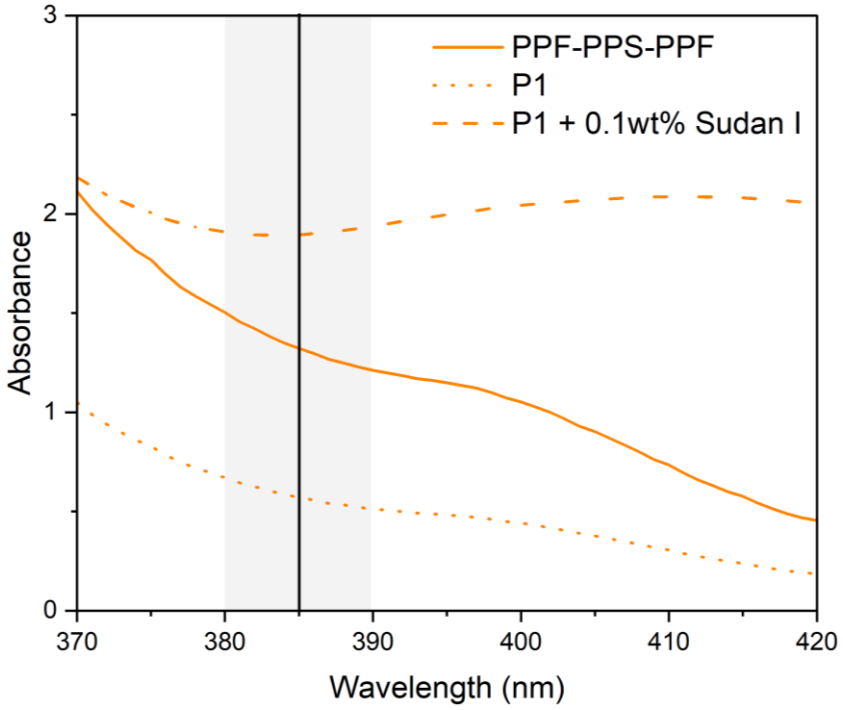

Figure S7.4.7: UV-vis spectroscopy of diluted resins (10 wt% in ethyl acetate). Comparison of **P1** with and without Sudan I dye relative to poly(propylene fumarate-*b*-propylene succinate-*b*-propylene fumarate) triblock copolymer known to successfully print. Shaded region covers wavelengths used by DLP printer.

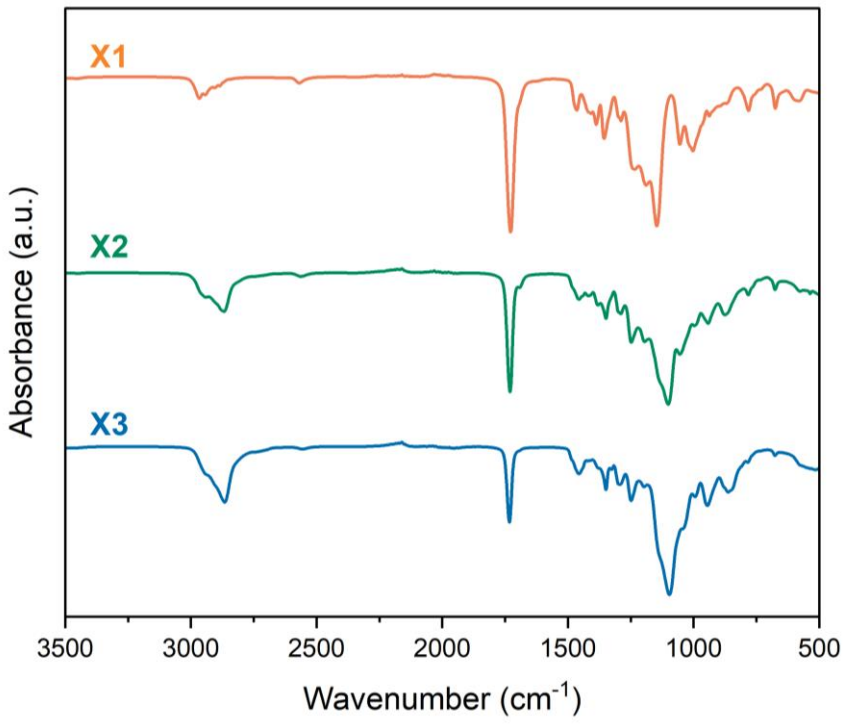

Figure S7.4.8: FTIR spectra of **X1**, **X2** and **X3**.

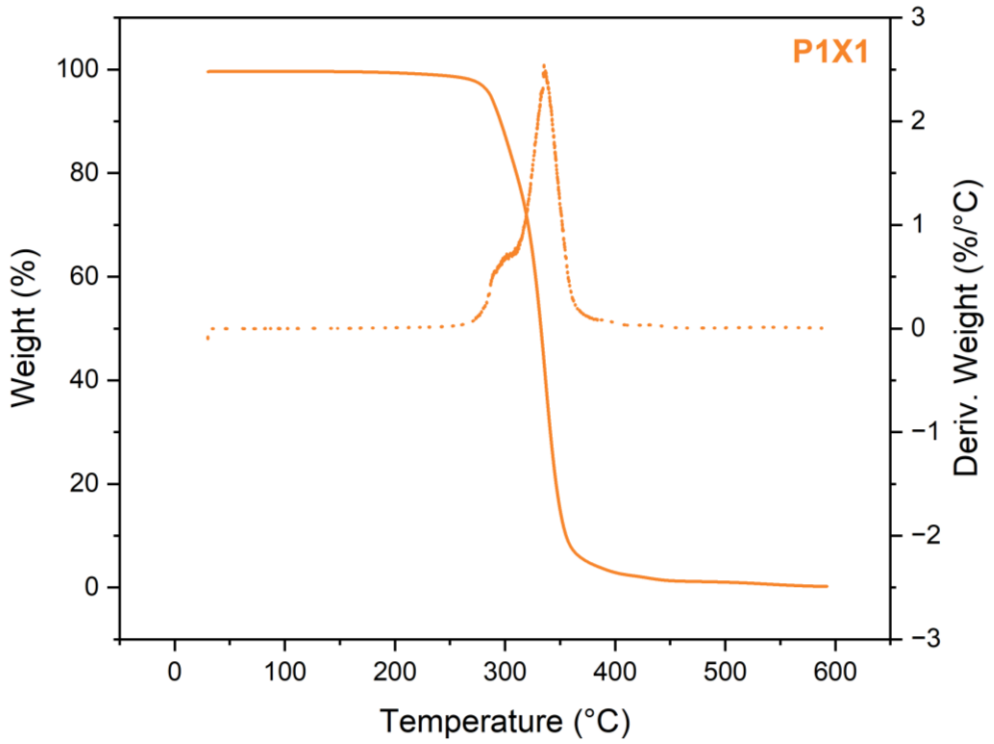

Figure S7.4.9: Thermogravimetric Analysis (TGA) trace of **P1X1**.

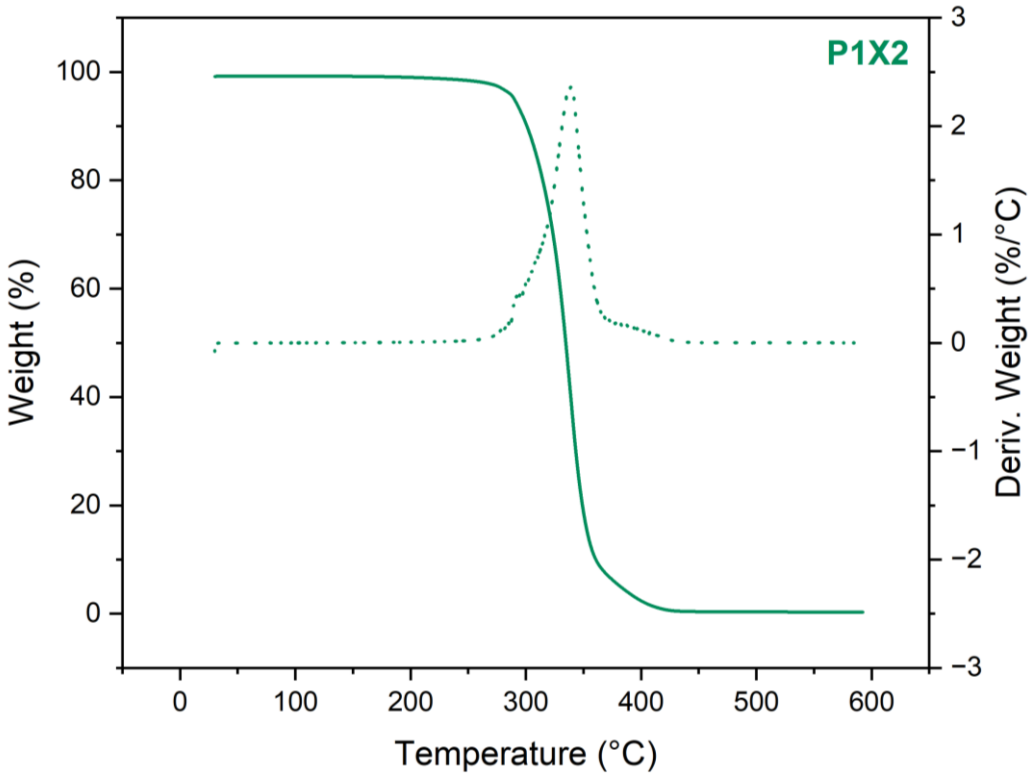

Figure S7.4.10: Thermogravimetric Analysis (TGA) trace of **P1X2**.

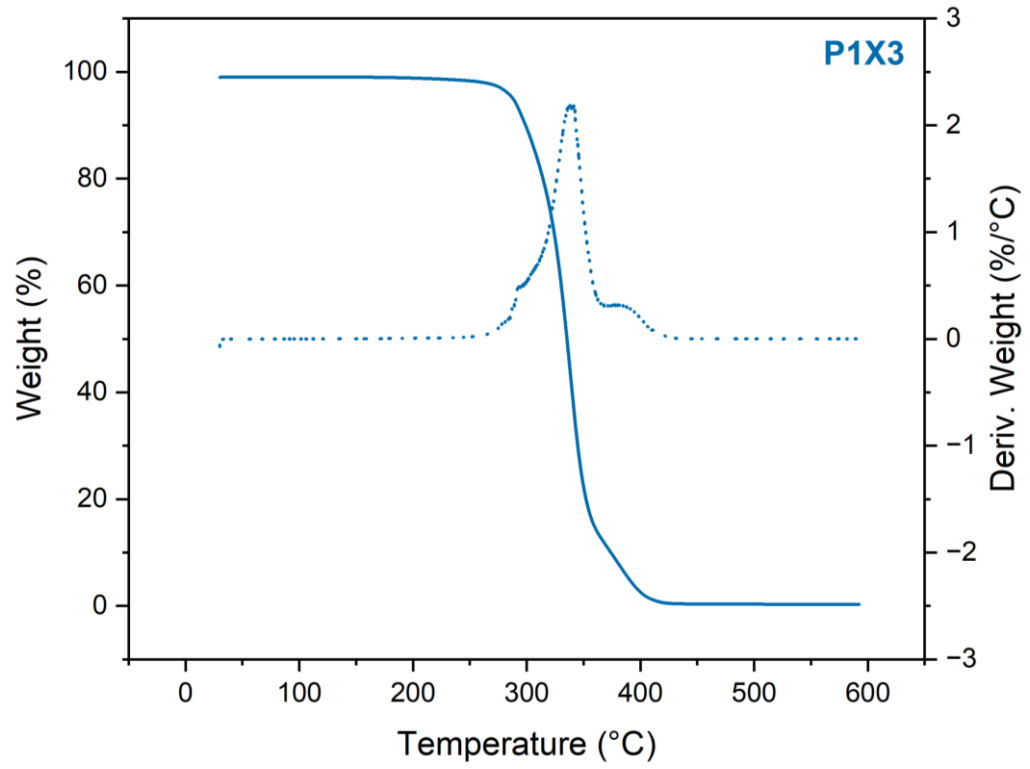

Figure S7.4.11: Thermogravimetric Analysis (TGA) trace of **P1X3**.

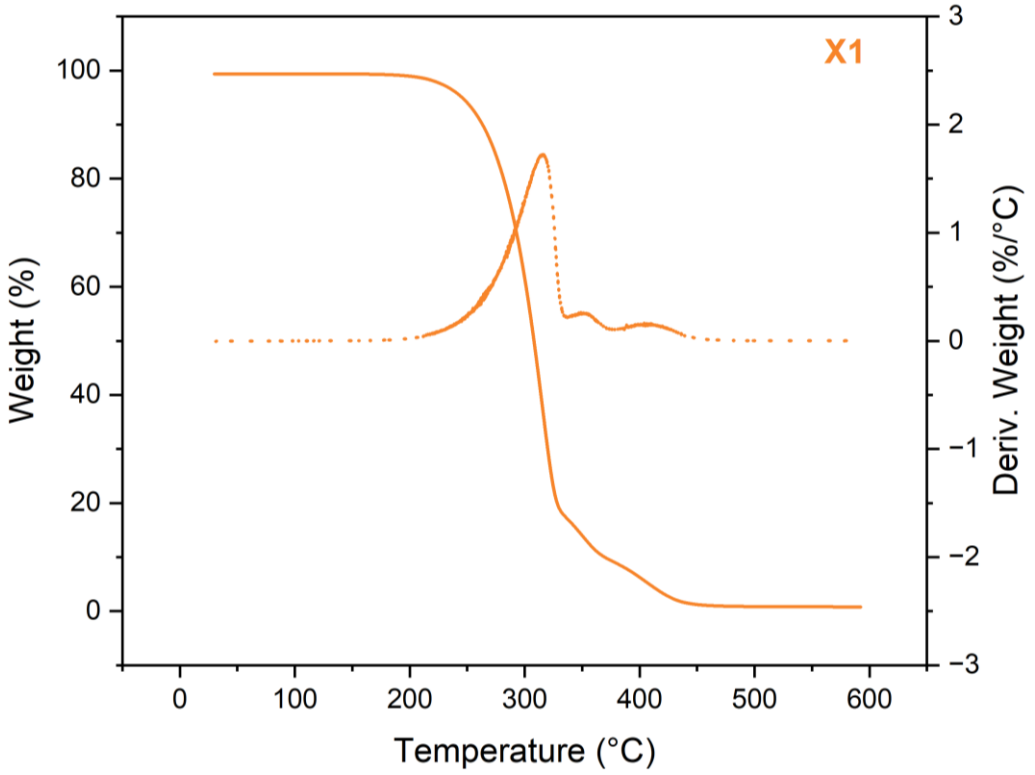

Figure S7.4.12: Thermogravimetric Analysis (TGA) trace of **X1**.

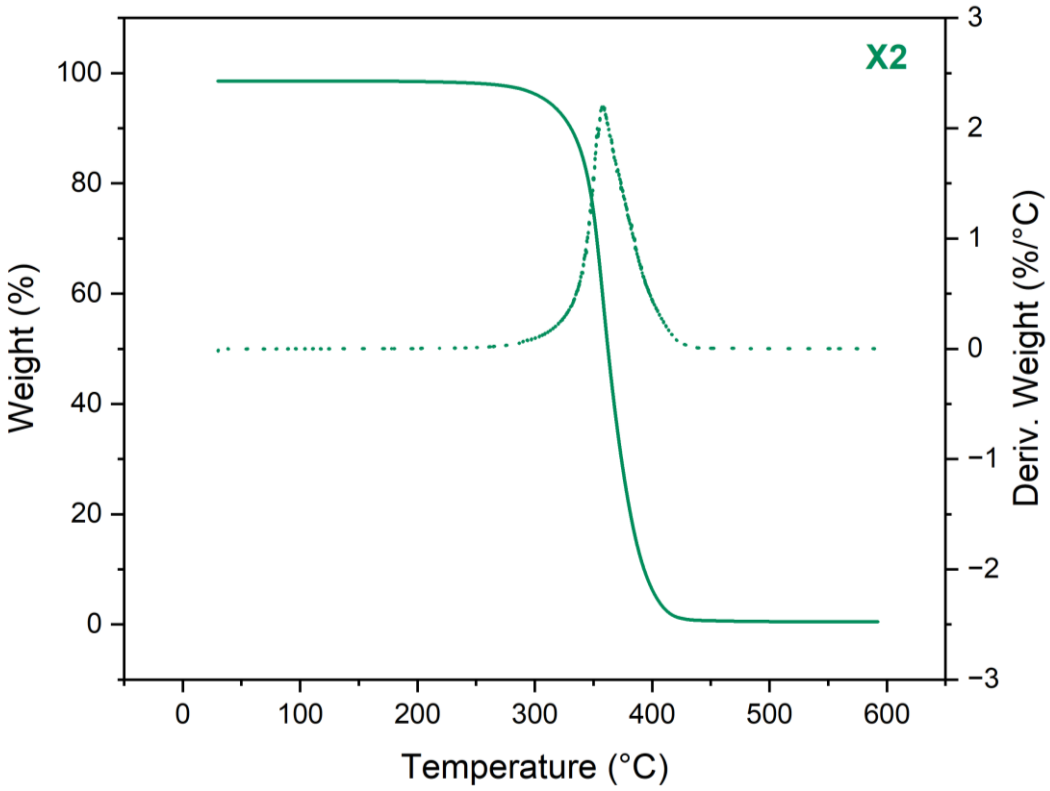

Figure S7.4.13: Thermogravimetric Analysis (TGA) trace of **X2**.

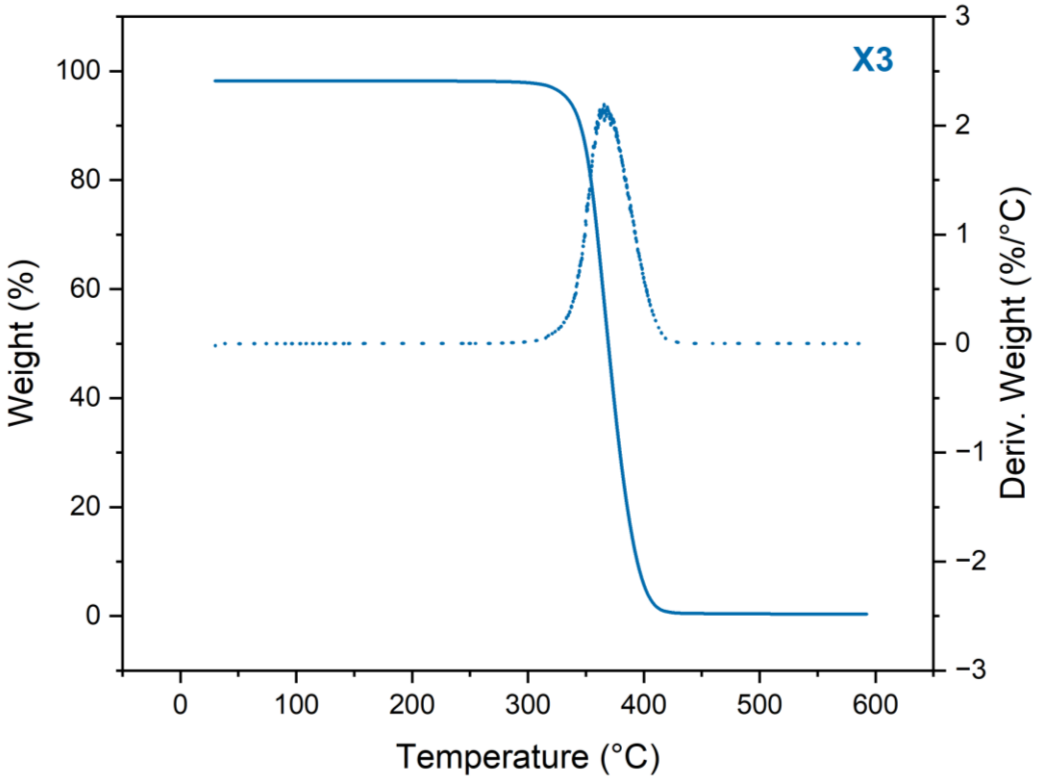

Figure S7.4.14: Thermogravimetric Analysis (TGA) trace of **X3**.

Table S7.4.1: Statistical analysis of uniaxial tensile testing.

	Samples	Young's modulus (E_y)	Tensile strength (σ)	Strain at break (ε_b)	Toughness (U_T)
Tukey's multiple comparisons test	**P1X1 vs. P1X2**	ns (0.4876)	ns (0.7559)	ns (0.9584)	ns (0.6509)
	P1X1 vs. P1X3	ns (0.1061)	ns (0.1137)	ns (0.9584)	ns (0.6011)
	P1X2 vs. P1X3	ns (0.5601)	ns (0.3401)	ns (>0.9999)	ns (0.9962)
ANOVA Results	**P1X1 vs. P1X2 vs. P1X3**	ns (0.1246)	ns (0.1248)	ns (0.9500)	ns (0.5676)

Significance and p-values are listed, where ns = no significance, *p<0.05, **p<0.01, ***p<0.001, ****p<0.0001.

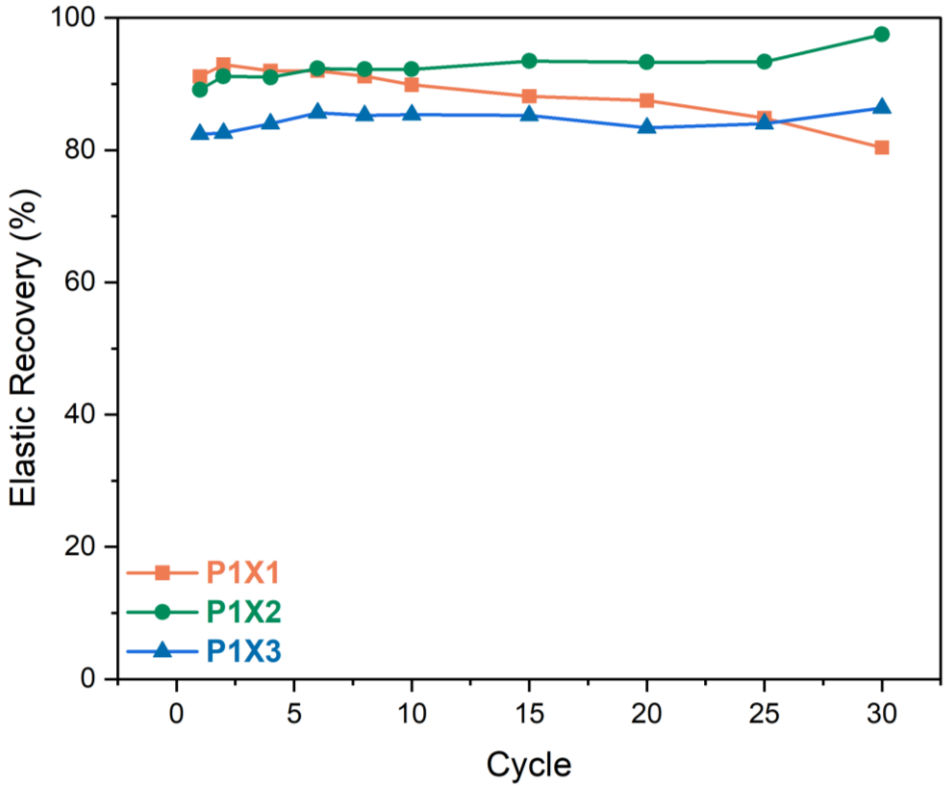

Figure S7.4.15: Elastic recovery as a function of cycle number for **P1X1**, **P1X2** and **P1X3.**

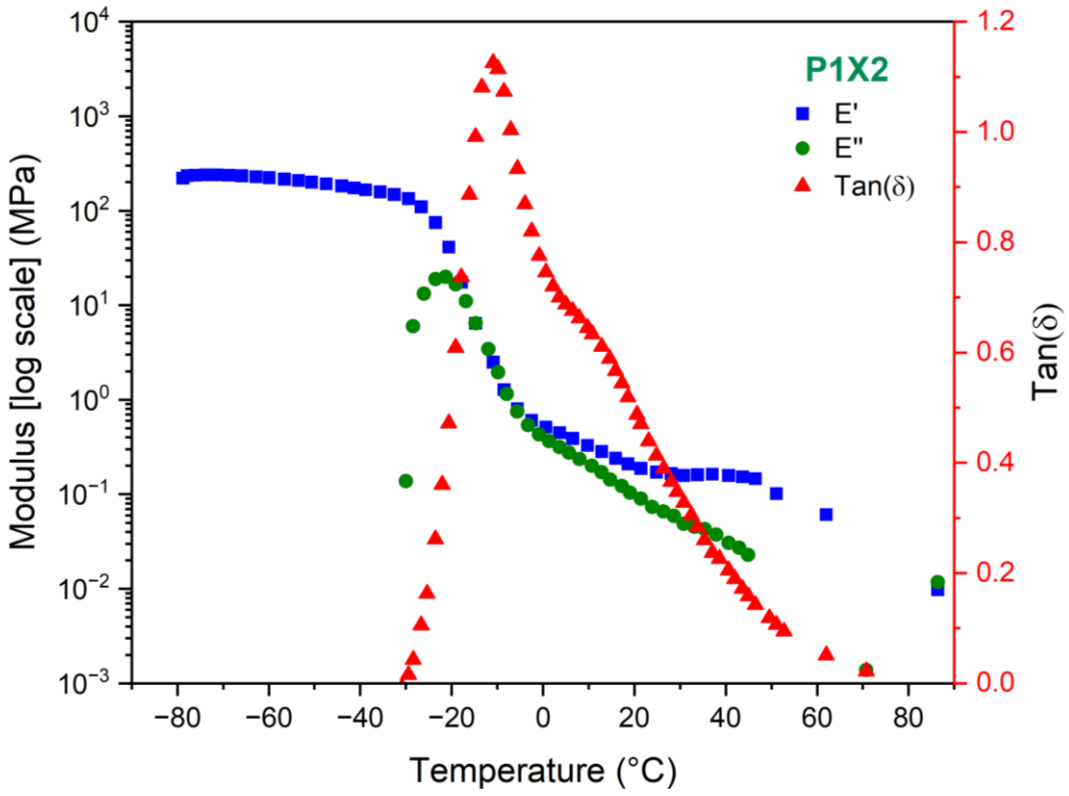

Figure S7.4.16: Dynamic mechanical thermal analysis (DMTA) temperature sweep for **P1X2**.

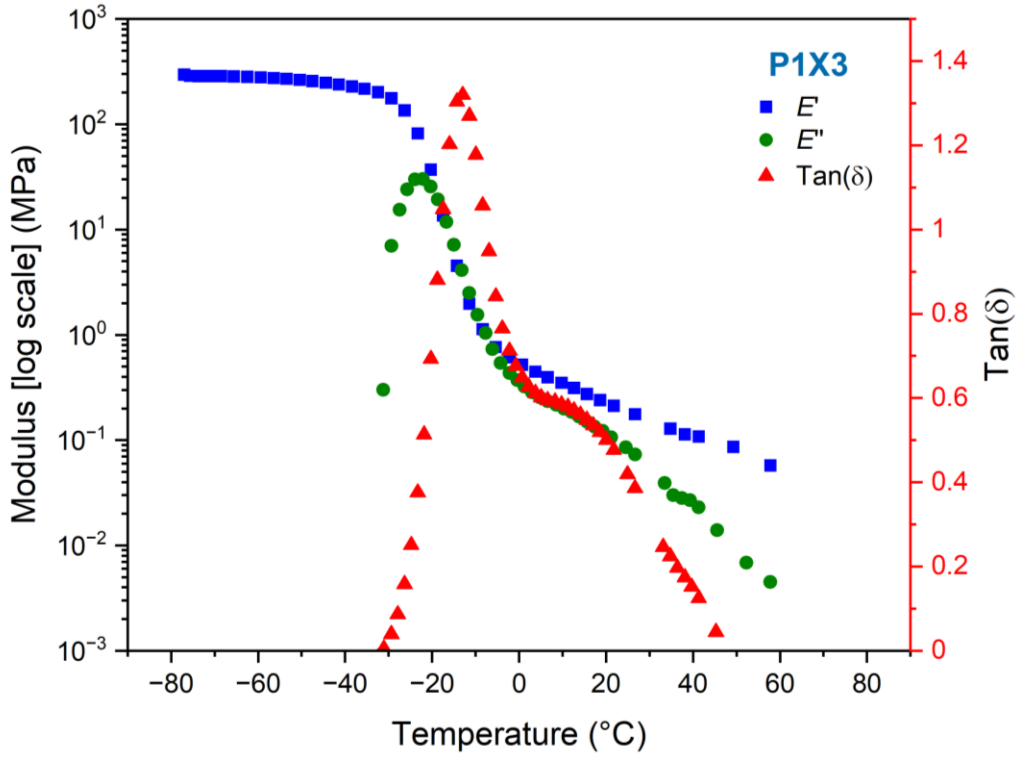

Figure S7.4.17: Dynamic mechanical thermal analysis (DMTA) temperature sweep for **P1X3**.

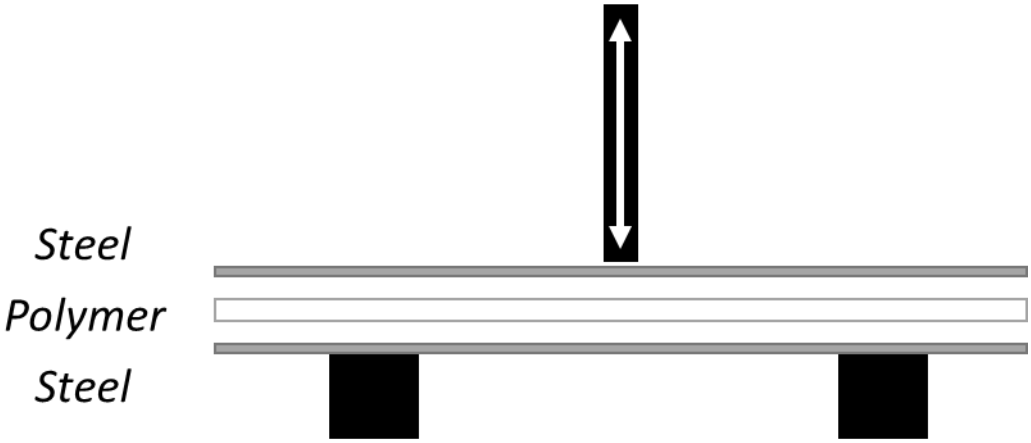

Figure S7.4.18: Schematic of dynamic mechanical thermal analysis (DMTA) set-up for **P1**, resin between 2 x 0.25 mm thick steel sheets in 3-point bend geometry.

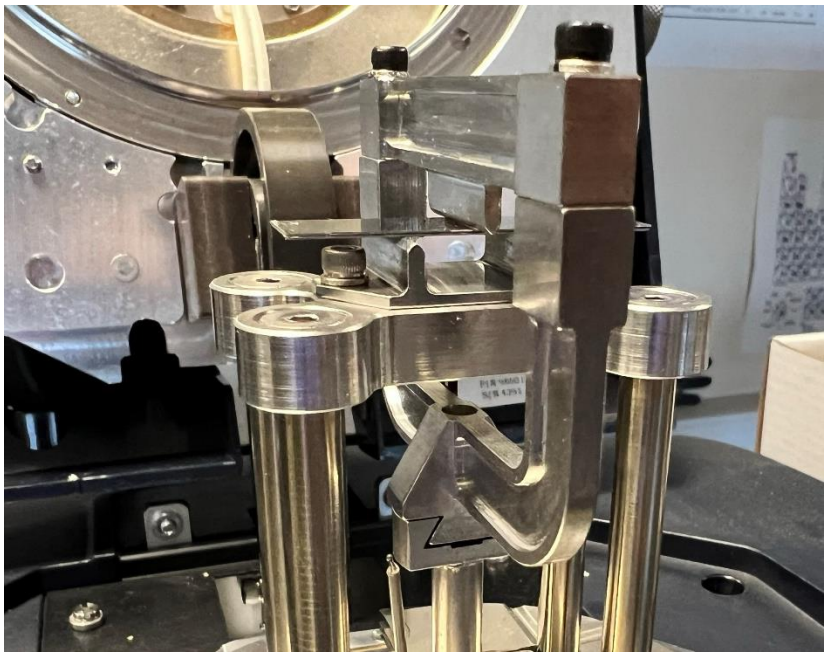

Figure S7.4.19: Digital photograph of dynamic mechanical thermal analysis (DMTA) set-up for **P1**.

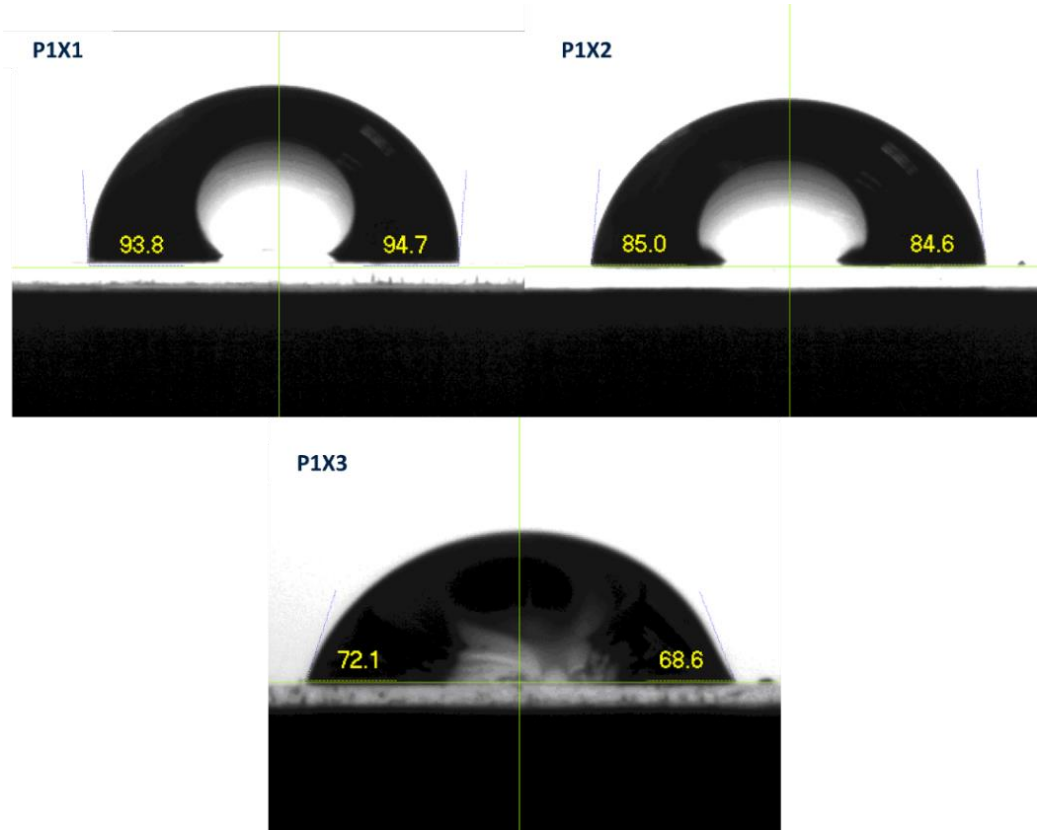

Figure S7.4.20: Representative of water contact angle measurements on thin films of **P1X1**, **P1X2** and **P1X3**.

Table S7.4.2: Statistical analysis of swelling index, gel content, and water contact angles.

	Samples	Swelling index	Gel content	Water contact angle
Tukey's multiple comparisons test	**P1X1 vs. P1X2**	** (0.010)	ns (0.6852)	** (<0.0019)
	P1X1 vs. P1X3	*** (<0.001)	ns (0.8778)	**** (<0.0001)
	P1X2 vs. P1X3	** (0.004)	ns (0.9305)	**** (<0.0001)
ANOVA Results	**P1X1 vs. P1X2 vs. P1X3**	*** (<0.001)	ns (0.7063)	**** (<0.0001)

Significance and p-values are listed, where ns = no significance, *p<0.05, **p<0.01, ***p<0.001, ****p<0.0001

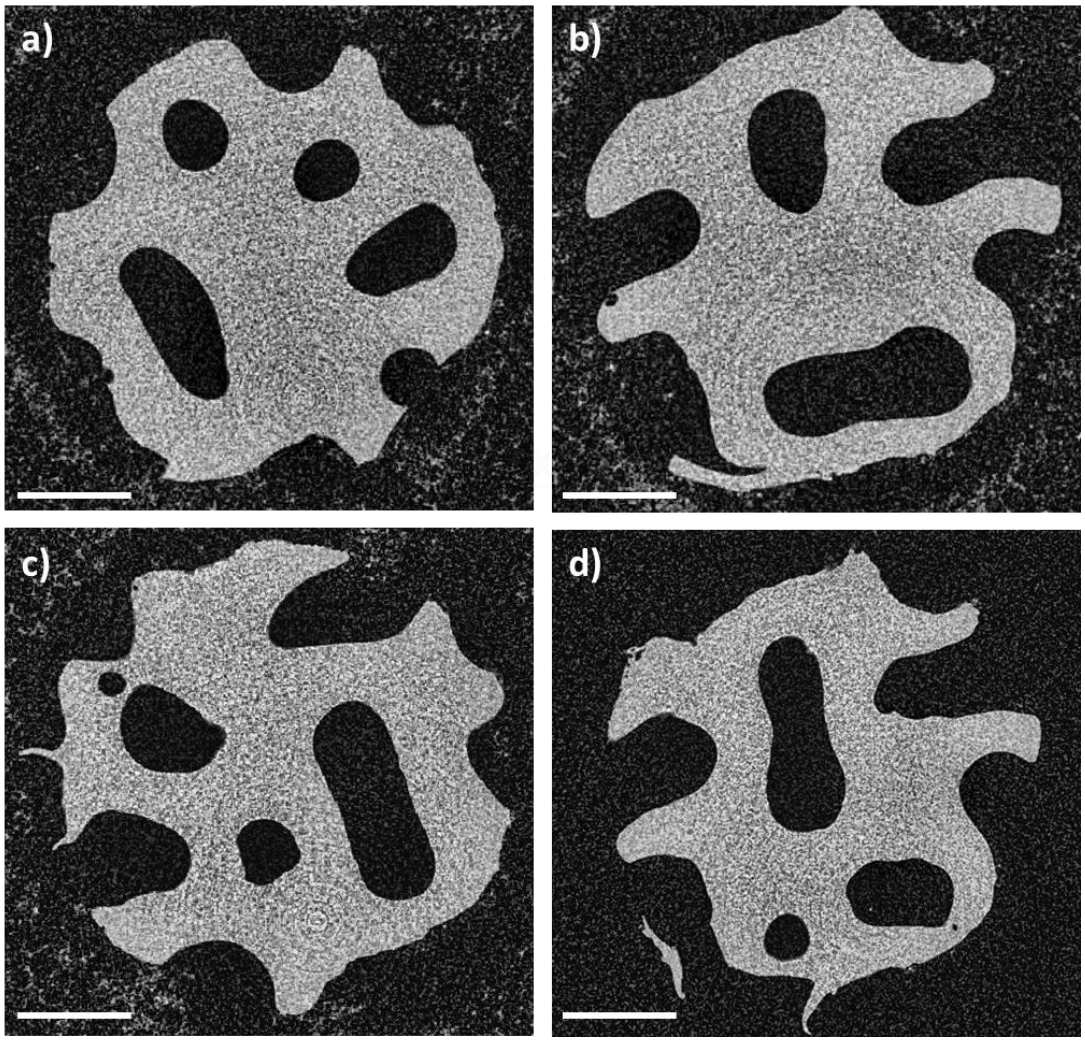

Figure S7.4.21: Selection of cross-sectional image of **P1X1** gyroid (5.9 mm tall) from micro-CT scan. Slices a) 171, b) 232, c) 293 and d) 444 of 615. Scale bar: 1000 µm.

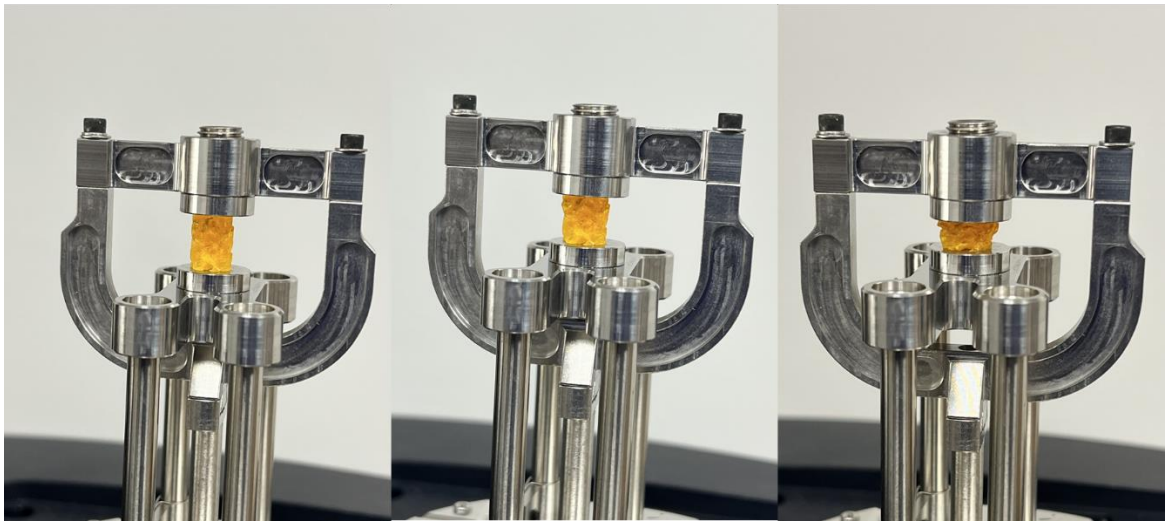

Figure S7.4.22: Digital photographs of gyroid compression testing.

7.4. Chapter 5

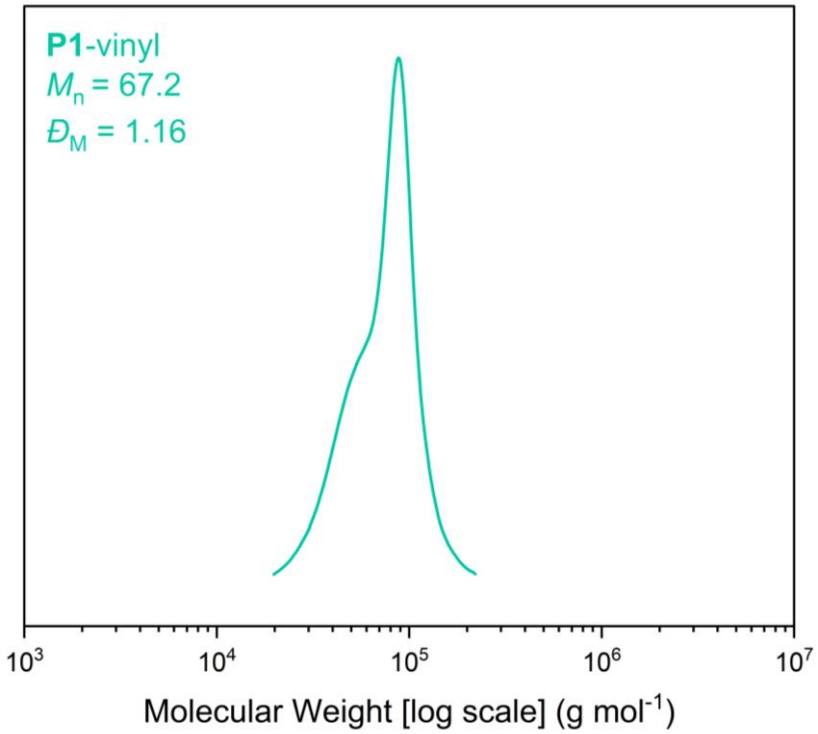

Figure S7.5.1: SEC (THF, 1 mL min^{-1}) data for **P1**-vinyl

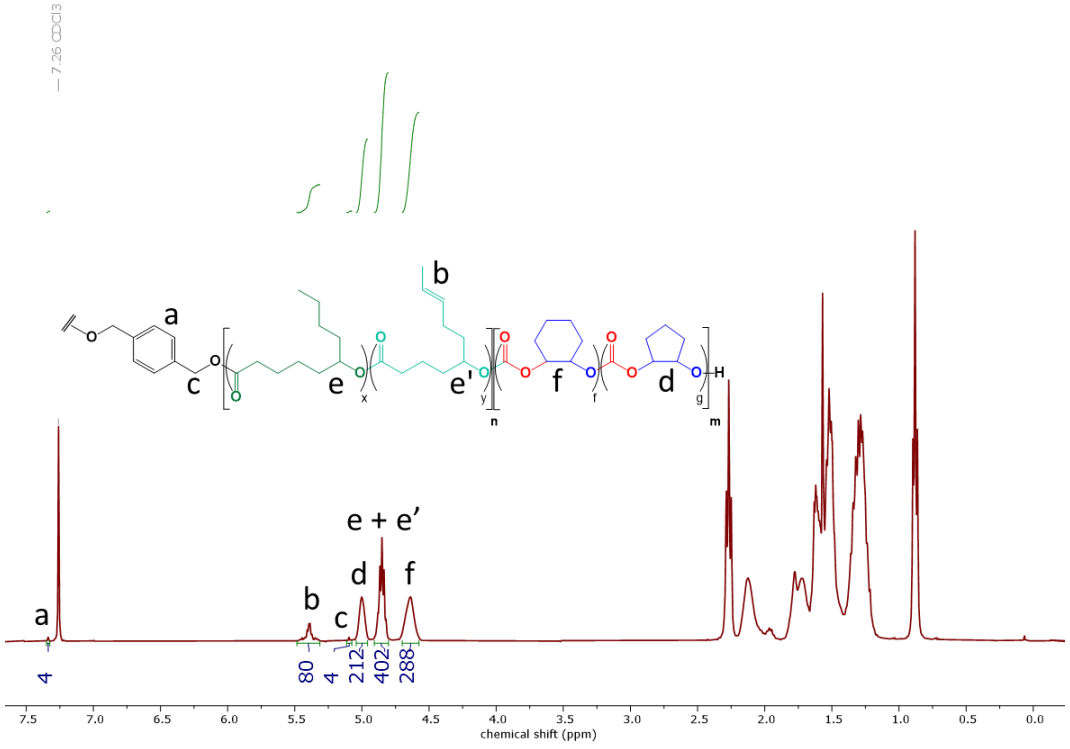

Figure S7.5.2: ^{1}H NMR spectrum (400 MHz, $CDCl_3$) of **P1**-vinyl.

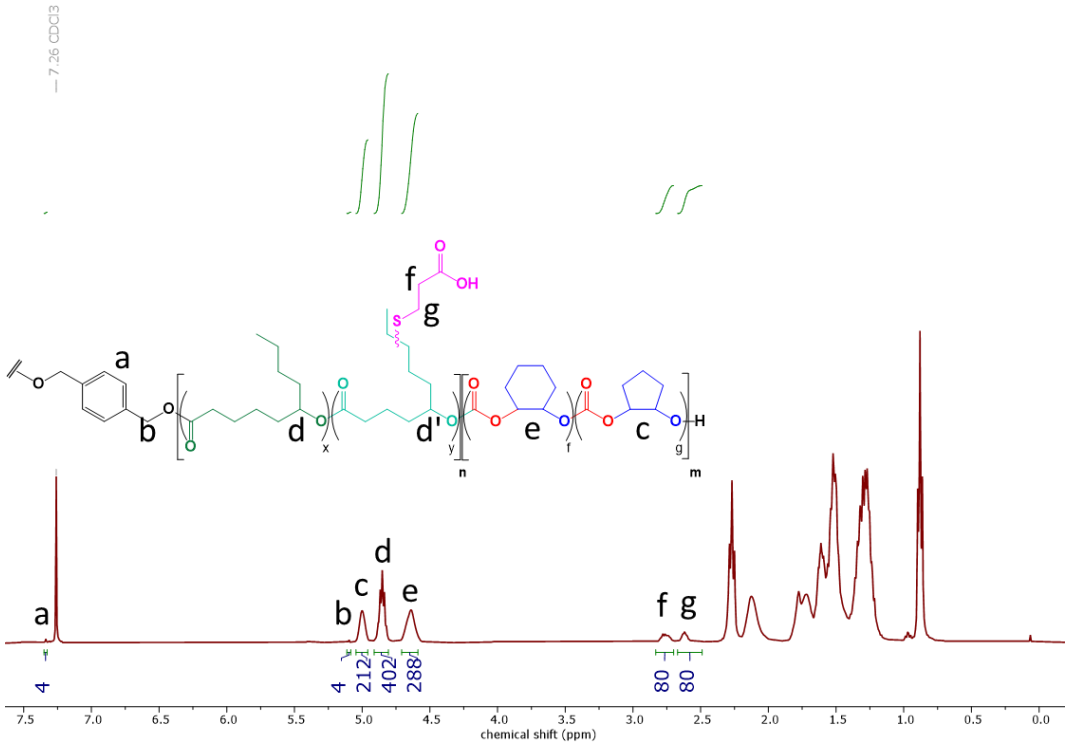

Figure S7.5.3: ^{1}H NMR spectrum (400 MHz, $CDCl_3$) of **P1**-COOH.

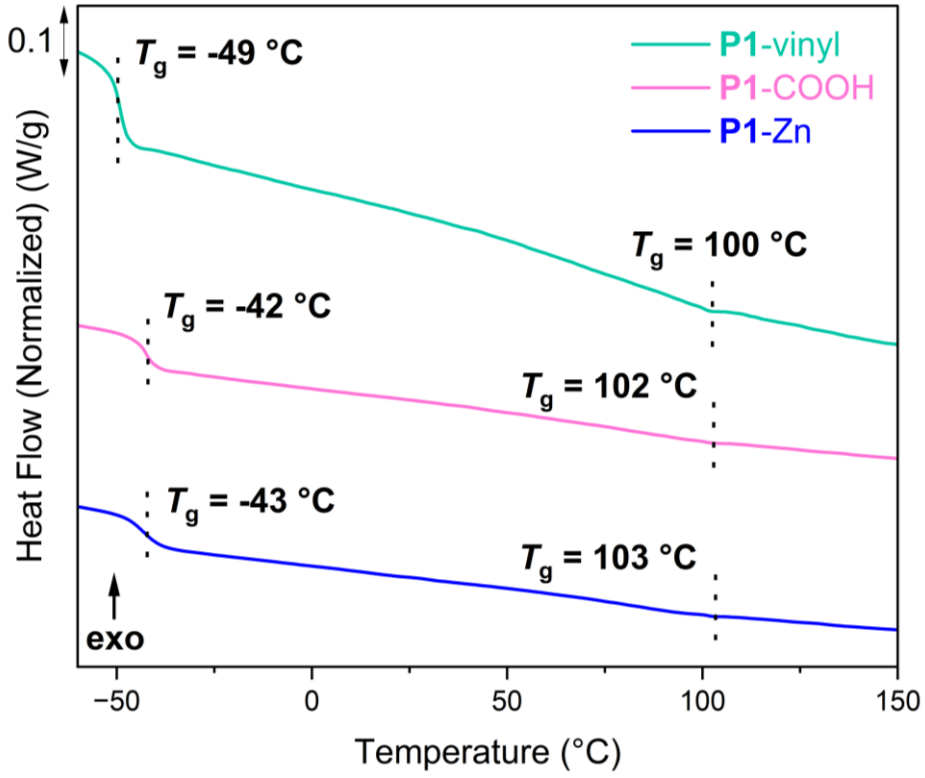

Figure S7.5.4: Differential Scanning Calorimetry (DSC) traces of **P1** resin and printed materials.

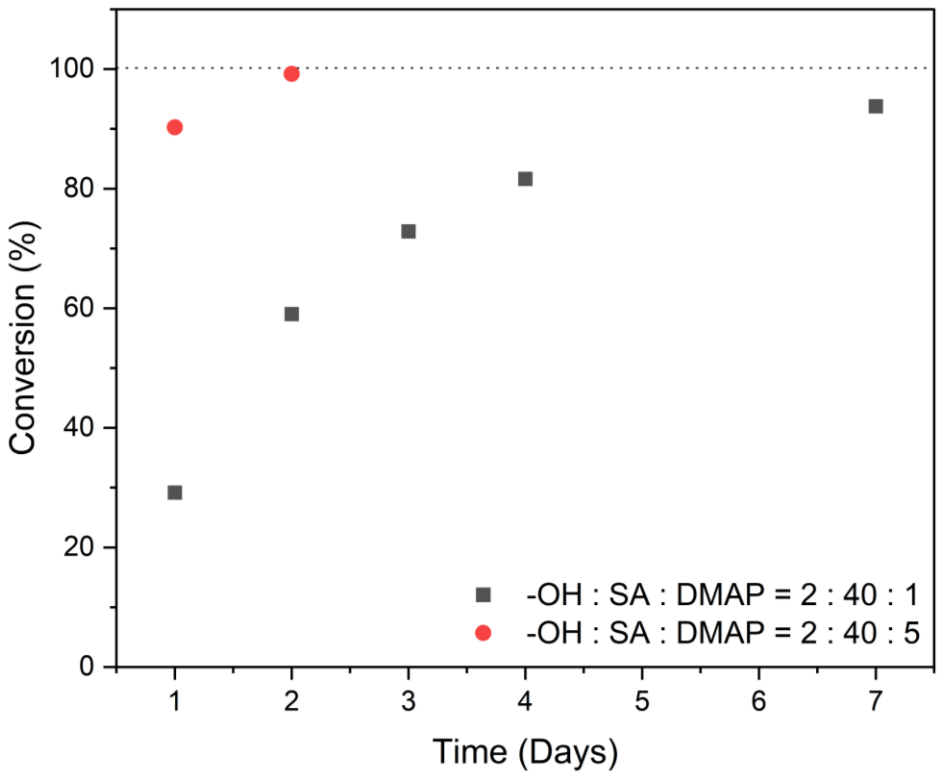

Figure S7.5.5: Conversion of hydroxyl end groups to carboxylic acid end-groups over time.

7.5. Chapter 6

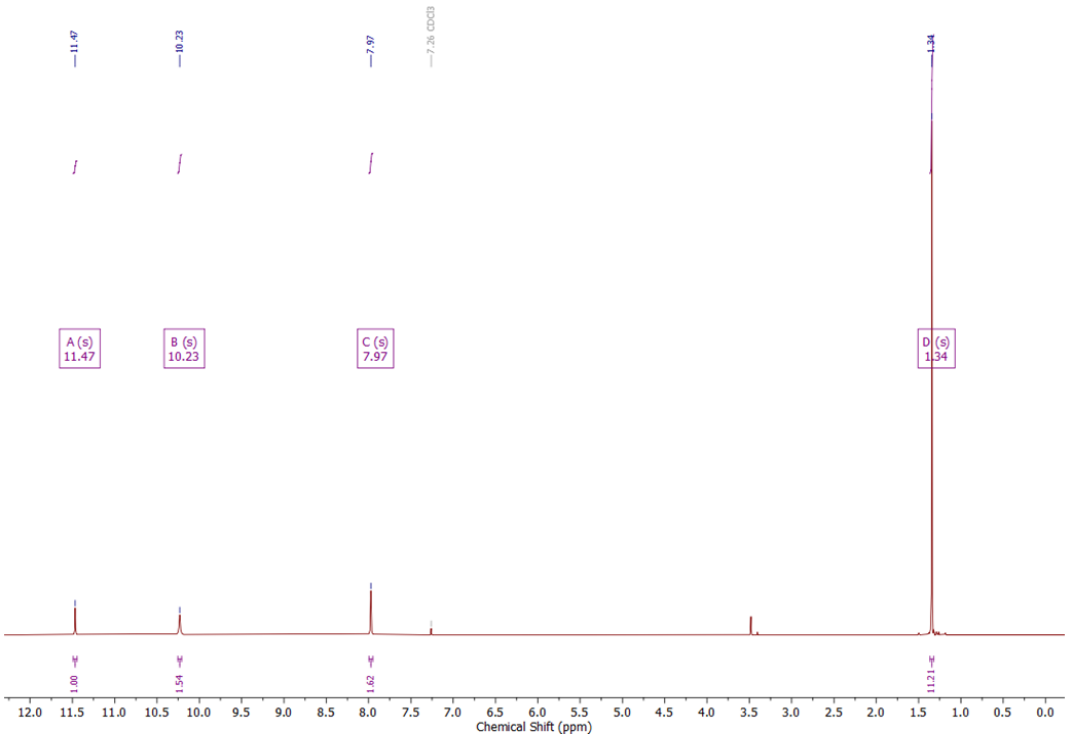

Figure S7.6.1: ^{1}H NMR (400 MHz, $CDCl_3$, 298 K) spectrum of 4-tert-butly-2,6-diformyl phenol.

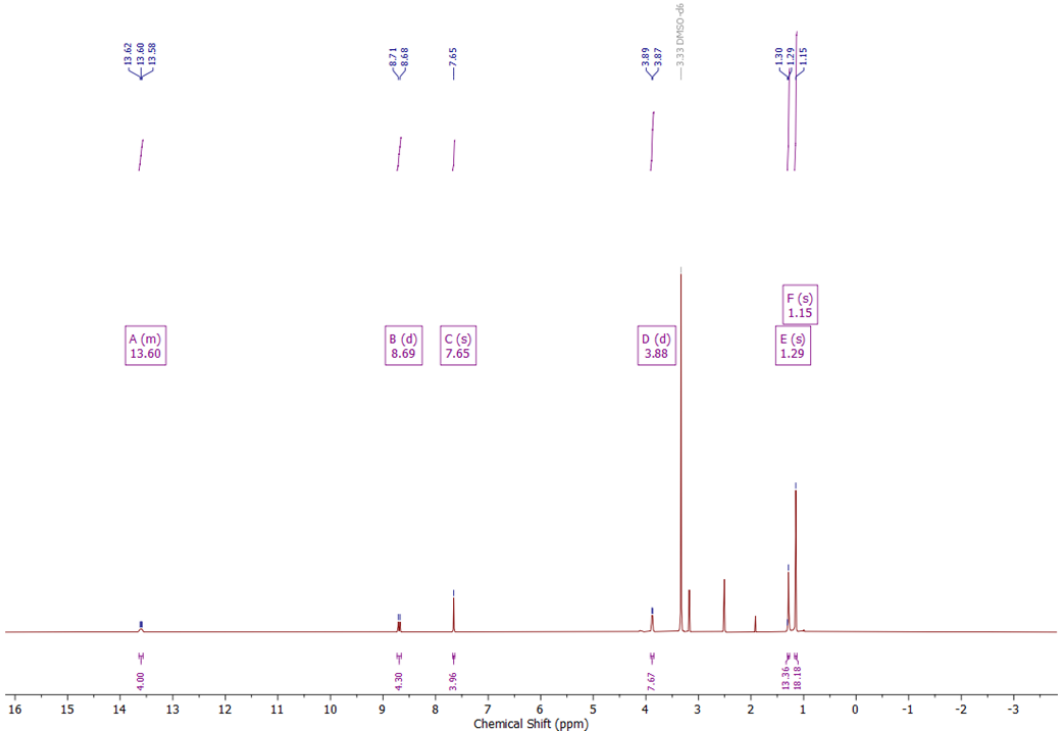

Figure S7.6.2: ^{1}H NMR (400 MHz, DMSO-d_6, 298 K) spectrum of $[H_4L](ClO_4)_2$.

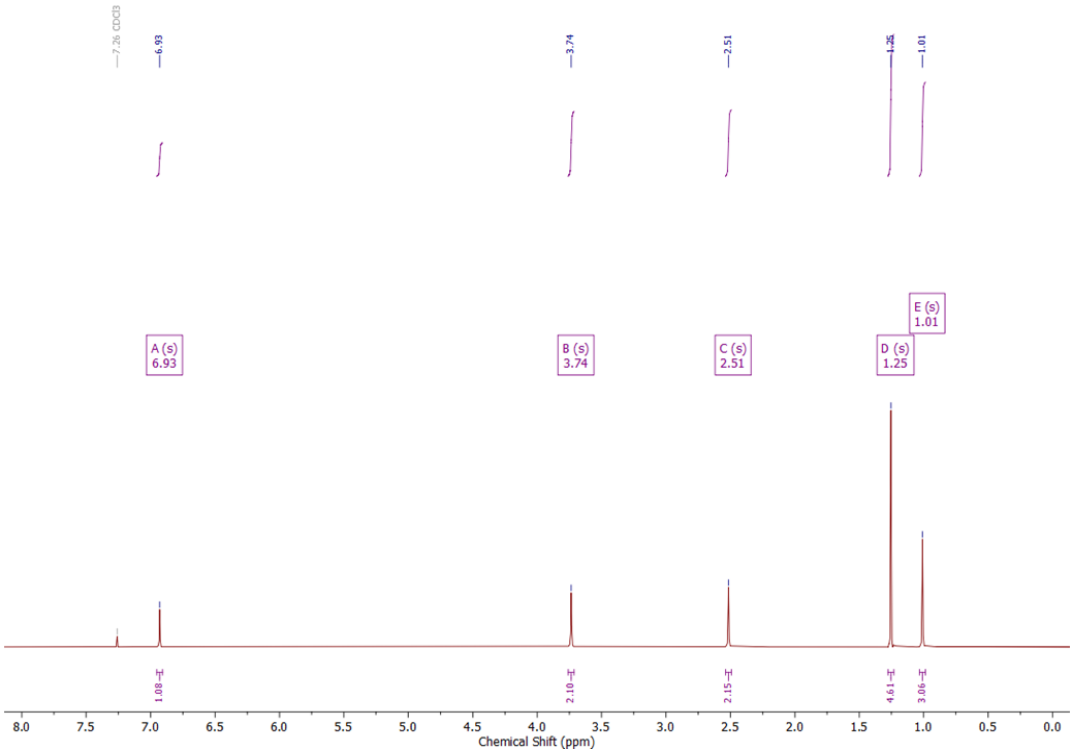

Figure S7.6.3: ^{1}H NMR (400 MHz, $CDCl_3$, 298 K) spectrum of H_2L.

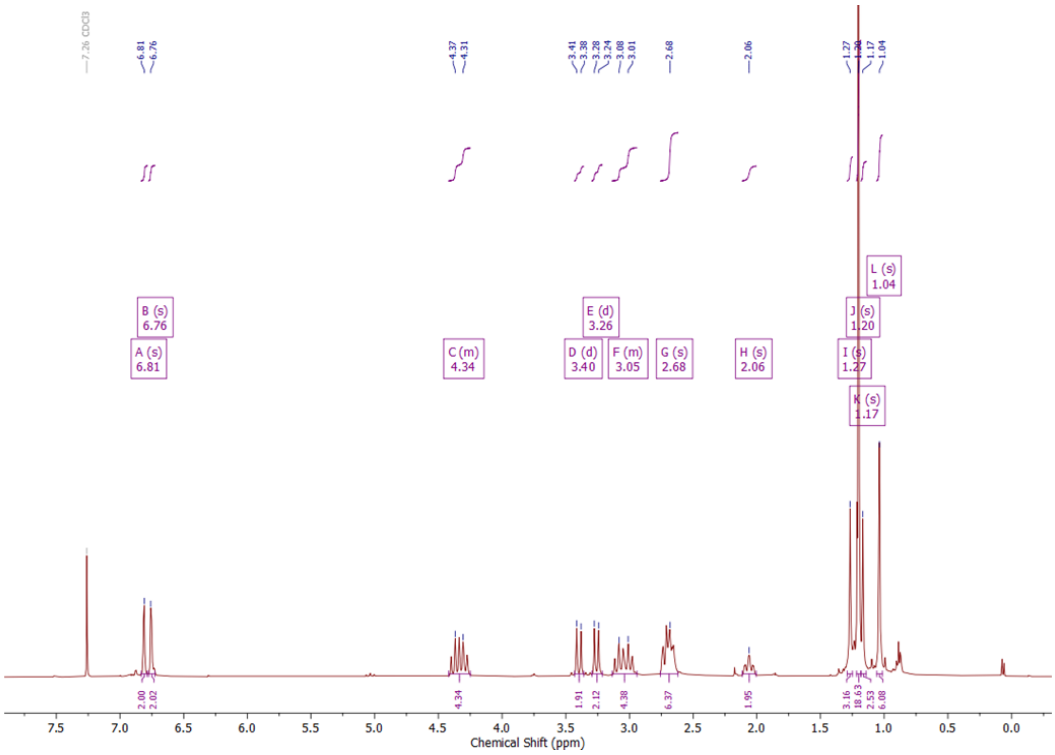

Figure S7.6.4: ^{1}H NMR (400 MHz, $CDCl_3$, 298 K) spectrum of $LZnMg(C_6F_5)_2$.

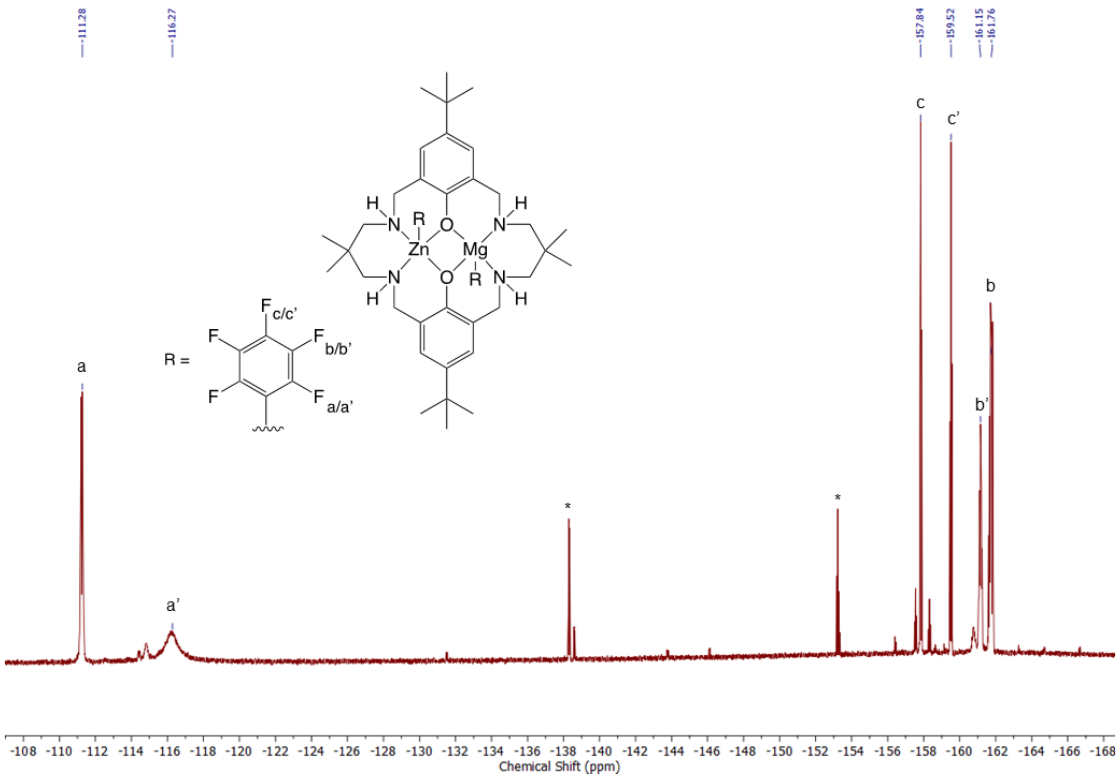

Figure S7.6.5: $^{19}F\{^{1}H\}$ NMR (376 MHz, $CDCl_3$) spectrum of the heterodinuclear catalyst [$LZnMg(C_6F_5)_2$]. *Signals corresponding to C_6F_5H

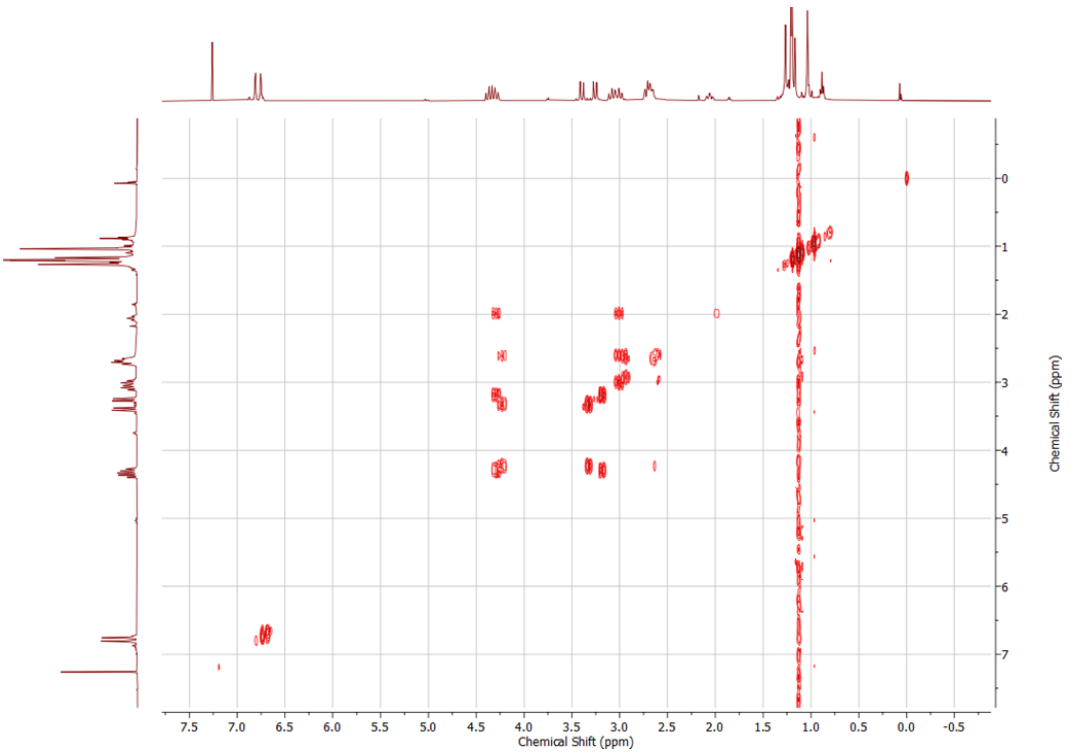

Figure S7.6.6: ^{1}H-^{1}H COSY (400 MHz, $CDCl_3$, 298 K) of $LZnMg(C_6F_5)_2$.

7.6. References

(1) Watts, A.; Kurokawa, N.; Hillmyer, M. A. Strong, Resilient, and Sustainable Aliphatic Polyester Thermoplastic Elastomers. *Biomacromolecules* **2017**, *18* (6), 1845-1854. DOI: 10.1021/acs.biomac.7b00283.
(2) Wanamaker, C. L.; Bluemle, M. J.; Pitet, L. M.; O'Leary, L. E.; Tolman, W. B.; Hillmyer, M. A. Consequences of Polylactide Stereochemistry on the Properties of Polylactide-Polymenthide-Polylactide Thermoplastic Elastomers. *Biomacromolecules* **2009**, *10* (10), 2904-2911. DOI: 10.1021/bm900721p.
(3) Gregory, G. L.; Williams, C. K. Exploiting Sodium Coordination in Alternating Monomer Sequences to Toughen Degradable Block Polyester Thermoplastic Elastomers. *Macromolecules* **2022**, *55* (6), 2290-2299. DOI: 10.1021/acs.macromol.2c00068.
(4) Gregory, G. L.; Sulley, G. S.; Kimpel, J.; Lagodzinska, M.; Hafele, L.; Carrodeguas, L. P.; Williams, C. K. Block Poly(carbonate-ester) Ionomers as High-Performance and Recyclable Thermoplastic Elastomers. *Angew. Chem. Int. Edit.* **2022**, *61* (47). DOI: 10.1002/anie.202210748.